Calhoun
Institutional Archive of the Naval Postgraduate School

Calhoun: The NPS Institutional Archive

DSpace Repository

Theses and Dissertations | 1. Thesis and Dissertation Collection, all items

1989-06

Effect of vortex circulation on injectant from a single film-cooling hole and a row of film-cooling holes in a turbulent boundary layer: part 1: injection beneath the vortex downwash

Craig, Douglas William

Monterey, California. Naval Postgraduate School

https://hdl.handle.net/10945/27010

This publication is a work of the U.S. Government as defined in Title 17, United States Code, Section 101. Copyright protection is not available for this work in the United States.

Downloaded from NPS Archive: Calhoun

http://www.nps.edu/library

Calhoun is the Naval Postgraduate School's public access digital repository for research materials and institutional publications created by the NPS community. Calhoun is named for Professor of Mathematics Guy K. Calhoun, NPS's first appointed -- and published -- scholarly author.

Dudley Knox Library / Naval Postgraduate School
411 Dyer Road / 1 University Circle
Monterey, California USA 93943

NAVAL POSTGRADUATE SCHOOL
Monterey, California

THESIS

C192233

EFFECT OF VORTEX CIRCULATION ON INJECTANT FROM A SINGLE FILM-COOLING HOLE AND A ROW OF FILM-COOLING HOLES IN A TURBULENT BOUNDARY LAYER, PART 1: INJECTION BENEATH THE VORTEX DOWNWASH

by

Douglas W. Craig

June 1989

Thesis Advisor: P. M. Ligrani
Co-Advisor: Chelakara S. Subramanian

Approved for public release; distribution is unlimited.

T244060

REPORT DOCUMENTATION PAGE

1a REPORT SECURITY CLASSIFICATION UNCLASSIFIED	1b RESTRICTIVE MARKINGS
2a SECURITY CLASSIFICATION AUTHORITY	3 DISTRIBUTION/AVAILABILITY OF REPORT Approved for public release; distribution is unlimited
2b DECLASSIFICATION/DOWNGRADING SCHEDULE	
4 PERFORMING ORGANIZATION REPORT NUMBER(S)	5 MONITORING ORGANIZATION REPORT NUMBER(S)
6a NAME OF PERFORMING ORGANIZATION Naval Postgraduate School 6b OFFICE SYMBOL (If applicable) Code 69	7a NAME OF MONITORING ORGANIZATION
6c ADDRESS (City, State, and ZIP Code) Monterey, California 93943-5000	7b ADDRESS (City, State, and ZIP Code) Wright-Paterson Air Force Base Dayton, Ohio 45433
8a NAME OF FUNDING/SPONSORING ORGANIZATION Wright Aeronautical Laboratories 8b OFFICE SYMBOL (If applicable)	9 PROCUREMENT INSTRUMENT IDENTIFICATION NUMBER MIPR FY 1455-88-N0608
8c ADDRESS (City, State, and ZIP Code) Wright-Patterson Air Force Base Dayton, Ohio 45433	10 SOURCE OF FUNDING NUMBERS PROGRAM ELEMENT NO / PROJECT NO / TASK NO / WORK UNIT ACCESSION NO

11 TITLE (Include Security Classification) Effect of Vortex Circulation on Injectant from a Single Film-Cooling Hole and a Row of Film-Cooling Holes in a Turbulent Boundary Layer, Part I: Injection Beneath the Vortex Downwash

12 PERSONAL AUTHOR(S)
Douglas W. Craig

13a TYPE OF REPORT	13b TIME COVERED	14 DATE OF REPORT (Year, Month, Day)	15 PAGE COUNT
Master's Thesis	FROM _____ TO _____	1989 June	314

16 SUPPLEMENTARY NOTATION
The views expressed on this thesis are those of the arthor and do not reflect the official policy or position of the Department of Defense or the U.S. Government.

17 COSATI CODES			18 SUBJECT TERMS (Continue on reverse if necessary and identify by block number)
FIELD	GROUP	SUB-GROUP	Embedded vortex, vortex circulation film-cooled turbulent boundary layer

19 ABSTRACT (Continue on reverse if necessary and identify by block number)

The effects of longitudinal vortices on film-cooling injectant from a single injection hole and from a row of injection holes in a turbulent boundary layer are investigated. Attention is focussed on the effects of vortex circulation when the injection hole is located beneath the vortex downwash. Heat transfer measurements, mean velocity and mean temperature surveys, and surface flow visualization results are discussed The embedded vortex considerably disturbs the injectant when $\Gamma/(U_c \cdot d)$ is greater than 1.0 where Γ is the vortex circulation, U_c is the injectant mean velocity and d is the injection hole diameter.

20 DISTRIBUTION/AVAILABILITY OF ABSTRACT	21 ABSTRACT SECURITY CLASSIFICATION
☒ UNCLASSIFIED/UNLIMITED ☐ SAME AS RPT ☐ DTIC USERS	UNCLASSIFIED
22a NAME OF RESPONSIBLE INDIVIDUAL Phillip M. Ligrani	22b TELEPHONE (Include Area Code) (408) 646-3382 / 22c OFFICE SYMBOL 69Li

DD FORM 1473, 84 MAR 83 APR edition may be used until exhausted
All other editions are obsolete

SECURITY CLASSIFICATION OF THIS PAGE

☆ U.S. Government Printing Office: 1986—606-24.

Approved for public release; distribution is unlimited

EFFECT OF VORTEX CIRCULATION ON INJECTANT FROM A SINGLE FILM-COOLING HOLE AND A ROW OF FILM-COOLING HOLES IN A TURBULENT BOUNDARY LAYER, PART 1: INJECTION BENEATH THE VORTEX DOWNWASH

by

Douglas William Craig
Lieutenant Commander, United States Navy
B.S., Miami University, 1977

Submitted in partial fulfillment of the
requirements for the degree of

MASTER OF SCIENCE IN MECHANICAL ENGINEERING

from the

NAVAL POSTGRADUATE SCHOOL
June 1989

ABSTRACT

The effects of longitudinal vortices on film-cooling injectant from a single injection hole and from a row of injection holes in a turbulent boundary layer are investigated. Attention is focused on the effects of vortex circulation when the injection hole is located beneath the vortex downwash. Heat transfer measurements, mean velocity and mean temperature surveys, and surface flow visualization results are discussed. The embedded vortex considerably disturbs the injectant when $\Gamma/(U_c \cdot d)$ is greater than 1.0, where Γ is the vortex circulation, U_c is the injectant mean velocity and d is the injection hole diameter.

C.1

TABLE OF CONTENTS

		PAGE
I.	INTRODUCTION	1
	A. BACKGROUND	1
	B. RELATED STUDIES	2
	C. ONGOING RESEARCH AT NAVAL POSTGRADUATE SCHOOL	4
	D. OBJECTIVES OF PRESENT STUDY	6
	E. OUTLINE OF EXPERIMENTATION	8
	F. THESIS ORGANIZATION	9
II.	EXPERIMENTAL APPARATUS AND PROCEDURES	10
	A. WIND TUNNEL AND COORDINATE SYSTEM	10
	B. VORTEX GENERATOR	12
	C. INJECTION SYSTEM	14
	D. HEAT TRANSFER SURFACE	16
	E. TEMPERATURE MEASUREMENTS	21
	F. MEAN VELOCITY MEASUREMENTS	23
	G. FLOW VISUALIZATION	24
III.	EXPERIMENTAL RESULTS	27
	A. DEFINITIONS OF KEY PARAMETERS	27
	B. FIVE HOLE PRESSURE PROBE SURVEYS	32
	1. STREAMWISE VORTICITY CONTOURS	34
	A. VORTICITY CONTOURS: NO FILM COOLING	34
	B. VORTICITY CONTOURS: FILM COOLING FROM A SINGLE INJECTION HOLE	37

C. VORTICITY CONTOURS:---------- 39
FILM COOLING FROM 13
INJECTION HOLES

D. DEPENDENCE OF VORTEX---------- 40
PARAMETERS

2. SECONDARY FLOW VECTORS---------- 42
STREAMWISE VELOCITY, AND
TOTAL PRESSURE DISTRIBUTIONS

A. VELOCITY AND PRESSURE---------- 42
DISTRIBUTIONS: NO FILM COOLING

B. VELOCITY AND PRESSURE---------- 45
DISTRIBUTIONS: FILM COOLING
FROM A SINGLE INJECTION HOLE

C. VELOCITY AND PRESSURE---------- 46
DISTRIBUTIONS: FILM COOLING
FILM COOLING FROM 13
INJECTION HOLES

3. AVERAGE VORTEX STRENGTH---------- 48

C. MEAN TEMPERATURE SURVEYS---------- 49

1. TEMPERATURE SURVEYS AT x/d=41.9--------- 52
FILM COOLING FROM A SINGLE
INJECTION HOLE

2. TEMPERATURE SURVEYS AT x/d=41.9--------- 53
FILM COOLING FROM 13 INJECTION
HOLES

3. STREAMWISE DEVELOPMENT:---------- 53
FILM COOLING FROM A SINGLE
INJECTION HOLE

4. STREAMWISE DEVELOPMENT:---------- 54
FILM COOLING FROM 13 INJECTION
HOLES

D. HEAT TRANSFER MEASUREMENTS---------- 55

1. HEAT TRANSFER MEASUREMENTS:---------- 56
NO FILM COOLING

2. HEAT TRANSFER MEASUREMENTS:---------- 58
FILM COOLING FROM A SINGLE
INJECTION HOLE

3. HEAT TRANSFER MEASUREMENTS:---------- 64
FILM COOLING FROM 13 INJECTION
HOLES

E. FLOW VISUALIZATION RESULTS---------- 69

IV. SUMMARY AND CONCLUSIONS---------- 74

APPENDIX A FIGURES---------- 76

APPENDIX B UNCERTAINTY ANALYSIS----------262

APPENDIX C DATA ACQUISITION, DATA----------264
PROCESSING AND PLOTTING PROGRAMS

APPENDIX D DATA FILE DIRECTORY----------273

LIST OF REFERENCES----------282

INITIAL DISTRIBUTION LIST----------284

LIST OF TABLES

PAGE

I. VORTEX GENERATOR POSITIONS---------- 14

II. FIVE-HOLE PRESSURE PROBE SURVEY DATA--------- 33

III. VORTEX PARAMETERS: NO FILM COOLING---------- 36
(M=0.0)

IV. VORTEX PARAMETERS: FILM COOLING---------- 38
FROM A SINGLE INJECTION HOLE (M=0.50)

V. VORTEX PARAMETERS: FILM COOLING---------- 40
FROM 13 INJECTION HOLES (M=0.50)

VI. AVERAGE VORTEX STRENGTH AND---------- 49
CIRCULATION VALUES AT x/d = 41.9

VII. TEMPERATURE SURVEYS: EXPERIMENTAL---------- 51
CONDITIONS AND PARAMETERS

VIII. HEAT TRANSFER SURVEYS: EXPERIMENTAL--------- 57
CONDITIONS AND PARAMETERS: NO FILM COOLING

IX. HEAT TRANSFER SURVEYS: EXPERIMENTAL--------- 59
CONDITIONS AND PARAMETERS: SINGLE
INJECTION HOLE FILM COOLING

X. SPANWISE VARIATION OF LOCAL STANTON---------- 61
NUMBER RATIOS: SINGLE INJECTION HOLE
FILM COOLING

XI. HEAT TRANSFER SURVEYS: EXPERIMENTAL--------- 65
CONDITIONS AND PARAMETERS: 13
INJECTION HOLE FILM COOLING

XII. SPANWISE VARIATION OF LOCAL STANTON---------- 67
NUMBER RATIOS: 13 INJECTION
HOLE FILM COOLING

XIII. SURFACE FLOW VISUALIZATION: FLOW---------- 70
CONDITIONS AND PARAMETERS

XIV. MEAN VELOCITY UNCERTAINTY----------262

XV. STANTON NIMBER UNCERTAINTY----------263

LIST OF FIGURES

FIGURES		PAGE
1.	Test Section Coordinate System----------	76
2.	Top View Schematic of Wind Tunnel---------- Test Section	77
3.	Vortex Generator Details----------	78
4.	Vortex Generator Orientation---------- in X-Z Plane For Various Vortex Generator Angles	79
5.	Coordinate Locations of Vortex---------- Generator Mounting Plate For Various Vortex Generator Angles	80
6.	Stanton Number Comparison Between---------- Exact Solution And Empirical Relationships	81
7.	Stanton Number Comparison Between---------- Exact Solution and Experimental Measurements	82
8.	Streamwise Vorticity Contours, m=0,---------- x/d=41.9, Γ =.149 m^2/s, Vortex r	83
9.	Streamwise Vorticity Contours, m=0---------- x/d=41.9, Γ =.115 m^2/s, Vortex s	84
10.	Streamwise Vorticity Contours, m=0---------- x/d=41.9, Γ =.085 m^2/s, Vortex t	85
11.	Streamwise Vorticity Contours, m=0---------- x/d=41.9 Γ= .041 m^2/s, Vortex u	86
12.	Streamwise Vorticity Contours, m=0---------- x/d=41.9 Γ=.019 m^2/s, Vortex v	87
13.	Streamwise Vorticity Contours, x/d=41.9-------- m=0.5, Single Injection Hole Γ = .151 m^2/s, S=3.17, Vortex r	88

14. Streamwise Vorticity Contours, x/d=41.9-------- 89
m=0.5, Single Injection Hole
Γ = .121 m^2/s, S=2.55, Vortex w

15. Streamwise Vorticity Contours, x/d=41.9-------- 90
m=0.5, Single Injection Hole
Γ = .089 m^2/s, S=1.88, Vortex x

16. Streamwise Vorticity Contours, x/d=41.9-------- 91
m=0.5, Single Injection Hole
Γ =.051 m^2/s, S=1.08, Vortex y

17. Streamwise Vorticity Contours, x/d=41.9-------- 92
m=0.5, Single Injection Hole
Γ =.014 m^2/s, S=0.29, Vortex z

18. Streamwise Vorticity Contours, x/d=41.9-------- 93
m=0.5, 13 Injection Holes,
Γ =.134 m^2/s, S=2.81, Vortex r

19. Streamwise Vorticity Contours, x/d=41.9-------- 94
m=0.5, 13 Injection Holes,
Γ =.111, m^2/s, S=2.33, Vortex w

20. Streamwise Vorticity Contours, x/d=41.9-------- 95
m=0.5, 13 Injection Holes,
Γ =.088 m^2/s, S=1.86, Vortex x

21. Streamwise Vorticity Contours, x/d=41.9-------- 96
m=0.5, 13 Injection Holes,
Γ =.042 m^2/s, S=0.89, Vortex y

22. Streamwise Vorticity Contours, x/d=41.9-------- 97
m=0.5, 13 Injection Holes,
Γ =.008 m^2/s, S=0.17, Vortex z

23. Spanwise Location of Vortex Center (Zcen)------ 98
vs. Vortex Generator Angle

24. Maximum Streamwise Vorticity (Wxmax)---------- 99
vs. Vortex Generator Angle

25. Vortex Circulation vs. Vortex----------------- 100
Generator Angle

26. Vortex Strength [$\Gamma/(Uc \cdot d)$]-------------------- 101
vs Vortex Generator Angle

27. Secondary Flow Vectors, m=0, x/d=41.9---------- 102
Γ =.149 m^2/s, Vortex r

28. Streamwise Velocity Field, m=0, x/d=41.9------- 103
Γ =.149 m^2/s, Vortex r

29. Total Pressure Field, m=0, x/d=41.9----------104
Γ =.149 m^2/s, Vortex r

30. Secondary Flow Vectors, m=0, x/d=41.9----------105
Γ =.115 m^2/s, Vortex s

31. Streamwise Velocity Field, m=0, x/d=41.9--------106
Γ =.115 m^2/s, Vortex s

32. Total Pressure Field, m=0, x/d=41.9----------107
Γ =.115 m^2/s, Vortex s

33. Secondary Flow Vectors, m=0, x/d=41.9----------108
Γ =.085 m^2/s, Vortex t

34. Streamwise Velocity Field, m=0, x/d=41.9--------109
Γ =.085 m^2/s, Vortex t

35. Total Pressure Field, m=0, x/d=41.9----------110
Γ =.085 m^2/s, Vortex t

36. Secondary Flow Vector, m=0, x/d=41.9----------111
Γ =.041 m^2/s, Vortex u

37. Streamwise Velocity Field, m=0, x/d=41.9--------112
Γ =.041 m^2/s, Vortex u

38. Total Pressure Field, m=0, x/d=41.9----------113
Γ =.041 m^2/s, Vortex u

39. Secondary Flow Vectors, m=0, x/d=41.9----------114
Γ =.019 m^2/s, Vortex v

40. Streamwise Velocity Field, m=0, x/d=41.9--------115
Γ =.019 m^2, Vortex v

41. Total Pressure Field, m=0, x/d=41.9----------116
Γ =.019 m^2/s, Vortex v

42. Secondary Flow Vecors, x/d=41.9----------117
m=0.5, Single Injection Hole,
Γ =.151 m^2/s, S=3.17, Vortex r

43. Streamwise Velocity Field, x/d=41.9----------118
m=0.5, Single Injection Hole,
Γ =.151 m^2/s, S=3.17, Vortex r

44. Total Pressure Field, x/d=41.9----------119
m=0.5, Single Injection Hole,
Γ =.151 m^2/s, S=3.17, Vortex r

45. Secondary Flow Vectors, x/d=41.9----------120
m=0.5, Single Injection Hole,
Γ =.121 m^2/s, S=2.55, Vortex w

46. Streamwise Velocity Field, x/d=41.9----------121
m=0.5, Single Injection Hole,
Γ =.121 m^2/s, S=2.55, Vortex w

47. Total Pressure Field x/d=41.9----------122
m=0.5, Single Injection Hole,
Γ =.121 m^2/s, S=2.55, Vortex w

48. Secondary Flow Vectors, x/d=41.9----------123
m=0.5, Single Injection Hole,
Γ =.089 m^2/s, S=1.88, Vortex x

49. Streamwise Velocity Field, x/d=41.9----------124
m=0.5, Single Injection Hole,
Γ =.089 m^2/s, S=1.88, Vortex x

50. Total Pressure Field, x/d=41.9----------125
m=0.5, Single Injection Hole,
Γ =.089 m^2/s, S=1.88, Vortex x

51. Secondary Flow Vectors, x/d=41.9----------126
m=0.5, Single Injection Hole,
Γ =.051 m^2/s, S=1.08, Vortex y

52. Streamwise Velocity Field, x/d=41.9----------127
m=0.5, Single Injection Hole,
Γ =.051 $m^2.s$, S=1.08, Vortex y

53. Total Pressure Field, x/d=41.9----------128
m=0.5, Single Injection Hole,
Γ =.051 m^2/s, S=1.08, Vortex y

54. Secondary Flow Vectors, x/d=41.9----------129
m=0.5, Single Injection Hole,
Γ =.014 m^2/s, S=0.29, Vortex z

55. Streamwise Velocity Field, x/d=41.9----------130
m=0.5, Single Injection Hole,
Γ =.014 m^2/s, S=0.29, Vortex z

56. Total Pressure Field, x/d=41.9----------131
m=0.5, Single Injection Hole,
Γ =.014 m^2/s, S=0.29, Vortex z

57. Secondary Flow Vectors, x/d=41.9----------132
m=0.5, 13 Injection Holes,
Γ =.134 m^2/s, S=2.81, Vortex r

58. Streamwise Velocity Field, x/d=41.9----------133
m=0.5, 13 Injection Holes,
Γ =.134 m^2/s, S=2.81, Vortex r

59. Total Pressure Field, x/d=41.9----------134
m=0.5, 13 Injection Holes,
Γ =.134 m^2/s, S=2.81, Vortex r

60. Secondary Flow Vectors, x/d=41.9----------135
m=0.5, 13 Injection Holes
Γ =.111 m^2/s, S=2.33, Vortex w

61. Streamwise Velocity Field, x/d=41.9----------136
m=0.5, 13 Injection Holes,
Γ =.111 m^2/s, S=2.33, Vortex w

62. Total Pressure Field, x/d=41.9----------137
m=0.5, 13 Injection Holes,
Γ =.111 m^2/s, S=2.33, Vortex w

63. Secondary Flow Vectors, x/d=41.9----------138
m=0.5, 13 Injection Holes,
Γ =.088 m^2/s, S=1.86, Vortex x

64. Streamwise Velocity Field, x/d=41.9----------139
m=0.5, 13 Injection Holes,
Γ =.088 m^2/s, S=1.86, Vortex x

65. Total Pressure Field, x/d=41.9----------140
m=0.5, 13 Injection Holes,
Γ =.088 m^2/s, S=1.86, Vortex x

66. Secondary Flow Vectors, x/d=41.9----------141
m=0.5, 13 Injection Holes
Γ =.042 m^2/s, S=0.89, Vortex y

67. Streamwise Velocity Field, x/d=41.9----------142
m=0.5, 13 Injection Holes,
Γ =.042 m^2/s, S=0.89, Vortex y

68. Total Pressure Field, x/d=41.9----------143
m=0.5, 13 Injection Holes,
Γ =.042 m^2/s, S=0.89, Vortex y

69. Secondary Flow Vectors, x/d=41.9----------144
m=0.5, 13 Injection Holes,
Γ =.008 m^2/s, S=0.17, Vortex z

70. Streamwise Velocity Field, x/d=41.9----------145
m=0.5, 13 Injection Holes,
Γ =.008 m^2/s, S=0.17, Vortex z

71. Total Pressure Field, x/d=41.9----------146
m=0.5, 13 Injection Holes,
Γ =.008 m^2/s, S=0.17, Vortex z

72. Secondary Flow Vectors, x/d=41.9----------147
m=0.5, 13 Injection Holes, No Vortex,
Film Cooled Turbulent Boundary Layer

73. Streamwise Velocity Field, x/d=41.9----------148
m=0.5, 13 Injection Holes, No Vortex,
Film Cooled Turbulent Boundary Layer

74. Total Pressure Field, x/d=41.9----------149
m=0.5, 13 Injection Holes, No Vortex
Film Cooled Turbulent Boundary Layer

75. Local Temperature Distribution----------150
With Heated Injectant, No Wall Heating,
x/d=41.9, m=0.5, Single Injection Hole, No Vortex

76. Local Temperature Distribution----------151
With Heated Injectant, No Wall Heating,
x/d=41.9, m=0.5, Single Injection Hole
Γ =.014 m^2/s, S=0.23, Vortex z

77. Local Temperature Distribution----------152
With Heated Injectant, No Wall Heating,
x/d=41.9, m=0.5, Single Injection Hole
Γ =.045 m^2/s, S=0.98, Vortex y

78. Local Temperature Distribution----------153
With Heated Injectant, No Wall Heating,
x/d=41.9, m=0.5, Single Injection Hole
Γ =.088 m^2/s, S=1.87, Vortex x

79. Local Temperature Distribution----------154
With Heated Injection, No Wall Heating,
x/d=41.9, m=0.5, Single Injection Hole
Γ =.116 m^2/s, S=2.44, Vortex w

80. Local Temperature Distribution----------155
With Heated Injectant, No Wall Heating,
x/d=41.9, m=0.5, Single Injection Hole
Γ =.145 m^2/s, S=2.99, Vortex r

81. Local Temperature Distribution----------156
With Heated Injectant, No Wall Heating, No Vortex,
x/d=41.9, m=0.5, 13 Injection Holes

82. Local Temperature Distribution----------157
With Heated Injectant, No Wall Heating,
x/d=41.9, m=0.5, 13 Injection Holes
Γ =.014 m^2/s, S=0.23, Vortex z

83. Local Temperature Distribution----------158
With Heated Injectant, No Wall Heating,
x/d=41.9, m=0.5, 13 Injection Holes
Γ =.045 m^2/s, S=0.98, Vortex y

84. Local Temperature Distribution----------159
With Heated Injectant, No Wall Heating,
x/d=41.9, m=0.5, 13 Injection Holes
Γ =.088 m^2/s, S=1.87, Vortex x

85. Local Temperature Distribution----------160
With Heated Injectant, No Wall Heating,
x/d=41.9, m=0.5, 13 Injection Holes
Γ =.116 m^2/s, S=2.44, Vortex w

86. Local Temperature Distribution----------161
With Heated Injectant, No Wall Heating,
x/d=41.9, m=0.5, 13 Injection Holes
Γ =.145 m^2/s, S=2.44, Vortex r

87. Local Temperature Distribution----------162
With Heated Injectant, No Wall Heating,
x/d=5.2, m=0.5, Single Injection Hole Vortex w

88. Local Temperature Distribution----------163
With Heated Injectant, No Wall Heating,
x/d=41.9, m=0.5, Single Injection Hole
Γ =.116 m^2/s, S=2.44, Vortex w

89. Local Temperature Distribution----------164
With Heated Injectant, No Wall Heating,
x/d=82.9, m=0.5, Single Injection Hole, Vortex w

90. Local Temperature Distribution----------165
With Heated Injectant, No Wall Heating,
x/d=109.2, m=0.5, Single Injection Hole
Vortex w, Temp. Difference Range (.5 - 2.5) degrees

91. Local Temperature Distribution----------166
With Heated Injectant, No Wall Heating,
x/d=109.2, m=0.5, Single Injection Hole
Vortex w, Temp. Difference Range (.3 - .7) degrees

92. Local Temperature Distribution----------167
With Heated Injectant, No Wall Heating,
x/d=5.2, m=0.5, 13 Injection Holes Vortex w

93. Local Temperature Distribution----------168
With Heated Injectant, No Wall Heating,
x/d=41.9, m=0.5, 13 Injection Holes
Γ =.116 m^2/s, S=2.44, Vortex w

94. Local Temperature Distribution----------169
With Heated Injectant, No Wall Heating,
x/d=82.9, m=0.5, 13 Injection Holes, Vortex w

95. Local Temperature Distribution----------170
With Heated Injectant, No Wall Heating,
x/d=109.2, m=0.5, 13 Injection Holes, Vortex w

96. Local St/Sto Ratio Distribution with----------171
No Film Cooling, Embedded Vortex z

97. Local St/Sto Ratio Distribution with----------172
No Film Cooling, Embedded Vortex y

98. Local St/Sto Ratio Distribution with----------173
No Film Cooling, Embedded Vortex x

99. Local St/Sto Ratio Distribution with----------174
No Film Cooling, Embedded Vortex w

100. Local St/Sto Ratio Distribution with----------175
No Film Cooling, Embedded Vortex r

101. Local St/Sto and Stf/Sto Distributions with-----176
Film Cooling, m=0.5, Single Injection Hole
Without Embedded Vortex

102. Local St/Sto and Stf/Sto Distributions with-----177
Film Cooling, m=0.5, Single Injection Hole
With and Without Embedded Vortex z

103. Local St/Sto and Stf/Sto Distributions with-----178
Film Cooling, m=0.5, Single Injection Hole
With and Without Embedded Vortex y

104. Local St/Sto and Stf/Sto Distributions with-----179
Film Cooling, m=0.5, Single Injection Hole
With and Without Embedded Vortex x

105. Local St/Sto and Stf/Sto Distributions with-----180
Film Cooling, m=0.5, Single Injection Hole
With and Without Embedded Vortex w

106. Local St/Sto and Stf/Stop Distributions with----181
Film Cooling, m=0.5, Single Injection Hole
With and Without Embedded Vortex r

107. Spanwise Variation of St/Sto and Stf/Sto--------182
Ratios, m=0.5, Single Injection Hole
x/d=7.4, No Vortex

108. Spanwise Variation of St/Sto and Stf/Sto--------183
Ratios, m=0.5, Single Injection Hole
x/d=7.4, Vortex z

109. Spanwise Variation of St/Sto and Stf/Sto--------184
Ratios, m=0.5, Single Injection Hole
x/d=7.4, Vortex y

110. Spanwise Variation of St/Sto and Stf/Sto--------185
Ratios, m=0.5, Single Injection Hole
x/d=7.4, Vortex x

111. Spanwise Variation of St/Sto and Stf/Sto--------186
Ratios, m=0.5, Single Injection Hole
x/d=7.4, Vortex w

112. Spanwise Variation of St/Sto and Stf/Sto--------187
Ratios, m=0.5, Single Injection Hole
x/d=7.4, Vortex r

113. Spanwise Variation of St/Sto and Stf/Sto--------188
Ratios, m=0.5, Single Injection Hole
x/d=17.5, No Vortex

114. Spanwise Variation of St/Sto and Stf/Sto--------189
Ratios, m=0.5, Single Injection Hole
x/d=17.5, Vortex z

115. Spanwise Variation of St/Sto and Stf/Sto--------190
Ratios, m=0.5, Single Injection Hole
x/d=17.5, Vortex y

116. Spanwise Variation of St/Sto an Stf/Sto---------191
Ratios, m=0.5, Single Injection Hole
x/d=17.5, Vortex x

117. Spanwise Variation of St/Sto and Sto------------192
Ratios, m=0.5, Single Injection Hole
x/d=17.5, Vortex w

118. Spanwise Variation of St/Sto and Stf/Sto--------193
Ratios, m=0.5, Single Injection Hole
x/d=17.5, Vortex r

119. Spanwise Variation of St/Sto an Stf/Sto---------194
Ratios, m=0.5, Single Injection Hole
x/d=33.6, No Vortex

120. Spanwise Variation of St/Sto an Stf/Sto---------195
Ratios, m=0.5, Single Injection Hole
x/d=33.6, Vortex z

121. Spanwise Variation of St/Sto an Stf/Sto---------196
Ratios, m=0.5, Single Injection Hole
x/d=33.6, Vortex y

122. Spanwise Variation of St/Sto an Stf/Sto---------197
Ratios, m=0.5, Single Injection Hole
x/d=33.6, Vortex x

123. Spanwise Variation of St/Sto an Stf/Sto---------198
Ratios, m=0.5, Single Injection Hole
x/d=33.6, Vortex w

124. Spanwise Variation of St/Sto an Stf/Sto---------199
Ratios, m=0.5, Single Injection Hole
x/d=33.6, Vortex r

125. Spanwise Variation of St/Sto an Stf/Sto---------200
Ratios, m=0.5, Single Injection Hole
x/d=54.6, No Vortex

126. Spanwise Variation of St/Sto an Stf/Sto---------201
Ratios, m=0.5, Single Injection Hole
x/d=54.6, Vortex z

127. Spanwise Variation of St/Sto an Stf/Sto---------202
Ratios, m=0.5, Single Injection Hole
x/d=54.6, Vortex y

128. Spanwise Variation of St/Sto an Stf/Sto---------203
Ratios, m=0.5, Single Injection Hole
x/d=54.6, Vortex x

129. Spanwise Variation of St/Sto an Stf/Sto---------204
Ratios, m=0.5, Single Injection Hole
x/d=54.6, Vortex w

130. Spanwise Variation of St/Sto an Stf/Sto---------205
Ratios, m=0.5, Single Injection Hole
x/d=54.6, Vortex r

131. Spanwise Variation of St/Sto an Stf/Sto---------206
Ratios, m=0.5, Single Injection Hole
x/d=75.6, No Vortex

132. Spanwise Variation of St/Sto an Stf/Sto---------207
Ratios, m=0.5, Single Injection Hole
x/d=75.6, Vortex z

133. Spanwise Variation of St/Sto an Stf/Sto---------208
Ratios, m=0.5, Single Injection Hole
x/d=75.6, Vortex y

134. Spanwise Variation of St/Sto an Stf/Sto---------209
Ratios, m=0.5, Single Injection Hole
x/d=75.6, Vortex x

135. Spanwise Variation of St/Sto an Stf/Sto---------210
Ratios, m=0.5, Single Injection Hole
x/d=75.6, Vortex w

136. Spanwise Variation of St/Sto an Stf/Sto---------211
Ratios, m=0.5, Single Injection Hole
x/d=75.6, Vortex r

137. Spanwise Variation of St/Sto an Stf/Sto---------212
Ratios, m=0.5, Single Injection Hole
x/d=96.6, No Vortex

138. Spanwise Variation of St/Sto an Stf/Sto---------213
Ratios, m=0.5, Single Injection Hole
x/d=96.6, Vortex z

139. Spanwise Variation of St/Sto an Stf/Sto---------214
Ratios, m=0.5, Single Injection Hole
x/d=96.6, Vortex y

140. Spanwise Variation of St/Sto an Stf/Sto---------215
Ratios, m=0.5, Single Injection Hole
x/d=96.6, Vortex x

141. Spanwise Variation of St/Sto an Stf/Sto---------216
Ratios, m=0.5, Single Injection Hole
x/d=96.6, Vortex w

142. Spanwise Variation of St/Sto an Stf/Sto---------217
Ratios, m=0.5, Single Injection Hole
x/d=96.6, Vortex r

143. Local St/Sto and Stf/Sto Distributions----------218
with Film Cooling, m=0.5, 13 Injection Holes
Without Embedded Vortex

144. Local St/Sto and Stf/Sto Distributions----------219
with Film Cooling, m=0.5, 13 Injection Holes
With and Without Embedded Vortex z

145. Local St/Sto and Stf/Sto Distributions----------220
with Film Cooling, m=0.5, 13 Injection Holes
With and Without Embedded Vortex y

146. Local St/Sto and Stf/Sto Distributions----------221
with Film Cooling, m=0.5, 13 Injection Holes
With and Without Embedded Vortex x

147. Local St/Sto and Stf/Sto Distributions----------222
with Film Cooling, m=0.5, 13 Injection Holes
With and Without Embedded Vortex w

148. Local St/Sto and Stf/Sto Distributions----------223
with Film Cooling, m=0.5, 13 Injection Holes
With and Without Embedded Vortex r

149. Spanwise Variation of St/Sto and Stf/Sto--------224
Ratios, m=0.5, 13 Injection Holes
x/d=7.4, No Vortex

150. Spanwise Variation of St/Sto and Stf/Sto--------225
Ratios, m=0.5, 13 Injection Holes
x/d=7.4, Vortex z

151. Spanwise Variation of St/Sto and Stf/Sto--------226
Ratios, m=0.5, 13 Injection Holes
x/d=7.4, Vortex y

152. Spanwise Variation of St/Sto and Stf/Sto--------227
Ratios, m=0.5, 13 Injection Holes
x/d=7.4, Vortex x

153. Spanwise Variation of St/Sto and Stf/Sto--------228
Ratios, m=0.5, 13 Injection Holes
x/d=7.4, Vortex w

154. Spanwise Variation of St/Sto and Stf/Sto--------229
Ratios, m=0.5, 13 Injection Holes
x/d=7.4, Vortex r

155. Spanwise Variation of St/Sto and Stf/Sto--------230
Ratios, m=0.5, 13 Injection Holes
x/d=17.5, No Vortex

156. Spanwise Variation of St/Sto and Stf/Sto--------231
Ratios, m=0.5, 13 Injection Holes
x/d=17.5, Vortex z

157. Spanwise Variation of St/Sto and Stf/Sto--------232
Ratios, m=0.5, 13 Injection Holes
x/d=17.5, Vortex y

158. Spanwise Variation of St/Sto and Stf/Sto--------233
Ratios, m=0.5, 13 Injection Holes
x/d=17.5, Vortex x

159. Spanwise Variation of St/Sto and Stf/Sto--------234
Ratios, m=0.5, 13 Injection Holes
x/d=17.5, Vortex w

160. Spanwise Variation of St/Sto and Stf/Sto--------235
Ratios, m=0.5, 13 Injection Holes
x/d=17.5, Vortex r

161. Spanwise Variation of St/Sto and Stf/Sto--------236
Ratios, m=0.5, 13 Injection Holes
x/d=33.6, No Vortex

162. Spanwise Variation of St/Sto and Stf/Sto--------237
Ratios, m=0.5, 13 Injection Holes
x/d=33.6, Vortex z

163. Spanwise Variation of St/Sto and Stf/Sto--------238
Ratios, m=0.5, 13 Injection Holes
x/d=33.6, Vortex y

164. Spanwise Variation of St/Sto and Stf/Sto--------239
Ratios, m=0.5, 13 Injection Holes
x/d=33.6, Vortex x

165. Spanwise Variation of St/Sto and Stf/Sto--------240
Ratios, m=0.5, 13 Injection Holes
x/d=33.6, Vortex w

166. Spanwise Variation of St/Sto and Stf/Sto--------241
Ratios, m=0.5, 13 Injection Holes
x/d=33.6, Vortex r

167. Spanwise Variation of St/Sto and Stf/Sto--------242
Ratios, m=0.5, 13 Injection Holes
x/d=54.6, No Vortex

168. Spanwise Variation of St/Sto and Stf/Sto--------243
Ratios, m=0.5, 13 Injection Holes
x/d=54.6, Vortex z

169. Spanwise Variation of St/Sto and Stf/Sto--------244
Ratios, m=0.5, 13 Injection Holes
x/d=54.6, Vortex y

170. Spanwise Variation of St/Sto and Stf/Sto--------245
Ratios, m=0.5, 13 Injection Holes
x/d=54.6, Vortex x

171. Spanwise Variation of St/Sto and Stf/Sto--------246
Ratios, m=0.5, 13 Injection Holes
x/d=54.6, Vortex w

172. Spanwise Variation of St/Sto and Stf/Sto--------247
Ratios, m=0.5, 13 Injection Holes
x/d=54.6, Vortex r

173. Spanwise Variation of St/Sto and Stf/Sto--------248
Ratios, m=0.5, 13 Injection Holes
x/d=75.6, No Vortex

174. Spanwise Variation of St/Sto and Stf/Sto--------249
Ratios, m=0.5, 13 Injection Holes
x/d=75.6, Vortex z

175. Spanwise Variation of St/Sto and Stf/Sto--------250
Ratios, m=0.5, 13 Injection Holes
x/d=75.6, Vortex y

176. Spanwise Variation of St/Sto and Stf/Sto--------251
Ratios, m=0.5, 13 Injection Holes
x/d=75.6, Vortex x

177. Spanwise Variation of St/Sto and Stf/Sto--------252
Ratios, m=0.5, 13 Injection Holes
x/d=75.6, Vortex w

178. Spanwise Variation of St/Sto and Stf/Sto--------253
Ratios, m=0.5, 13 Injection Holes
x/d=75.6, Vortex r

179. Spanwise Variation of St/Sto and Stf/Sto--------254
Ratios, m=0.5, 13 Injection Holes
x/d=96.6, No Vortex

180. Spanwise Variation of St/Sto and Stf/Sto--------255
Ratios, m=0.5, 13 Injection Holes
x/d=96.6, Vortex z

181. Spanwise Variation of St/Sto and Stf/Sto--------256
Ratios, m=0.5, 13 Injection Holes
x/d=96.6, Vortex y

182. Spanwise Variation of St/Sto and Stf/Sto--------257
Ratios, m=0.5, 13 Injection Holes
x/d=96.6, Vortex x

183. Spanwise Variation of St/Sto and Stf/Sto--------258
Ratios, m=0.5, 13 Injection Holes
x/d=96.6, Vortex w

184. Spanwise Variation of St/Sto and Stf/Sto--------259
Ratios, m=0.5, 13 Injection Holes
x/d=96.6, Vortex r

185. Surface Flow Patterns: 13 Injection Holes------260

186. Surface Flow Patterns: Single------------------261
Injection Hole

LIST OF SYMBOLS

A	-	area
c	-	average vortex core radius
Cp	-	constant pressure specific heat (air)
Cpy, Cpp Cpt, Cpts	-	five-hole probe calibration coefficients
Cr, Cr2	-	vortex circulation, symbols used in vorticity plots representing circulation values derived from different vortex core models
d	-	injection hole diameter (0.952 cm)
h	-	heat transfer coefficient: $\dot{q}''/(T_{r\infty} - T_w)$
Kp, Ky	-	five-hole probe calibration curve slopes for pitch and yaw angles
m, M	-	blowing ratio: $\rho_c \cdot U_c/(\rho_\infty \cdot U_\infty)$
P	-	static pressure
Pamb	-	ambient pressure
Pr	-	Prandtl number
$\dot{q}''$	-	heat flux
$\dot{q}_w$	-	convective heat transfer rate from the wall to the freestream
Re_x	-	Reynolds number
r, s, t, u, v, w, x, y, z	-	specific vortex designators
S, $\Gamma/(U_c \cdot d)$	-	non-dimensional vortex circulation, vortex strength
St	-	stanton number
Stf	-	stanton number, film-cooling only

Sto	-	baseline Stanton number, no film-cooling no vortex
T	-	static temperature
U	-	mean velocity
w_x	-	streamwise vorticity
Wxmax	-	maximum streamwise vorticity, occuring at vortex core center
x/d	-	dimensionless streamwise position: streamwise distance measured from the downstream edges of the injection holes, divided by injection hole diameter
X	-	downstream distance measured from the leading edge of the boundary layer trip
Y	-	vertical distance measured upwards from the test surface wall
Z	-	spanwise distance measured from the test surface centerline
Zcen	-	spanwise location of vortex core center
Zcore, Ycore Z2core, Y2core	-	core radii in the Z and Y directions, symbols used in vorticity plots representing values derived from different vortex core models
2c/d	-	dimensionless core size parameter: twice the average core radius divided by the injection hole diameter
α	-	pitch angle of the five-hole probe
β	-	yaw angle of the five-hole probe
β_1	-	complete Beta function
β_{u1}	-	incomplete Beta function
ε	-	unheated starting length
Γ	-	circulation of streamwise vorticity
ρ	-	density

Θ - non-dimensional coolant temperature: $(T_{rc} - T_{r^\infty})/(T_w - T_{r^\infty})$

δ_1 - boundary layer displacement thickness

Subscripts

c - coolant at exit of the injection holes

o - stagnation condition

r - recovery condition

w - wall

∞ - freestream

ACKNOWLEDGEMENTS

This research was supported by Wright Aeronautical Laboratories, Wright-Patterson Air Force Base; Dr. Dick Rivir, program monitor.

The composition of this study was greatly influenced by P. M. Ligrani along with the work of S. L. Joseph, A. Ortiz, G. E. Schwartz and W. W. Williams.

Technical contributions were made by Dr. Chelakara Subramanian through his expert adaptation of computer software and his knowledgable instruction in surface flow visualization techniques.

I wish to express my thanks and appreciation to Professor Phil Ligrani for his expert guidance and patient instruction, and for the many hours of consultation which he devoted to this study.

I. INTRODUCTION

A. BACKGROUND

In modern gas turbines, maximum turbine inlet temperatures are in the range of 1600-1800 degrees Celsius. The resulting thermal loading of turbine blades and turbine endwalls necessitates the development of efficient cooling configurations. Film cooling is one cooling scheme employed to protect the turbine surfaces from exposure to hot gases and the resulting thermal stresses. However, the effectiveness of film cooling may be significantly reduced due to the presence of turbine passage secondary flows. Studies by Ligrani et al. [Ref. 1, 2, and 3] show that embedded vortices in particular may cause significant changes to wall heat transfer rates and distributions of film injectant. In some cases, hot spots may form just downstream of injectant sites at locations where film cooling would ordinarily be expected to provide adequate protection.

Embedded vortices in turbine cascades originate from at least two different fluid mechanisms. In the first case, they form from intense local pressure gradients at locations such as the intersection between the turbine

blade and the endwall. Here, pressure forces the flow toward the end wall where it rolls into the leading edge or horseshoe vortex. One leg of this vortex flows along the suction side of the turbine blade and one leg flows along the pressure side. The passage vortex arises on the pressure side of the turbine blade as a consequence of the cross-passage static pressure gradient, then moves in the channel crossflow towards the suction (convex) side of the turbine blade [Ref. 2, p. 347]. The concave curvature of the turbine blade is a second source of vortices. Here, Taylor-Gortler vortices or roll cells form as a result of centrifugal instabilities.

B. RELATED STUDIES

Studies of the interactions between film cooling injection and embedded vortices are scarce. Blair [Ref. 4] reports large variations in heat transfer on a film cooled turbine endwall. These variations are attributed to the presence of an embedded vortex in the corner, between the endwall and the suction surface of the cascade. Goldstein and Chen [Ref. 5 and 6] investigated the influence of the endwall on film cooling from blades using one and two rows of injection holes. They discovered a triangular region which exists on the

convex side of the blade where film coolant is swept away from the surface by the passage vortex. The research of Sto, Aoki, Takeishi, and Matsuura [Ref. 7] examines the heat transfer and film cooling effectiveness on the endwall and airfoil within an annular low aspect ratio cascade. [Ref. 1, pp. 2-3].

Kobayashi [Ref. 8 and 9] reports that film suction minimizes the effects of centrifugal instabilities and delays the onset of longitudinal vortices in laminar boundary layers near concave surfaces. El-Hady and Verma [Ref. 10] conclude that the overall effect of suction or cooling is to stabilize laminar boundary layers by reducing the amplitude ratio of the vortices.

Honami and Fukagawa [Ref. 11] examined the effects of concave curvature upon a film cooled turbulent boundary layer with a blowing ratio of 0.47. They conclude that concave curvature causes little change in film cooling effectiveness when lateral injection is employed. Conversely they report a significant decrease in film cooling effectiveness when streamwise injection is used. Schwarz and Goldstein [Ref. 12] examined local film cooling effectiveness downstream of a row of film cooling jets in turbulent flows near concave surfaces. They report that lateral mixing between jets is enhanced as a

result of Taylor-Gortler cells at a blowing ratio(m) of 0.4. For m values of 0.8 to 1.8 the mixing and lateral sway of the jets is less pronounced [Ref. 1, p. 2].

C. ONGOING RESEARCH AT NAVAL POSTGRADUATE SCHOOL

Research at the Naval Postgraduate School focuses on the investigation of the influence of embedded longitudinal vortices on film cooled turbulent boundary layers. In the work of Joseph [Ref. 13], film cooling is supplied by a single row of 13 film cooling jets. The diameters (d) of the injection holes are 0.952 cm, scaled such that the boundary layer displacement thickness is approximately 0.38 d. The 13 injection nozzles are inclined 30 degrees to the test surface, with a three diameter spacing between centerlines. Γ/U_∞ of the longitudinal vortex used is estimated to be -.95 cm with film cooling, and -1.10 cm without film cooling, where Γ is the vortex circulation and U_∞ is the freestream velocity. Joseph's results indicate that heat transfer is augmented near the downwash side of the vortex, and the protective benefits of film cooling are reduced. Near the upwash side of the vortex, the effects of film cooling may sometimes be augmented. Evans [Ref. 14] presents measurements of the three mean velocity

components in film cooled boundary layers with vortices. Vortex secondary flows are indicated to be the major cause of the observed disturbances to film injectant. Ortiz [Ref. 15] repeated Joseph's measurements [Ref. 13] with a new heat transfer surface. He varied blowing ratio and spanwise vortex position relative to the film cooling jet location. Results show that the change in spanwise position of the vortex affects the magnitude, shape and spanwise position of heat transfer (Stanton Number) peaks. Additionally, Ortiz indicates that the secondary heat transfer peaks associated with regions of high streamwise velocity become larger in magnitude and more persistent with downstream distance as the blowing ratio increases from 0.47 to 1.26 [Ref. 15, pp. 58-60]. References 2 and 3 summarize the extensive research conducted by Ligrani, Joseph, Evans, and Ortiz.

The experimental investigation undertaken by Ligrani and Williams [Ref. 1] and Williams [Ref. 16] was pursued to study the interaction between an embedded vortex and injectant from a single film-cooling hole. This was done so that the interactions with injectant from neighboring injection holes are eliminated. For a blowing ratio of approximately 0.50, and a freestream velocity of approximately 10 m/s, these investigators focused on the

influence of spanwise vortex position with respect to the injection hole location. The Γ/U_∞ value of the embedded vortex was 1.42 cm. In order to characterize the vortex strength relative to injection rate and cooling jet size, the parameter $\Gamma/(U_c \cdot d)$ is used, where U_c is the injectant mean velocity and d is the injection hole diameter. For this study, the value of this vortex parameter at x/d=41.9 is 2.80. Ligrani and Williams report that the injectant provides near-wall protection if it is located at least 2.0 -2.8 core diameters[1] away from the vortex center in the spanwise direction. If the vortex position is closer to the injectant location, the vortex perturbs the injectant distribution and the local heat transfer. These perturbations persist as far as 97 hole diameters downstream of the injection hole. [Ref. 1]

D. OBJECTIVES OF PRESENT STUDY

The present study is an extension of the work of References 1, 2, 3, 13, 14, 15, and 16. In those studies, attention is focused on effects of blowing ratio

---

[1] The derivation of Core Diameter, Vortex Circulation, and Non-Dimensional Circulation, is discussed in full detail in Section III. A. (DEFINITION OF KEY PARAMETERS) of this Thesis.

and spanwise vortex position. In the present study, vortex strength (vortex circulation) is varied from 0 m^2/s to .151 m^2/s, as the position of the vortex with respect to the injection hole is maintained constant. For all tests presented, the injection is always located beneath the vortex downwash. The circulation of embedded vortices is altered by changing the angle between the leading edge of the vortex generator and the wind tunnel spanwise centerline. This angle is varied in specified discrete values from four to 18 degrees. Tests are also conducted with no embedded vortex. The effects on heat transfer and coolant distribution of the various strength vortices are then measured. Both a single film coolant injection hole and a single row of 13 film coolant injection holes are employed. In both cases a constant blowing ratio (m) of approximately 0.50 is maintained. According to Goldstein et al. [Ref. 17] a blowing ratio maintained at 0.50-0.53 is optimal in providing thermal protection, when coolant is injected into a turbulent boundary layer from a single hole or a single row of holes inclined at 35 degrees.

E. OUTLINE OF EXPERIMENTATION

The present study consists of four experiments:

1. Measurement of fluid mechanics properties (mean velocities, total pressure, vortex parameters), in the Y-Z plane, at x/d=41.9.

2. Surveys of mean temperature ($T-T_\infty$) in the Y-Z plane, at x/d=41.9; for embedded vortices of varying strength, and at x/d=5.2, 41.9, 82.9, and 109.2 for a single embedded vortex.

3. Heat transfer measurements (Stanton Number and Stanton Number ratios) measured at 21 spanwise locations for each of the following streamwise locations: X=1.15, 1.25, 1.40, 1.60, 1.80, and 2.0 meters.

4. Visualization of surface flow patterns.

Three different cooling configurations are employed for these experiments:

1. No film cooling (m=0).

2. Film cooling (m=0.50) from a single injection hole, located beneath the vortex downwash at x/d=0.0.

3. Film cooling (m-0.50) from a single row of 13 injection holes, with the centerline injection hole located beneath the vortex downwash at x/d=0.0.

For each of the above film cooling configurations the embedded vortex strength was varied by positioning the

vortex generator to achieve the following angles with the wind tunnel spanwise centerline: 4, 8, 12, 15, and 18 degrees.

F. THESIS ORGANIZATION

In the remainder of this thesis, Chapter II discusses experimental apparatus and procedures. Chapter III gives experimental results, and Chapter IV contains a summary and conclusions. Appendix A consists of all the Figures referenced throughout the text of this thesis. Appendix B presents the uncertainty levels for the parameters measured and calculated. Appendix C lists and describes the data acquisition, data processing and plotting software programs used. A directory of experimental data files is given in Appendix D.

II. EXPERIMENTAL APPARATUS AND PROCEDURES

A. WIND TUNNEL AND COORDINATE SYSTEM

Experiments were conducted in an open-circuit, subsonic wind tunnel located in the laboratories of the Department of Mechanical Engineering at the Naval Postgraduate School. This facility is the same wind tunnel used in the research and experimentation reported in References 1, 2, 3, 13, 14, 15, 16, and 18. Joseph [Ref. 13] discusses the qualification tests of the facility. The source of the wind tunnel streamwise flow is a variable speed centrifugal blower. Air from the surrounding room passes through a coarse filter to the inlet of this blower and is discharged to a diffuser. The diffuser contains a fine grade filter to remove small particulates from the airstream as well as four baffle vanes to minimize the likelihood of flow separation. Following the diffuser, the inlet air passes through a header box containing a honeycomb and three screens used to reduce the spatial non-uniformities of the flow. After exiting the header, the air stream enters a 16 to 1 contraction ratio nozzle which then leads to the wind tunnel test section.

The test section is a 3.05 m long and 0.61 m wide rectangular duct, containing a single row of 13 film coolant injection holes and a constant flux heat transfer surface. The height of the test section top wall is adjustable to permit changes in the streamwise pressure gradient. For the present study, a zero pressure gradient is maintained without vortex or film cooling to within 0.005 inches of water differential pressure along the length of the test section. The test section free stream velocity is adjustable from 1 m/s to 40 m/s. The freestream turbulence intensity is approximately 0.1 percent based on the freestream velocity of 30 m/s. The boundary layer is tripped near the exit of the nozzle, 0.48 meters upstream of the vortex generator streamwise location. Figure 1 shows the test section coordinate system and the streamwise location of test section components. The schematic of the wind tunnel test section floor, in Figure 2, (adapted from Reference 1) provides a top view of the test section. Locations of the vortex generator, the film coolant injection holes and the heat transfer surface are shown. Also shown in Figures 1 and 2, are the streamwise locations of the thermocouple rows along the constant flux heat transfer surface. With the heat transfer surface at elevated

temperatures, an unheated starting length of 1.10 m exists. Freestream air is maintained at ambient temperature, and thus the direction of the heat transfer is from the wall to the gas.

B. VORTEX GENERATOR

A single half delta wing is used as the vortex generator. The generator design is similar to the one employed by Williams [Ref. 16]. As depicted in Figure 3, the height of the half delta wing is 3.2 cm., and the length of the base is 7.6 cm. The half delta wing is attached to a 1/16 inch thick Lexan mounting plate which, in turn, is attached to the wind tunnel floor. The Lexan base is rectangular in shape with the dimensions: 4.32 cm X 9.2 cm. It is scribed with lines which form angles of 18, 15, 12, 8, 4, and 0 degrees with respect to the tunnel floor centerline.

In order to generate vortices of varying vortex strength and circulation, the 7.6 cm side of the delta wing is attached to the Lexan base along the appropriate scribed line to obtain the desired angle. For all angles, the delta wing is pivoted about the same point on the Lexan base with the generator apex pointing upstream [Figures 3, 4]. The Lexan base is taped to the tunnel

floor, with its forward edge positioned at X=.48 meters downstream from the boundary layer trip. The circulation (strength) of the resulting vortex increases as the aspect angle is increased from 0 to 18 degrees.

With the edge of the Lexan base aligned with the tunnel floor centerline, vortices r, s, t, u, and v were produced by using the respective aspect angles of 18, 15, 12, 8, and 4 degrees (see Figure 4). The downwash of vortex r at x/d=0.0 is located directly above the centerline hole injectant, while the downwash of vortices s through v is is displaced from the spanwise location of the injectant in the negative Z direction. For generator angles of 15, 12, 8, and 4, the edge of the Lexan base was repositioned at Z=-.51 cm, -1.53 cm, -3.56 cm, and -4.07 cm, respectively (see Figure 5). The vortex downwash of the resulting vortices, w, x, y, and z (respective angles of 15, 12, 8 and 4 degrees), at x/d=0.0, is located directly above the injectant issuing from the centerline hole. Figures 4 and 5 show vortex generator coordinate locations for vortices r through z. Table I lists the generator aspect angle and generator placement corresponding to each of these vortices.

TABLE I. VORTEX GENERATOR POSITIONS

VORTEX	Vortex Generator Angle (degrees)	Z Alignment of right edge of Lexan Base (cm)
r	18	0.0
s	15	0.0
t	12	0.0
u	8	0.0
v	4	0.0
w	15	-0.51
x	12	-1.53
y	8	-3.56
z	4	-4.07

C. INJECTION SYSTEM

Film coolant is injected from the single row of injection holes into the boundary layer developing along the bottom wall of the test section. The downstream edges of the injection holes are located at 1.08 m downstream of the boundary layer trip, 0.60 m downstream of the vortex generator leading edge and 0.02 m upstream of the constant heat flux text surface. The injection system is fully described in References 13 and 15. Injection system qualification tests are discussed by

Joseph [Ref. 13, pp. 23-26] and Williams [Ref. 16, pp. 10-11]. The diameter (d) of each injection hole is .952 cm., scaled such that the boundary layer displacement thickness (δ_1) is approximately 0.38 (d). Values of blowing ratio (m) and non-dimensionalized coolant temperature (Θ) are chosen to resemble values used in gas turbine design. The 13 injection nozzles are inclined at an angle of 30 degrees with respect to the horizontal test surface, with a three diameter spanwise spacing between hole centerlines. The centerline of the middle injection hole is located at the test surface centerline.

Film coolant injection air originates in a ten horsepower, two stage, 150 psig Ingersol-Rand air compressor. From the compressor the injection air flows through a pressure regulator, moisture separators, a flow regulator, a rotometer, a diffuser and finally into the injectant heat exchanger and plenum chambers. The heat exchanger provides the capability of heating the injectant to temperatures of 40° C-50° C above ambient temperature. The top surface of the plenum contains 13

plexiglass injection tubes, each 8.0 cm long with a length to diameter ratio of 8.4:1. The injection tubes extend through the wind tunnel floor, terminating in the single row of 13 film cooling holes.

For the present study, the film cooling blowing ratio was maintained at approximately 0.50, using either three injection holes or 13 injection holes. When three injection holes are employed, the centerline hole and the two outer holes located at Z=-17.1 cm and Z=+17.1 cm are used. The two peripheral holes are required to maintain steady flow in the injection system at measurable flow rates. In this case, the vortex affects film coolant from the centerline injection hole only. Injectant from the peripheral holes does not touch the heat transfer surface or affect the heat transfer measurements. When only three of the 13 injection holes are used, the remaining ten holes are plugged and covered with cellophane tape.

D. HEAT TRANSFER SURFACE

The heat transfer surface provides a constant heat flux over its area. The plate is inserted into the bottom wall of the wind tunnel test section. The upper surface of the plate is adjacent to the wind tunnel air

stream and is maintained level with the test surface. The heat transfer test surface consists of a stainless steel foil 1.3 m X 0.476 m X 0.20 mm, and is painted black with seven layers of liquid crystals. Attached to the underside of the foil are 126 copper-constantan thermocouples in six rows. Each row contains 21 thermocouples with a spanwise spacing of 1.27 cm. This spacing provides adequate spanwise resolution of surface temperature distributions. Thermocouple lead wires are embedded in grooves cut into a triple sheet of 0.254 mm thick double sided tape. The thermocouple lead wire grooves are filled with epoxy. A thin foil heater, 1.0 mm X 1.118 m X 0.438 m, is attached to the underside of the double sided tape with Electrobond epoxy. The heater is rated at 120 volts and 1500 watts and is manufactured by the Electrofilm Corporation. The foil within the heater is custom designed with adjacent braces sufficiently close together to maintain a uniform heat flux boundary condition. The insulation and support substructure consists of a 12.7 mm (1/2 in.) thick Lexan sheet followed by 25.4 mm of foam insulation; a 82.55 mm thick styrofoam layer, three sheets of .254 mm thick Lexan and one 9.53 mm thick sheet of balsa wood. The portion of the constant flux heat assembly which

protrudes from the bottom of the test section is encased in a plexiglass support frame which is mounted to the underside of the wind tunnel [Ref. 15, pp. 27-28].

Heat transfer surface height adjustment, to accommodate thermal expansion, is achieved through the use of height adjustment screws mounted in the plexiglass support frame. During heat transfer tests, the top surface of the plate (the stainless steel foil) is maintained level with the wind tunnel test surface and remains flat and remarkably smooth with minimum surface irregularities. Surface temperature is controlled by adjusting the input voltage to the heater foil using a Standard Electrical Company variac, type 3000B. For all heat transfer tests, heater foil power levels are adjusted to maintain overall temperature differences less than 30 degrees Celsius to minimize the influence of variable parameters.

In order to determine the heat loss by conduction from the heat transfer plate, the results of the energy balance performed by Ortiz are used [Ref. 1, pp. 29-33]. When heat is convicted from the surface, conduction losses are 1.5 percent to 2.5 percent of the total power into the heater. For an average plate temperature of 40 $^{\circ}$ C and a 10 m/s freestream flow at 18 $^{\circ}$ C, radiation

heat losses are approximately 8.5 percent of the total power into the test plate [Ref. 13, p. 32]. The thermal contact resistance between thermocouples and the upper foil are given by Joseph [Ref. 13, p. 34] and also verified by Williams [Ref. 16, pp. 14, 15]. The contact resistance is estimated based on the thermocouple output and measurements from calibrated liquid crystals on the surface of the foil. The Chameleon encapsulated liquid crystals, manufactured by Appleton Papers Division of the National Cash Register Company, are calibrated to allow foil surface temperatures to be measured within $\pm$ 0.3 degrees Celsius [Ref. 1, p. 3]. This uncertainty is included in the determination of the overall experimental uncertainty. Stanton number and Stanton number ratio uncertainties, as presented in Appendix B, are based on Schwartz' original estimates [Ref. 18, pp. 267-269]. Typically the uncertainty of these parameters are about 4.4 percent and 5.5 percent respectively.

Contact resistance for each of the 126 individual thermocouples sometimes deviates slightly from the above experimentally determined value. The effects of these variations are minimized by presenting results for local conditions in terms of Stanton number ratios. Local Stanton number values are normalized with Stanton number

baseline values. Baseline Stanton number measurements were made without film cooling and without an embedded vortex.

To confirm the validity of the baseline Stanton number data, baseline experimental results are compared to empirical relationships, between Stanton numbers ad Reynolds numbers, given by Kays and Crawford [Ref. 19]. For a constant wall temperature downstream of an unheated starting length (ε), the following relationship is valid:

$$St_x \, P_r^{0.4} = 0.0287 \, Re_x^{-0.2} \, [1-(\varepsilon/x)^{9/10}]^{-1/9} \quad \text{(Eq. 2.1)}$$

An approximation for a turbulent boundary layer with an unheated starting length followed by constant heat flux is achieved by altering Equation 2.1 to obtain:

$$St_x \, Pr^{0.4} = 0.030 \, Re_x^{-0.2} [\, 1-(\varepsilon/x)^{9/10}]^{-1/9} \quad \text{(Eq. 2.2)}$$

A more exact equation to account for constant heat flux surface beyond the unheated starting length is given by:

$$St_x Pr^{0.4} = 0.030 \, Re_x^{-0.2} \cdot \frac{\beta_1(1/9,10/9)}{\beta_{u1}(1/9,\ 10/9)} \quad \text{(Eq. 2.3)}$$

Here, β_1 and β_{u1} are analytically determined values of the complete Beta function and the incomplete Beta function, respectively.

Equations 2.1, 2.2, and 2.3 are compared in Figure 6. Experimental data are compared with equation 2.3 in Figure 7. Four baseline Stanton number data sets show agreement with the equation, with a maximum deviation of $\pm$ 5.0 percent.

E. TEMPERATURE MEASUREMENTS

Calibrated copper-constantan thermocouples are used for all temperature measurements. These include the heat transfer surface temperature, the freestream temperature, the injection plenum temperature, and local boundary layer temperature. The calibration equation for the 126 thermocouples used to measure surface temperature on the heat transfer plate is given by Ortiz [Ref. 15, p. 34]. All 126 thermocouples are of similar manufacture and their outputs agree to within $\pm$ 2 microvolts. The same calibration equations for the freestream thermocouple and the injection plenum thermocouple used by Williams are used in the present study [Ref. 16, pp. 15, 16]. A new calibration was performed for the thermocouple used to measure local temperatures within the turbulent boundary

layer. A temperature bath regulated through the use of electric heaters and liquid nitrogen, along with a platinum resistance temperature reference (±0.01 °C) were used for this purpose. The third-order polynomial representing temperature as a function of thermocouple output voltage (E=millivolts) is given by:

$$T=-.033367+26.2327\ E - .833808\ E^2+.0[illegible]6587\ E^3 \quad \text{(Eq. 2.4)}$$

Temperature surveys of $(T - T_\infty)$ are performed utilizing the freestream temperature (T_∞) thermocouple and the boundary layer temperature (T) thermocouple, which is mounted in the automated traversing device. During these surveys freestream temperature is maintained at ambient temperature, while film cooling injectant is heated within the injection plenum to 50 (+2, -0) degrees Celsius. The constant heat flux plate is not energized during the $(T-T_\infty)$ surveys. Local temperature is measured at 800 (20 X 40) locations in the Y-Z plane at a specified x/d location. Spatial resolution between sampling points is 0.2 inches in both the horizontal and the vertical directions, with overall dimensions of the sampling plane equal to 12 cm X 22 cm. The two degree of freedom traversing device consists of a spanwise and vertical traversing block, each mounted on separate

assemblies consisting of a 20 thread per inch pitch drive screw and two steel case hardened support shafts. Each of the two drive shafts is coupled to a separate M092-FD310 stepping motor. These motors are controlled by a two axis Motion Controller (MITAS), which is equipped with 2K bytes of memory and a MC6800 16 bit microprocessor. Both stepping motors and the MITAS controller are manufactured by the Superior Electric Company. The MITAS controller was operated by a Hewlett-Packard Series 200, Model 9836S computer.

Voltages from the thermocouples during all temperature data collection are read by a Hewlett-Packard 3497A Data Acquisition/Control Unit with a Hewlett-Packard 3498A extender. These units are controlled by the Hewlett-Packard 9836S computer equipped with a MC6800, 8MHz 16/32 bit processor, dual 5 1/4 in. floppy disk drives and 1 megabyte of memory.

F. MEAN VELOCITY MEASUREMENTS

The three mean velocity components are measured using a DC-250-24CD five hole pressure probe manufactured by the United Sensors and Control Corporation. The conical pressure probe, with a tip diameter of 6.35 mm, is mounted on the automated traversing device. Probe

calibration is given by Williams [Ref. 16, pp. 17, 18] over a range of yaw angles from -20 degrees to +20 degrees; and a range of pitch angles from -20 degrees to +20 degrees. The Williams calibration data is used in the present study to convert pressure coefficients to velocity components. Each of the five pressures sensed by the pressure probe is directed to a separate Celesco model LCVR differential pressure transducer. The full scale pressure range of each transducer is 2.0 cm of water differential pressure. The five Celesco CD-10D carrier demodulators convert transducer output signals to D. C. voltage. Demodulator voltages are then sent to the HP-3497A Data Acquisition Unit.

G. FLOW VISUALIZATION

Surface flow patterns are visualized through the use of a suspension of titanium dioxide (pigment), penetrating oil (low viscosity and low surface tension), vacuum pump oil (high viscosity) and oleic acid (dispersing agent). This oil-pigment mixture is applied in varying proportions to a 1/16 in. thick, nonporous, black fiberboard sheet. The painted fiberboard sheet is positioned over the wind tunnel test surface downstream of the injection holes. Then, the freestream air flow

and film cooling injection flow are gradually increased to establish the desired blowing ratio. The composition of the suspension paint is a modification of the mixture described by Bradshaw in Reference 20.

This technique is used to gain qualitative information about the flow in the immediate vicinity of the test surface. As long as the flow does not undergo rapid transients, the deviation of flow parameters, caused by the presence of the oil film, is less than two percent of flow parameters for flow with no oil film. The use of this technique reveals the direction of flow of the limiting streamlines because the oil pigment mixture flows in filaments over the surface. Miniscule concentrations of pigment form and act as a resistance to the flow. A portion of the pigment, which is carried by the oil as it is blown over and around the concentrated pigment flocs, is deposited in the wake of the pigment concentrations. The deposits will continue to grow into long streaks until all of the oil is blown from the surface. The amount and scale of the streaking obtained is directly dependent on the proportion of oleic acid (anti-coagulant) used in the mixture [Ref. 21].

The mixing proportions of the suspension paint used in the present study yielding the most satisfactory streaking patterns are: two parts titanium dioxide; one part oleic acid; 33 parts penetrating oil; and three parts vacuum pump oil. Once satisfactory surface flow streaking patterns are obtained, the wind tunnel flow rates are gradually reduced to zero, and photographs of the flow visualization patterns are taken through the clear plexiglass wind tunnel top wall.

III. EXPERIMENTAL RESULTS

A. DEFINITIONS OF KEY PARAMETERS

Circulation over a region A in the Y-Z plane is given by:

$$\Gamma = \int_A w_x dA \qquad \text{(Eq. 3.1)}$$

w_x represents the streamwise vorticity, which is expressed by:

$$w_x = \frac{\partial Uz}{\partial y} - \frac{\partial Uy}{\partial z} \qquad \text{(Eq. 3.2)}$$

Streamwise vorticity in the Y-Z plane at a given x/d location is estimated using a central finite difference equation for each sampled point:

$$w_x(y,z) = \frac{U_z(y+\Delta yY,z) - Uz(y-\Delta y,z)}{2\ \Delta\ y} - \frac{U_y(y,z+\Delta\ z) - U_y(y,z-\Delta z)}{2 \cdot \Delta z} \qquad \text{(Eq. 3.3)}$$

Here Δy and Δz are the incremental probe positions in the Y and Z directions, respectively.

To determine circulation using Equation 3.1, all vorticity levels below a threshold level are set equal to zero. Schwartz [Ref. 18] utilizes a threshold vorticity

of 100 s^{-1}. In order to provide continuity between Schwartz' results and those of the present study, circulation is estimated based on the same value of threshold vorticity. Additionally, a second estimate of circulation is made using a threshold vorticity value of 76.03 s^{-1}. This latter value is ten percent of the maximum vorticity (measured at x/d=41.9) of vortex r (generator aspect angle of 18 degrees and no film cooling), [Data Run #101588.1145, Figure 8]. The latter choice of threshold vorticity allows for a better evaluation of the circulation of lower strength vortices (e.g., for a four degree generator angle, maximum vorticity is 117 1/s). Once threshold vorticity is established, circulation is estimated using Equation 3.1. For this calculation, the product of the differential node value of vorticity (w_x) and the differential element area ($\Delta z \times \Delta y = .258$ cm^2) is summed over all sample points with values of w_x greater than the threshold vorticity.

The following dimensionless parameter is used as a measure of vortex strength relative to cooling jet strength:

$$S = \Gamma/(U_c \cdot d) \qquad \text{(Eq. 3.4)}$$

Here U_c is the average injection velocity at the wall, and d is the diameter of the injection hole. With no film cooling (m=0 & U_c=0), the parameter S is meaningless and therefore not used.

The dimensionless parameter used to compare vortex core size relative to injection hole size is given by:

$$2c/d = \frac{2\ ((Zcore + Ycore)/2)}{d} \qquad \text{(Eq. 3.5)}$$

Here c represents the average vortex core radius. Two separate schemes for calculating the average vortex core diameter [2((Zcore + Ycore)/2)] are now discussed.

In the first scheme, the embedded longitudinal vortices are assumed to be modified a Rankine vortices. All streamwise vorticity created by a Rankine vortex is contained within its core. The core of Rankine vortex extends from the point of minimum secondary flow velocity (center of core) to the point of maximum secondary flow velocity. Here, secondary flow velocity is defined as $\sqrt{Uy^2 + Uz^2}$. The use of this method to estimate average core diameter, at best, is accurate to within $\pm$ .51 cm, since this is the spacing between sample points in both the Z and Y directions.

To obtain a more accurate measure of average core radius, a second approach is used which is similar to the method used by Westphal et al. [Ref. 22]. With this approach, the finite difference matrix point with the maximum streamwise vorticity (Wxmax) is defined as the center of the core. The average radial distance from the center to the point of 0.4 Wxmax is then determined in both the Y and Z directions. With the previous approach, linear interpolation between matrix points cannot be used to identify local minima and maxima. However, if the outer boundary of the core is defined as a certain percentage of Wxmax, linear interpolation can be employed to estimate the location of this boundary between measurement locations. By using a specific percentage (40) of Wxmax to define the core boundary, a more accurate estimate of core diameter is obtained. The resulting estimates of average core diameter show reasonable agreement with the average values reported in References 1 and 16 for similar strength vortices. Core diameter values reported in those studies are calculated from secondary velocity maxima and minima.

Figures 8-22 show the vorticity contours for all combinations of film cooling and vortex strengths employed in this study. The subsequent section discusses

this data in detail. In order to provide continuity between studies, two separate values are listed on these figures for vortex circulation, and vortex core size parameters. The value of circulation based on the 100 1/s vorticity threshold is denoted on these Figures as Cr, while the value of circulation based on the 76.03 1/s threshold is annotated as Cr2. Vortex core radii calculated from secondary velocity maxima and minima are denoted on the Figures as Zcore and Ycore, while core radii calculated using the 0.4 Wxmax approach are denoted as Z2core and Y2core. Two separate values are also given for the dimensionless parameters of core strength and core diameter, annotated in accordance with this scheme.

Data tables, presented in the following section, summarize the key parameters calculated from the vorticity contours. These tables also list two separate values for vortex circulation, strength, and core diameter. Within the text of this thesis, the circulation values and core strength values quoted are those based on circulation values using the 76.03 1/s vorticity threshold. The values cited for core radii and core size are those derived using the 0.4 Wxmax approach.

B. FIVE HOLE PRESSURE PROBE SURVEYS

Distributions of streamwise vorticity, streamwise mean velocity, secondary flow vectors and total pressure are presented in Figures 8-74. These surveys are obtained using the five hole pressure probe. For each survey the probe is positioned at 800 different locations in the spanwise plane at x/d = 41.9. The freestream velocity (U_∞) is maintained at 10.0 $\pm$ .2 m/s. The surveys are conducted for three separated film cooling configurations: (1) No film cooling, m=0.0; (2) Film cooling from a single injection hole, m=0.50; (3) Film cooling from a row of 13 injection holes, m-=0.50. The number (2) film cooling configuration is alternately referred to as film cooling with single injection hole or film cooling with three injection holes.

The strength of the embedded vortex is varied by incrementally changing the aspect angle of the vortex generator over a range of 18 to 4 degrees. For each of the three film cooling configurations, a separate mean velocity/mean vorticity survey is conducted for each of the five incremental settings of vortex generator angle. The surveys with no film cooling are conducted with the generator spanwise position maintained at Z=0.0 cm, while generator angle is varied. For the surveys with film

cooling, the spanwise generator position is changed as indicated in Table I. This is done to ensure that the vortex is positioned with injectant from the centerline hole directly beneath the vortex downwash as the vortex passes over the injection hole.

Table II lists the data file number, experimental conditions and corresponding Figures for all five hole pressure probe surveys.

TABLE II. FIVE HOLE PRESSURE PROBE SURVEY DATA

Figure	m	Number of Injection Holes	Vortex (Table I)	Survey Data Run Number
8, 27-29	0.0	0	r	101588.1145
9, 30-32	0.0	0	s	101588.1659
10,33-35	0.0	0	t	101688.1054
11,36-38	0.0	0	u	101688.1524
12,39-41	0.0	0	v	101688.2023
13,42-44	0.50±.03	3	r	101988.1701
14,45-47	0.50±.03	3	w	101988.2347
15,48-50	0.50±.03	3	x	102088.1025
16,51-53	0.50±.03	3	y	102088.1718
17,54-56	0.50±.03	3	z	102088.2031
18,57-59	0.50±.03	13	r	102288.2315
19,60-62	0.50±.03	13	w	102288.1839
20,63-65	0.50±.03	13	x	102288.1323
21,66-68	0.50±.03	13	y	102288.0834
22,69-71	0.50±.03	13	z	102188.2359
72-74	0.50±.03	13	no vortex	102188.1933

Probe Location: x/d = 41.9
Freestream Velocity: U_∞ = 10.0 ± .2 m/s

The results from the five-hole pressure probe surveys are presented in the following order: first, the streamwise vorticity contours (Figures 8-22) for all pressure probe surveys are presented. Next, secondary flow vector distributions, streamwise velocity fields, and total pressure fields (Figures 27-74) are discussed.

1. Streamwise Vorticity Contours

a. Vorticity Contours: No Film Cooling

Streamwise vorticity contours of single embedded vortices, with no film cooling (m=0.0), are measured at x/d = 41.9 and presented in Figures 8-12. Vortices r, s, t, u, and v are employed (see Tables I and II). For these five contour plots the dimensionless parameter $S = \Gamma/(U_c \cdot d)$ has no meaning since $U_c = 0.0$. Therefore, the circulation (Γ) of each vortex is used as a measure of vortex strength. Vortex circulation values range from .149 m^2/s for the strongest vortex (r) to 0.19 m^2/s for the weakest vortex (v).

Figures 8-12 show that the spanwise location of the vortex center (Zcen) changes from Z = -3.56 cm to Z = +0.51 cm, as the circulation decreases from .149 m^2/s to .019 m^2/s. As a result, only vortex r was positioned with its downwash directly above the wind tunnel centerline (location of injection hole) for x/d = 0.0.

When film cooling is employed, the spanwise position of the vortex generator is moved, in the case of the four weaker vortices, to insure that the downwash of each of these vortices is also directly above the spanwise centerline for x/d = 0.0, as the vortex passes the injectant hole. The Zcen information of Figures 8-12 was used to calculate the spanwise displacement of the vortex generator required to insure appropriate vortex positioning at x/d = 0.0.

Figures 8-12 show that the vortex core is approximately circular in shape. The Z and Y radii of the core are relatively constant for all vortices regardless of strength. Radii values range from .70 cm to .77 cm. This leads to a relatively constant dimensionless core size parameter, 2c/d, ranging from 1.47 to 1.62. This constant core size for all vortex strengths is a direct result of the method used to define core radii. These average radii are calculated for the area which encompasses all vorticity values greater than or equal to 40 percent of the vorticity encountered at the vortex center (Wxmax). If the core were defined as

the area encompassing a given percentage of an absolute constant value of vorticity (i.e., 100 1/s for example), the vortex core size would decrease with decreasing vortex strength.

Figures 8 and 9 each display a region of negative vorticity located appproximately 3 cm in the negative Z direction from the center of the vortex.

Table III lists vortex parameter information obtained from the streamwise vorticity contours of Figures 8-12.

TABLE III. VORTEX PARAMETERS: NO FILM COOLING (M=0.0)

VORTEX	(5) Wxmax (1/s)	(1) Γ (m^2/s)	(2) Γ (m^2/s)	(3) Zcore (cm)	(3) Ycore (cm)	(3) 2c/d	(4) Zcore (cm)	(4) Ycore (cm)	(4) 2c/d
r	760.3	.14029	.14955	.76	.76	1.604	.77	.77	1.621
s	626.2	.11556	.11556	.51	.76	1.337	.72	.73	1.521
t	522.3	.08282	.08523	.51	.76	1.337	.71	.70	1.490
u	278.2	.02991	.04130	1.02	.76	1.872	.70	.70	1.469
v	179.2	.01500	.01925	.25	.76	1.069	.72	.72	1.514

Freestream Velocity = 10 $\pm$ .2 m/s
x/d = 41.9

1. Based on vorticity threshold of 100 1/s (Reference 18).
2. Based on vorticity threshold of 76.03 1/s (10% of Wxmax Run #101588.1145.
3. Based on core radius measurement from minimum secondary velocity to maximum secondary velocity.
4. Based on core radius measurement from center of vortex to .40 Wxmax.
5. Denotes maximum streamwise vorticity.

b. Vorticity Contours: Film Cooling From A Single Injection Hole

Streamwise vorticity contours of single embedded vortices with single injection hole film cooling (m = 0.50) are presented in Figures 13-17. With film cooling, the vortices employed (in order of decreasing strength) are r, w, x, y, and z. Vortices w, x, y, and z have approximately the same strength and circulation, respectively, as vortices s, t, u, and v. The downwash of each of the vortices r, w, x, y and z passes over the centerline injection hole at x/d = 0.0. This spanwise positioning is achieved for the latter four vortices (w, x, y and z) by changing the spanwise location of the vortex generator as described earlier and as indicated in Table I.

The nondimensional strength parameter is represented as $Cr_2/(U_c \cdot d)$ on Figures 13-17. Values of $\Gamma/(U_c \cdot d)$ for vortices r, w, x, y, and z at x/d = 41.9 are 3.17, 2.55, 1.88, 1.08, and 0.29 respectively. At x/d = 41.9, the spanwise location of the core center (Zcen) for each of these five vortices is $Z = -3.56 \pm .51$ cm. The core radius values in both the Z and Y directions (Z2core and Y2core) fall within the range of .69 cm to .76 cm. As a result, the dimensionless core size parameter of 2 c/d,

[denoted on the figures as 2(Z2core + Y2core)/(2 d)], is relatively constant for all five vortices, ranging from 1.46 to 1.58. Circulation of the five vortices changes from .151 m^2/s to .014 m^2/s. Figures 13 and 14 also show small areas of negative streamwise vorticity which are near the vortex upwash, to the left of the vortex cores.

Table IV summarizes vortex data from Figures 13-17.

TABLE IV. VORTEX PARAMETERS: FILM COOLING FROM A SINGLE INJECTION HOLE (M=0.50)

VORTEX	(5) Wxmax (1/s)	Γ (m^2/s)	S Γ/(U_∞·d)	(2) Γ (m^2/s)	(2) S Γ/(U_∞·d)	(3) Zcore (cm)	(3) Ycore (cm)	(3) Zc/d	(4) Zcore (cm)	(4) Ycore (cm)	(4) 2c/d
r	831.9	.151867	2.98670	.150776	3.17379	.76	1.02	1.871	.76	.74	1.560
s	690.8	.126468	2.49432	.121000	2.54734	.25	.25	.535	.76	.71	1.486
x	534.1	.084321	1.77516	.080924	1.87876	.51	.76	1.337	.71	.72	1.510
y	322.9	.042566	.89594	.050115	1.07693	1.02	.76	1.872	.69	.70	1.457
z	154.1	.008947	.11939	.013693	.29330	2.03	.76	2.941	.74	.73	1.552

Freestream Velocity = 10 ± .2 m/s
x/d = 41.9

1. Based on vorticity threshold of 100 1/s (Reference 18).
2. Based on vorticity threshold of 76.03 1/s (10% of Wxmax Run #101588.1145.
3. Based on core radius measurement from minimum secondary velocity to maximum secondary velocity.
4. Based on core radius measurement from center of vortex to .40 Wxmax.
5. Denotes maximum streamwise vorticity.

c. Vorticity Contours: Film Cooling From 13 Injection Holes

Streamwise vorticity contours for film cooling from 13 injection holes (m=.50), measured at x/d = 41.9, are presented in Figures 18-22. Values of $\Gamma/(U_c \cdot d)$ for vortices r, w, x, y, and z are 2.81, 2.33, 1.86, 0.89, and 0.17 respectively. Vortex circulation decreases from .134 m^2/s to .008 m^2/s. The spanwise location of the vortex center for all five vortices is again Z = -3.56$\pm$ .51 cm. 2c/d ranges from 1.48 to 1.61, while the core radii in both the Z and Y directions are approximately constant for all vortex strengths, ranging from .68 cm to .76 cm.

Vorticity contours for the three strongest vortices, in Figures 18, 19, and 20, show areas of negative vorticity to the left of the vortex upwash.

Table V. summarizes the vortex parameter data measured for film cooling from a single row of 13 injection holes.

TABLE V. VORTEX PARAMETERS: FILM COOLING FROM 13 INJECTION HOLES (m = 0.50)

VORTEX	(5) Wxmax (1/s)	(1) Γ (m^2/s)	(1) S $\Gamma/(U_c \cdot d)$	(2) $^2\Gamma$ (m^2/s)	(2) S $\Gamma/(U_c \cdot d)$	(3) Zcore (cm)	(3) Ycore (cm)	(3) 2c/d	(4) Z2core (cm)	(4) Y2core (cm)	(4) 2c/d
r	716.5	.13126	2.76342	.13367	2.81419	.25	.76	1.069	.76	.76	1.605
w	693.9	.09908	2.08588	.11080	2.33265	.76	.51	1.337	.72	.73	1.524
x	555.5	.08424	1.77337	.08843	1.86169	.25	.51	.802	.68	.72	1.477
y	328.1	.03997	.84146	.04209	.88607	.51	.76	1.337	.69	.72	1.487
z	126.7	.00594	.12498	.00829	.17459	2.54	.76	3.476	.73	.74	1.549

Freestream Velocity = 10 $\pm$ .2 m/s
x/d = 41.9

1. Based on vorticity threshold of 100 1/s (Reference 18).
2. Based on vorticity threshold of 76.03 1/s (10% of Wxmax Run #101588.1145.)
3. Based on core radius measurement from minimum secondary velocity to maximum secondary velocity.
4. Based on core radius measurement from center of vortex to .40 Wxmax.
5. Denotes maximum streamwise vorticity.

d. Dependence of Vortex Parameters

Vortex parameter dependence is indicated in Figures 23-26, which show the relationship between vortex generator angle and various vortex parameters. Figure 23, shows the varying spanwise location of the vortex center, for x/d=41.9 and blowing ratio of 0.0. For this case, the generator angle was varied from 18 to 4 degrees

to produce vortices r, s, t, u, and v. Figure 23 additionally, shows that the vortex center spanwise location is essentially constant at Z=-3.56 $\pm$ .51 cm, for x/d=41.9 and blowing ratio=0.5 (for both single injection hole and 13 injection holes). This constant spanwise vortex position for x/d=41.9 is accomplished by changing the spanwise position of the generator from Z=0.0 to Z=-4.07 cm as the generator angle is changed from 18 to 4 degrees to produce vortices r, w, x, y, and z.

Maximum vorticity (Wxmax) and circulation (Cr), at x/d=41.9, for all cooling configurations, are plotted with respect to vortex generator angle in Figures 24 and 25. These plots show that film cooling, regardless of configuration, has minimal effect upon vorticity and circulation. Vortex strength, determined by the generator angle, determines these characteristic parameters. Figure 26 shows the non-dimensional circulation [Γ /(U_c · d)] versus generator angle, at x/d=41.9, for single hole injection and 13 hole injection for a blowing ratio of 0.50. The curves for the two injection hole configurations are very nearly the same.

Thus, vortex generator aspect angle, and not film cooling, is the dominating factor contributing to the magnitude of maximum vorticity, vortex circulation, and vortex strength (non-dimensional circulation).

2. Secondary Flow Vectors, Streamwise Velocity, and Total Pressure Distributions

Distributions of secondary flow vectors, streamwise velocity and total pressure are presented in Figures 27-74. Measurements are made at x/d=41.9, with freestream velocity equal to 10.0 $\pm$ .2 m/s. This data is presented in the following order: (a) m=0, no film cooling, Figures 27-41; (b) m=0.5, single injection hole, Figures 42-56; (c) m=0.5, 13 injection holes, Figures 57-71. The effects of the embedded vortex on the boundary layer are qualitatively similar to those observed by Ligrani et al., and reported in References 1, 2, and 3.

a. Velocity and Pressure Distributions: No Film Cooling

Data for m=0.0 are shown in Figures 27-41. Figures 27-29 show the effects of vortex r with a circulation (Γ) equal to .149 m^2/s. Figure 27 shows the secondary flow velocity vector field, Figure 28 depicts the streamwise velocity field, and Figure 29 displays the total pressure field.

The presence of a vortex is indicated in Figure 27 by the strong secondary clockwise rotating cross flow. The downwash region of the vortex is distinguishable by strong downwards secondary crossflow velocities directed towards the wall (-Y direction). The secondary crossflow velocities in the upwash region (left portion of vortex) are directed upwards, away from the wall (+Y direction). Figure 27 also shows the dominating feature of strong secondary velocities, with a -Z direction, between the wall and the vortex. The area to the left of the vortex upwash where the secondary flow vectors indicate a weak counter clockwise rotating crossflow is coincidental to the region of negative vorticity cited in the discussion of vorticity contours. Figure 28 shows high streamwise velocities near the wall on the downwash side of the vortex (Z = 0), while low streamwise velocities exist near the wall in the vortex upwash region (-10.0 <Z<-6.0). Low streamwise velocity fluid is swept up (convected) into the upwash region by the strong secondary crossflow between the wall and vortex. As a result, the boundary layer thickness is increased in the upwash region and decreased in the downwash region. Figure 29 indicates that high pressure (high momentum) fluid is found in close proximity to the

wall, within the area of the vortex downwash, while low pressure (low momentum) fluid is swept up and away from the wall within the upwash region.

Figures 30-32 show the effects of vortex s, with circulation equal to .115 m^2/s. Figures 33-35 depict the boundary layer as affected by vortex t, with circulation of .085 m^2/s. The data presented in Figures 36-39 display the effects of vortex u with Γ = .041 m^2/s. Figures 39-41 correspond to vortex v and Γ= .019 m^2/s. The local structure of vortices s, t, u, and v (Figures 30-41) is qualitatively similar to that of vortex r, discussed above (Figures 27-29). The extent of the area affected by each vortex, i.e., the size of the downwash region and the size of the upwash region, decreases with decreasing vortex circulation. Additionally, the magnitude of the perturbations to the local boundary layer within the upwash and downwash regions also decreases as the circulation decreases from .115 m^2/s to .014 m^2/s.

A comparison of secondary flow vector distributions (Figures 27, 30, 33, 36, 39) reveals that the vortex center, at x/d=41.9, is located further to the left (negative Z direction) as the strength (circulation) of the vortex is increased. This is a result of spanwise

migration of the vortex core as the vortex travels in the streamwise direction. This phenomenon, caused by the secondary flow between the core and the wall, is discussed by Ligrani and Williams [Ref. 1].

b. Velocity and Pressure Distributions: Film Cooling from a Single Injection Hole

Results for m=0.5, single injection hole film cooling are presented in Figures 42-56. Figures 42-44 show the effects of vortex r (S = 3.17 and Γ = .151 m^2/s). Vortex w (S = 2.55 and Γ = .121 m^2/s) data are shown in Figures 45-47. Figures 48-50 present the effects of vortex x, with S=1.88 and = .089 m^2/s. The distributions of Figures 51-53 show the effects of vortex y with S=1.08 and =.051 m^2/s, while Figures 54-56 correspond to vortex z with S = 0.29 and circulation (Γ) = .014 m^2/s.

All vortex core centers are located at approximately Z = -3.56 cm for x/d=41.9. This is accomplished by displacing the vortex generator in the spanwise direction as its angle is changed.

Magnitudes of perturbations in the vortex upwash region and in the vortex downwash region decrease as vortex strength (S) decreases from 3.17 to 0.29. Vortices r, w, and x cause substantial thinning of the

boundary layer in their downwash regions which extend roughly from Z = -3.0 cm to Z = +1.0 cm. The upwash regions of these three relatively strong vortices are distinguishable by the abundant presence of low velocity, low pressure fluid. This low momentum fluid, which is convected into the upwash region, blankets the wall and is swept up away from the wall in a clockwise direction (looking downstream).

For vortices r, w, and x the upwash region extends from approximately Z = -9.0 cm to approximately Z =-4.0 cm. The two lower strength vortices, y and z, produce minimal boundary layer thinning, in the downwash region, and minimal boundary layer thickening in the upwash region. This is due to significantly reduced magnitudes of the cross flow convection velocities between the vortex and the wall.

c. Velocity and Pressure Distributions: Film Cooling from 13 Injection Holes

Figures 57-71 present the data for m=0.5, and a single row of 13 injection holes. For this situation the strengths of vortices r, w, x, y, and z are 2.81, 2.33, 1.86, 0.89, and 0.17, respectively. Respective values of vortex circulation are .133 m^2/s, .111 m^2/s, .088 m^2/s, .042 m^2/s, and .008 m^2/s.

Figures 57, 58, and 59 respectively show the secondary flow vectors, the streamwise velocity field and the total pressure field, corresponding to vortex r. Figures 60-62 apply to vortex w, and Figures 63-65 show the effects of vortex x. Figures 66-68 depict the effects of vortex y, while Figures 69-71 correspond to vortex z.

As before, the magnitude of the boundary layer perturbations is directly dependent upon the strength of the embedded vortex. The resulting boundary layer dimensions in the upwash and downwash regions are identically similar to the boundary layer dimensions for an equal strength embedded vortex with one film cooling hole. For this film cooling configuration, the mass flow of injectant into the turbulent boundary layer is 4.3 times the amount encountered in the single hole configuration. Yet the boundary layer perturbations caused by the vortex are not altered by this additional injectant issuing from holes adjacent to the upwash and downwash regions. Therefore, for a constant blowing ratio, the vortex, and not the film-cooling, is most important in regard to the resulting boundary layer pressure and velocity distributions.

The streamwise velocity and total pressure distributions display nearwall velocity and pressure deficits at discrete spanwise locations away from the vortex core. Figures 73 and 74 show the location of these deficits in a film cooled turbulent boundary layer with no embedded vortex. These locations correspond to the spanwise locations of the film cooling holes. Inspection of the data with embedded vortices (Figures 57-71) indicates that these velocity and pressure deficit locations shift towards the vortex upwash. The magnitude of this shift increases as vortex strength is increased. This skewing of the injectant from its nominal streamwise direction as it is redistributed by secondary flow convection is also discussed by Ligrani and Williams [Ref. 1 and 16].

3. Average Vortex Strength

Vortices r, w, x, y, and z, are used when mean temperature surveys and heat transfer measurements are made. These data are presented in subsequent sections of this thesis. The strength and circulation of vortices r, w, x, y, and z are measured in the five-hole probe surveys, in an isothermal flow field. Because Figures 25-26 indicate that vortex strength and circulation are nearly independent of cooling configuration, the values

of Γ and $\Gamma/(U_c \cdot d)$ used in subsequent sections are obtained by averaging values for single hole injection with values for 13 hole injection. These average values of vortex circulation and non-dimensional circulation for vortices z, y, x, w, and r are listed in Table VI.

TABLE VI. AVERAGE VORTEX STRENGTH AND CIRCULATION VALUES AT x/d=41.9

VORTEX	Generator Angle (degrees)	Vortex Circulation (Γ) (m^2/s)	Vortex Strength ($\Gamma/(U_c \cdot d)$)
z	4	.01382	.2340
y	8	.04485	.9815
x	12	.08763	1.8702
w	15	.11579	2.4400
r	18	.14466	2.9940

C. MEAN TEMPERATURE SURVEYS

The mean temperature surveys of Figures 75-95 are obtained using an experimental approach introduced by Ligrani et al. [Ref. 3] in which injectant is heated to approximately 50 degrees Celsius, while the test plate remains unheated. The temperature field, given as $(T - T_\infty)$, shows how the fluid from the injection holes

is convected and distorted by the vortex. Higher temperatures indicate greater amounts of injectant. Ligrani and Williams [Ref. 1 and 16] discuss additional details of this technique.

Experimental results are presented for mean temperature surveys in the following order: (1) mean temperature surveys conducted at x/d = 41.9 with film cooling from a single injection hole, (2) mean temperature surveys conducted at x/d = 41.9, with film cooling from a row of 13 injection holes (3) mean temperature surveys conducted at x/d = 5.2, 41.9, 82.9, and 109.2, for film cooling from a single injection hole, (4) mean temperature surveys conducted at x/d = 5.2, 41.9, 82.9, and 109.2, for film cooling from 13 injection holes. For (1) and (2) separate surveys are conducted using no vortex and vortices r, w, x, y, and z. For (3) and (4) surveys are conducted using vortex w.

The following parameters are maintained constant for all mean temperature surveys: injection temperature = 51 (+2,-0) $^{\circ}$C, m $\doteq$ 0.50 $\pm$ .03, freestream velocity (U_{∞}) = 10.0$\pm$ .2 m/s, and nondimensional injection temperature (θ) =1.5 (+0.1, -0.0). Figure numbers, film cooling conditions, streamwise locations and survey data run numbers for each mean temperature survey are given in Table VII.

TABLE VII. TEMPERATURE SURVEYS: EXPERIMENTAL CONDITIONS AND PARAMETERS

FIGURE	Survey Data Run Number	Film Cooling Holes	x/d Location	VORTEX
75	122388.1632	1	41.9	no vortex
76	122388.1414	1	41.9	z
77	122288.1653	1	41.9	y
78	123088.1914	1	41.9	x
79,88	122288.1339	1	41.9	w
80	122188.1744	1	41.9	r
81	122888.1154	13	41.9	no vortex
82	122888.1652	13	41.9	z
83	122888.1345	13	41.9	y
84	123088.1444	13	41.9	x
85,93	122988.1142	13	41.9	w
86	122888.1629	13	41.9	r
87	010389.1818	1	5.2	w
89	010489.1712	1	82.9	w
90,91	010589.1237	1	109.2	w
92	010389.2158	13	5.2	w
94	010489.1251	13	82.9	w
95	010689.1136	13	109.2	w

1. Temperature Surveys at x/d=41.9: Film Cooling from a Single Injection Hole

Figures 75-80 show injectant distributions within a turbulent boundary layer with film cooling from a single injection hole. Figure 75 shows injectant unperturbed by a vortex. Figures 76 and 77 show the effects of the relatively weak vortices z and y [$\Gamma/(U_c \cdot d)$ = 0.23 and 0.98 respectively]. Here, some injectant is convected into the vortex upwash, the remaining injectant is located near the wall in sufficient quantity to provide some protection. Figure 78, for vortex x ($\Gamma/(U_c \cdot d)$=1.87), shows that the bulk of the injectant is swept into the upwash which extends from Z=-8 cm to Z=-4 cm. Most injectant beneath the downwash of vortex x is depleted. The effects of vortex w and r with respective vortex strengths [$\Gamma/(U_c \cdot d)$] of 2.44 and 2.99 are shown in Figures 79 and 80. These figures show that the majority of the injectant is located in the upwash region. Additionally, injectant beneath the vortex downwash is almost entirely depleted for Z locations from -3.00 cm to +1.00 cm.

2. Temperature Surveys at x/d=41.9: Film Cooling from 13 Injection Holes

The results in Figures 81-86 present injectant distributions with film cooling from a single row of 13 injection holes. Figure 81 shows results obtained with no embedded vortex. Figures 82 and 83 display the effects of the relatively weak vortices z and y [$\Gamma/(U_c \cdot d) < 1.0$]. Here some redistribution of the injectant is evident. Major perturbations to injectant distributions are present with vortex x, w, and r, with respective $\Gamma/(U_c \cdot d)$ values of 1.87, 2.44, and 2.99. The magnitude of perturbations increases with increasing vortex strength, as shown in Figures 84-86.

3. Streamwise Development: Film Cooling from a Single Injection Hole

The streamwise development of the turbulent boundary layer with one film cooling hole and vortex w is shown in Figures 87-91. Figure 87 (x/d=5.2) shows that the majority of injectant is present in a concentrated area at the location of the film cooling jet, near Z=-1.5 cm. Secondary convection velocities have swept the injectant away from the wind tunnel spanwise centerline, and some injectant is accumulated in thee upwash region near Z=-6.0 cm. At x/d=41.9, Figure 88 indicates that the majority of injectant is swept into

the vortex upwash located near Z=-6.0 cm. The injectant is entirely depleted in the region from Z=-2.5 cm to Z=+0.5 cm. Figure 89 shows that for x/d = 82.9 the injectant is now entirely contained within the vortex upwash which extends from Z=-12.0 cm to Z=-6.0 cm. The near wall region between Z=-6.0 cm to Z=+1.0 cm, is completely devoid of injectant. Figure 90 shows that for x/d = 109.2 the injectant remains in the upwash region of the vortex which has begun to dissipate. Figure 91 shows the same temperature survey depicted in Figure 90, only here the lower limit on the differential temperature range has been expanded to show how the injectant is spread out.

4. Streamwise Development: Film Cooling from 13 Injection Holes

Figures 92-95 show the streamwise development of vortex w embedded in a turbulent boundary layer with film cooling from 13 injection holes. The same general pattern of development is repeated: as the vortex moves further downstream, a larger portion of the injectant is convected away from the wall and into the vortex upwash.

The vortex migrates in the negative Z direction with increasing streamwise distance. Due to the increased amount of injectant in the boundary layer, clear evidence of injectant is present for x/d values up to 109.2, even though it has been completely reorganized by the vortex.

D. HEAT TRANSFER MEASUREMENTS

Heat transfer measurements are presented in three parts: (1) measurements of boundary layers with an embedded vortex and no film cooling, (2) measurements of boundary layers with film cooling from a single injection hole, with and without an embedded vortex, and (3) measurements of boundary layers with film cooling from a single row of 13 injection holes, with and without an embedded vortex. These results are presented as Stanton number ratio distributions over the heat transfer test surface. The local Stanton numbers, measured in each heat transfer survey, are normalized with the baseline Stanton number values. Baseline Stanton number data files are described in Section II. D. (heat transfer surface description). For (1), (2), and (3), vortices r,

w, x, y, and z are employed. Parts (2) and (3) also include heat transfer measurements with no embedded vortex. Data reduction and plotting programs utilized were developed by Ligrani, et al. [Ref. 1, 2, and 3]

1. Heat Transfer Measurements: No Film Cooling

Measurements of local Stanton number ratios (St/Sto) are presented in Figures 96-100. Here, St represents Stanton number values with an embedded vortex and no film cooling, and Sto corresponds to Stanton number values with no vortex and no film cooling. Separate Stanton number distributions are presented for vortices r, w, x, y, and z. Freestream velocity is maintained at 10.0 $\pm$ .2 m/s with the test plate input parameters equal to 54.5 $\pm$ .1 volts and 6.0 amps. The injection system is not used, and the film cooling holes are sealed and taped.

Figures 96-100 show the Stanton number ratios for X=1.15, 1.25, 1.40, 1.60, 1.80, and 2.00. These X coordinate locations correspond to x/d locations of 7.4, 17.5, 33.6, 54.6, 75.6, and 96.6 respectively. In these figures, the St/Sto axes are expanded between .9 and 1.1 to prevent plotting data points on top of one another. Figures 96-100 show Stanton number ratio magnitudes which are greater than 1.0 in the vortex downwash region, and

less than 1.0 in the vortex upwash regions. Magnitudes of deviations from St/Sto = 1.0 increase with increasing vortex strength and downstream location. These figures also show the spanwise migration of the vortex in the negative Z direction as the streamwise distance is increased. Local distributions of St/Sto also show good agreement with the data of Ortiz [Ref. 15], Joseph [Ref. 13], and Williams [Ref. 16]. Experimental conditions for the measurements presented in Figures 96-100 are listed in Table VIII.

TABLE VIII. HEAT TRANSFER SURVEYS: EXPERIMENTAL CONDITIONS AND PARAMETERS: NO FILM COOLING

Figure	St Data Run Number	Vortex	X (m)	x/d
96	110388.0153	z	1.15-2.00	7.4-96.6
97	110388.0101	y	1.15-2.00	7.4-96.6
98	110388.0012	x	1.15-2.00	7.4-96.6
99	110288.2245	w	1.15-2.00	7.4-96.6
100	110288.2112	r	1.15-2.00	7.4-96.6

Sto Data Run Number: 110288.1805
Freestream Velocity (U_∞) = 10 $\pm$ .2 m/s

2. Heat Transfer Measurements: Film Cooling from a Single Injection Hole

Figures 101-106 are three-dimensional plots of Stanton number ratios which document the streamwise development of the film-cooled boundary layer. Figure 101 depicts the boundary layer streamwise development with no embedded vortex. Figures 102-106 show the effects of the embedded vortices z, y, x, w, and r, respectively. The effects of the vortex upon the film cooled boundary layer is indicated by comparing St/Sto values to Stf/Sto values. Here, St corresponds to Stanton number values with vortex and with film cooling, Stf corresponds to Stanton number values with film cooling only, and Sto represents baseline Stanton numbers for no vortex and no film cooling. When the boundary layer is unaffected by film cooling or vortex both Stanton number ratios, St/Sto and Stf/Sto, are close to 1.0. In the vortex upwash region, local St/Sto values are low compared to Stf/Sto values. In the downwash region, local St/Sto values are high compared to Stf/Sto values. Experimental conditions are listed in Table IX.

TABLE IX. HEAT TRANSFER SURVEYS: EXPERIMENTAL CONDITIONS AND PARAMETERS: SINGLE INJECTION HOLE FILM COOLING

Figure	St Data Run Number	Stf Data Run Number	VORTEX	M	Θ	U_∞ m/s
101	110488.2311	110488.2311	no vortex	.481	1.56	9.96
102	110488.2359	110488.2311	z	.481	1.58	9.96
103	110588.0147	110488.2311	y	.483	1.53	9.95
104	110588.0252	110488.2311	x	.482	1.57	9.95
105	110588.0351	110488.2311	w	.482	1.57	9.95
106	110588.0532	110488.2311	r	.482	1.59	9.94

Sto Data Run Number: 121988.1621
M = Blowing Ratio
Θ = Non-Dimensional Coolant Temperature
U_∞ = Freestream Velocity

In Figure 101, the pronounced decrease in Stanton number ratios at Z=0 cm and X=1.15 m (x/d=7.4) indicates the effects on the boundary layer caused by the injectant. These effects are significantly diminished as the boundary layer develops in the streamwise direction. At X=2.0 m (x/d=96.6) the centerline St/Sto and Stf/Sto values are nearly equal to 1.0, indicating that the effects of film cooling are very small.

Figures 102-106 show how St/Sto values change as the strength of the embedded vortex increases. A qualitative comparison of these figures indicates that at X=1.15 m

(x/d=7.4), the injectant is dominating the spanwise Stanton number distributions since values of both centerlne Stanton number ratios are significantly less than 1.0. At X=1.25 m (x/d=17.5) the beneficial effects of the injectant are diminished by the vortex downwash for the two strongest vortices w and r (Figures 105-106). This is indicated by peak values of St/Sto which are significantly greater than 1.0. For the lower strength vortices: z, y, and x (Figures 102, 103, and 104) similar phenomena occur at locations further downstream because the vortex retains its coherence as the influence of the injectant diminishes with streamwise development. St/Sto peak values in the downwash region and the Stf/Sto deficits in the upwash region both increase in magnitude with increasing vortex strength and greater downstream location.

Figures 107-142 show the spanwise variation of Stanton number ratios at specified streamwise locations as the vortex strength is varied. Data presented in these figures are the same as in Figures 101-106. Fluid parameters, streamwise location, and vortex designation corresponding to Figures 107-142 are listed in Table X.

TABLE X. SPANWISE VARIATION OF LOCAL STANTON NUMBER RATIOS: SINGLE INJECTION HOLE FILM COOLING

Figure	VORTEX	M	Θ	U_∞ m/s	X(m)	x/d
107	no vortex	.481	1.56	9.96	1.15	7.4
108	z	.481	1.58	9.96	1.15	7.4
109	y	.483	1.53	9.95	1.15	7.4
110	x	.482	1.57	9.95	1.15	7.4
111	w	.482	1.57	9.95	1.15	7.4
112	r	.482	1.59	9.94	1.15	7.4
113	no vortex	.481	1.56	9.96	1.25	17.5
114	z	.481	1.58	9.96	1.25	17.5
115	y	.483	1.53	9.95	1.25	17.5
116	x	.482	1.57	9.95	1.25	17.5
117	w	.482	1.57	9.95	1.25	17.5
118	r	.482	1.59	9.94	1.25	17.5
119	no vortex	.481	1.56	9.96	1.40	33.6
120	z	.481	1.58	9.96	1.40	33.6
121	y	.483	1.53	9.95	1.40	33.6
122	x	.482	1.57	9.95	1.40	33.6
123	w	.482	1.57	9.95	1.40	33.6
124	r	.482	1.59	9.94	1.40	33.6
125	no vortex	.481	1.56	9.96	1.60	54.6
126	z	.481	1.58	9.96	1.60	54.6
127	y	.483	1.53	9.95	1.60	54.6
128	x	.482	1.57	9.95	1.60	54.6
129	w	.482	1.57	9.95	1.60	54.6
130	r	.482	1.59	9.94	1.60	54.6
131	no vortex	.481	1.56	9.96	1.80	75.6
132	z	.481	1.58	9.96	1.80	75.6
133	y	.483	1.53	9.95	1.80	75.6
134	x	.482	1.57	9.95	1.80	75.6
135	w	.482	1.57	9.95	1.80	75.6
136	r	.482	1.59	9.94	1.80	75.6
137	no vortex	.481	1.56	9.96	2.00	96.6
138	z	.481	1.58	9.96	2.00	96.6
139	y	.483	1.53	9.95	2.00	96.6
140	x	.482	1.57	9.95	2.00	96.6
141	w	.482	1.57	9.95	2.00	96.6
142	r	.482	1.59	9.94	2.00	96.6

M - Blowing Ratio
Θ - Non-Dimensional Coolant Temperature
U_∞ - Freestream Velocity

Figures 107-112 for x/d=7.4 indicate that the injectant has a greater influence than the vortex on spanwise heat transfer distributions for all vortex strengths. Figures 111-112 show that the two strongest vortices, w and r create St/Sto peak values of approximately 1.05. However, at the same streamwise location, the film cooling jets are also important as indicated by St/Sto deficits at the centerline.

Figures 113-118 for x/d=17.5 indicate St/Sto deficits in the vortex upwash region for all vortices: z, y, x, w, and r. This deficit increases in magnitude with increasing vortex strength and is believed to be a result of accumulated injectant. For vortices x, w, and r (Figures 116, 117, 118), large St/Sto deficits in upwash regions extend from Z=-10.0 cm to z=-3.00 cm. St/Sto peaks near Z=0.0 cm for vortices x, w, and r indicate that little injectant is present in the vortex downwash region which extends from Z=0.0 cm to Z=+5.0 cm.

Figures 119-124 show Stanton number ratios for x/d=33.6. This data show evidence of film coolant only for no vortex and vortex z. Figure 121 for vortex y shows St/Sto peaks of approximately 1.0 in the downwash region and St/Sto minima of approximately 0.9 in the upwash region. St/Sto = 1.0 at the downwash indicates

that injectant protection is reduced considerably by the vortex downwash. Figures 122-124 show how St/Sto ratios vary as vortex strength increases for vortices x, w, and r. Here, downwash peaks and upwash deficits increase in magnitude as vortex circulation increases. Such behavior results as more injectant is connected into the vortex upwash, leaving less injectant near the wall to provide thermal protection in the vortex downwash region.

St/Sto and Stf/Sto ratios for x/d=54.6 are given in Figures 125-130. Evidence of injection protection exists for no vortex and for vortex z. Less evidence of injectant is present with vortices y, x, w, and r. Figure 127 shows that downwash St/Sto peaks are just above 1.0 for vortex y. Higher downwash peaks are present for stronger vortices r, w, and x in Figures 128-130. The St/Sto minima in upwash regions are approximately 0.9 for vortices y, x, w, and r.

Figures 131-136 for x/d=75.6 and Figures 137-142 for x/d=96.6 indicate that the protection provided by injectant is reduced considerably in the downwash region for all vortices. Figures 132 and 138 for vortex z show St/Sto peaks of approximately 1.0. For stronger vortices y, x, w, and r, St/Sto peaks grow in magnitude, as do the

St/Sto deficits in the upwash region relative to St/Sto =1.0. Additionally, spanwise distances over which the vortices affect the Stanton number ratios become larger as vortex strength increases.

The values of non-dimensional circulation [$\Gamma/(U_c \cdot d)$] at x.d=41.9 for vortices r, w, x, y, and z are 3.17, 2.55, 1.88, 1.07, and 0.29, respectively. When this parameter is less than 1.0, the injectant continues to provide some protection near the wall. When it is greater than 1.0, protection is reduced and high Stanton number regions exist.

3. Heat Transfer Measurements: Film Cooling from 13 Injection Holes

Figures 143-148 are three-dimensional plots showing streamwise development of film-cooled boundary layers, using a row of 13 injection holes spaced three hole diameters apart. Streamwise development is shown for the case of no embedded vortex (Figure 143) and for vortices z, y, x, w, and r (Figures 144-148). Experimental conditions for these heat transfer measurements are given in Table XI.

TABLE XI. HEAT TRANSFER SURVEYS: EXPERIMENTAL CONDITIONS AND PARAMETERS: 13 INJECTION HOLE FILM COOLING

Figure	St Data Run Number	Stf Data Run Number	VORTEX	M	Θ	U∞ m/s
143	110588.0835	110588.9835	No vortex	.471	1.55	9.96
144	110588.1214	110588.0835	z	.471	1.54	9.97
145	110588.1124	110588.0835	y	.472	1.55	9.97
146	110588.1009	110588.0835	x	.471	1.58	9.97
147	110588.0918	110588.0835	w	.470	1.59	9.96
148	110588.0718	110588.0835	r	.474	1.54	9.95

Sto Data Run Number. 121988.1621
M = Blowing Ratio
Θ = Non-Dimensional Coolant Temperature
U_∞ = Freestream Velocity

Figure 143 shows data in a film-cooled boundary layer without an embedded vortex. Stanton number ratios are nearly constant at different spanwise locations for each streamwise location. The values of ratios range from approximately 0.60 to 0.82, and increase with increasing downstream distance. The protection of film injection provided by the 13 injection holes diminishes only slightly over the streamwise distance shown, as evidenced by Stanton number ratios which are less than 1.0 at all locations.

Figures 144-148 show the familiar St/Sto peaks and deficits which occur in vortex downwash and upwash regions, respectively. The spanwise variations of St/Sto values indicate the redistribution of the injectant

caused by secondary flow convection. Unlike film cooling from a single injection hole, here the St/Sto peaks barely exceed 1.0, as a result of increased protection provided by injectant from 13 holes.

Figures 149-184 show individual plots of the same St/Sto data given in Figures 143-148. In each Figure, spanwise variations of Stanton number ratios are given at a particular streamwise location. Flow parameters, streamwise locations, and vortex designations corresponding to Figures 149-184 are listed in Table XII.

TABLE XII. SPANWISE VARIATION OF LOCAL STANTON NUMBER RATIOS: 13 INJECTION HOLE FILM COOLING

Figure	VORTEX	M	Θ	U_∞ m/s	X(m)	x/d
149	no vortex	.471	1.55	9.96	1.15	7.4
150	z	.471	1.54	9.97	1.15	7.4
151	y	.472	1.55	9.97	1.15	7.4
152	x	.471	1.58	9.97	1.15	7.4
153	w	.470	1.59	9.96	1.15	7.4
154	r	.474	1.54	9.95	1.15	7.4
155	no vortex	.471	1.55	9.96	1.25	17.5
156	z	.471	1.54	9.97	1.25	17.5
157	y	.472	1.55	9.97	1.25	17.5
158	x	.471	1.58	9.97	1.25	17.5
159	w	.470	1.59	9.96	1.25	17.5
160	r	.474	1.54	9.95	1.25	17.5
161	no vortex	.471	1.55	9.96	1.40	33.6
162	z	.471	1.54	9.97	1.40	33.6
163	y	.472	1.55	9.97	1.40	33.6
164	x	.471	1.58	9.97	1.40	33.6
165	w	.470	1.59	9.96	1.40	33.6
166	r	.474	1.54	9.95	1.40	33.6
167	no vortex	.471	1.55	9.96	1.60	54.6
168	z	.471	1.54	9.97	1.60	54.6
169	y	.472	1.55	9.97	1.60	54.6
170	x	.471	1.58	9.97	1.60	54.6
171	w	.470	1.59	9.96	1.60	54.6
172	r	.474	1.54	9.95	1.60	54.6
173	no vortex	.471	1.55	9.96	1.80	75.6
174	z	.471	1.54	9.97	1.80	75.6
175	y	.472	1.55	9.97	1.80	75.6
176	x	.471	1.58	9.97	1.80	75.6
177	w	.470	1.59	9.96	1.80	75.6
178	r	.474	1.54	9.95	1.80	75.6
179	no vortex	.471	1.55	9.96	2.00	96.6
180	z	.471	1.54	9.97	2.00	96.6
181	y	.472	1.55	9.97	2.00	96.6
182	x	.471	1.58	9.97	2.00	96.6
183	w	.470	1.59	9.96	2.00	96.6
184	r	.474	1.54	9.95	2.00	96.6

M = Blowing Ratio

Θ = Non-Dimensional Coolant Temperature

U_∞ = Freestream Velocity

Figures 149-154 present data obtained at x/d=7.4. Here spanwise St/Sto values are most influenced by the injectant rather than by the vortex for all vortex strengths. Small variations in the spanwise distributions of St/Sto and Stf/Sto are visible for the stronger vortices x, w, and r, but the distinctive profile resulting from the vortex downwash and upwash combination is not discernible.

x/d=17.5 data in Figures 155-160 show a maximum St/Sto peak of 0.84 at the downwash for vortex r (the strongest vortex, Figure 160). St/Sto deficits are distinguishable only for the two strongest vortices, w and r (Figures 159-160).

Figures 161-166 show data for x/d=33.6. Here, protection from the injectant is diminished significantly by the downwash of vortices x, w, and r (Figures 164, 165, and 166). The maximum St/Sto value is created by vortex r (Figure 166) and is about equal to 0.97.

The x/d=54.6 spanwise variations in Figures 167-172 and the x.d=75.6 spanwise variations in Figures 173-178 show that the three strongest vortices x, w, and r produce St/Sto peak values near 1.0 (Figures 170, 171, 172, and Figures 176, 177, and 178).

Figures 179-184 show data for x/d=96.6. All but the weakest vortex produce St/Sto peaks which approach or slightly exceed 1.0.

Values of $\Gamma/(U_c\ d)$ at x/d=41.9 for vortices r, w, x, y, and z, with film-cooling from 13 holes, are 2.81, 2.33, 1.86. 0.89, and 0.17, respectively. St/Sto data indicate film cooling protection in the vortex downwash region for the two weakest vortices, y and z ($\Gamma/(U_c \cdot d) < 1.0$). When $\Gamma/(U_c \cdot d) \geq 1.86$, St/Sto data vortices r, w, and x indicate minimum injectant protection in the downwash regions.

E. FLOW VISUALIZATION RESULTS

Flow visualization results for 13 holes film-cooling and for single hole film-cooling are presented in Figures 185 and 186, respectively. Each Figure consists of a series of six photographs. The photographs show a 1/16 inch, black fiberboard which is placed on top of the test surface, painted with an oil-pigment suspension (see Section II. G.) and exposed to the wind tunnel flow conditions specified in Table XIII.

TABLE XIII. SURFACE FLOW VISUALIZATION: FLOW CONDITIONS AND PARAMETERS

Figure	Photo-graph	U_∞ (m/s)	m	# of Injection Holes	Vortex
185	a	10	0.5	13	r
185	b	10	0.5	13	w
185	c	10	0.5	13	x
185	d	10	0.5	13	y
185	e	10	0.5	13	z
185	f	10	0.5	13	no vortex
186	a	10	0.5	1	r
186	b	10	0.5	1	w
186	c	10	0.5	1	x
186	d	10	0.5	1	y
186	e	10	0.5	1	z
186	f	10	0.5	1	no vortex

Injection --- unheated
Test Surface --- unheated

In each photograph, flow is moving from top (x.d=2.1) to bottom (x/d=23.1) as viewed looking down on the test surface. The white vertical lines at the top of the photographs correspond to the spanwise locations of the injection hole centerlines. The test surface spanwise centerline is annotated with a draftsman's centerline symbol. The negative Z direction lies to the left of this symbol, while the positive Z direction lies to the right. The arrow shown at the top of most photographs

indicates the spanwise position of the vortex generator at upstream location X=0.48 m. This arrow is not present in photographs of flow patterns for turbulent boundary layers with no embedded vortex. The wide horizontal band visable in the lower half of the photographs (x.d approximately 15.8) is due to a probe access slot in the test section top wall.

Figure 185 shows surface flow visualization with injection from 13 holes with vortices r, w, x, y, and z (185 a, b, c, d, e) and with no vortex (185 f). For photographs a, b, and c, $\Gamma/(U_c \cdot d) \geq 1.86$. The wide, dark path below the centerline symbol in these photographs follows the path of the vortex downwash and the vortex core. Here, secondary flow velocities sweep the white pigment in the transverse direction. The vortex upwash region is indicated in these photographs by the bright area just to the right of the dark region. Here, concentrated flocs of titanium dioxide pigment are deposited beneath the core upwash. Streamwise paths of the film-cooling jets are also evident in these photographs. The paths of these jets, which lie directly below the injection hole centerline markings, are indicated by narrow dark lines bordered on both sides by bright white lines. The centerline cooling jet, rather than being enveloped in the vortex, maintains its conformity as it is swept to the side of the vortex

upwash. The spanwise migration of the vortex in the -Z direction is also evident from these photographs as it travels in the streamwise direction.

Photographs 185d and 185e show surface flow effects from vortices y and z. Here, $\Gamma/(U_c \cdot d)$ equals 0.89 and 0.17, and the vortices disturb surface flow patterns only minimally. The only visable effect from vortex y (Figure 185 d) is the slight -Z direction displacement of centerline and adjacent film-cooling jet paths. Photograph 185 e for vortex z appears almost identical to photograph 185 f, which displays the surface flow patterns of a 13 hole film-cooled boundary layer with no vortex.

Photographs a, b, and c of Figure 186 show surface flow visualization for vortices r, w, and x in a film-cooled turbulent boundary layer using a single injection hole. $\Gamma/(U_c \cdot d)$ values are 3.17, 2.54, and 1.88, respectively. As for Figure 185, upwash and downwash regions are discernible by the varying concentrations of titanium dioxide pigment. The film-cooling path is not discernible from the vortex path in photographs 186 a and 186 b (vortices w and r). However, Figure 186 c for vortex x shows distinguishable film cooling and vortex paths. The marked contrast in photograph 186 e is due to a change in backround lighting.

Photograph 186 d shows the effects of vortex y ($\Gamma/(U_c \cdot d)=1.07$) on surface flow visualizations. The vortex slightly displaces film-injectant in the -Z direction. The effect of vortex z ($\Gamma/(U_c \cdot d)=0.29$) in photograph 185 e, is even less. Photograph 186 f shows surface flow patterns with film-cooling from a single hole layer with no vortex.

IV. SUMMARY AND CONCLUSIONS

The influences of circulation of an embedded vortex on injectant from a single film-cooling injection hole and from a row of 13 film-cooling injection holes are discussed. For all tests, the centerline injection hole is located beneath the vortex downwash (Williams' vortex position e) [Ref. 16]. A blowing ratio of approximately 0.50 and a freestream velocity of 10 m/s are employed. Non-dimensional coolant temperature (θ) is maintained at about 1.5. The non-dimensional circulation of the embedded vortex ($\Gamma/(U_c \cdot d)$) varies between 0.0 and 3.17.

Vortex core size is determined for the area where the streamwise vorticity is greater than or equal to 40 percent of the maximum vorticity at the vortex center. Based on this model, the average vortex core radius is relatively constant for all vortices examined and approximately equals 0.73 cm. The dimensionless core size parameter, 2c/d, is then about 1.5, where c is the average vortex radius and d is the injection hole diameter.

Local heat transfer distributions are altered significantly by embedded longitudinal vortices. For vortices with $\Gamma/(U_c \cdot d) < 1.0$, evidence of thermal protection from film cooling is seen for x/d values up to

54.6 for single hole film-cooling and x.d values up to 75.6 for 13 injection hole film-cooling. When $\Gamma/(U_c \cdot d)$ >1.0, evidence of injectant is present for x/d values only up to 7.4. At streamwise locations greater than x/d=7.4, injection protection is minimized in the downwash region, as indicated by augmented Stanton numbers which persist as far downstream as x/d=96.6.

Mean temperature and mean velocity surveys in spanwise normal planes and surface flow visualization results are consistent with heat transfer surveys. For $\Gamma/(U_c \cdot d) > 1.0$, injectant is swept from the downwash region into the vortex upwash by secondary flows. When $\Gamma/(U_c \cdot d)$ is less than 1.0, some injectant remains in the downwash region and thus continues to provide some thermal protection near the wall.

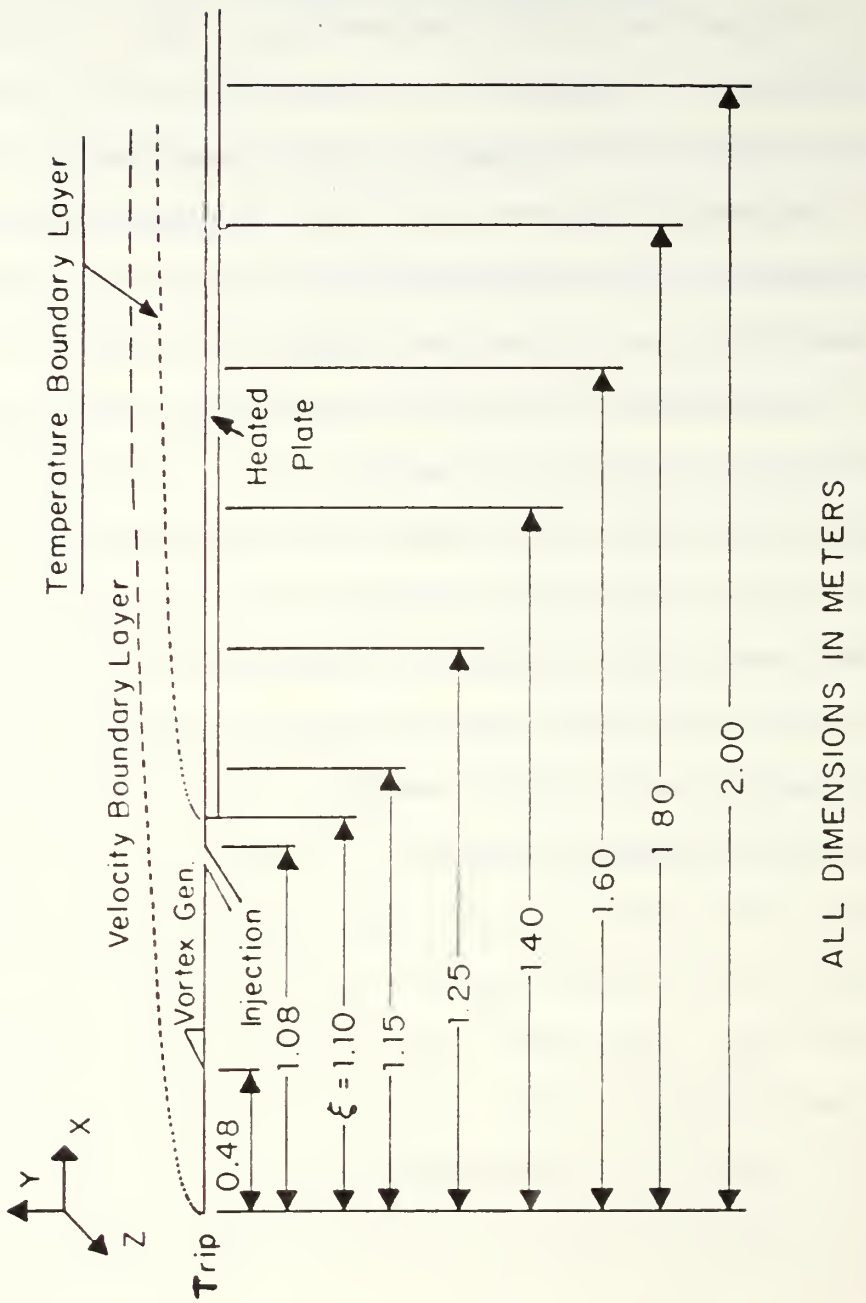

Figure 1. Test Section Coordinate System

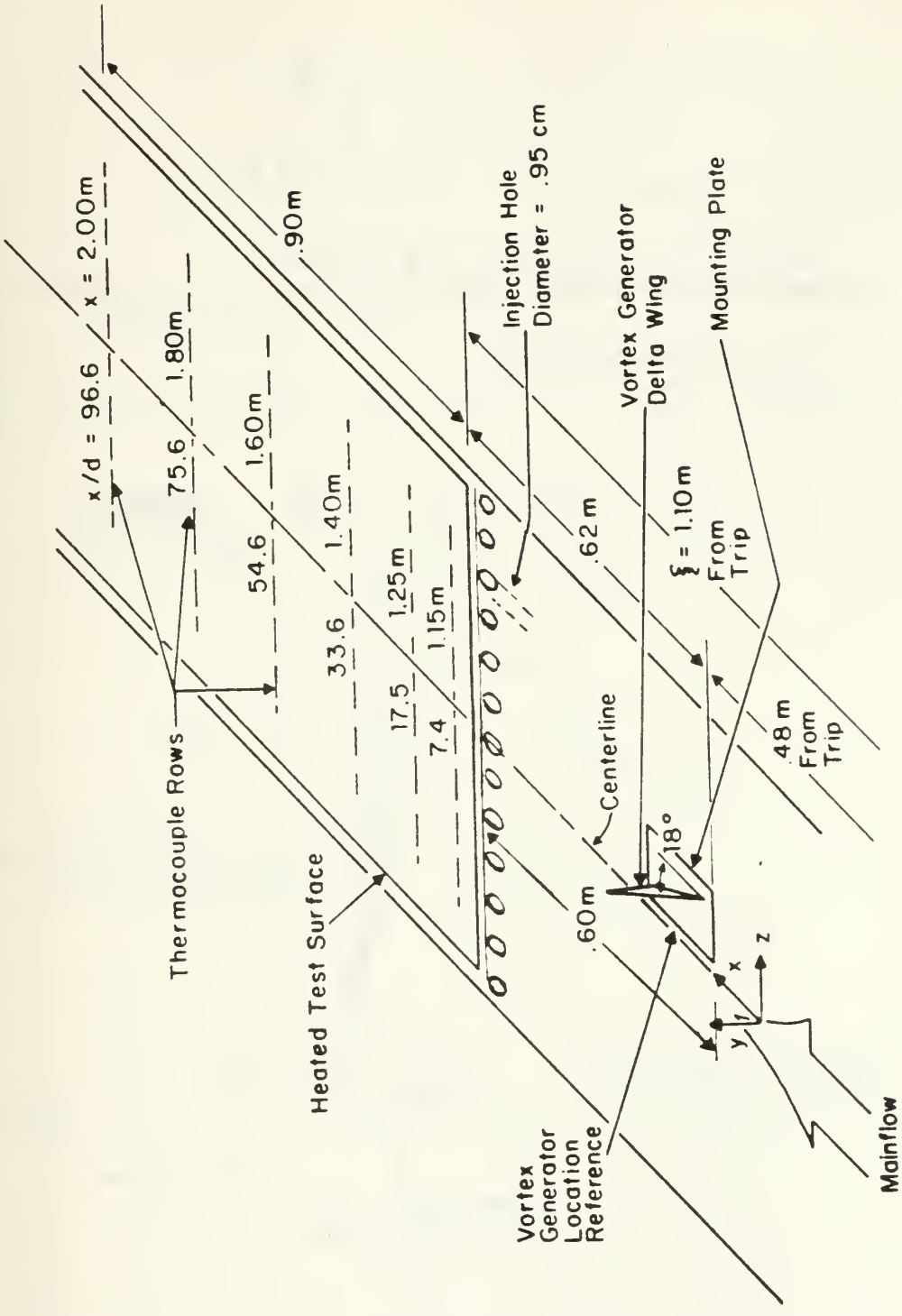

Figure 2. Top View Schematic Of Wind Tunnel Test Section

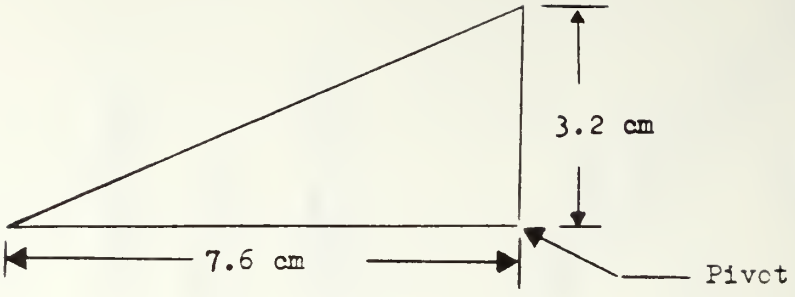

Half Delta Wing

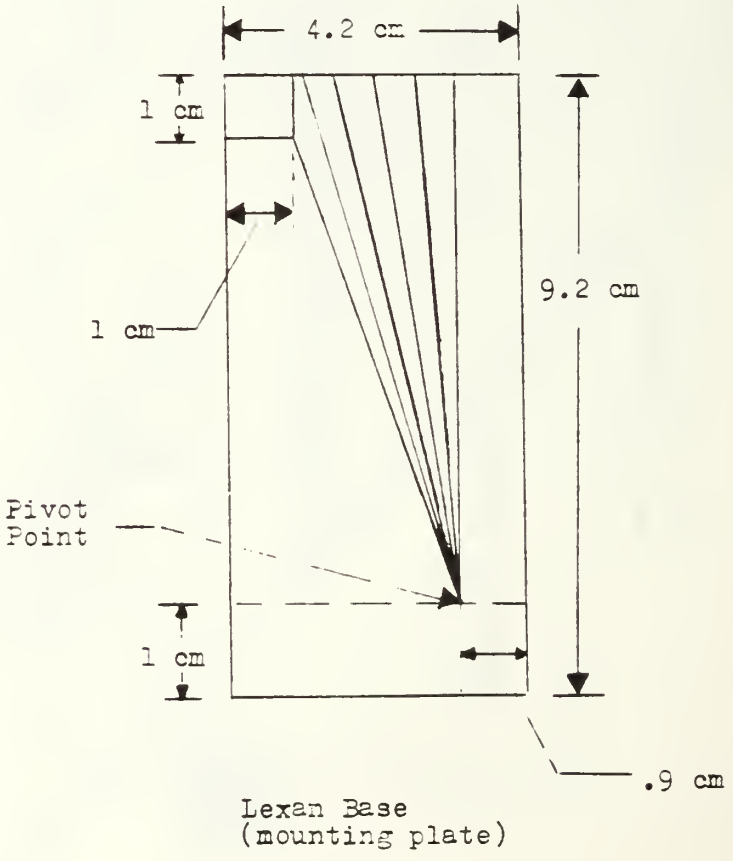

Figure 3. Vortex Generator Details

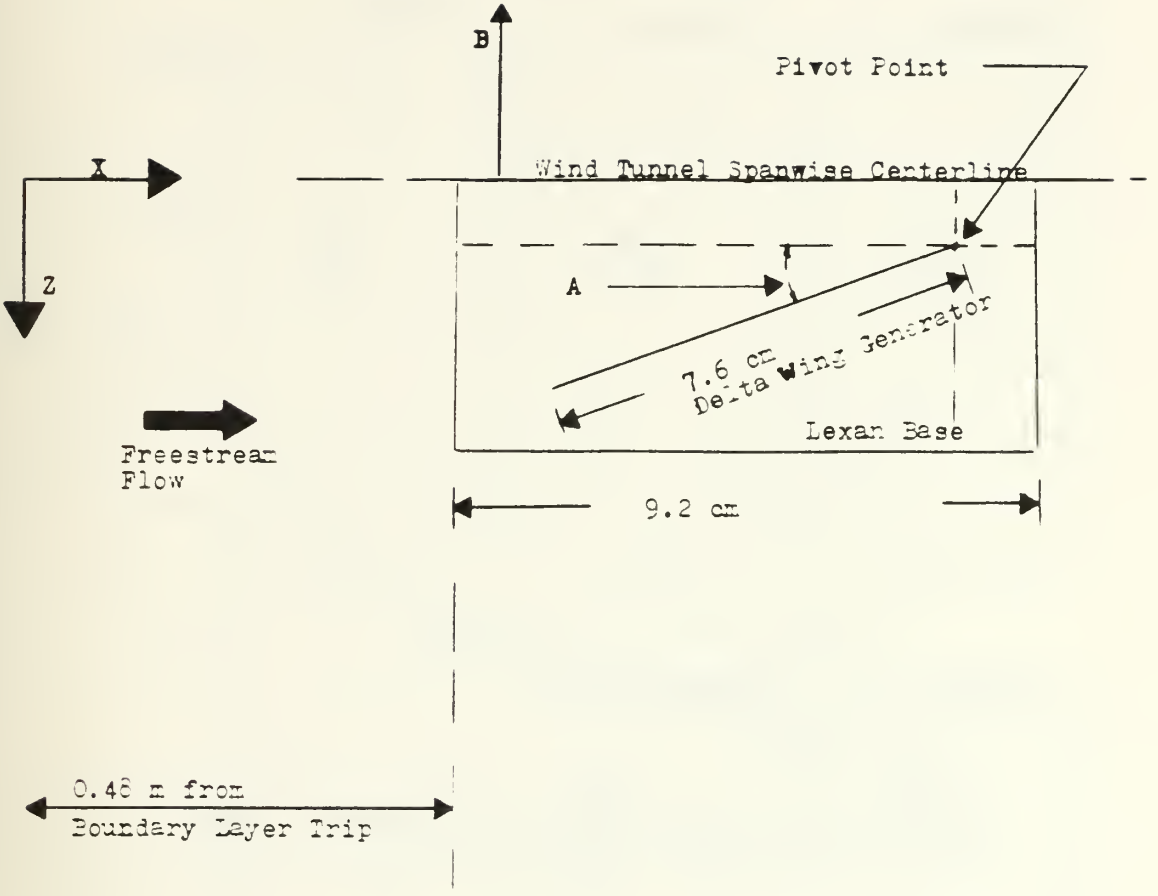

VORTEX	A Delta Wing Aspect Angle (degrees)	B Spanwise Location of the Lexan Base Edge (-Z direction) (cm)
r	18	0
s	15	0
t	12	0
u	8	0
v	4	0
w	15	-0.51
x	12	-1.53
y	8	-3.56
z	4	-4.07

Figure 4. Vortex Generator Orientation in X-Z Plane For Various Vortex Generator Angles

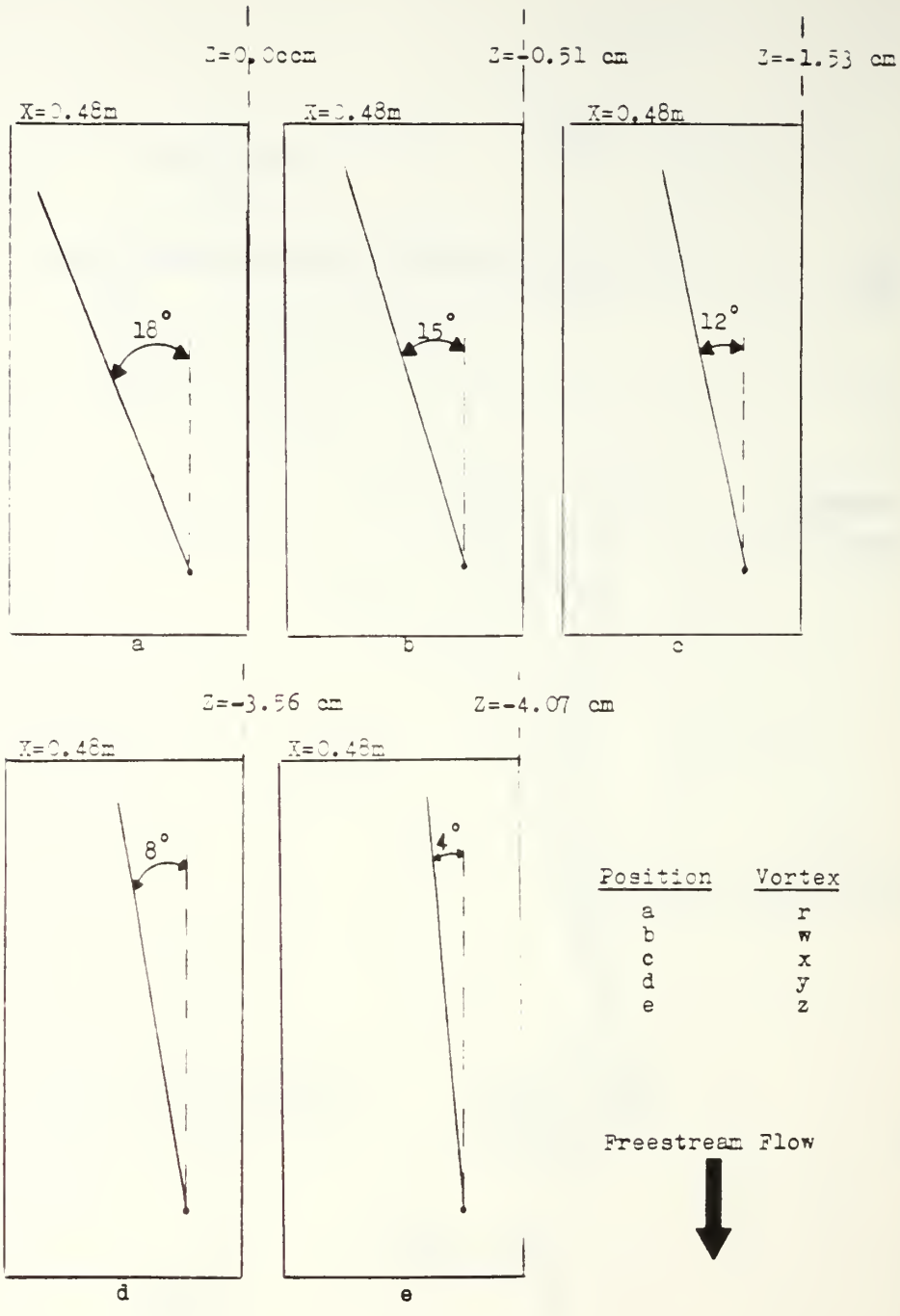

Figure 5. Coordinate Locations of Vortex Generator Mounting Plate For Various Vortex Generator Angles

Stanton No. (St_o) vs Reynolds No. (Re_x)

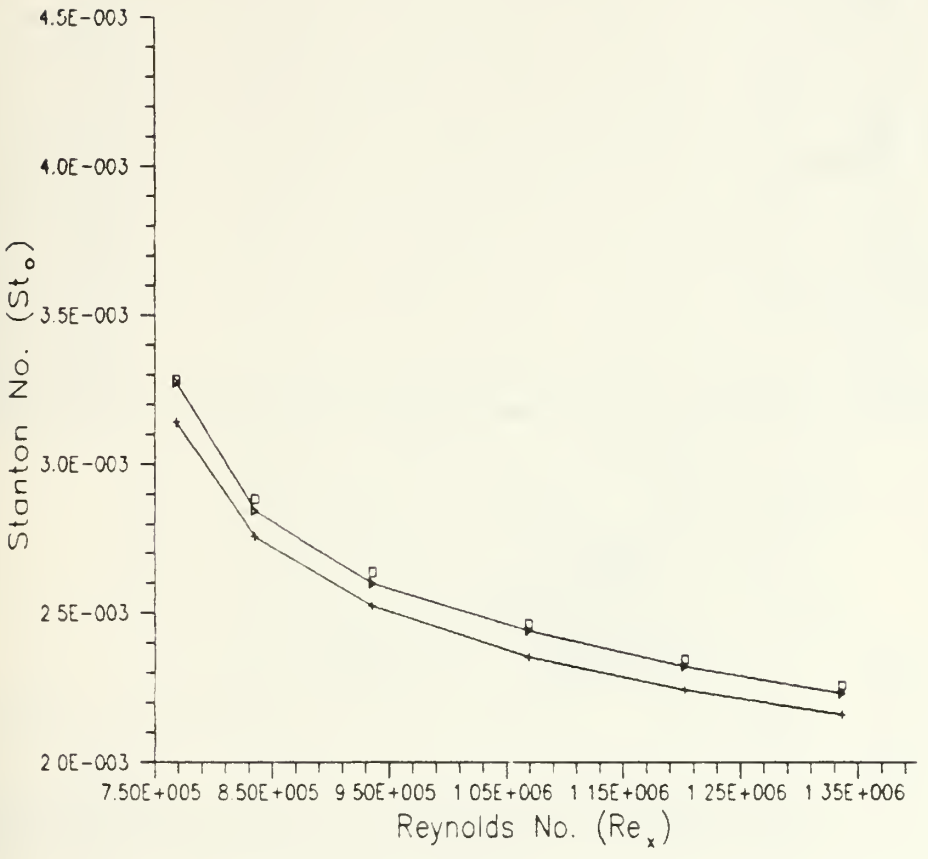

LEGEND:

+ = Equation 2.1 Constant Wall Temperature Beyond the Unheated Starting Length.

□ = Equation 2.2 Constant Heat Flux Approx. Single Step in Wall Heat Flux.

△ = Equation 2.3 Constant Heat Flux (exact) Empirical Relationship.

Figure 6. Stanton Number Comparison Between Exact Solution And Empirical Relationships

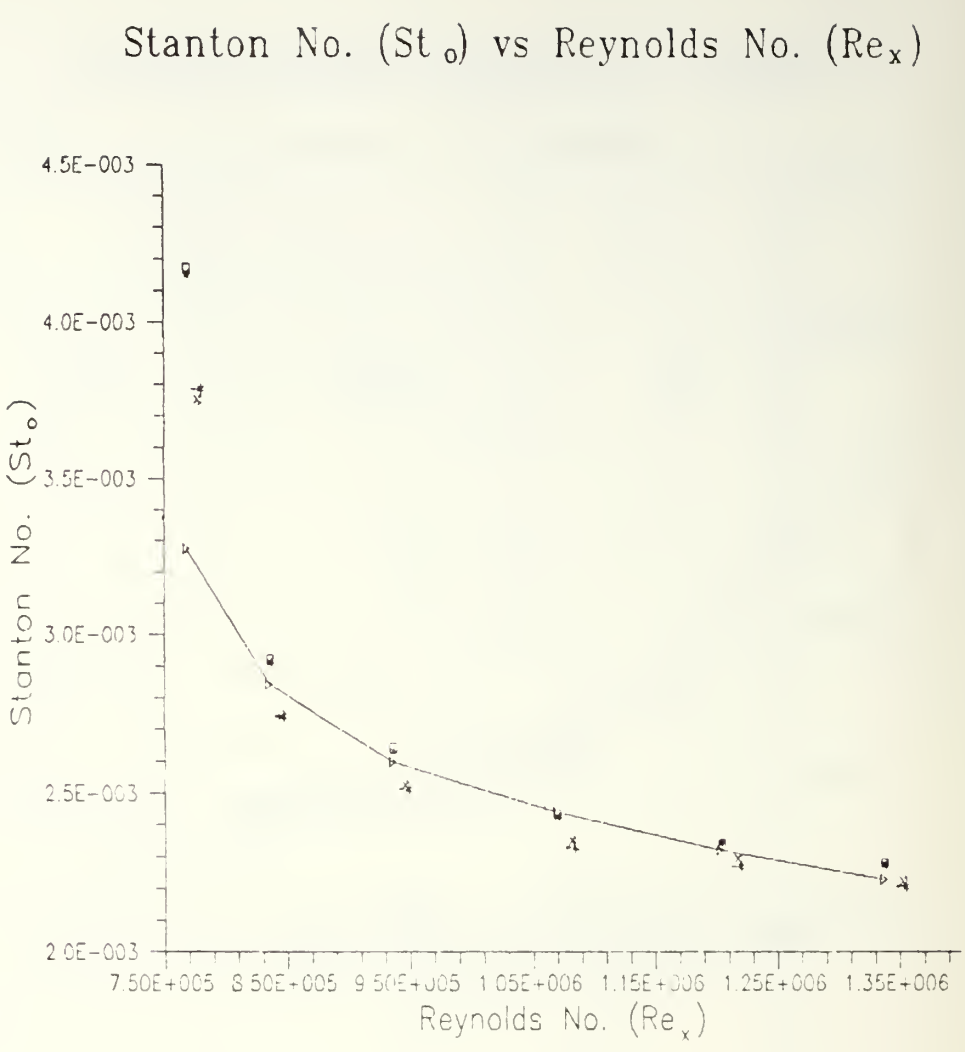

Figure 7. **Stanton Number Comparison Between Exact Solution and Experimental Measurements**

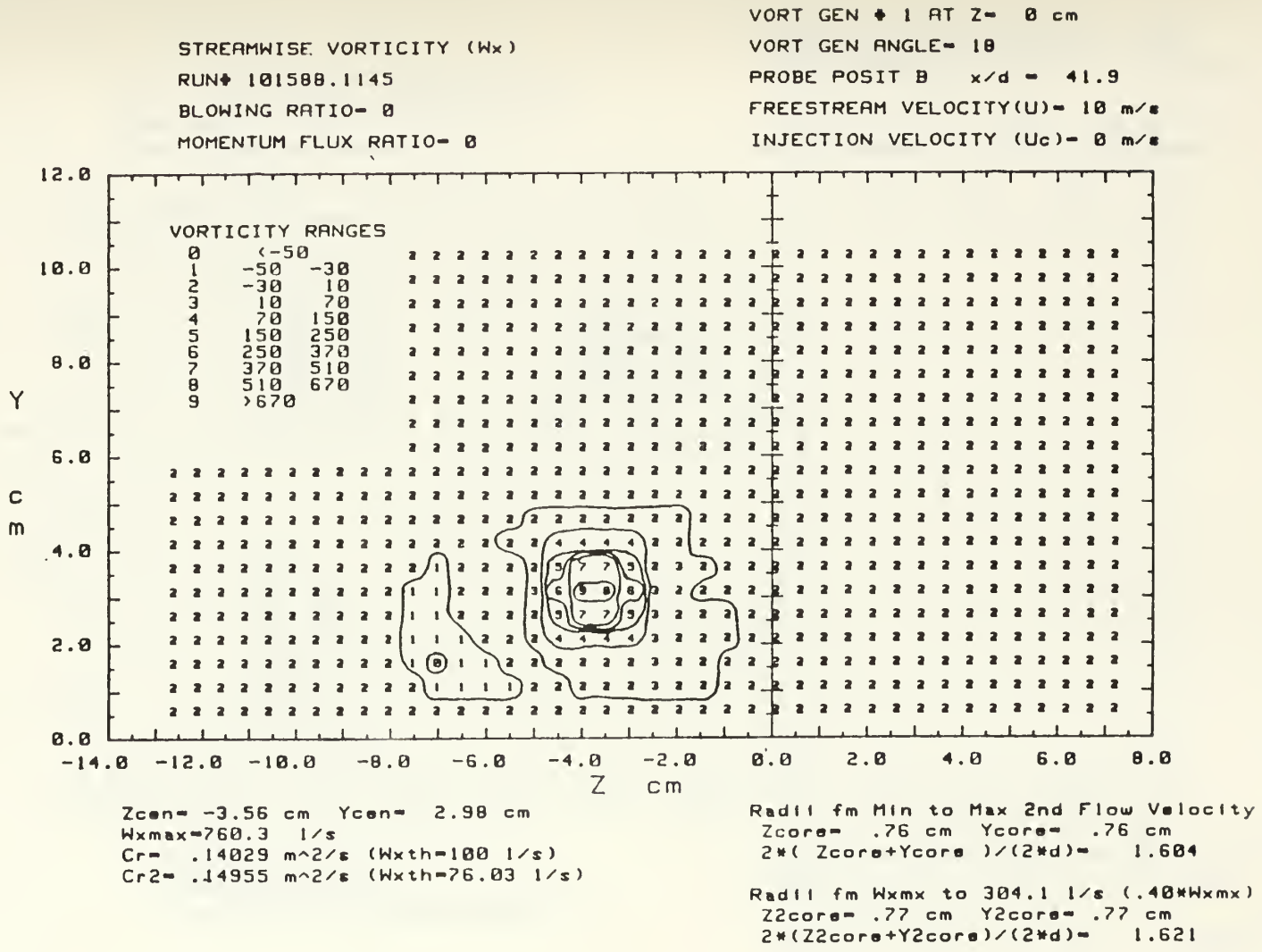

Figure 8. Streamwise Vorticity Contours, m=0, x/d=41.9 Γ = .149 m^2/s, Vortex r

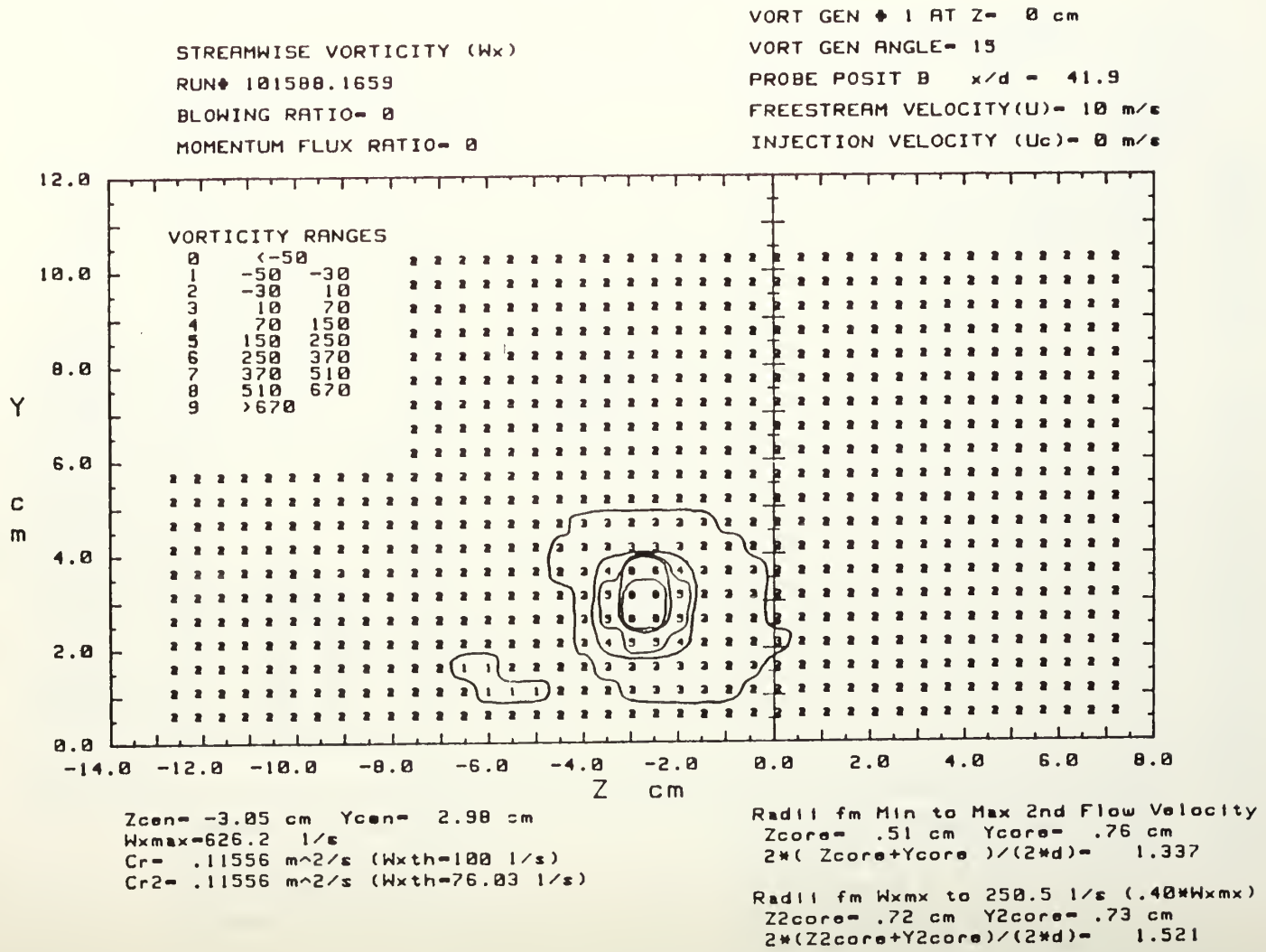

Figure 9. Streamwise Vorticity Contours, m=0 x/d=41.9 Γ = .115 m^2/s, Vortex s

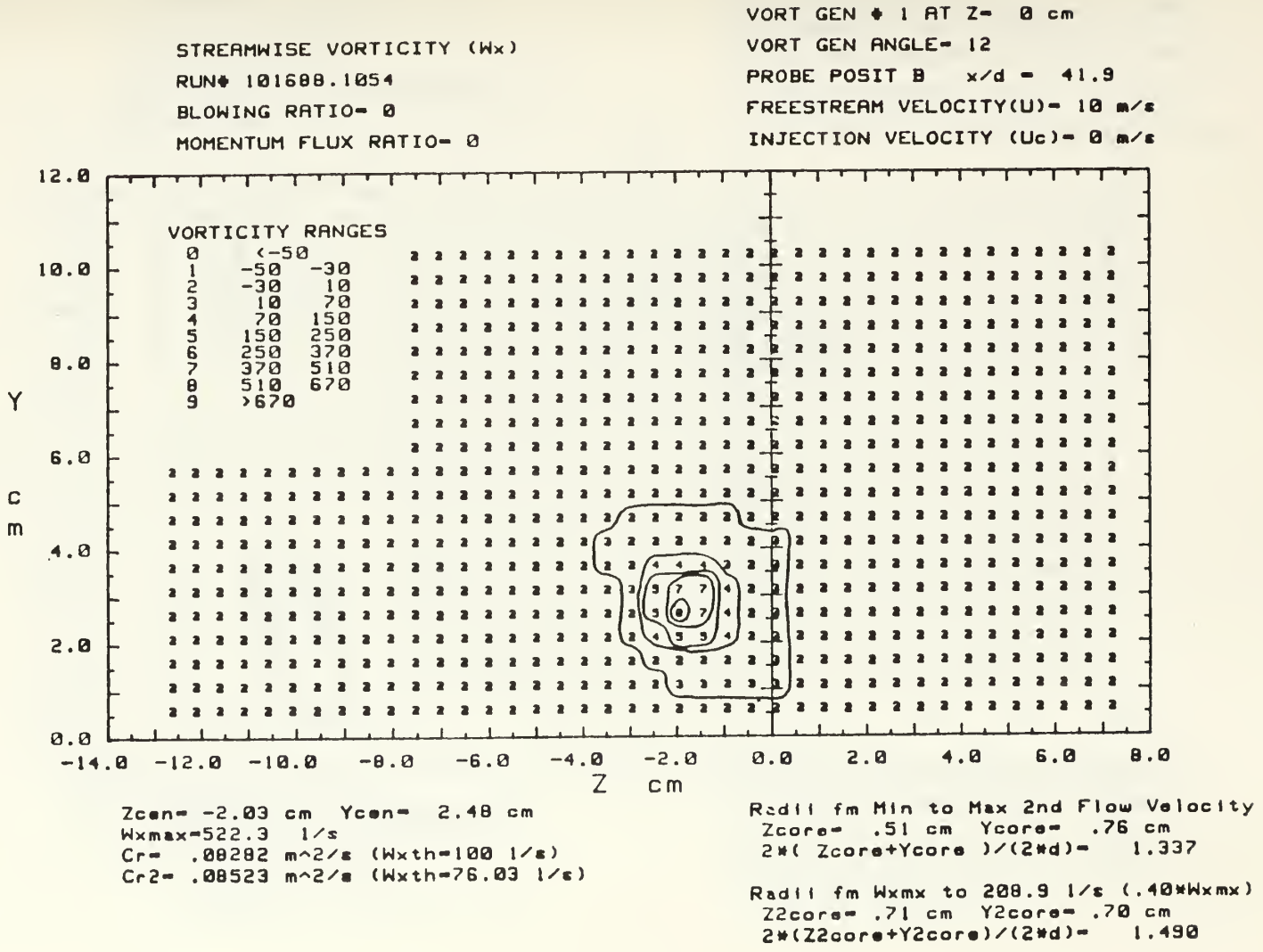

Figure 10. Streamwise Vorticity Contours, m=0
x/d=41.9 Γ = .085 m^2/s, Vortex t

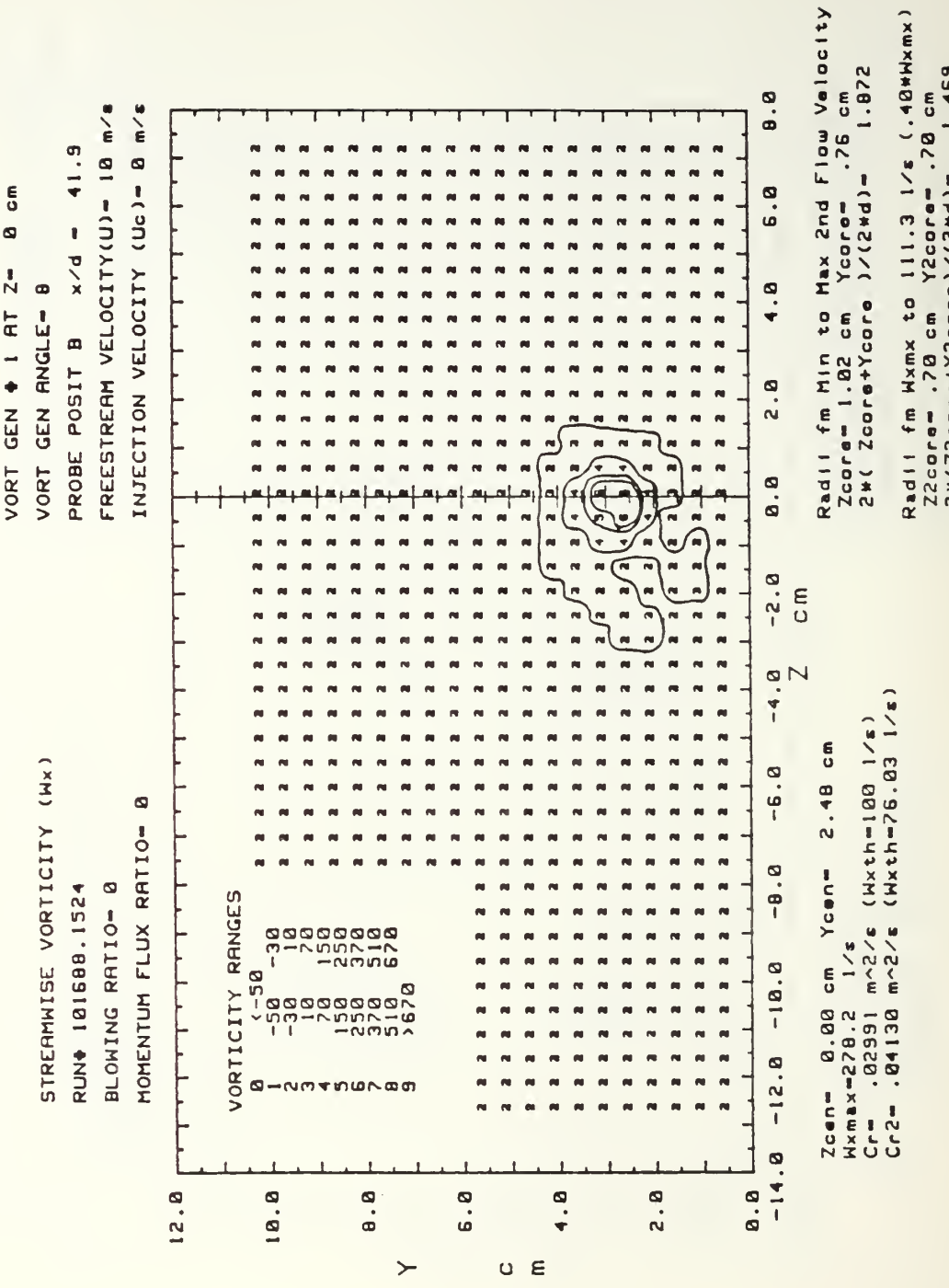

Figure 11. Streamwise Vorticity Contours, m=0
x/d=41.9Γ=.041 m^2/s, Vortex u

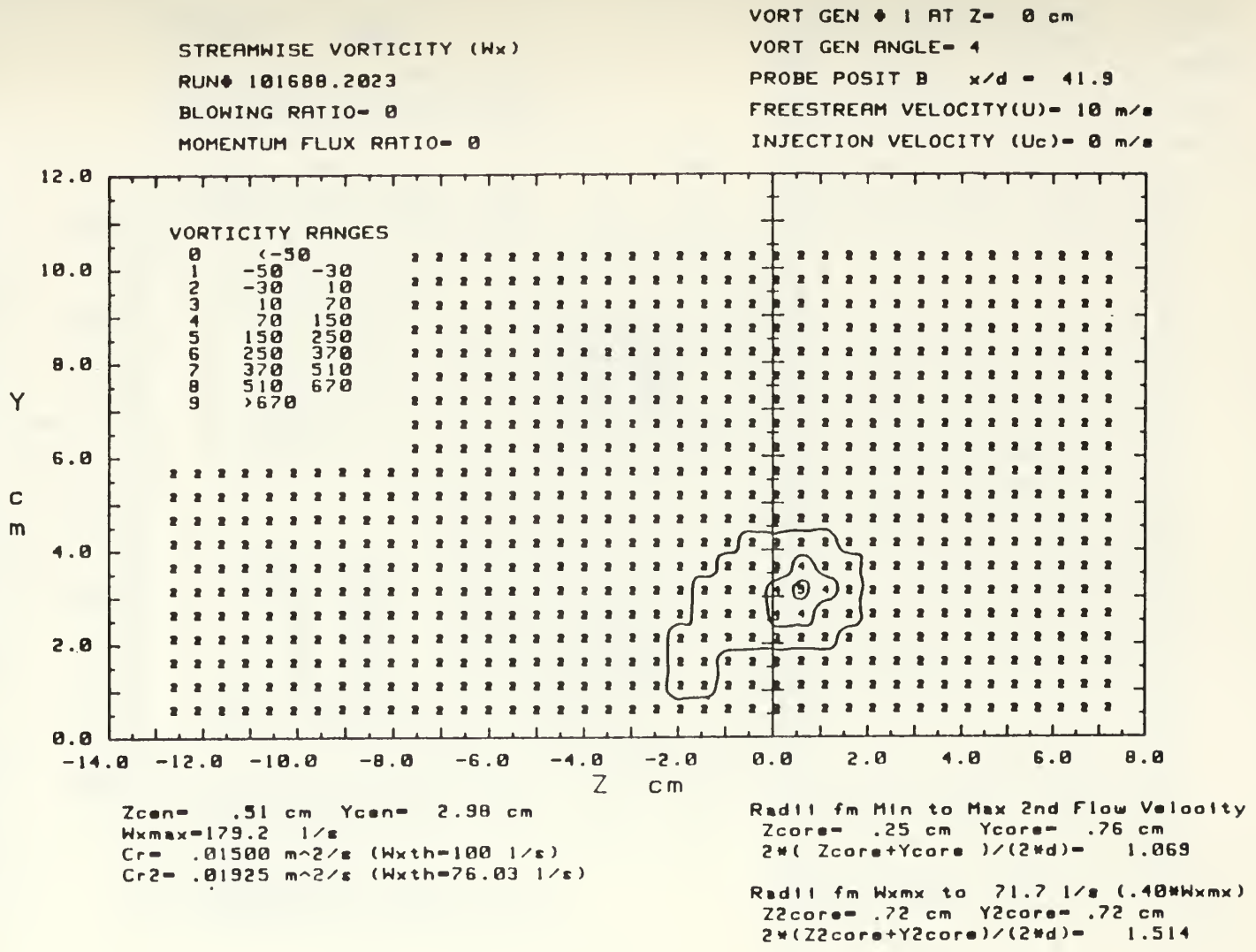

Figure 12. Streamwise Vorticity Contours, M=0 x/d=41.9 Γ=.019 m^2/s, Vortex v

Figure 13. Streamwise Vorticity Contours, x/d=41.9 m=0.5, Single Injection Hole Γ = .151 m^2/s, S=3.17, Vortex r

Figure 14. Streamwise Vorticity Contours, x/d=41.9 m=0.5, Single Injection Hole Γ = .121 m^2/s, S=2.55, Vortex w

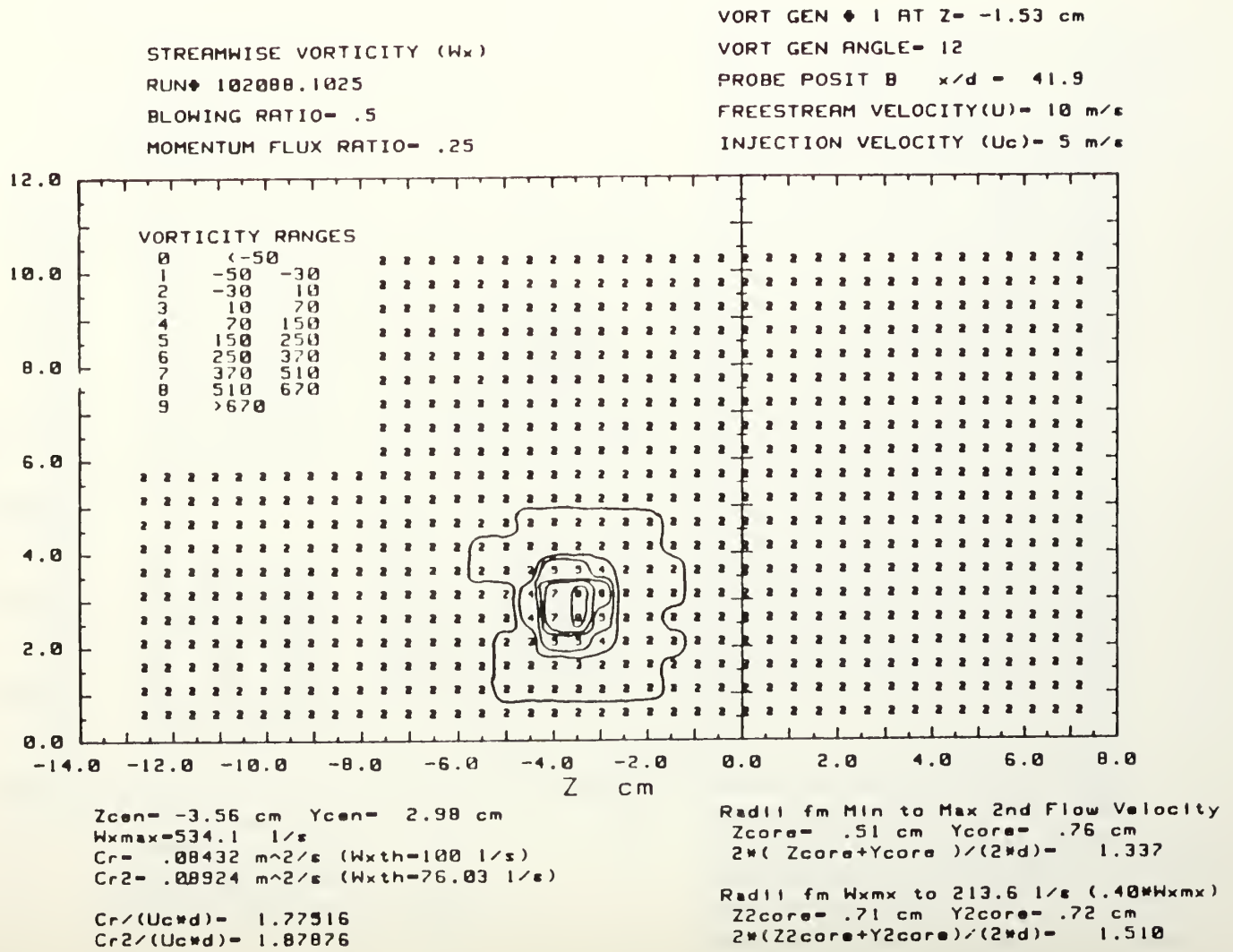

Figure 15. Streamwise Vorticity Contours x/d=41.9 m=0.5, Single Injection Hole Γ = .089 m^2/s, S=1.88, Vortex x

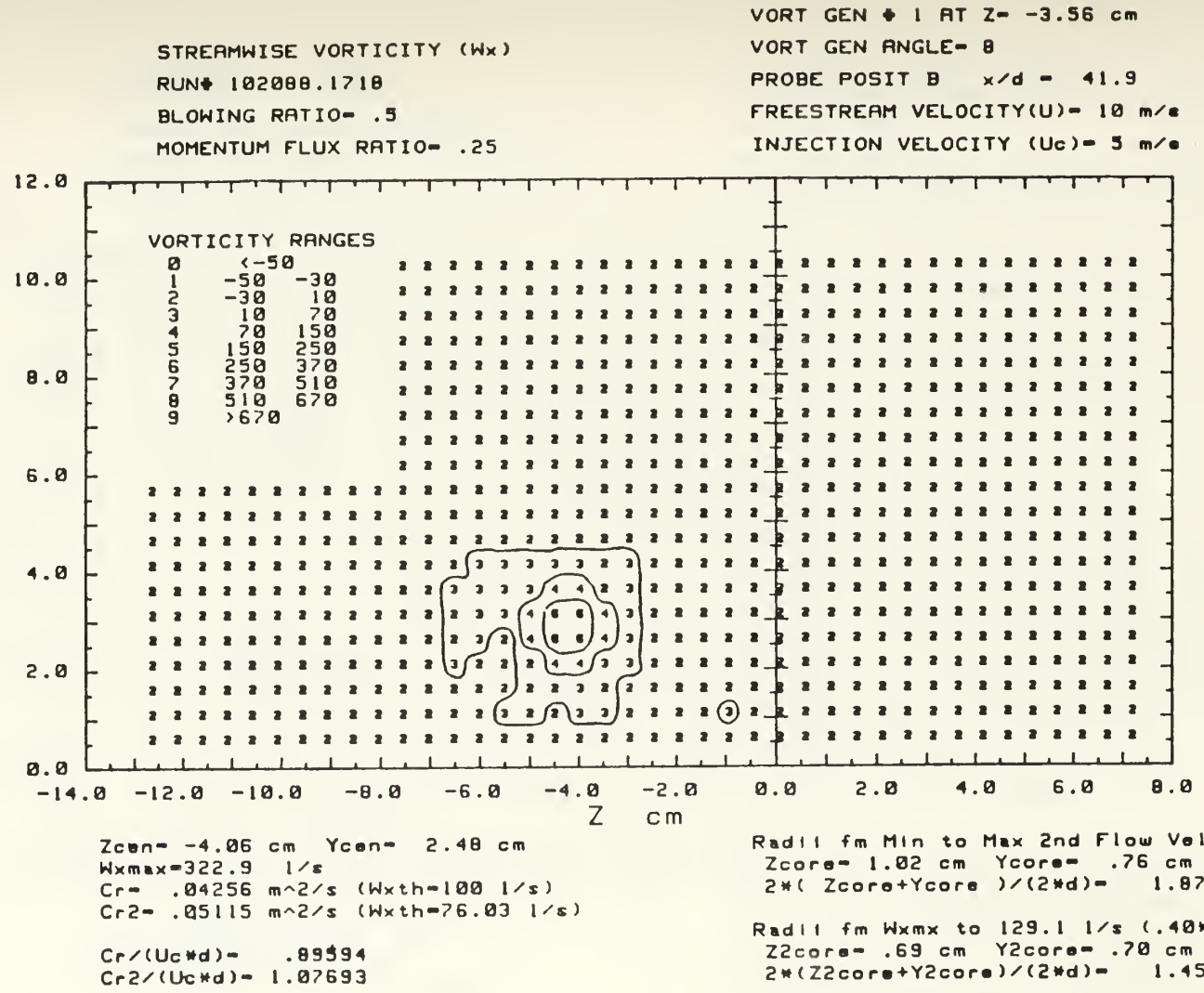

Figure 16. Streamwise Vorticity Contours, x/d=41.9 m=0.5, Single Injection Hole Γ =.051 m^2/s, S=1.08, Vortex Y

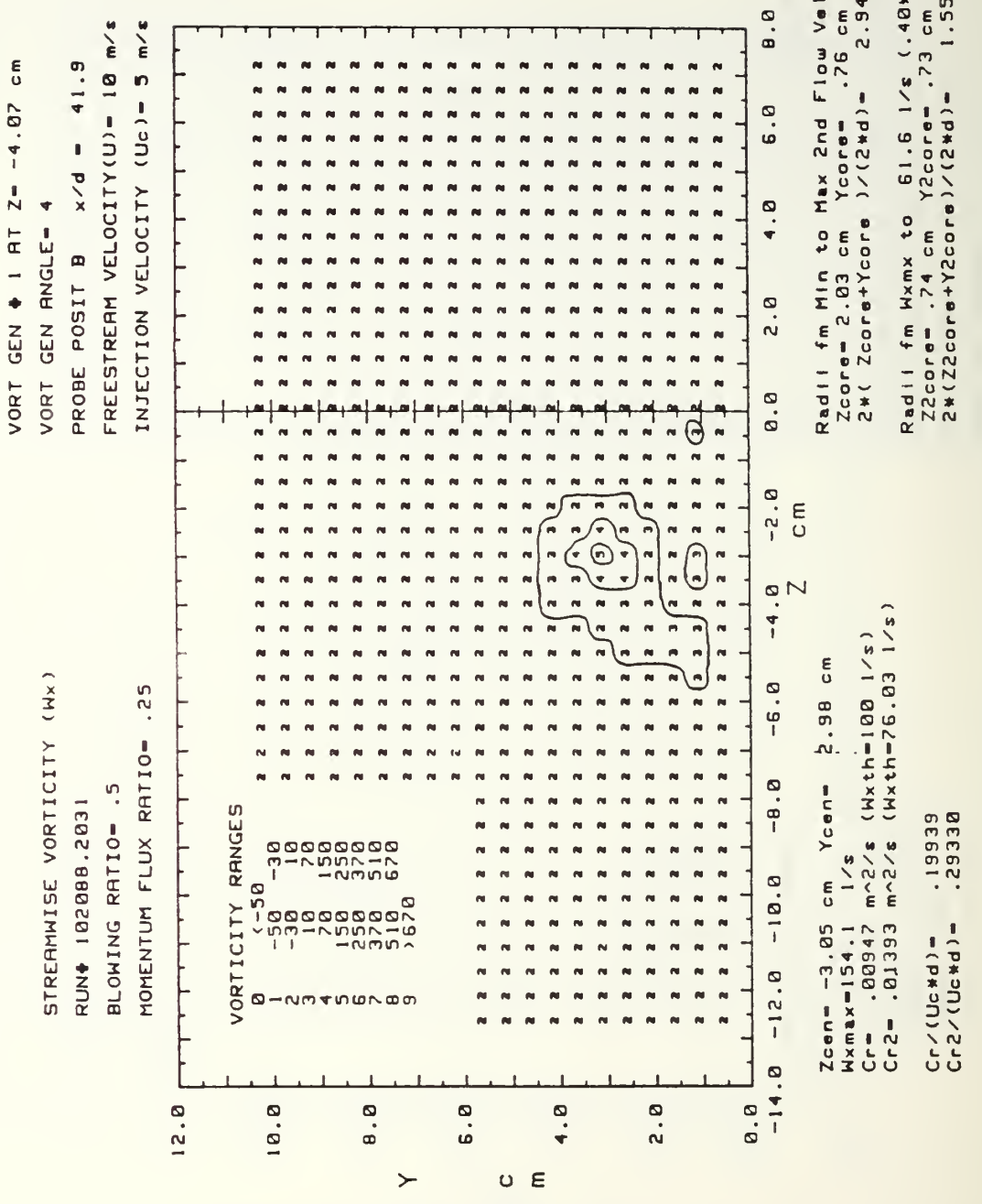

Figure 17. Streamwise Vorticity Contours, x/d=41.9 m=0.5, Single Injection Hole Γ=.014 m^2/s, S=0.29, Vortex z

Figure 18. Streamwise Vorticity Contours, x.d=41.9 m=0.5, 13 Injection Holes, Γ =.134 m^2/s, S=2.81, Vortex r

Figure 19. Streamwise Vorticity Contours, x/d=41.9 m=0.5, 13 Injection Holes, Γ=.111, m^2/s, S=2.33, Vortex w

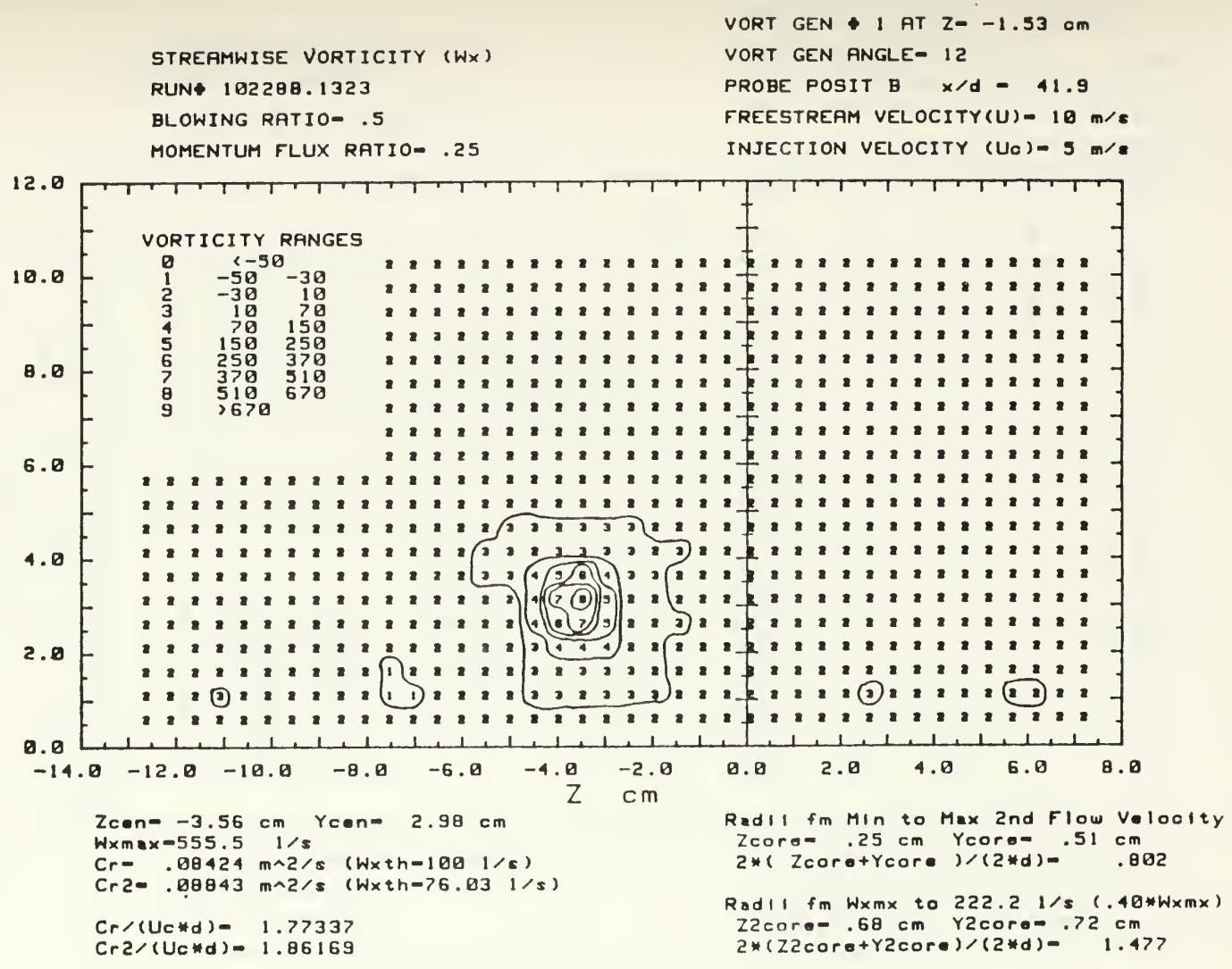

Figure 20. Streamwise Vorticity Contours, x/d=41.9 m=0.5, 13 Injection Holes, Γ =.088 m^2/s, S=1.86, Vortex x

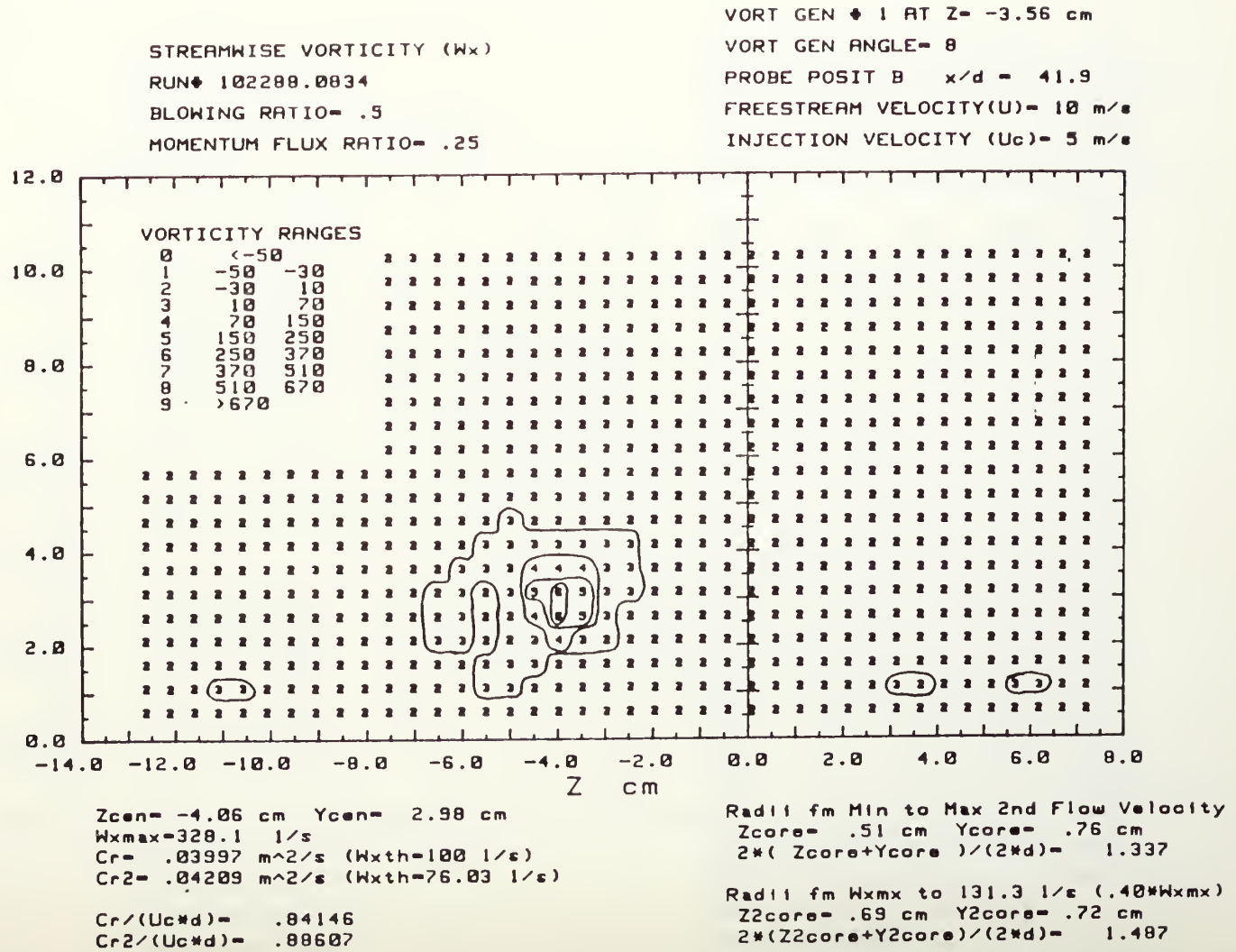

Figure 21. Streamwise Vorticity Contours, x/d=41.9 m=0.5, 13 Injection Holes, Γ =.042 m^2/s, S=0.89, Vortex y

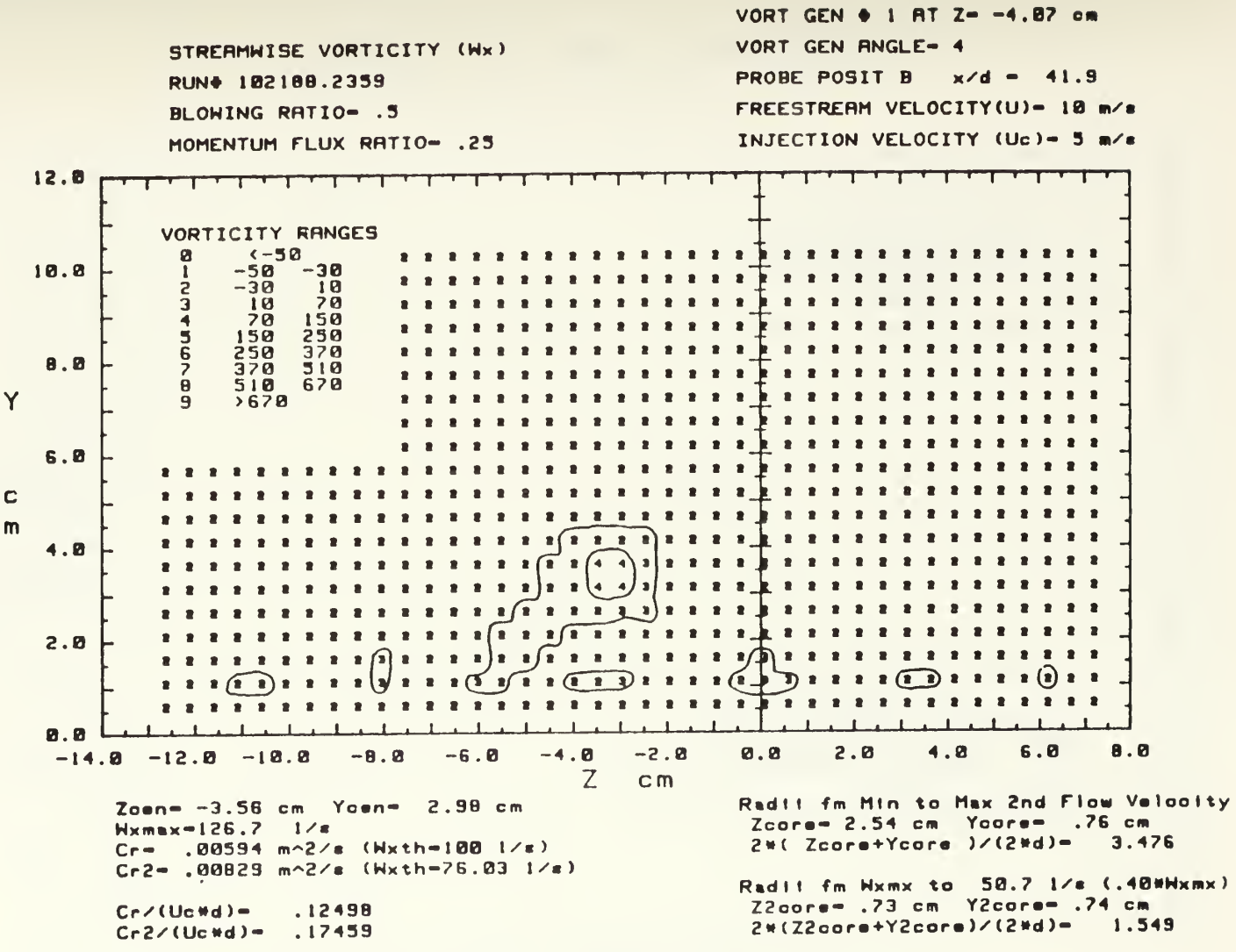

Figure 22. Streamwise Vorticity Contours, x/d=41.9 m=0.5, 13 Injection Holes, Γ =.008 m^2/s, S=0.17, Vortex 2

Figure 23. Spanwise Location of Vortex Center (Zcen) vs. Vortex Generator Angle

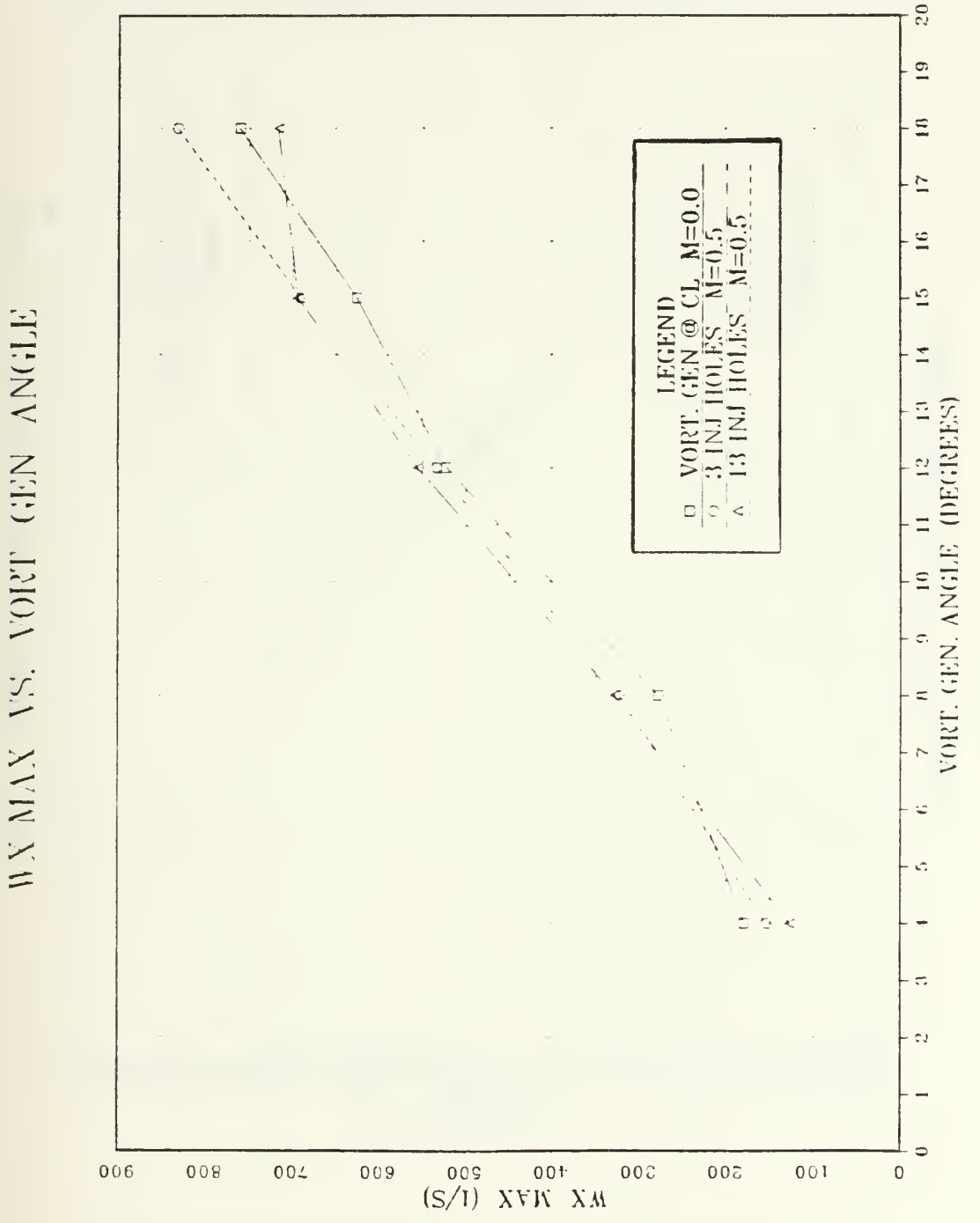

Figure 24. Maximum Streamwise Vorticity (Wxmax) vs. Vortex Generator Angle

Figure 25. Vortex Circulation vs. Vortex Generator Angle

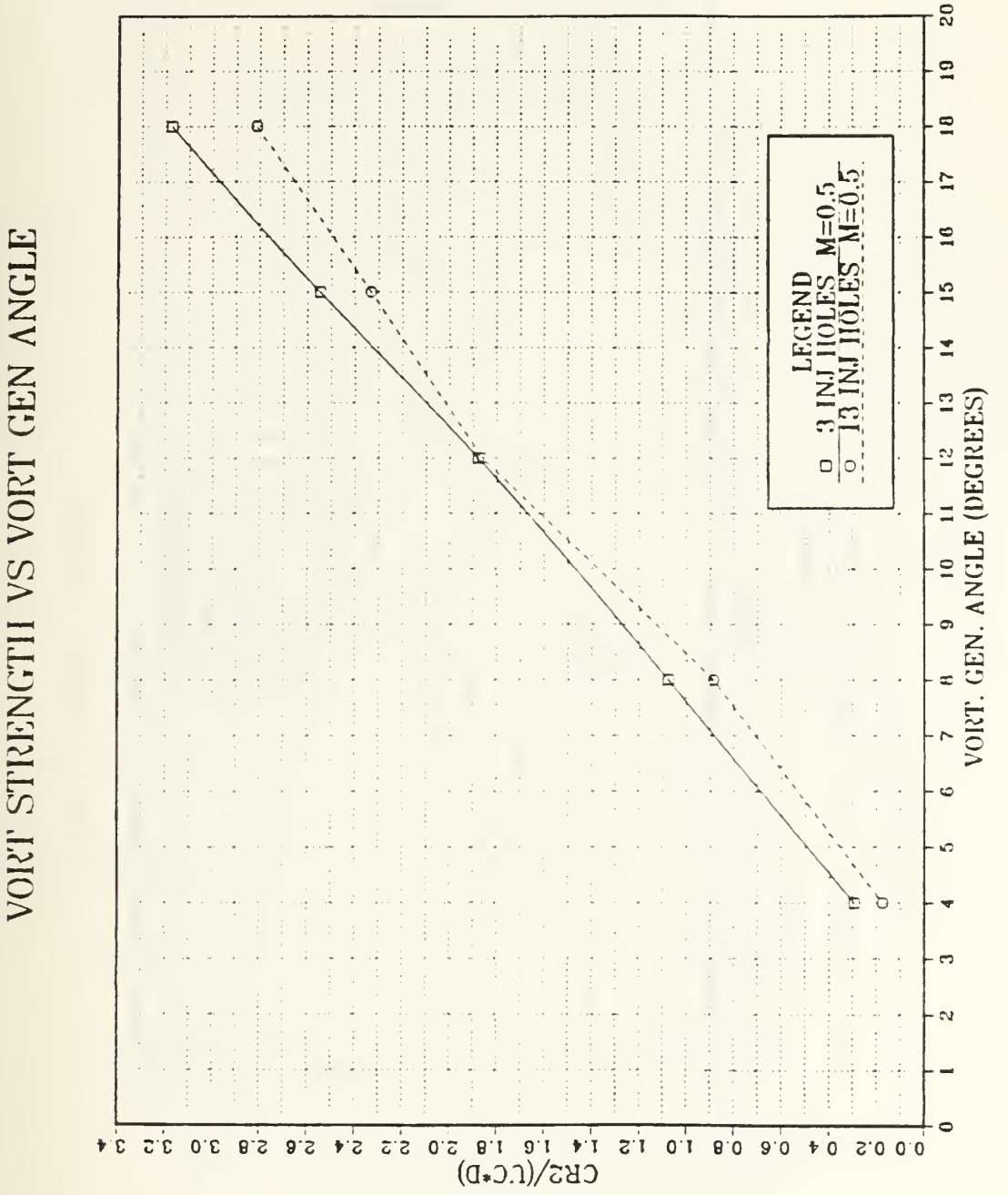

Figure 26. Vortex Strength [Γ /(Uc•d)] vs Vortex Generator Angle

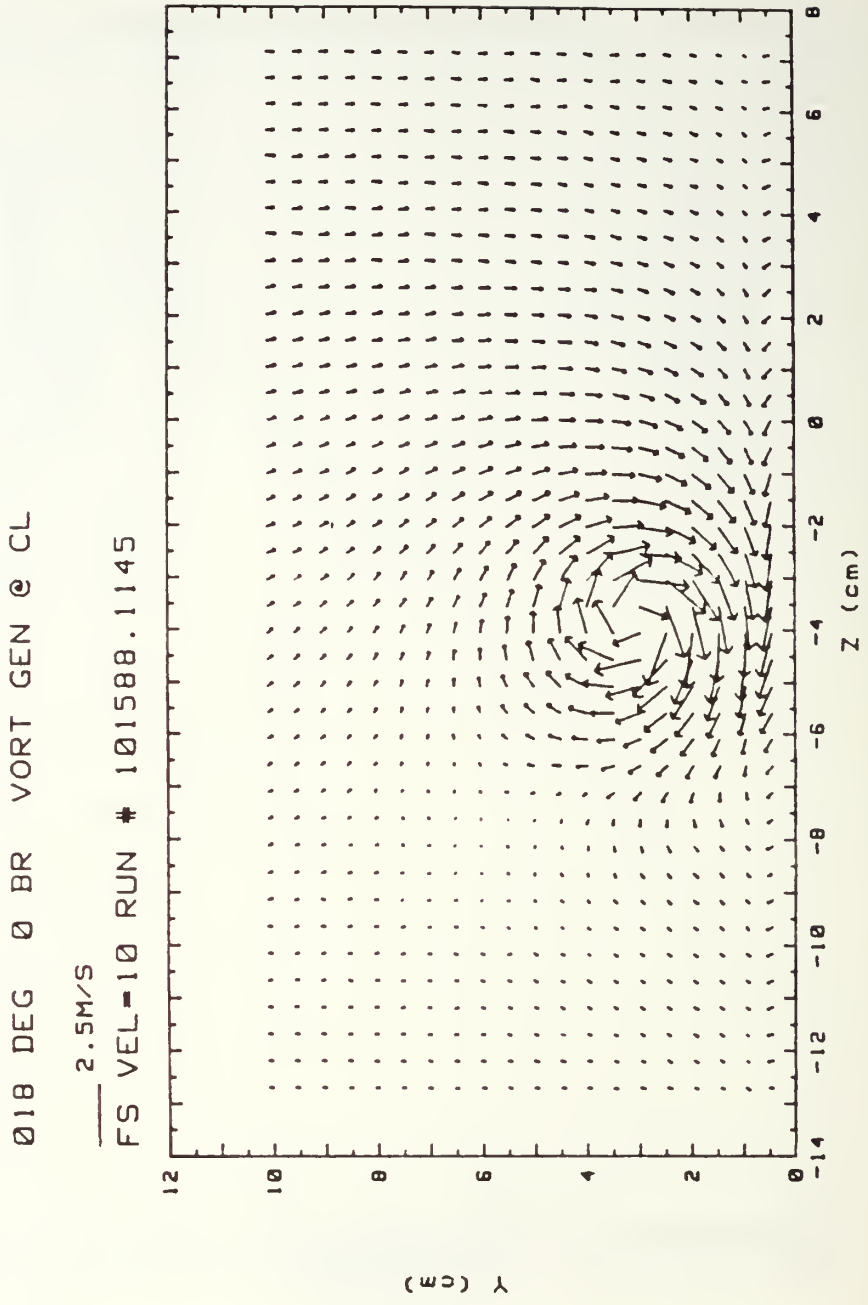

Figure 27. Secondary Flow Vectors, m=0, x/d= 41.9Γ=.149 m^2/s, Vortex r

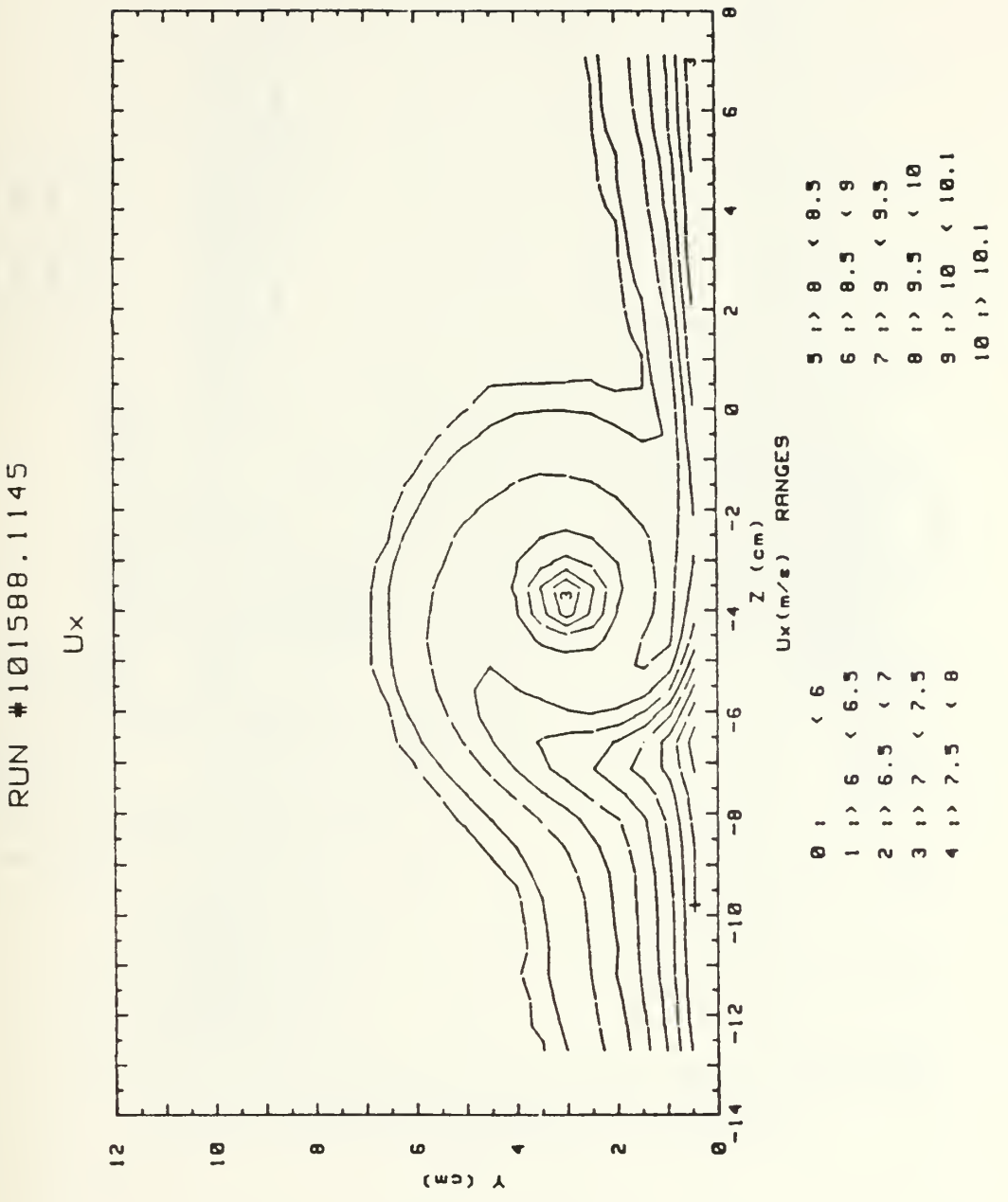

Figure 28. Streamwise Velocity Field, m-0, x/d=41.9 Γ=.149 m^2/s, Vortex r

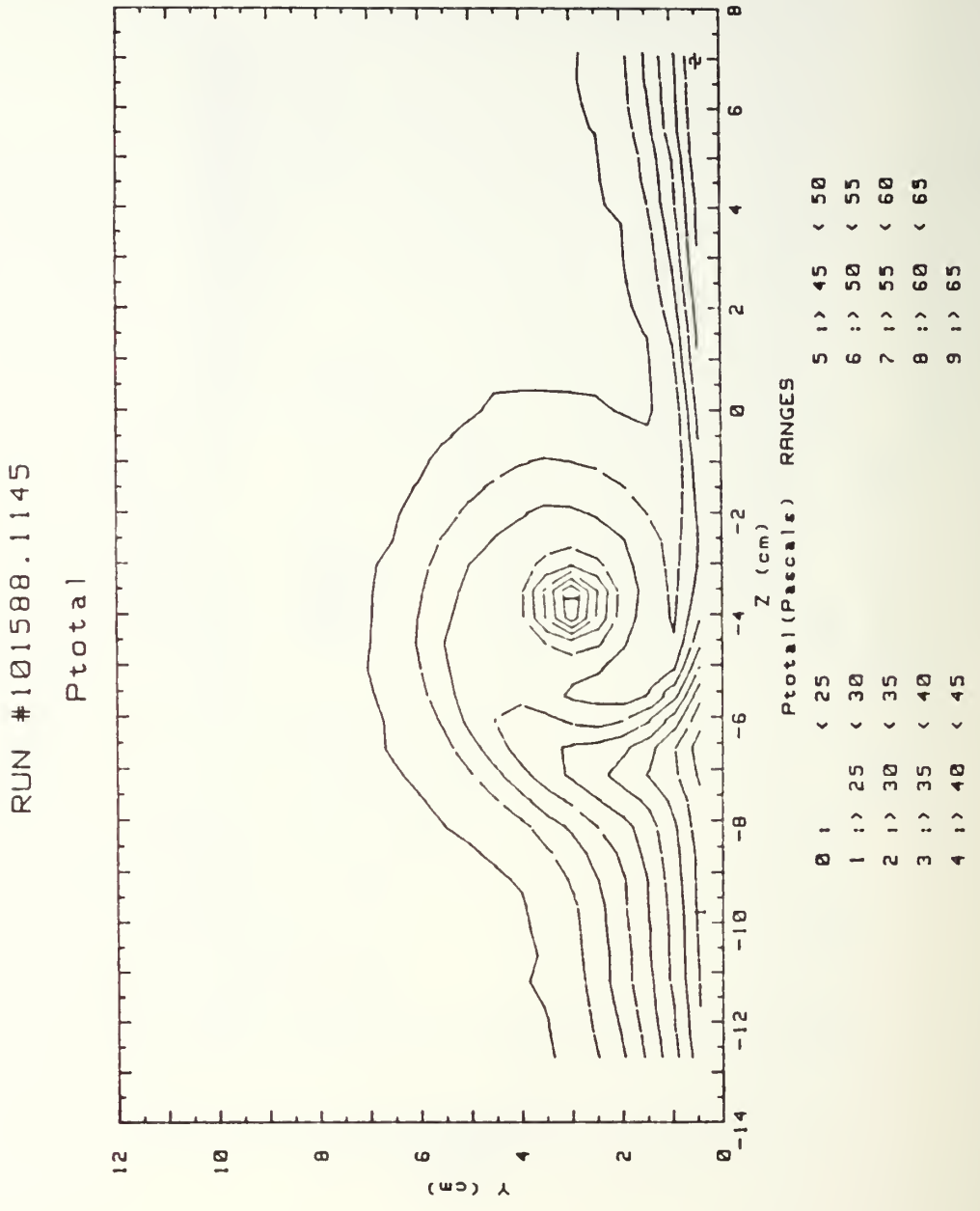

Figure 29. Total Pressure Field, m-0, x/d= 41.9Γ=.149 m^2/s, Vortex r

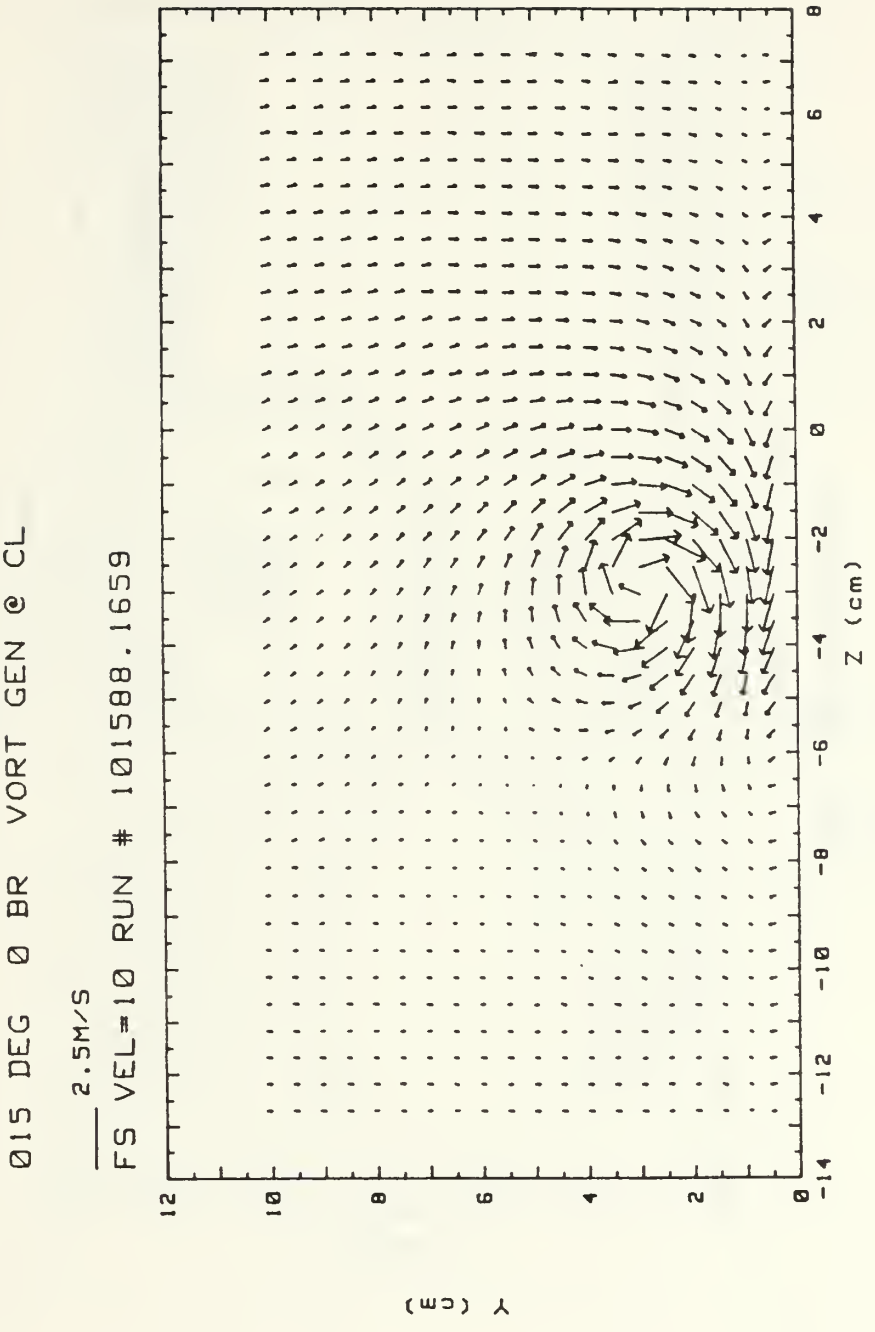

Figure 30. Secondary Flow Vectors, m-0, x/d=41.9Γ=.115 m^2/s, Vortex s

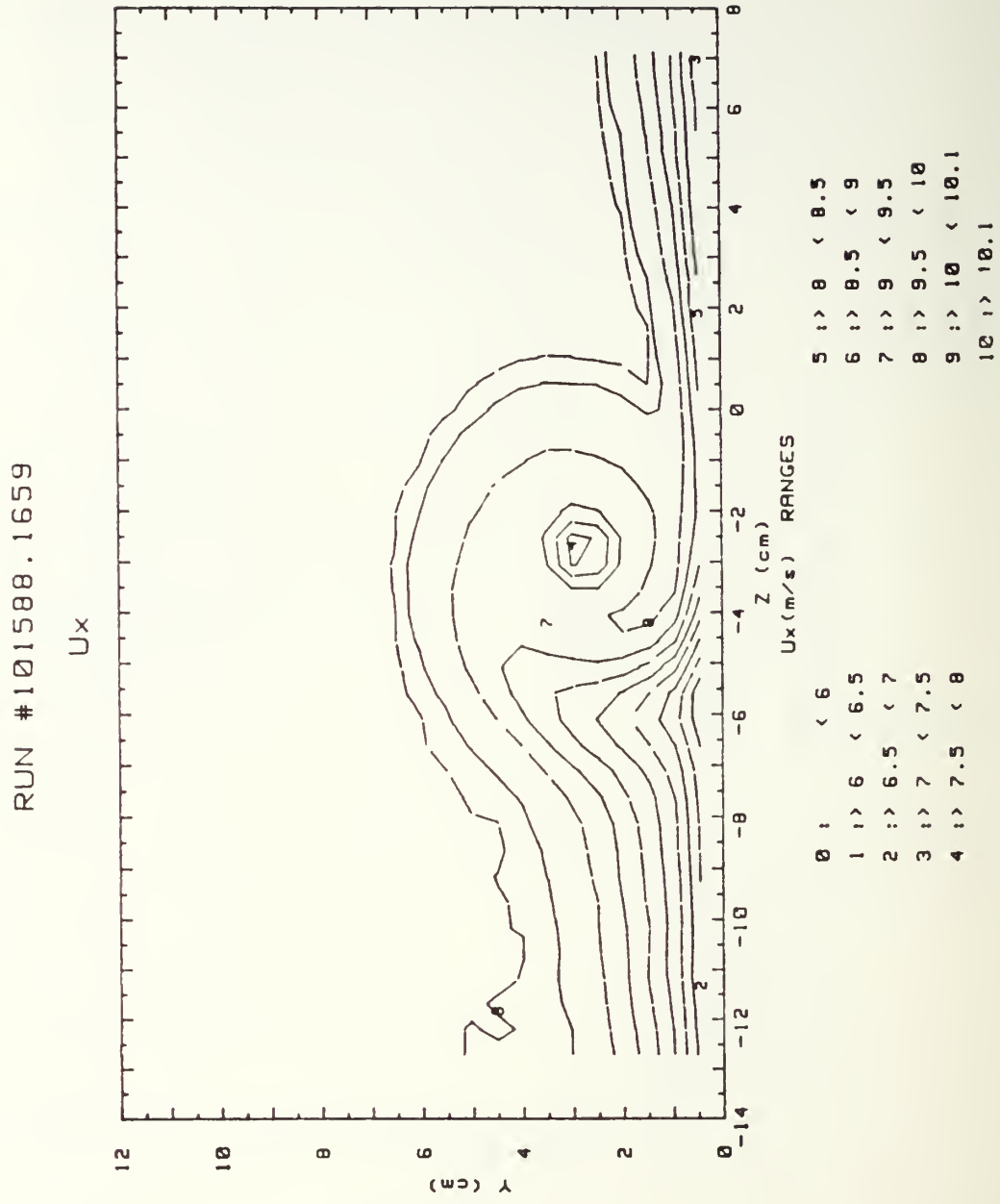

Figure 31. Streamwise Velocity Field, m-0, x/d=41.9Γ=.115 m^2/s, Vortex s

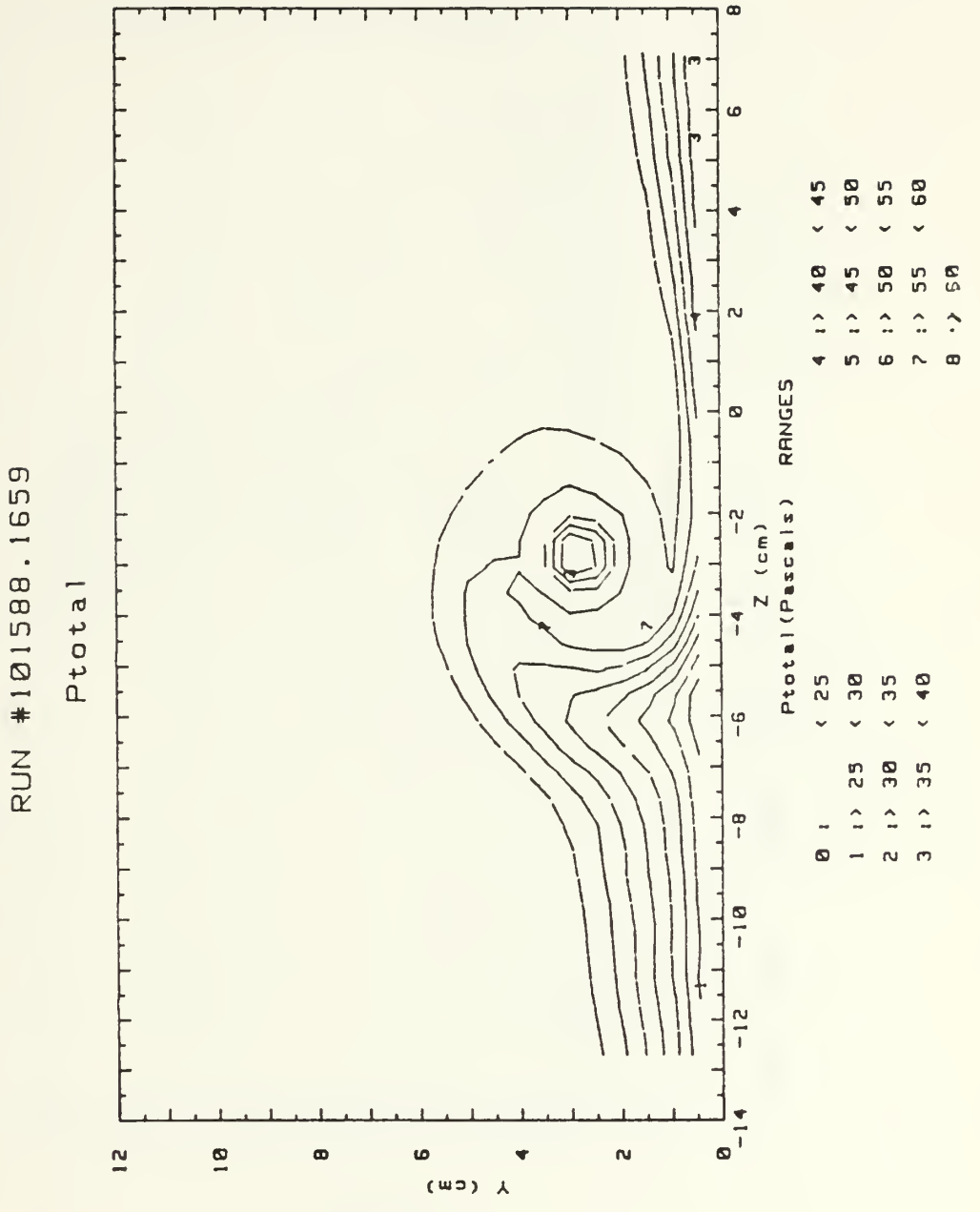

Figure 32. Total Pressure Field, m=0, x/d=41.9Γ=.115 m^2/s, Vortex s

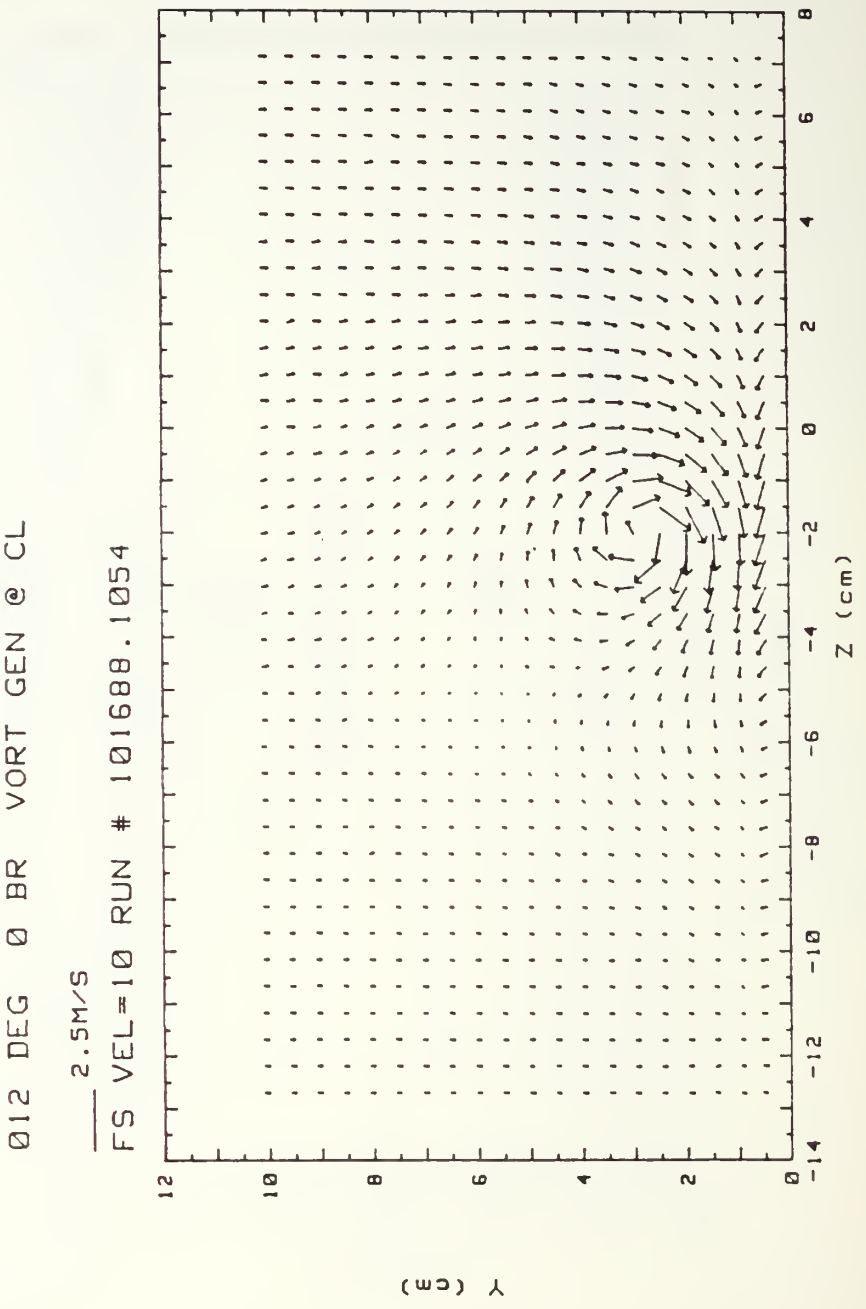

Figure 33. Secondary Flow Vectors, m=0, x/d=41.9Γ=.085 m^2/s, Vortex t

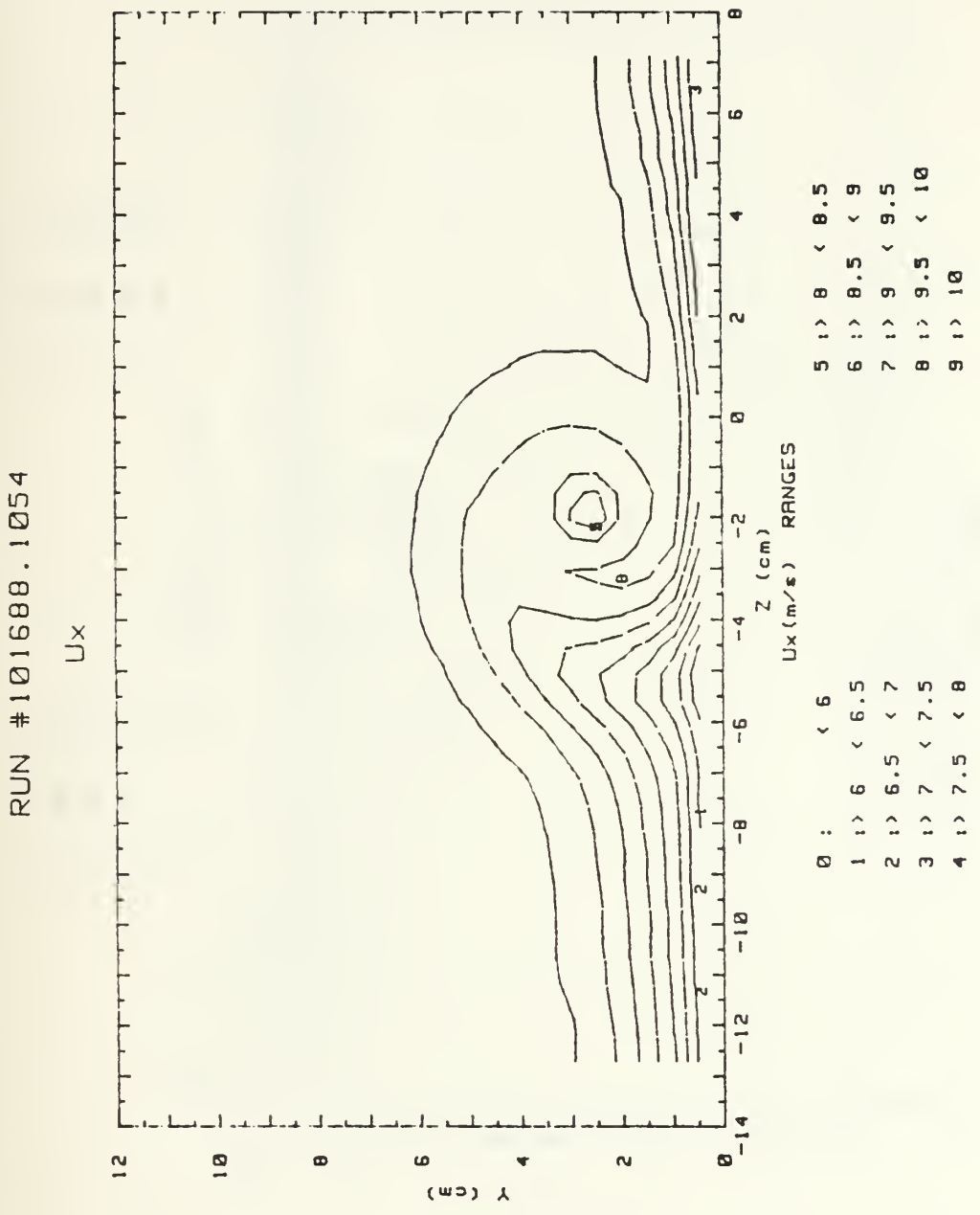

Figure 34. Streamwise Velocity Field, m=0, x/d=41.9 Γ=.085 m^2/s, Vortex t

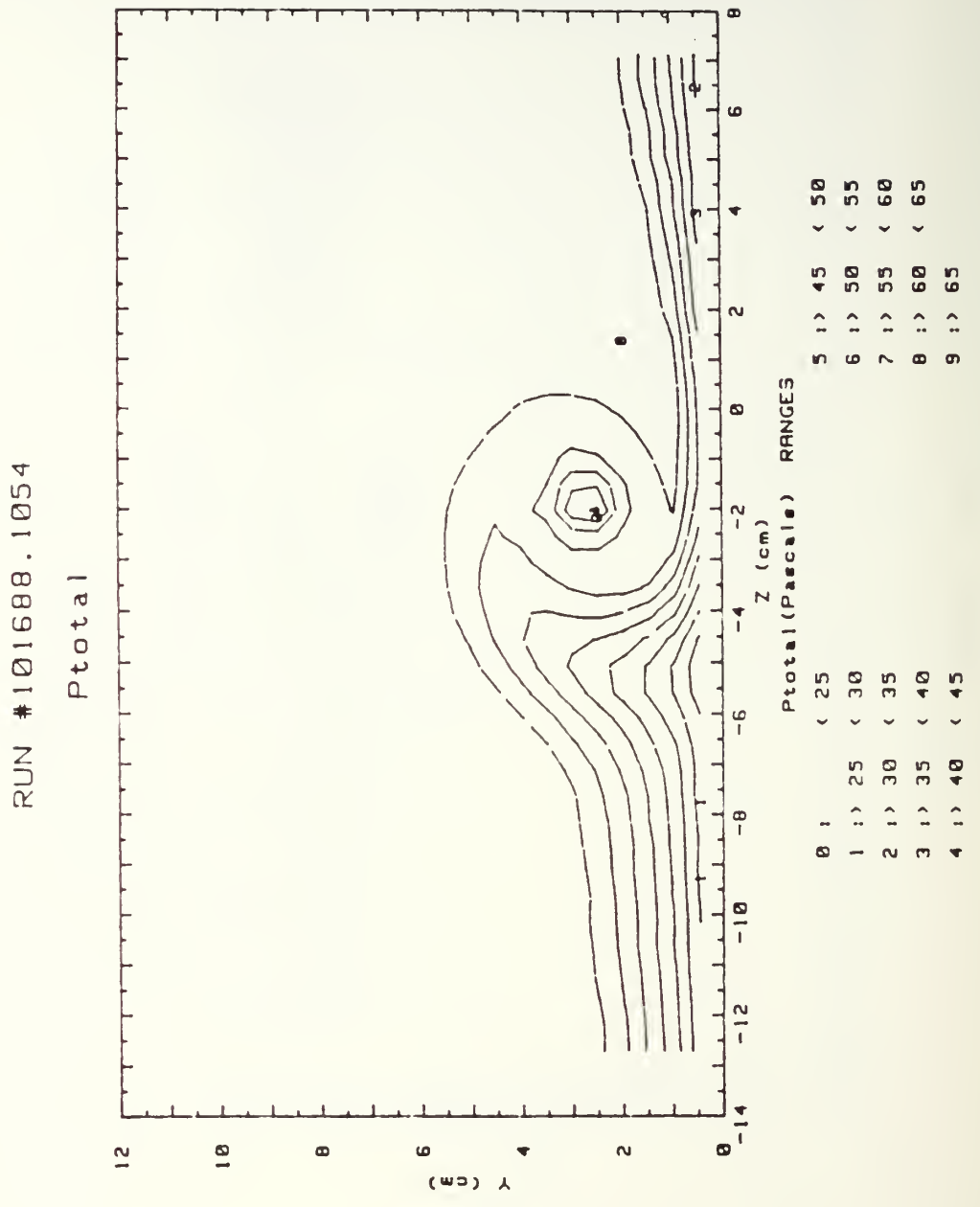

Figure 35. Total Pressure Field, m=0, x/d=41.9Γ=.085 m^2/s, Vortex t

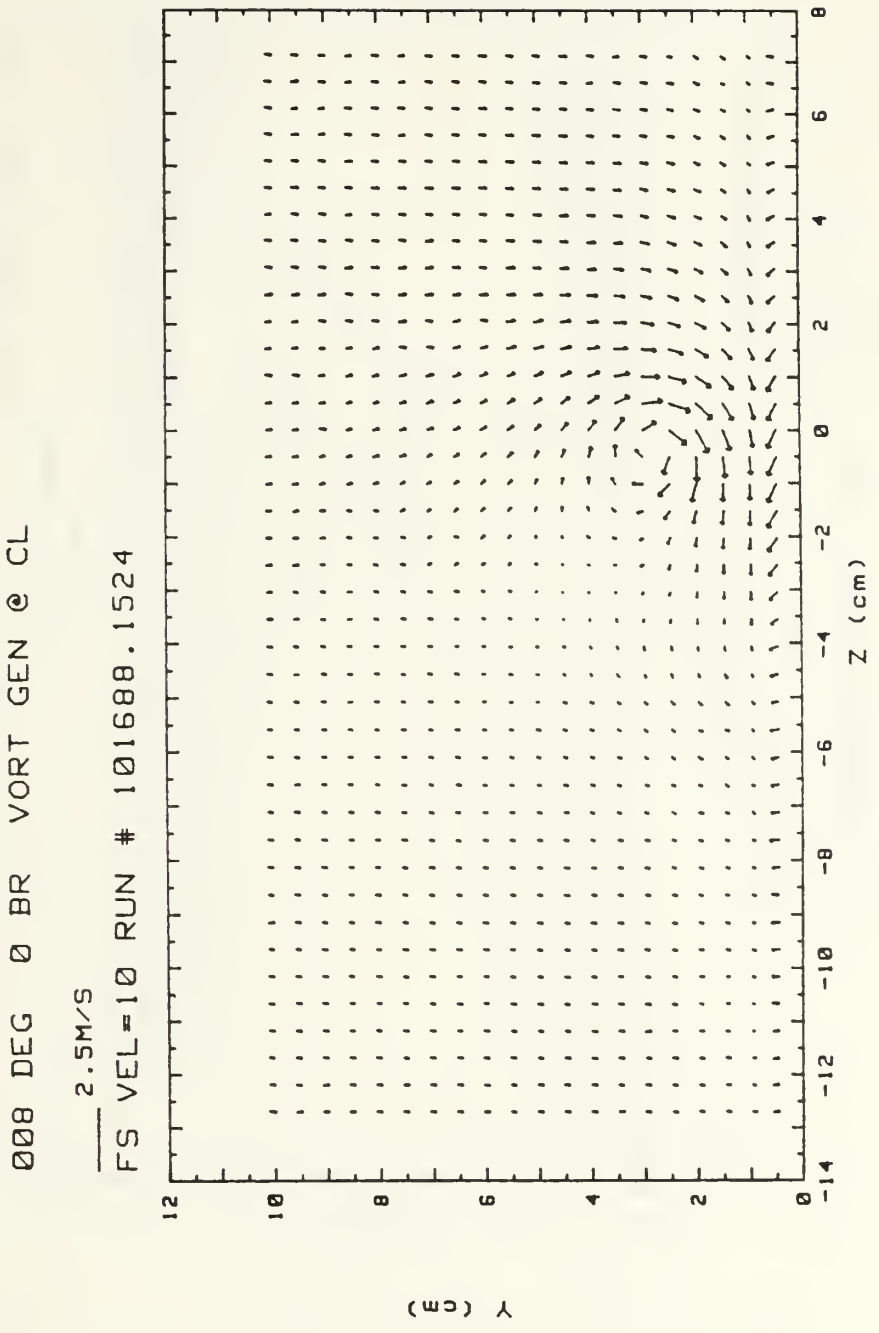

Figure 36. Secondary Flow Vector, m=0, x/d=41.9 Γ=.041 m^2/s, Vortex u

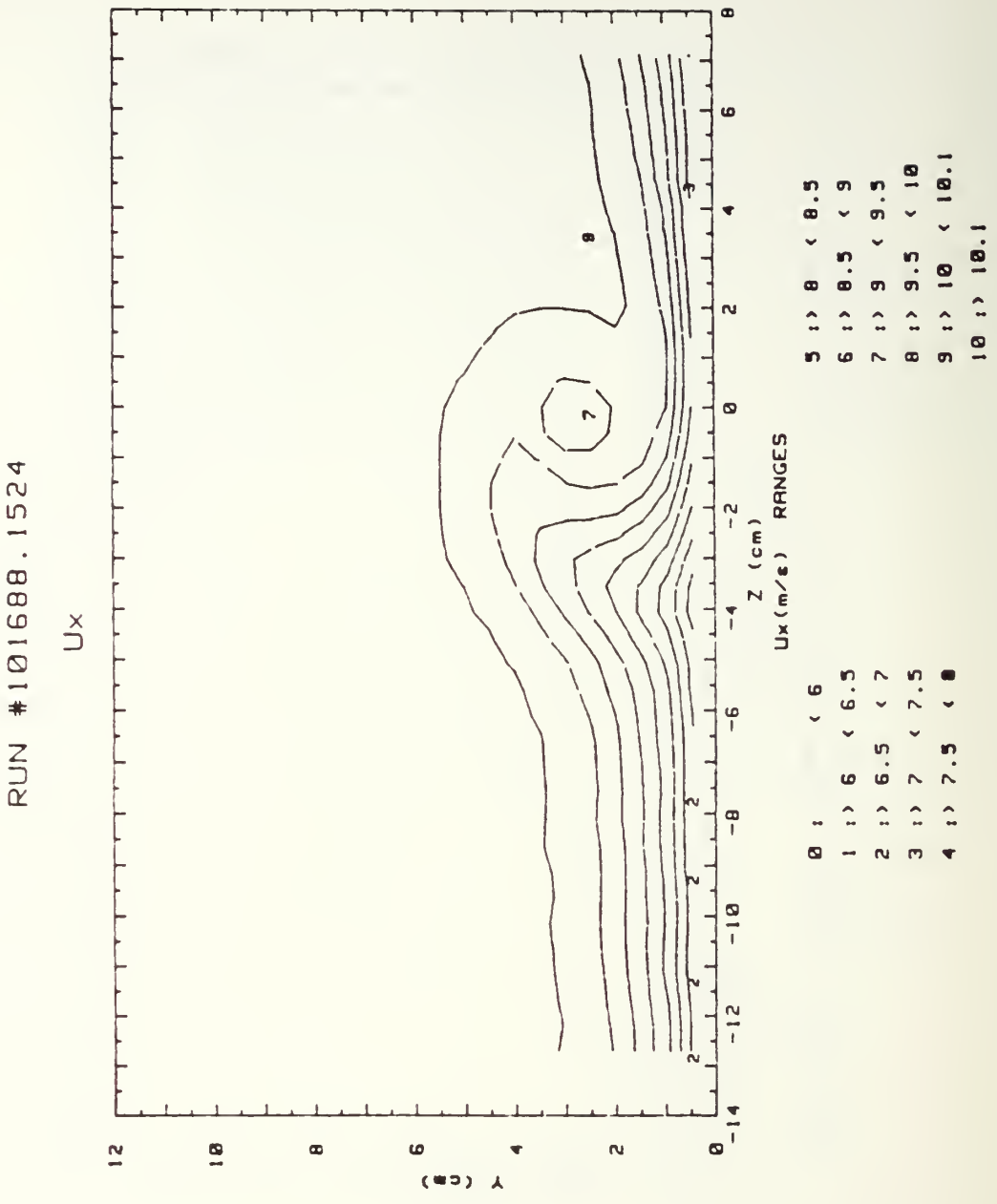

Figure 37. Streamwise Velocity Field, m=0, x/d=41.9Γ=.041 m^2/s, Vortex u

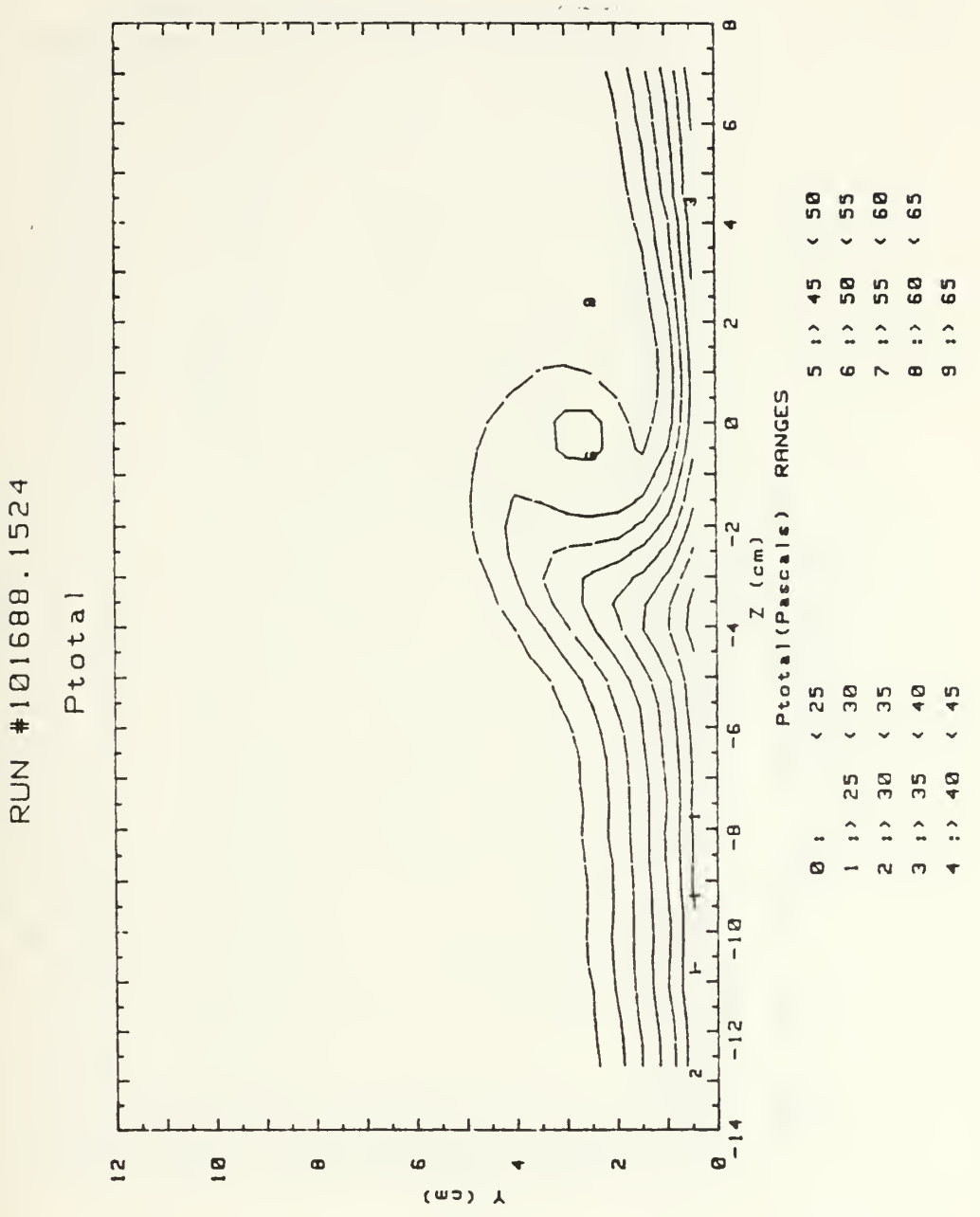

Figure 38. Total Pressure Field, m=0, x/d=41.9 Γ=.041 m^2/s, Vortex u

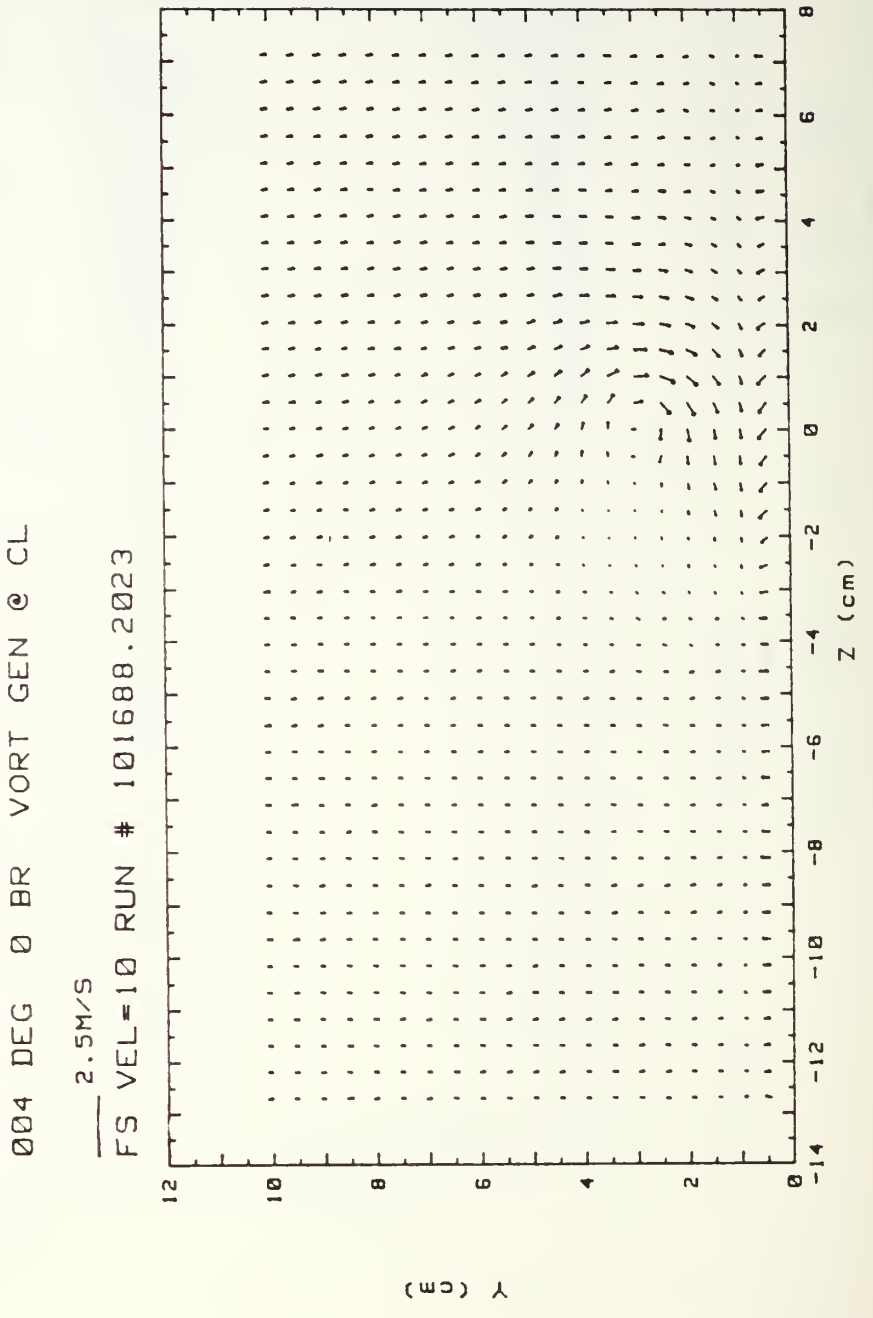

Figure 39. Secondary Flow Vectors, m=0, x/d=41.9 Γ=.019 m^2/s, Vortex v

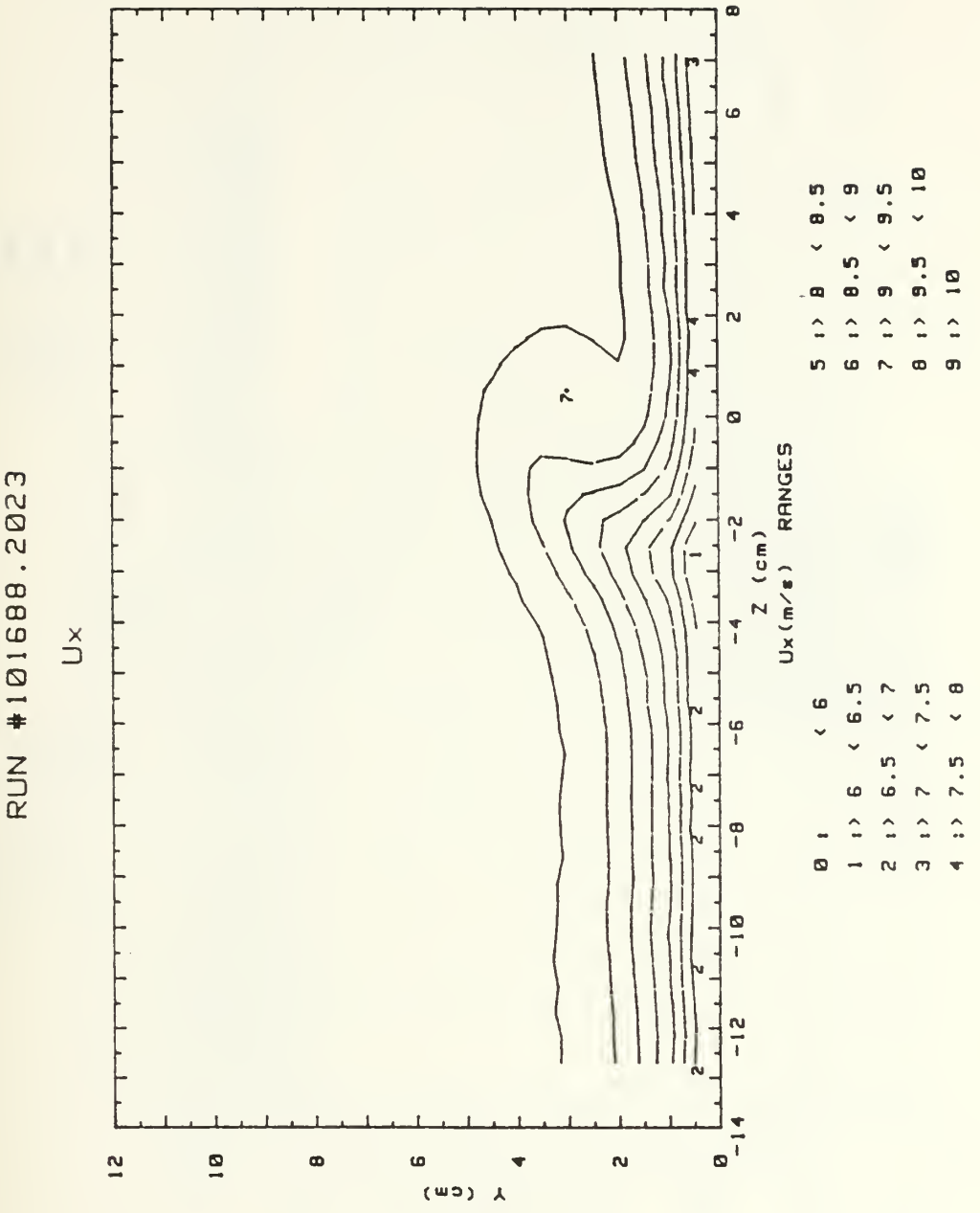

Figure 40. Streamwise Velocity Field, m=0, x/d=41.9 Γ=.019 m^2, Vortex v

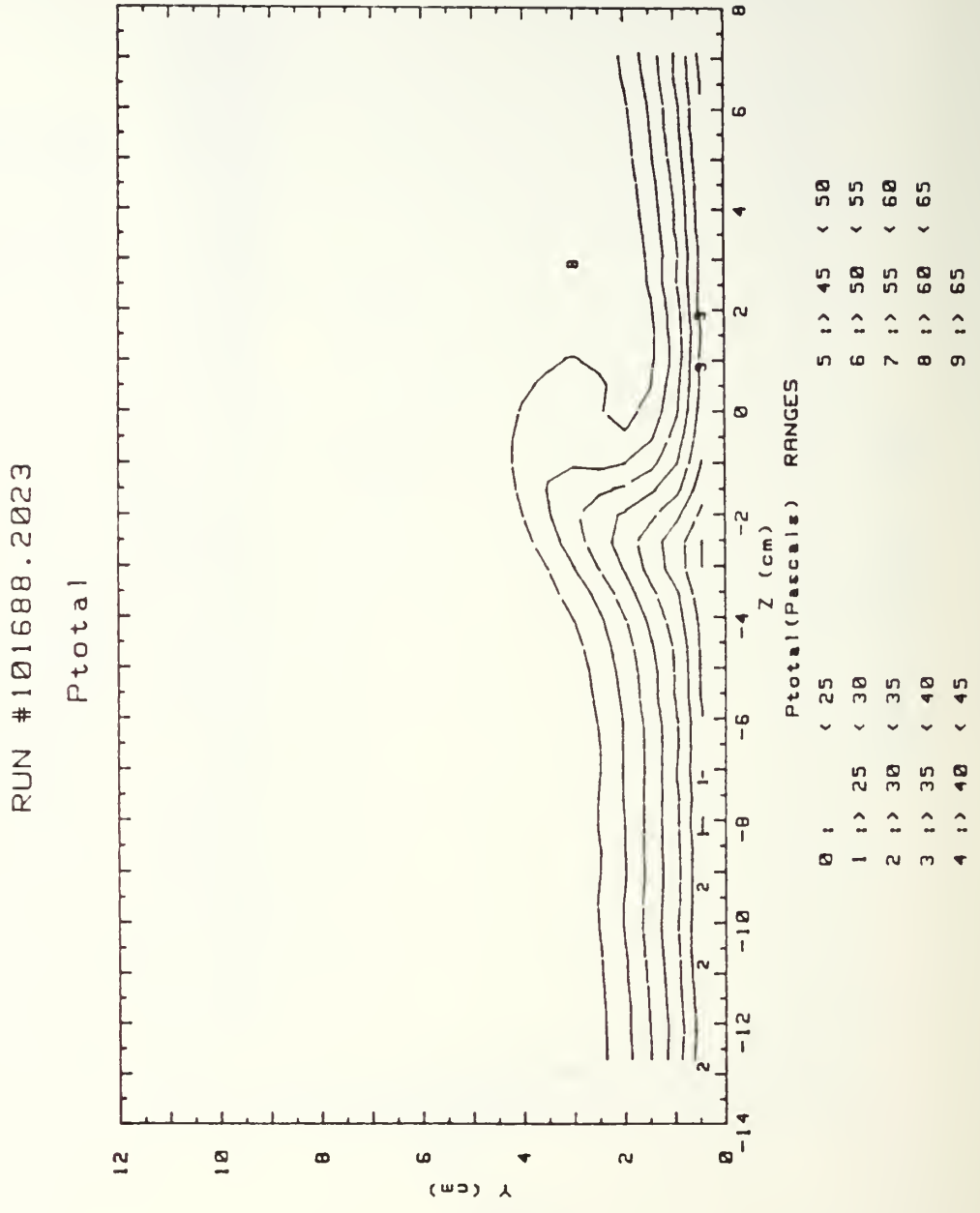

Figure 41. Total Pressure Field, m=0, x/d=41.9 Γ=.019 m^2/s, Vortex v

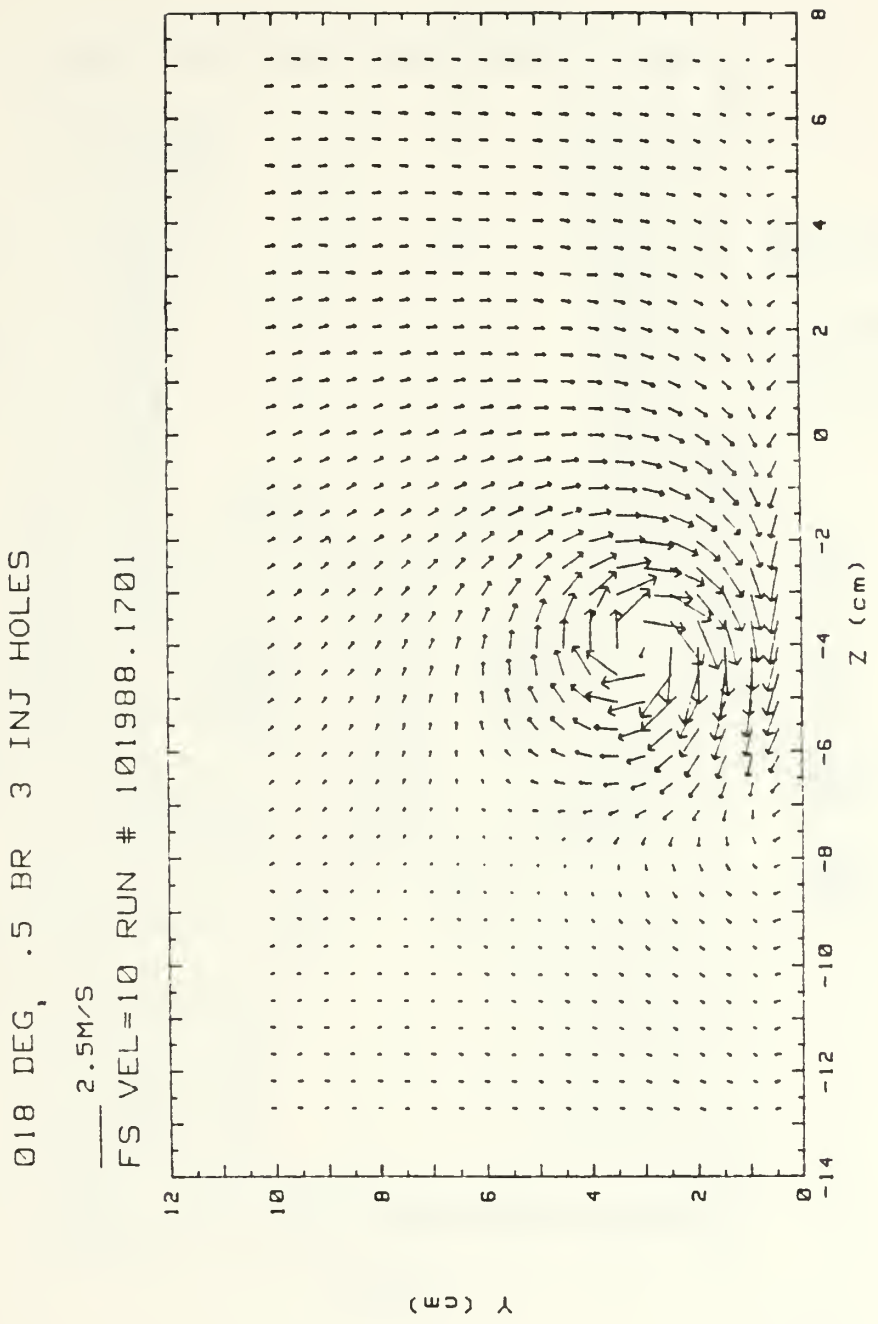

Figure 42. Secondary Flow Vectors, x/d=41.9 $\blacksquare$=0.5, Single Injection Hole, Γ =.151 m^2/s, S=3.17, Vortex r

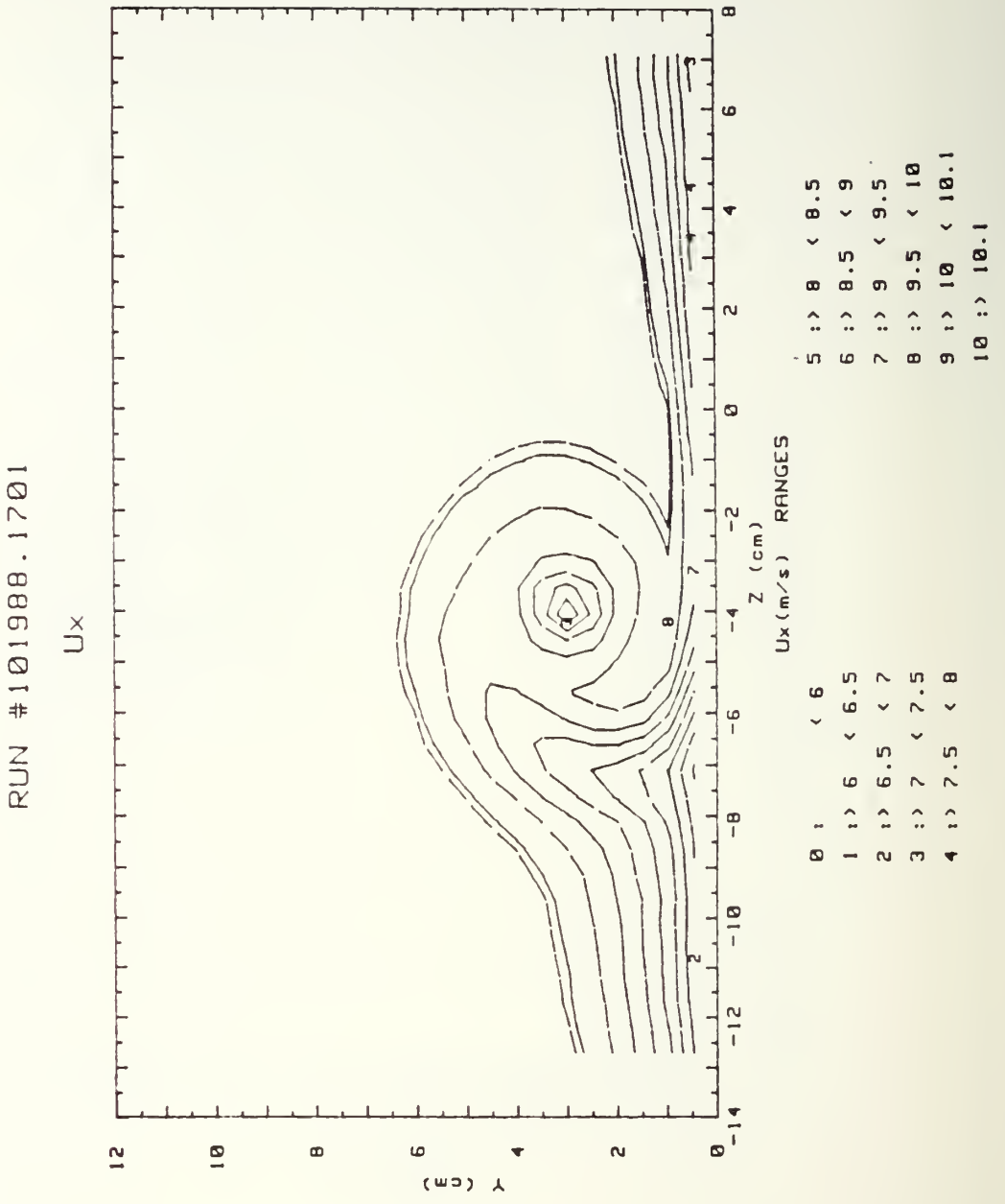

Figure 43. Streamwise Velocity Field, x/d=41.9 m=0.5, Single Injection Hole, Γ =.151 m^2/s, S=3.17, Vortex r

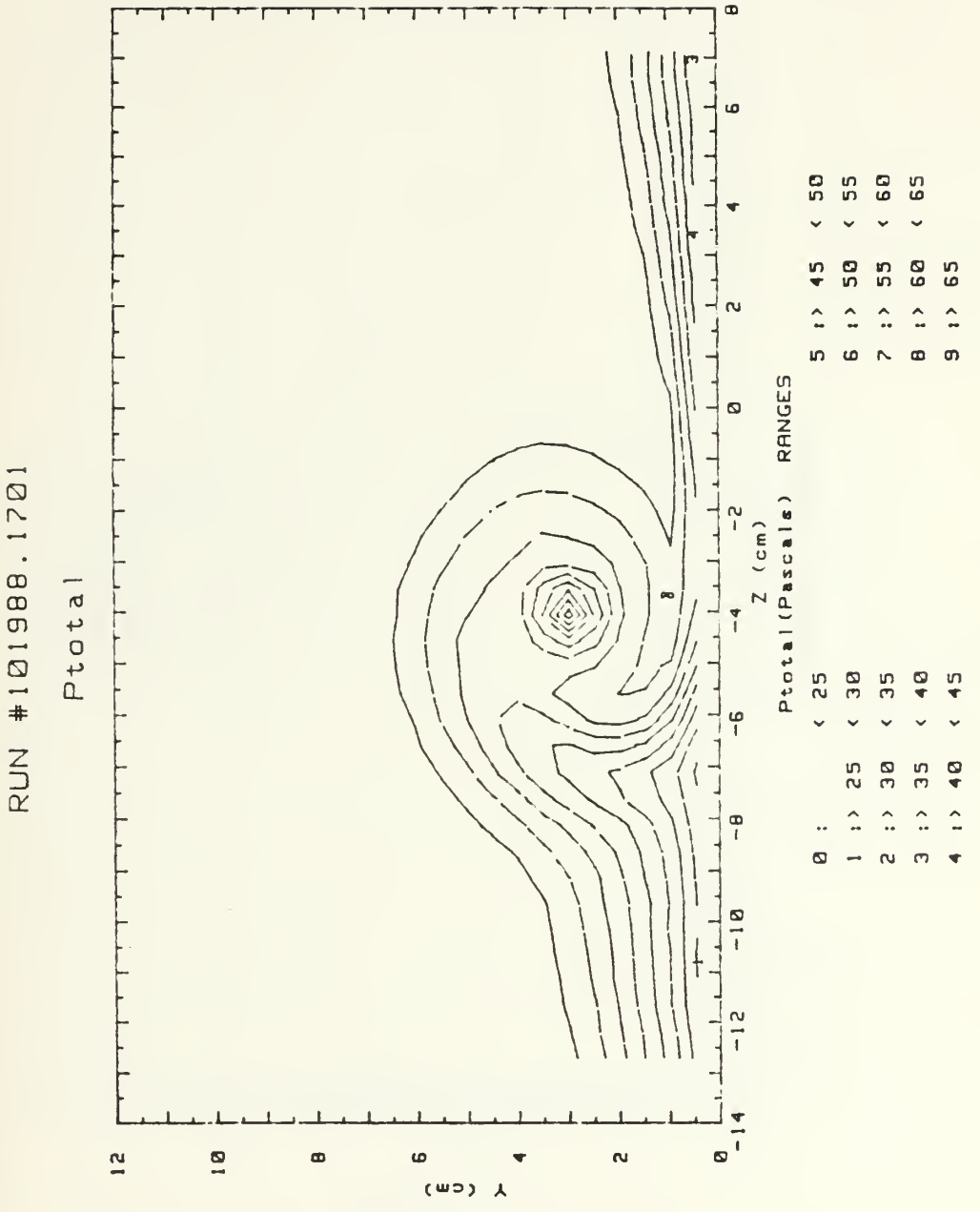

Figure 44. Total Pressure Field, x/d=41.9 m=0.5, Single Injection Hole, Γ=.151 m^2/s, S=3.17, Vortex r

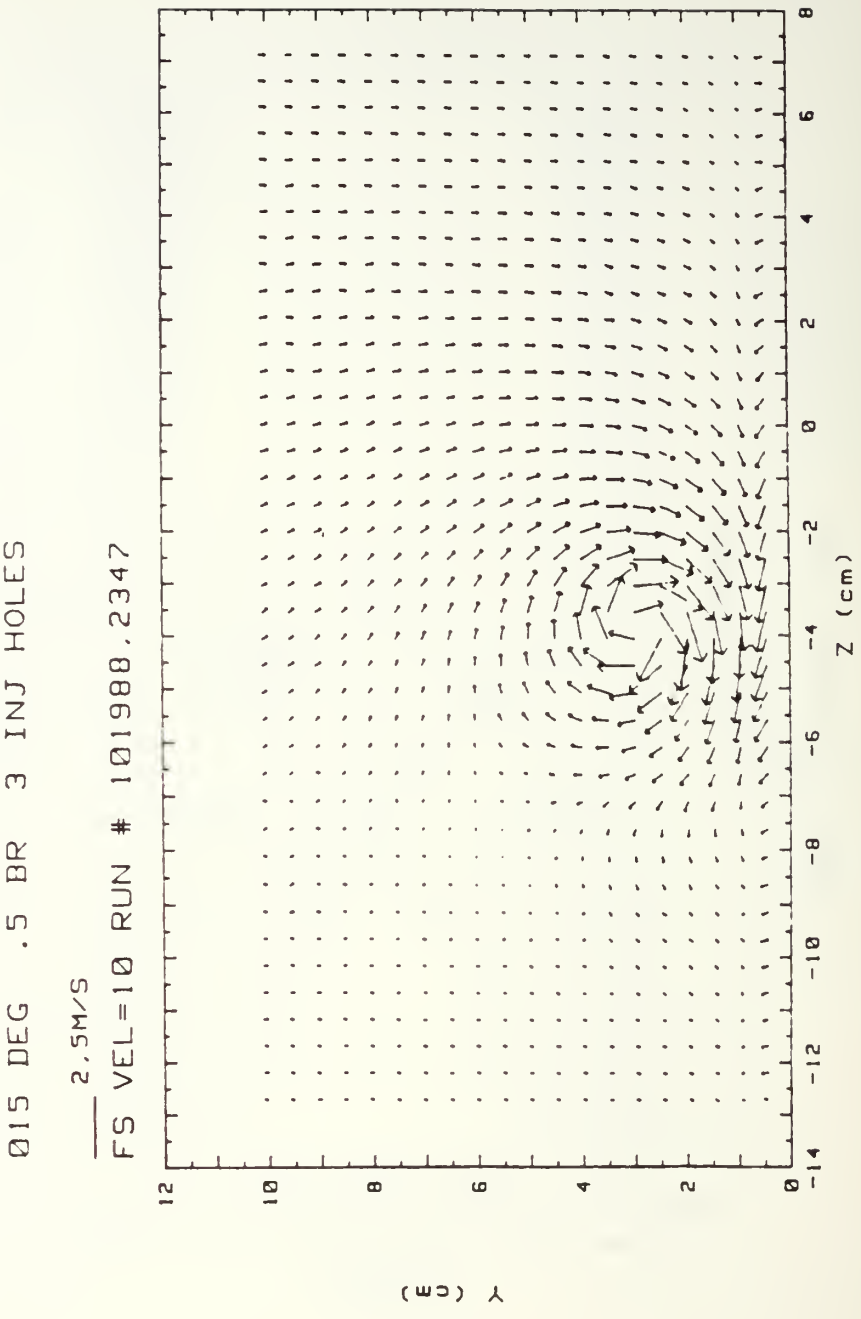

Figure 45. Secondary Flow Vectors, x/d=41.9 m=0.5, Single Injection Hole, Γ=.121 m^2/s, S=2.55, Vortex w

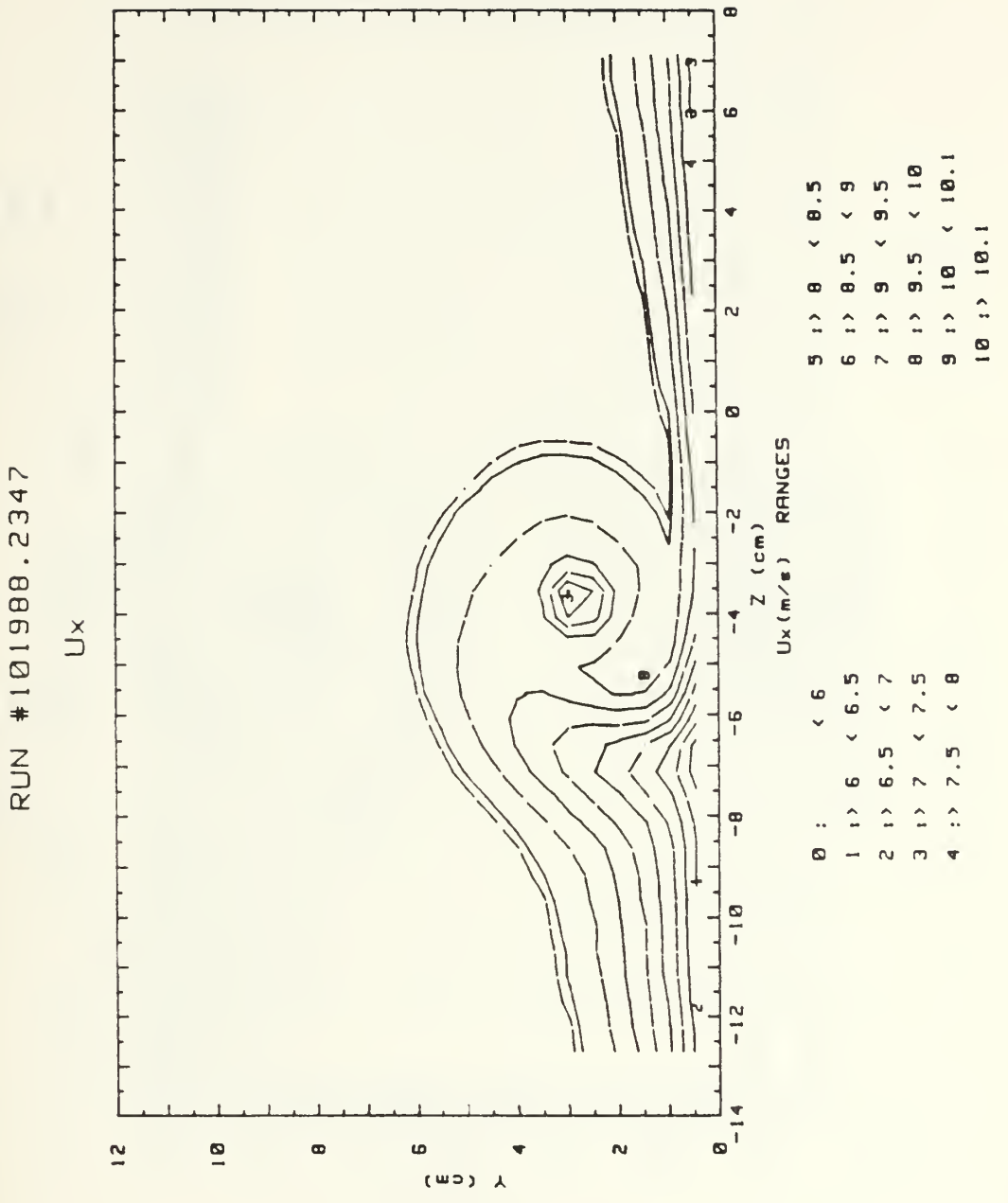

Figure 46. Streamwise Velocity Field, x/d=41.9 m=0.5, Single Injection Hole, Γ=.121 m^2/s, S=2.55, Vortex w

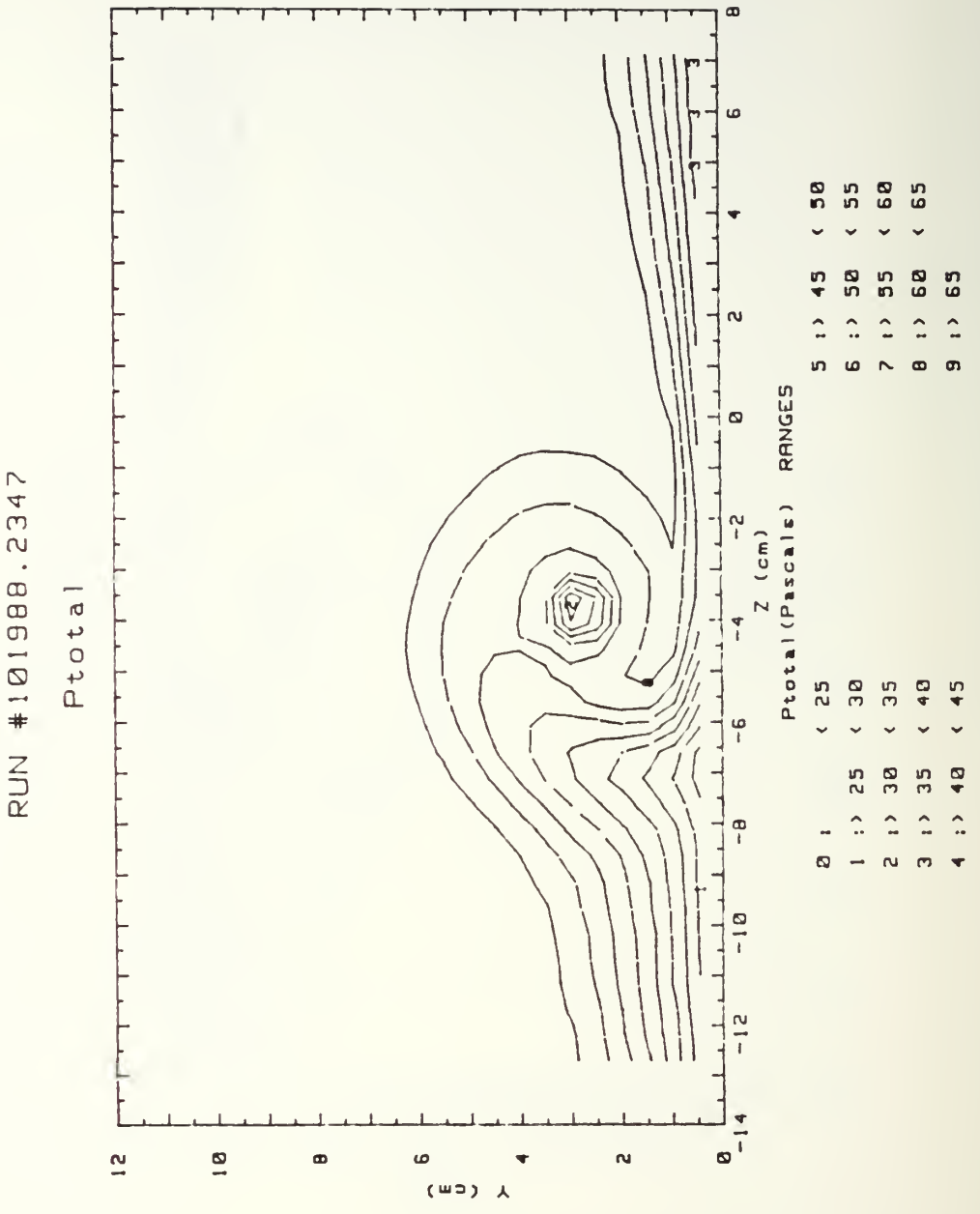

Figure 47. Total Pressure Field
x/d=41.9 m=0.5, Single Injection Hole,
Γ=.121 m^2/s, S=2.55, Vortex w

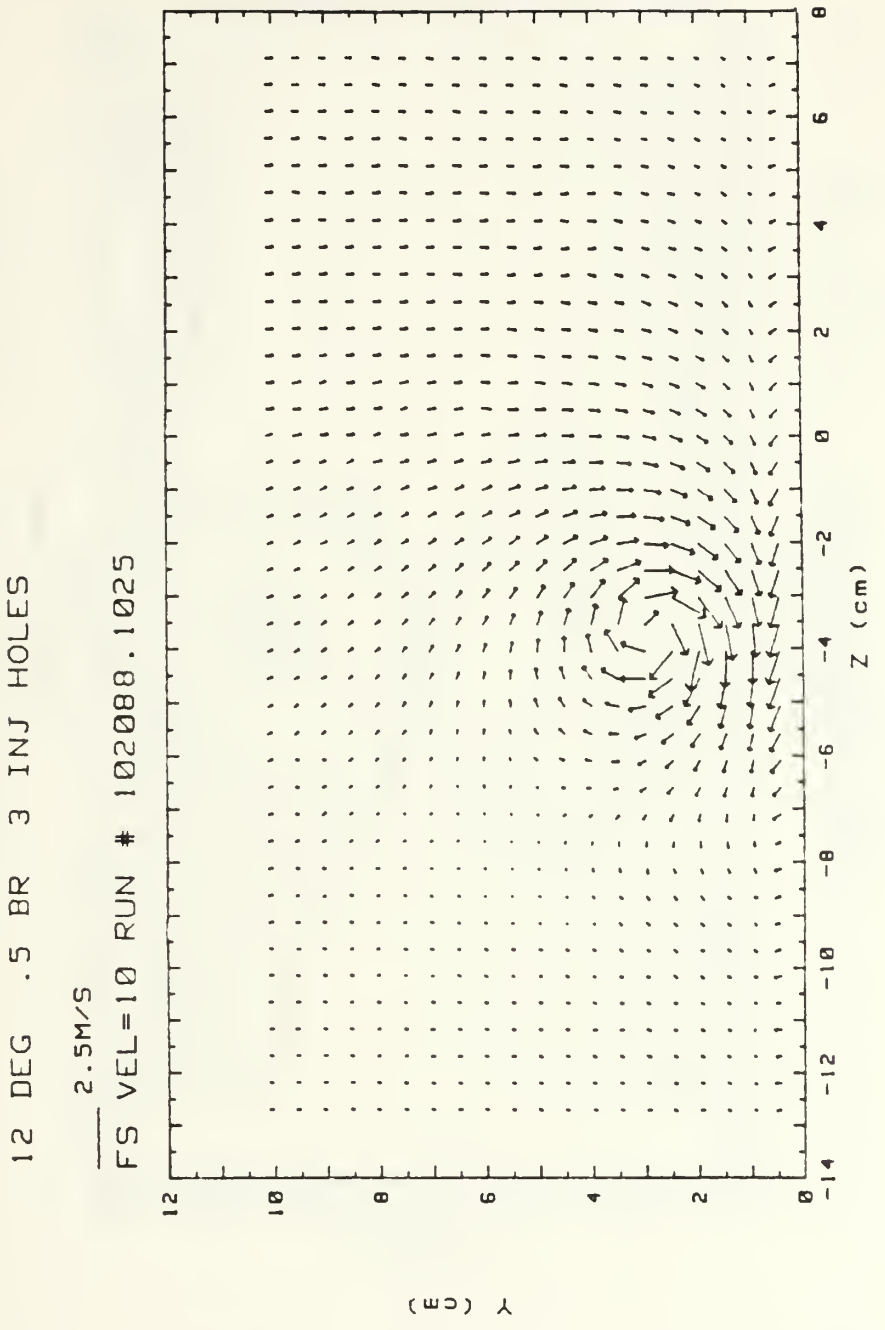

Figure 48. Secondary Flow Vectors, x/d=41.9 m=0.5, Single Injection Hole, Γ=.089 m^2/s, S=1.88, Vortex x

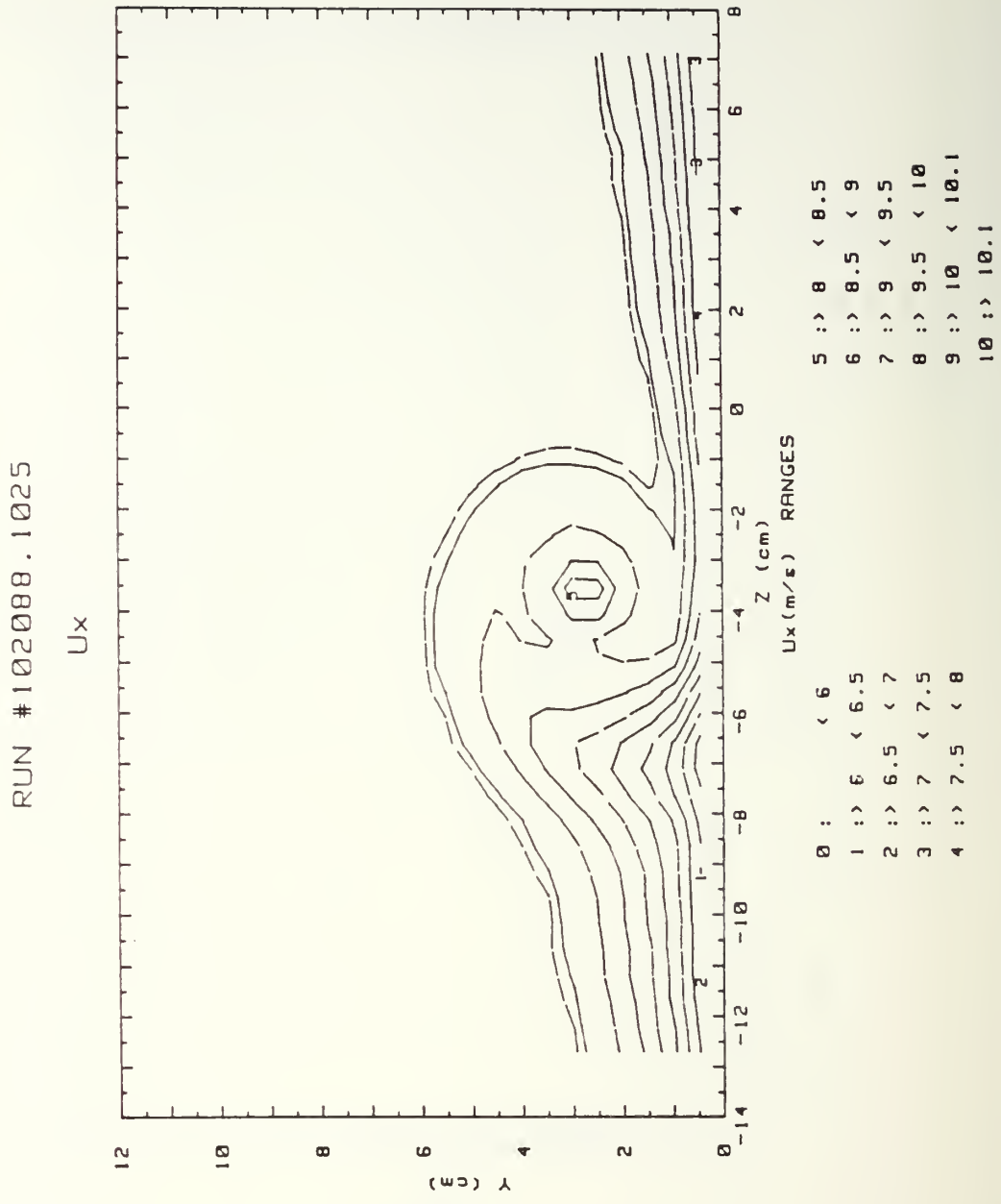

Figure 49. Streamwise Velocity Field, x/d=41.9 m=0.5, Single Injection Hole, Γ =0.89 m^2/s, S=1.88, Vortex x

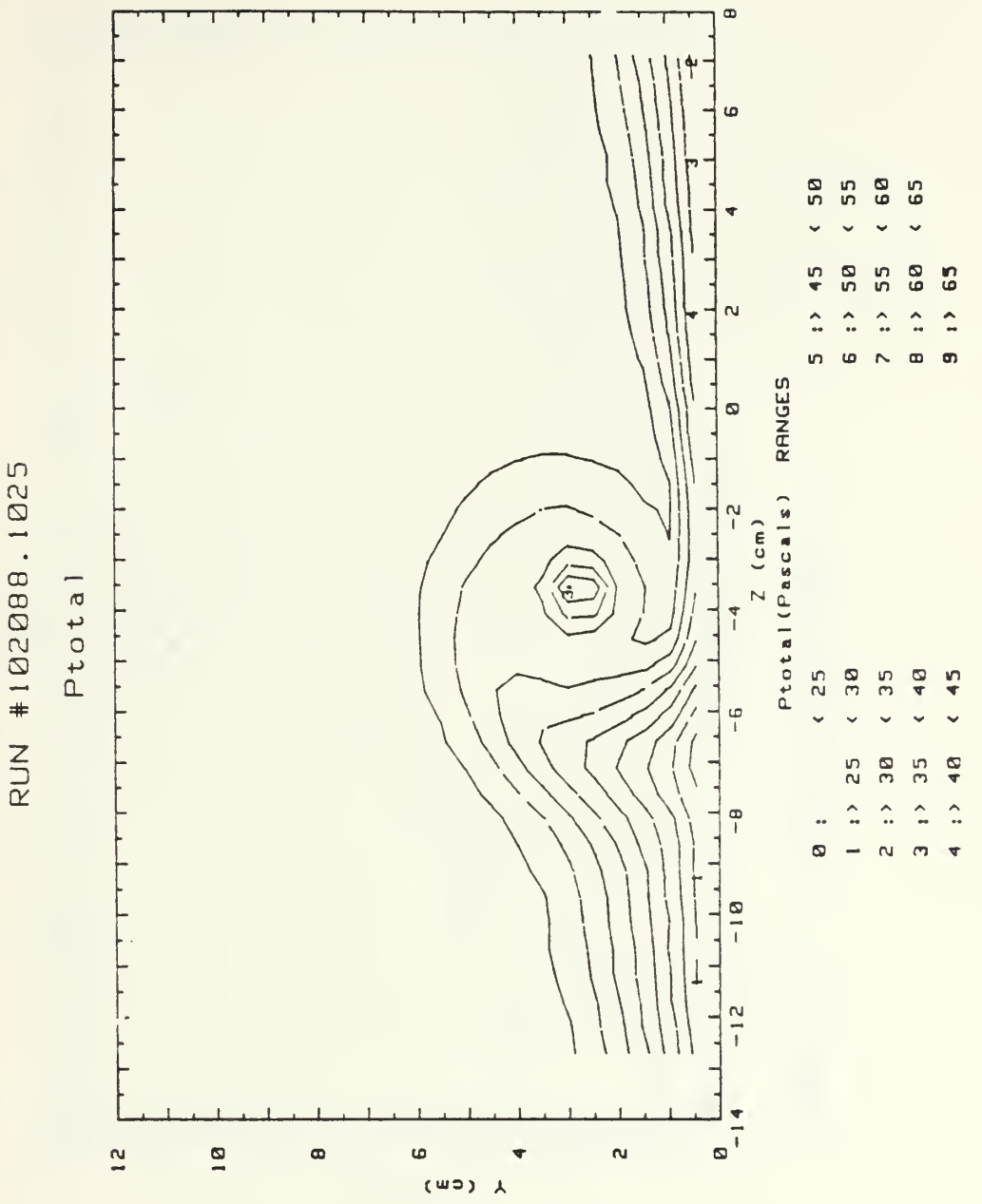

Figure 50. Total Pressure Field, x/d=41.9 m=0.5, Single Injection Hole, Γ=.089 m^2/s, S=1.88, Vortex x

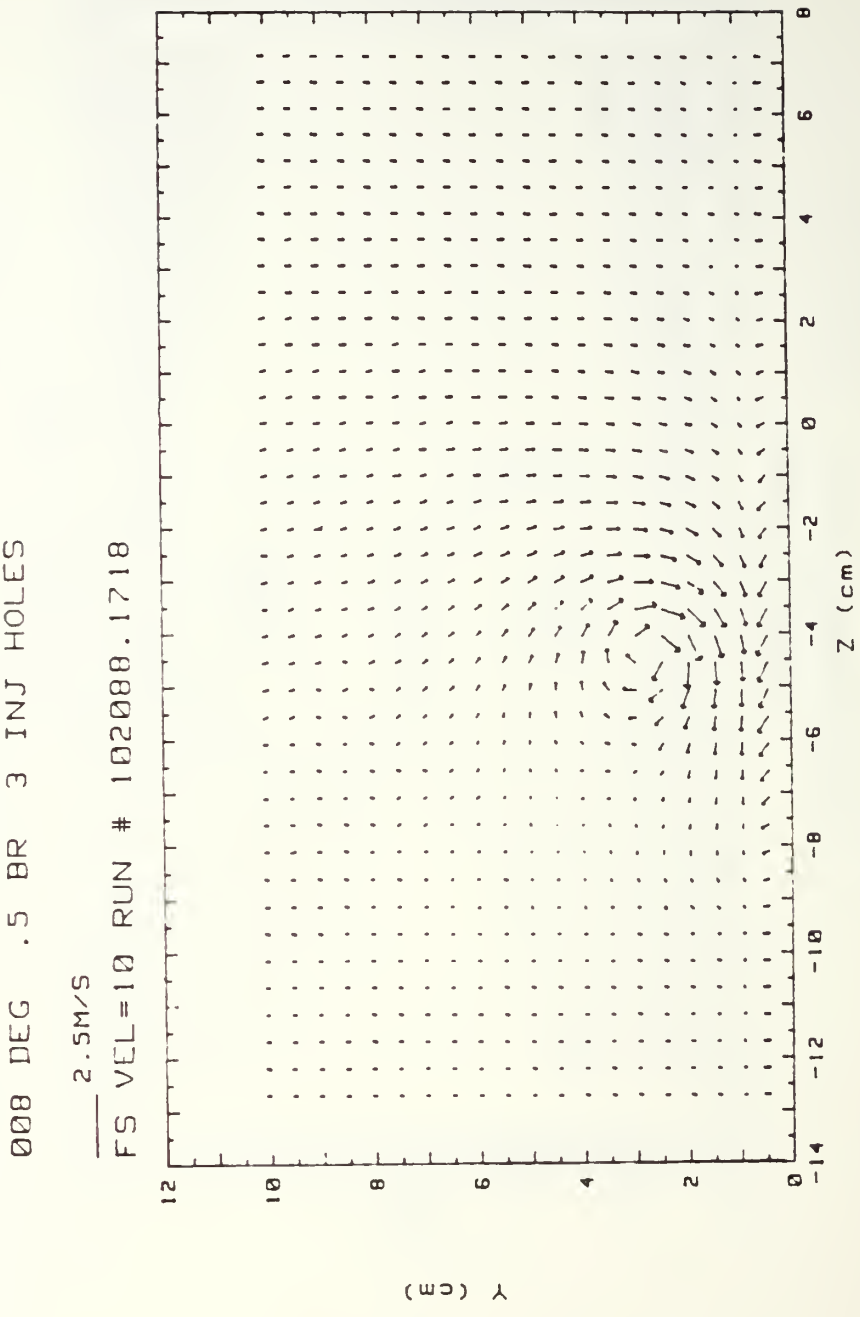

Figure 51. Secondary Flow Vectors, x/d=41.9 m=0.5, Single Injection Hole, Γ=.051 m^2/s, S=1.08, Vortex y

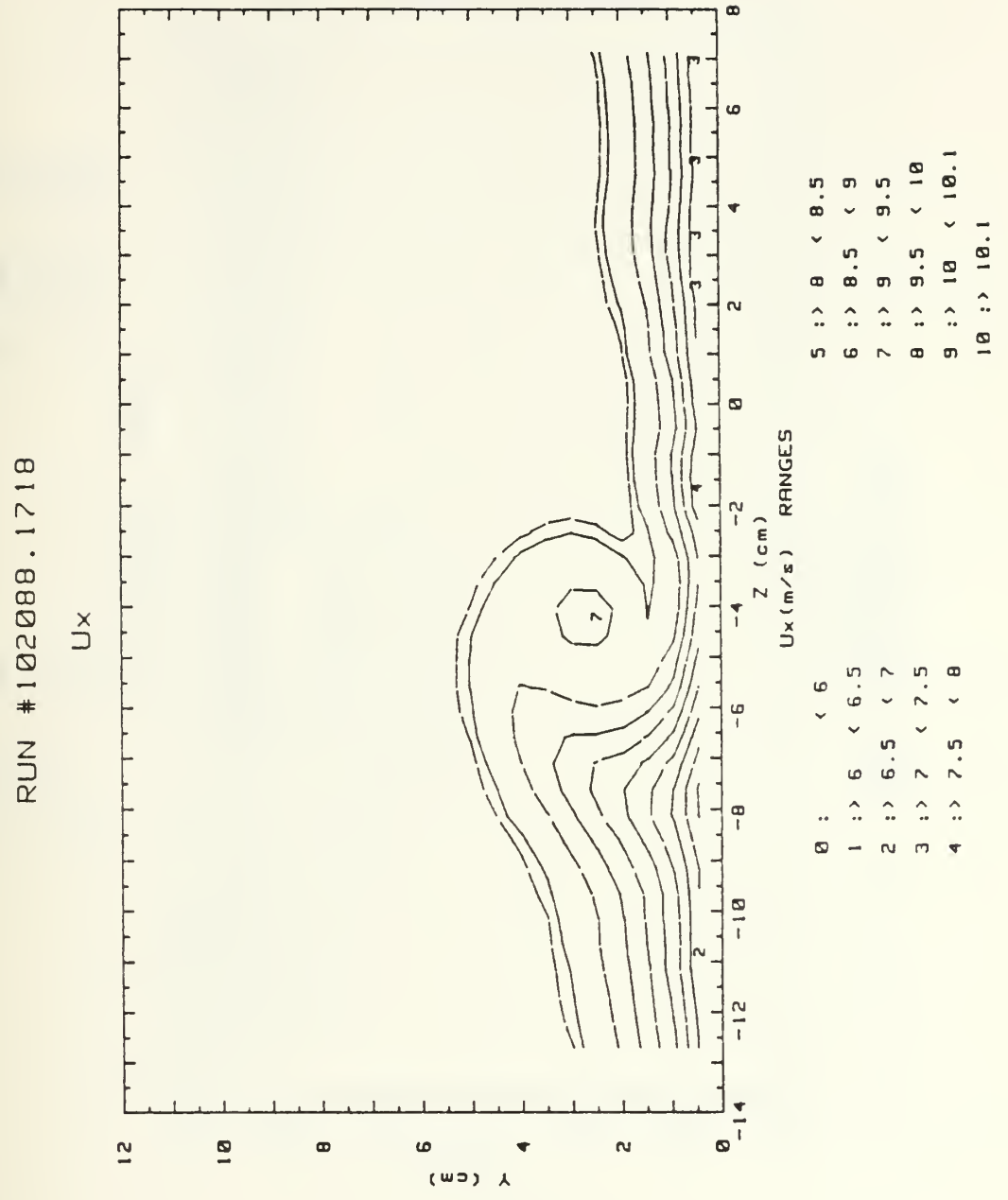

Figure 52. Streamwise Velocity Field, x/d=41.9 m=0.5, Single Injection Hole, Γ=.051 $m^2.s$, S=1.08, Vortex y

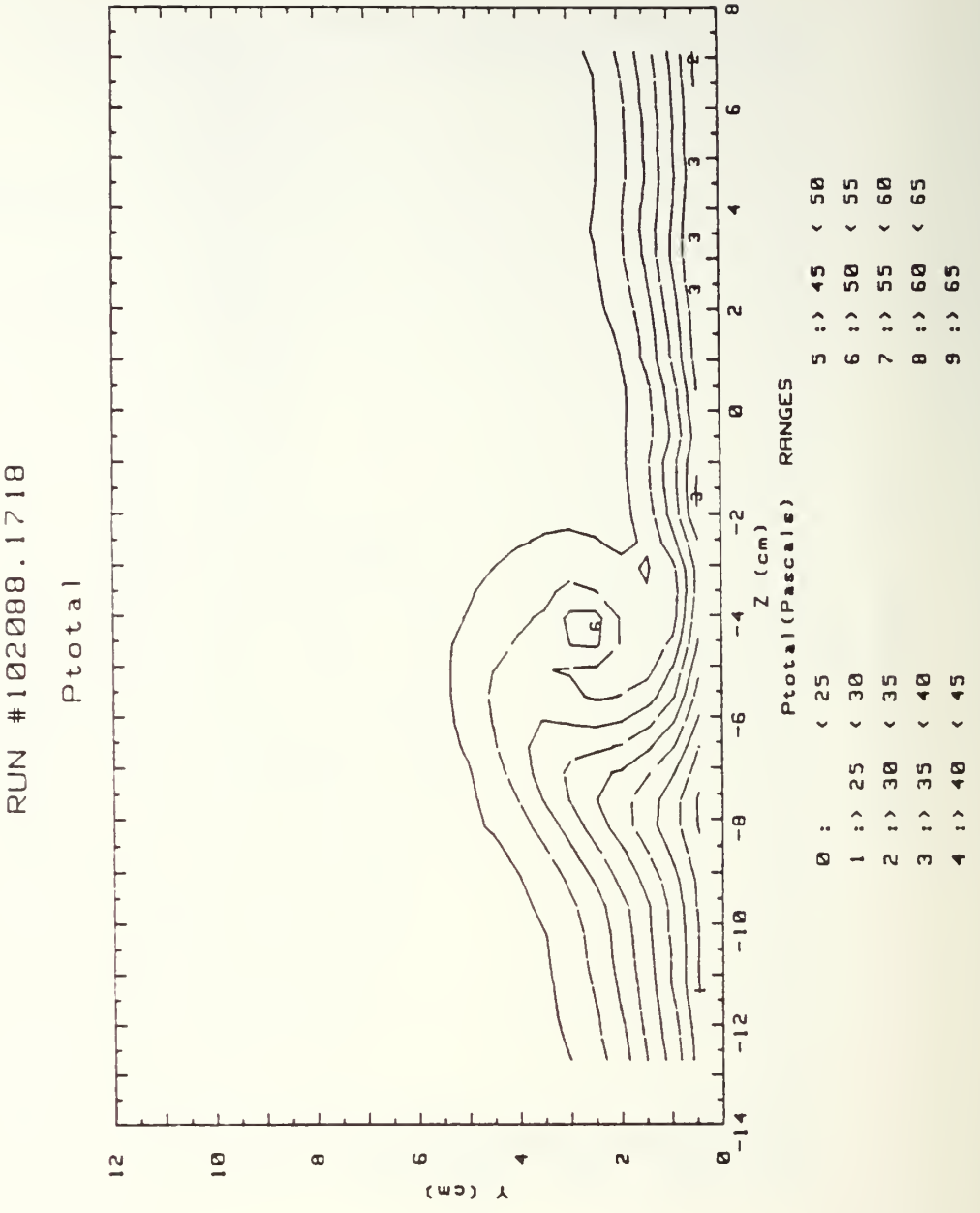

Figure 53. Total Pressure Field, x/d=41.9 m=0.5, Single Injection Hole, Γ=.051 m^2/s, S=1.08, Vortex y

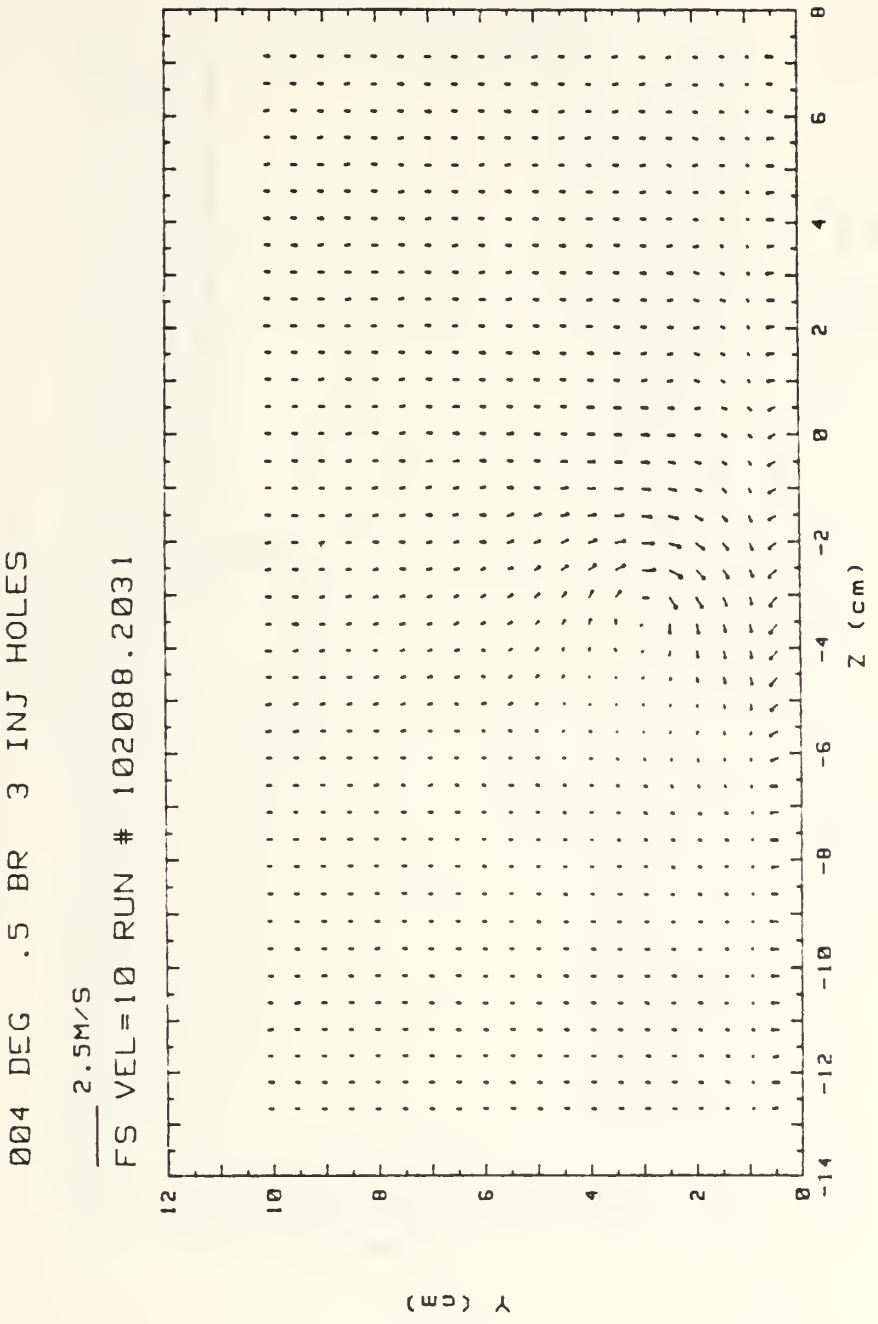

Figure 54. Secondary Flow Vectors, x/d=41.9 m=0.5, Single Injection Hole, Γ =.014 m^2/s, S=0.29, Vortex z

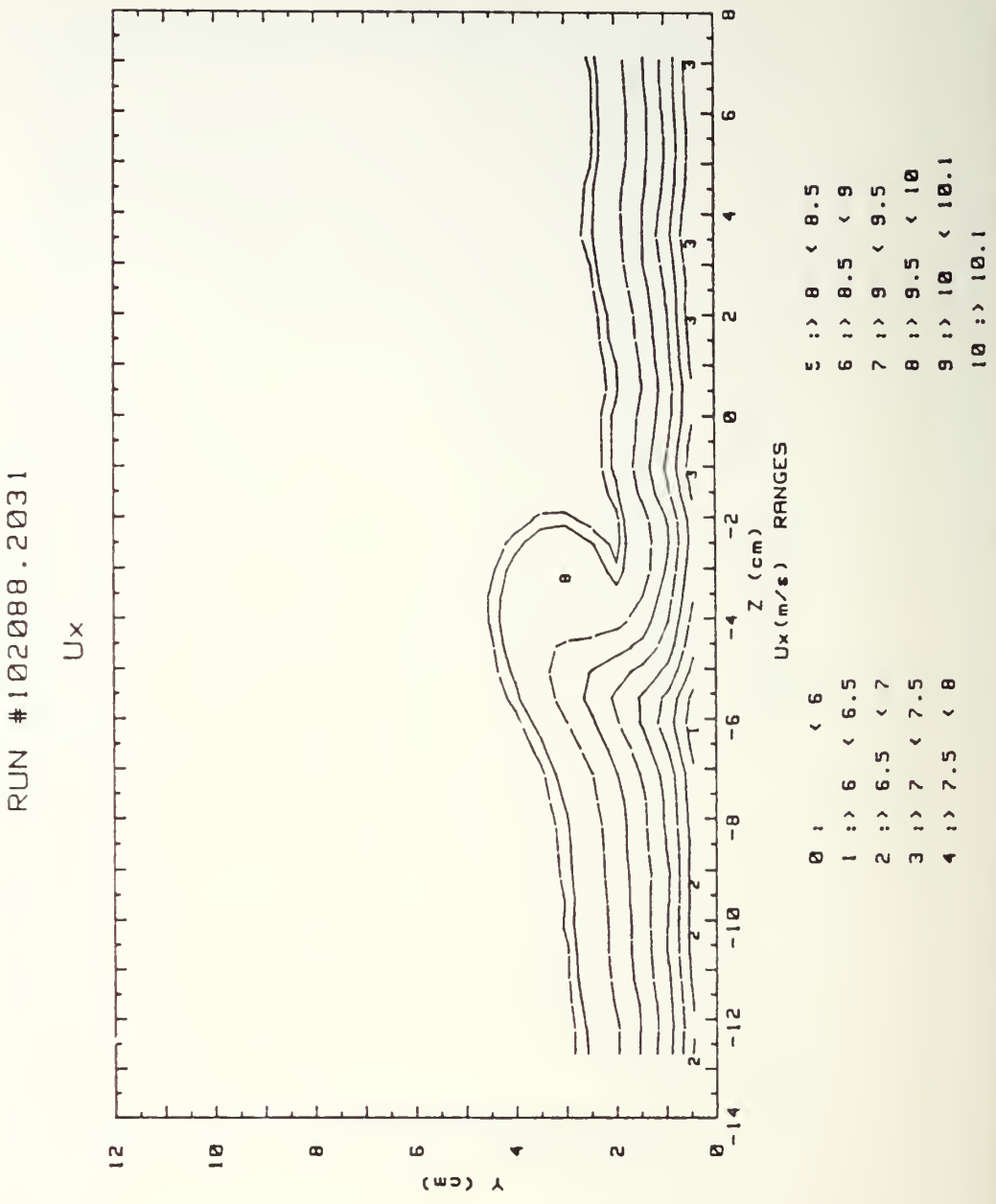

Figure 55. Streamwise Velocity Field, x/d=41.9 m=0.5, Single Injection Hole, Γ=.014 m^2/s, S=0.29, Vortex z

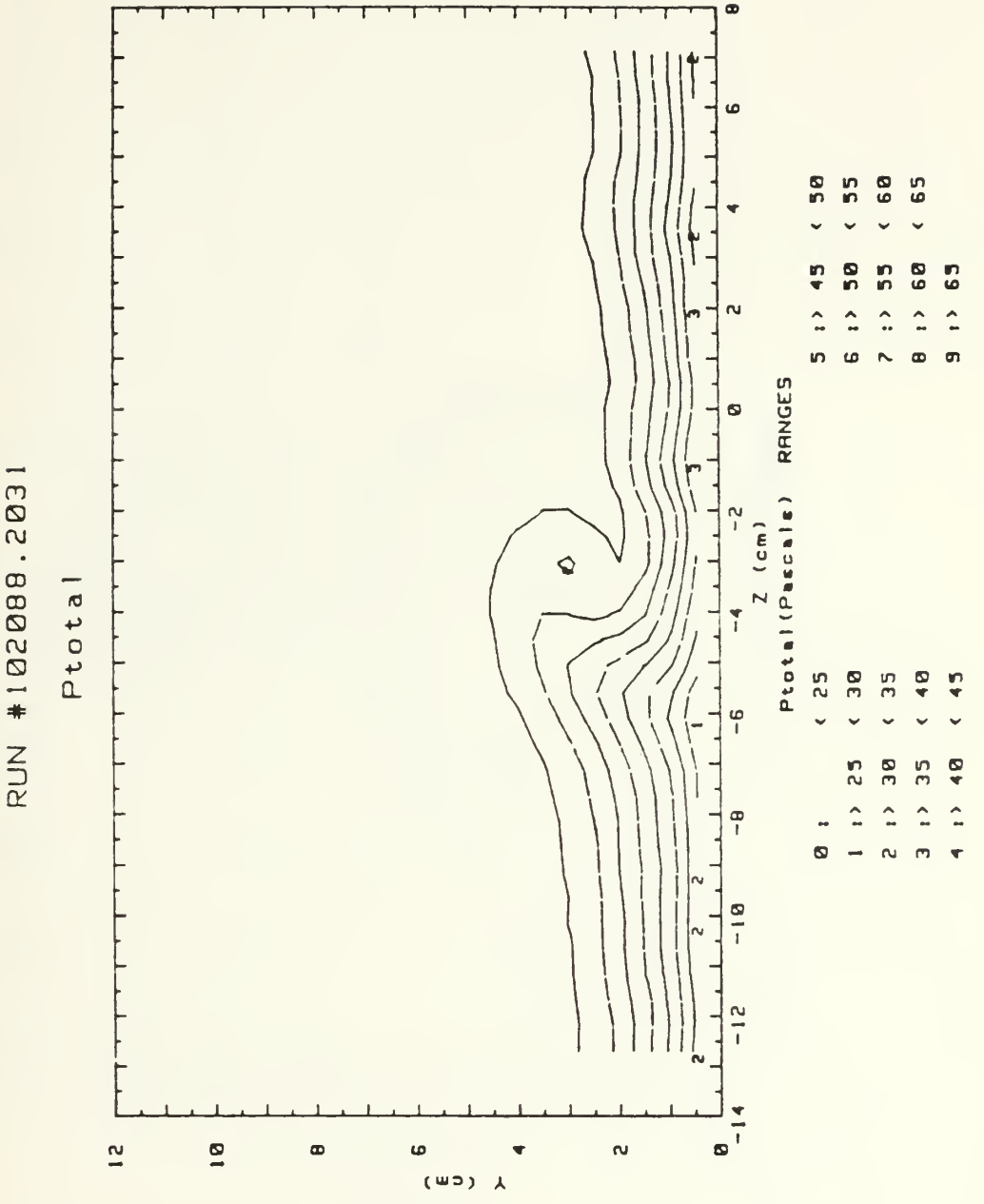

Figure 56. Total Pressure Field, x/d=41.9 m=0.5, Single Injection Hole, Γ=.014 m^2/s, S=0.29, Vortex z

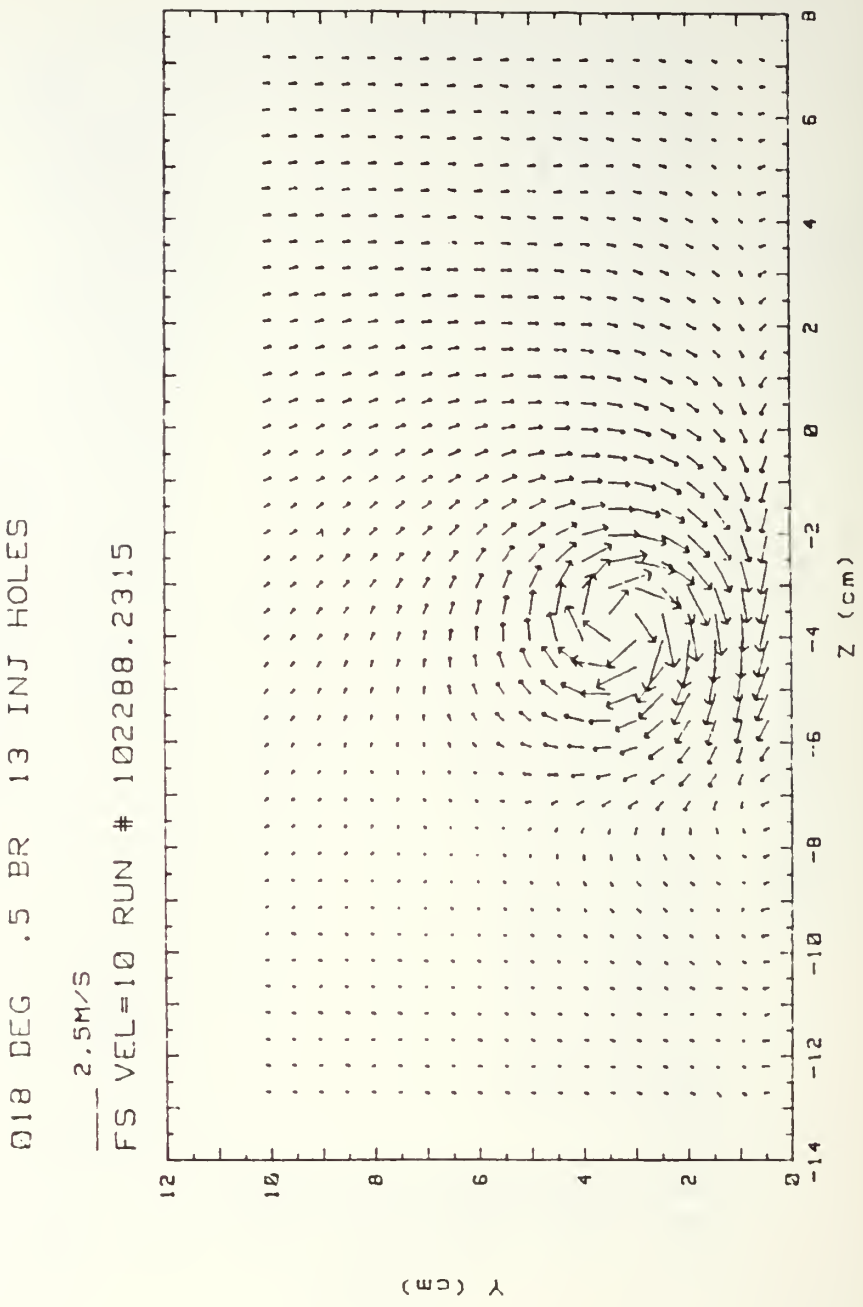

Figure 57. Secondary Flow Vectors, x/d=41.9 m=0.5, 13 Injection Holes, Γ=.134 m^2/s, S=2.81, Vortex r

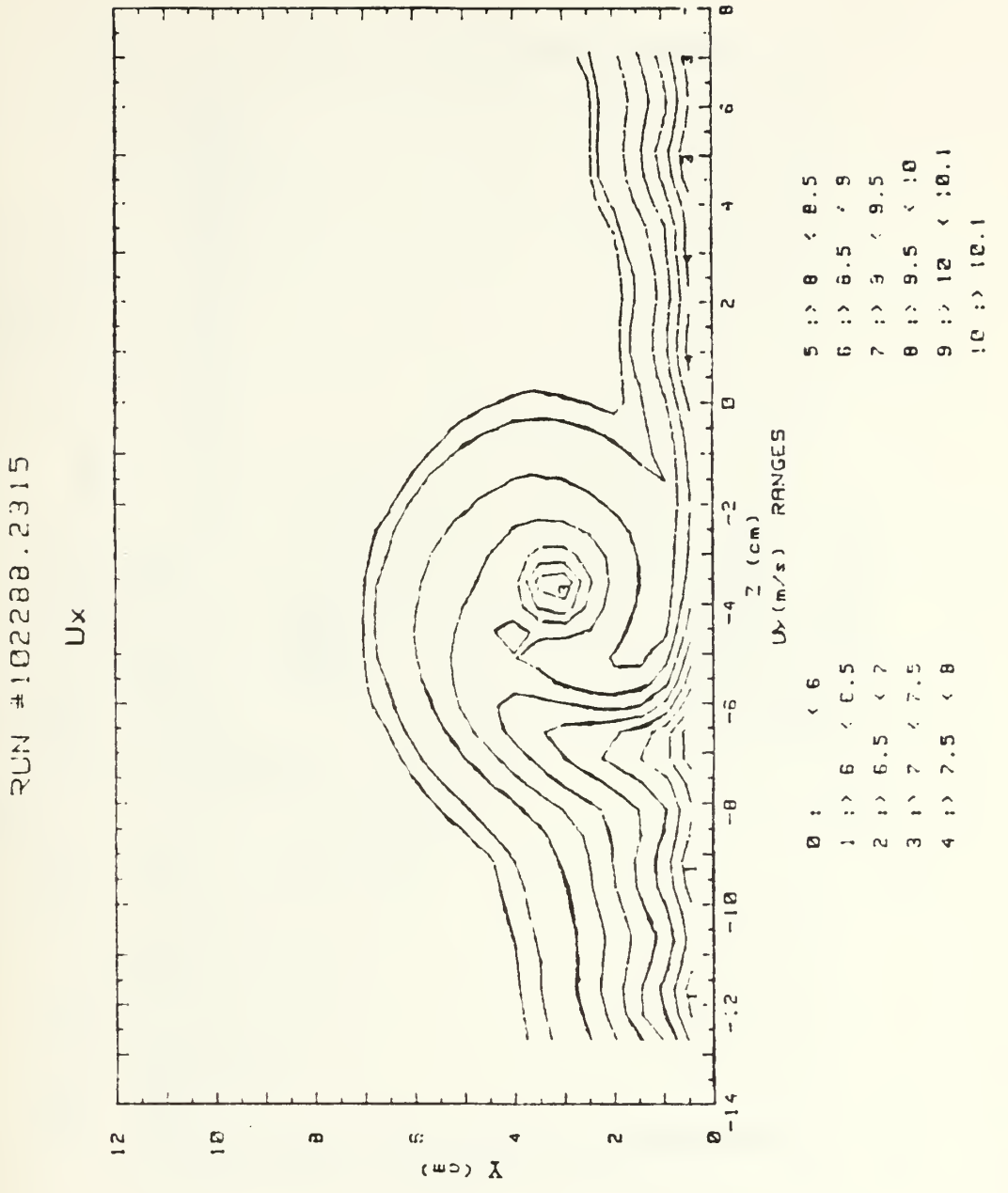

Figure 58. Streamwise Velocity Field, x/d=41.9 m=0.5, 13 Injection Holes, Γ=.134 m^2/s, S=2.81, Vortex r

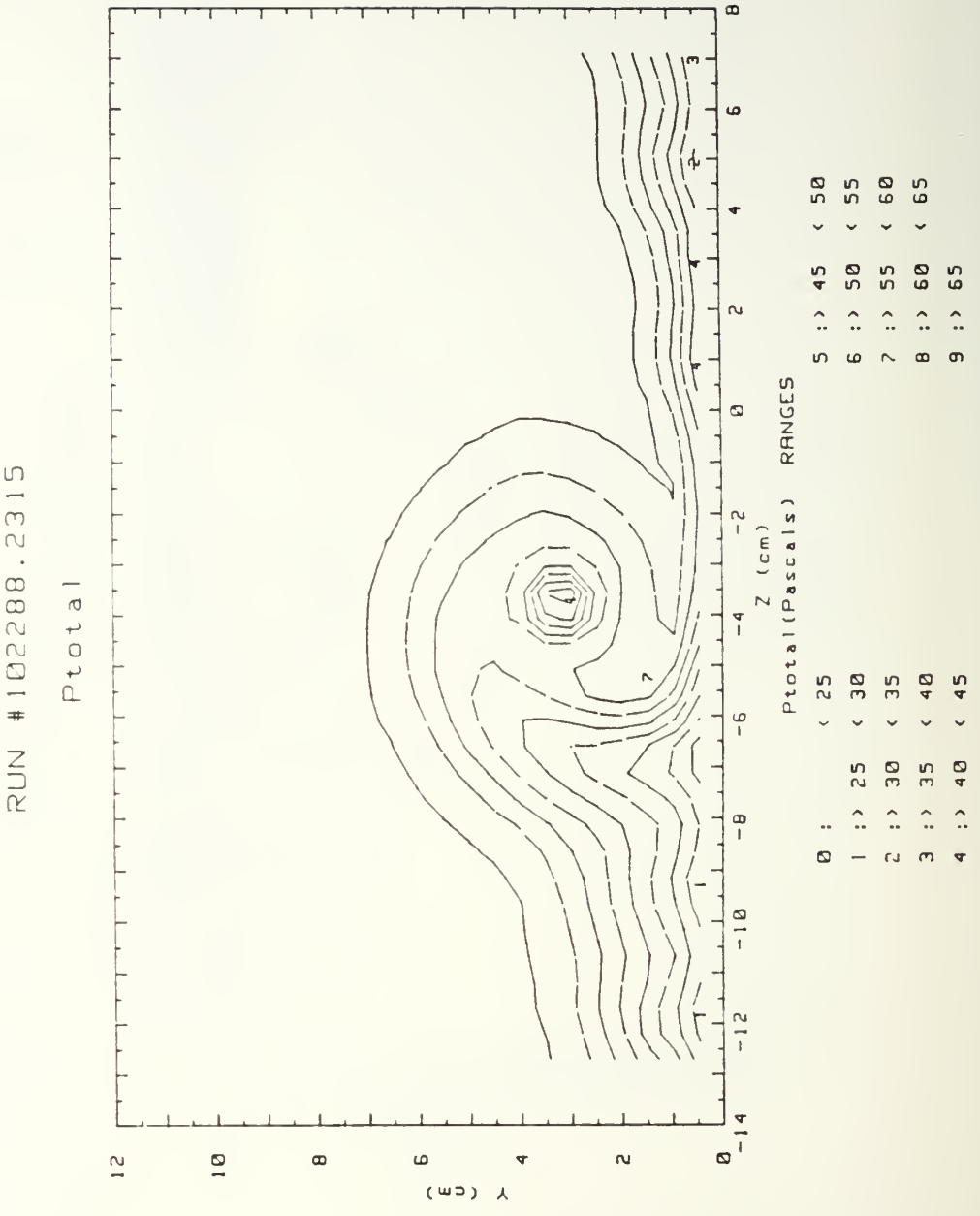

Figure 59. Total Pressure Field, x/d=41.9 m=0.5, 13 Injection Holes, Γ=.134 m^2/s, S=2.81, Vortex r

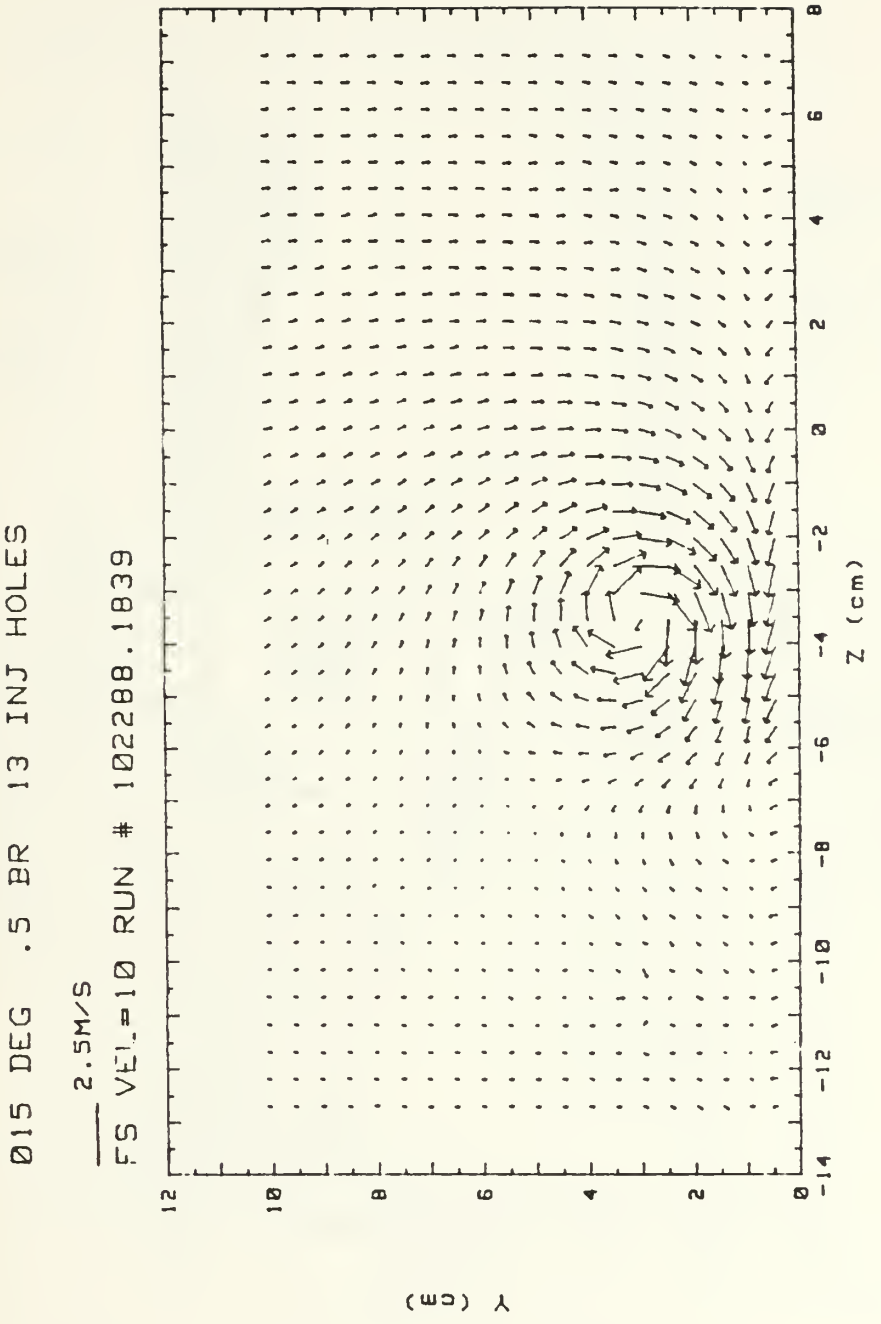

Figure 60. Secondary Flow Vectors,
x/d=41.9 m=0.5, 13 Injection Holes
Γ=.111 m^2/s, S=2.33, Vortex w

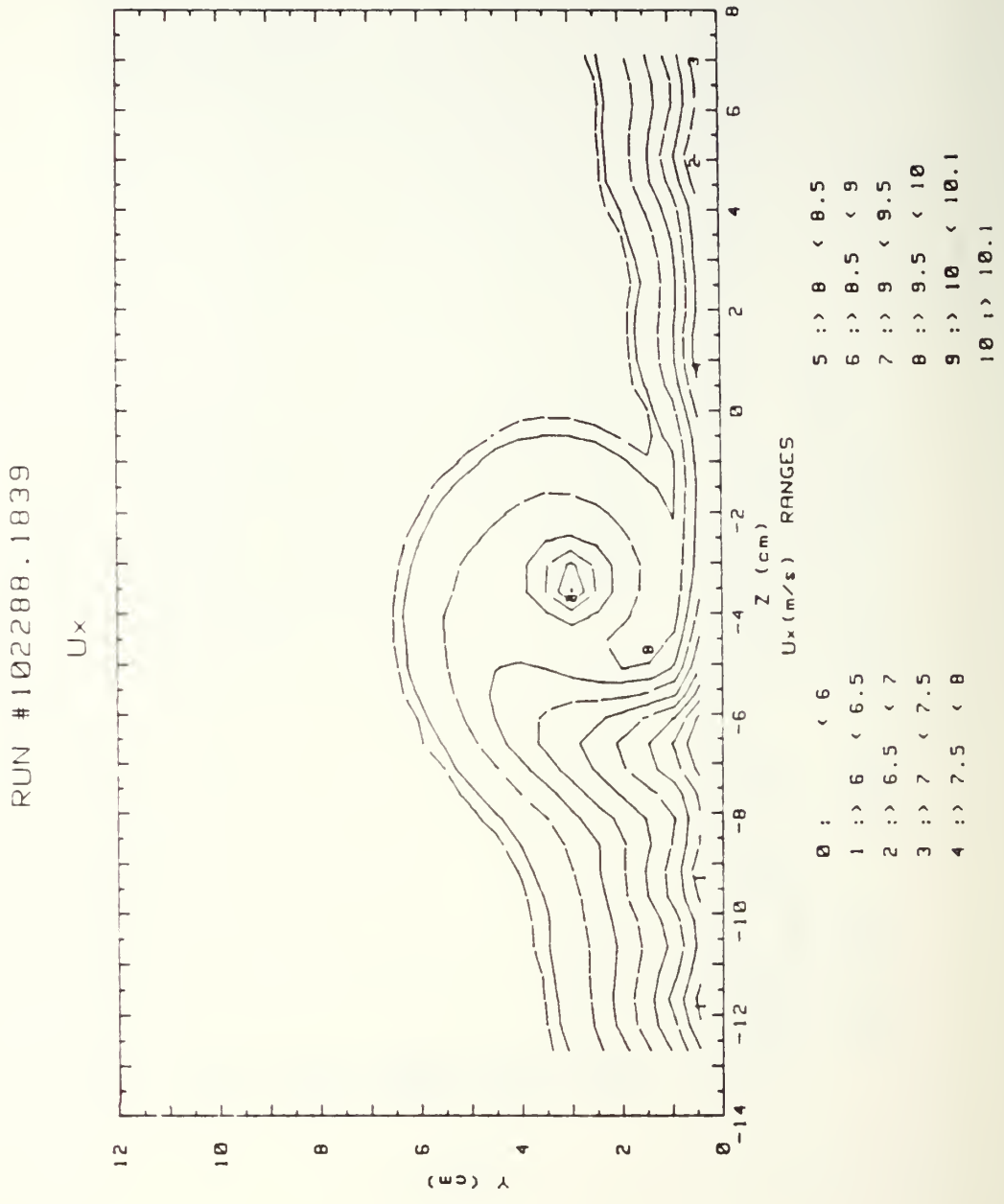

Figure 61. Streamwise Velocity Field, x/d=41.9 m=0.5, 13 Injection Holes, Γ=.111 m^2/s, S=2.33, Vortex w

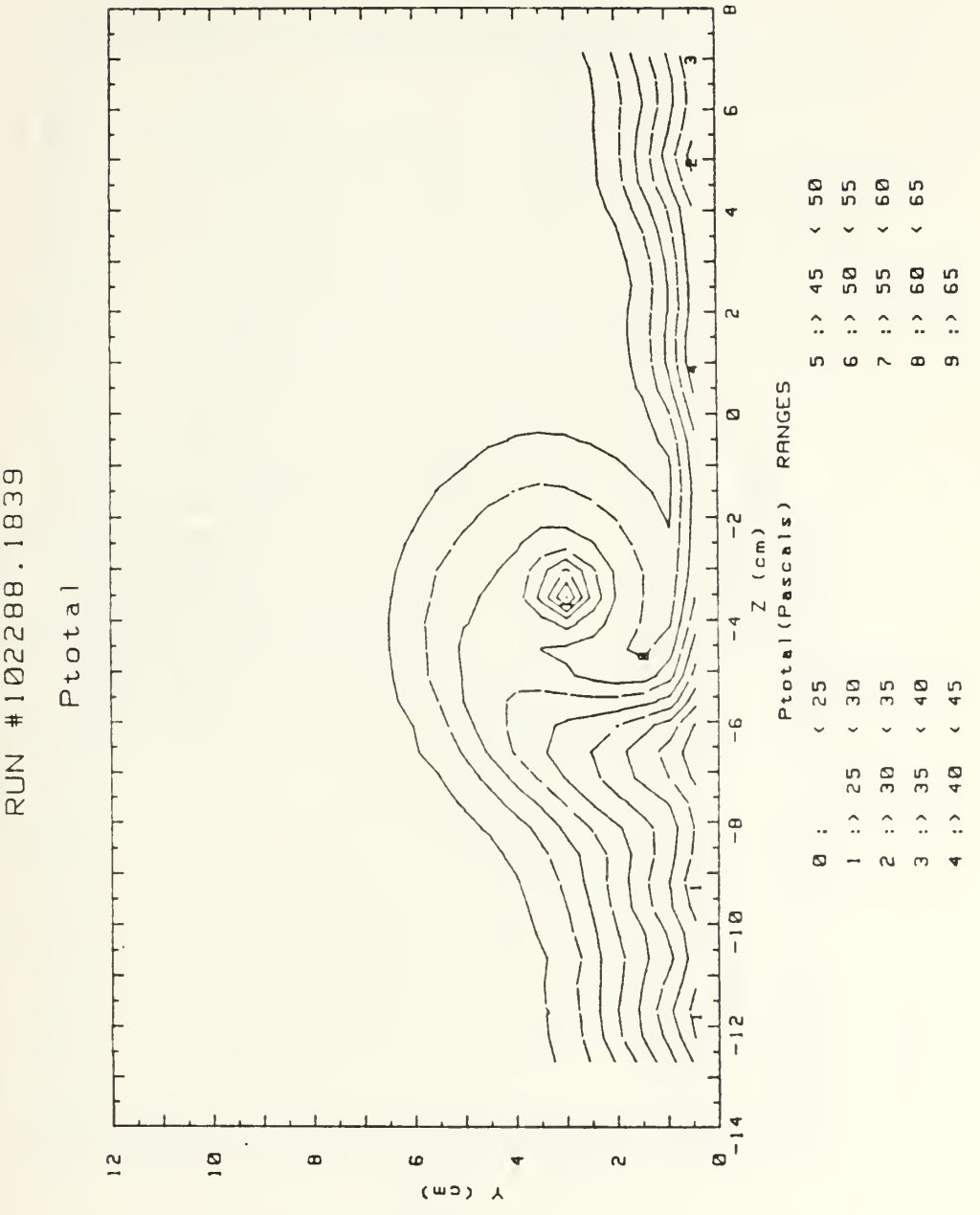

Figure 62. Total Pressure Field, x/d=41.9 m=0.5, 13 Injection Holes, Γ=.111 m^2/s, S=2.33, Vortex w

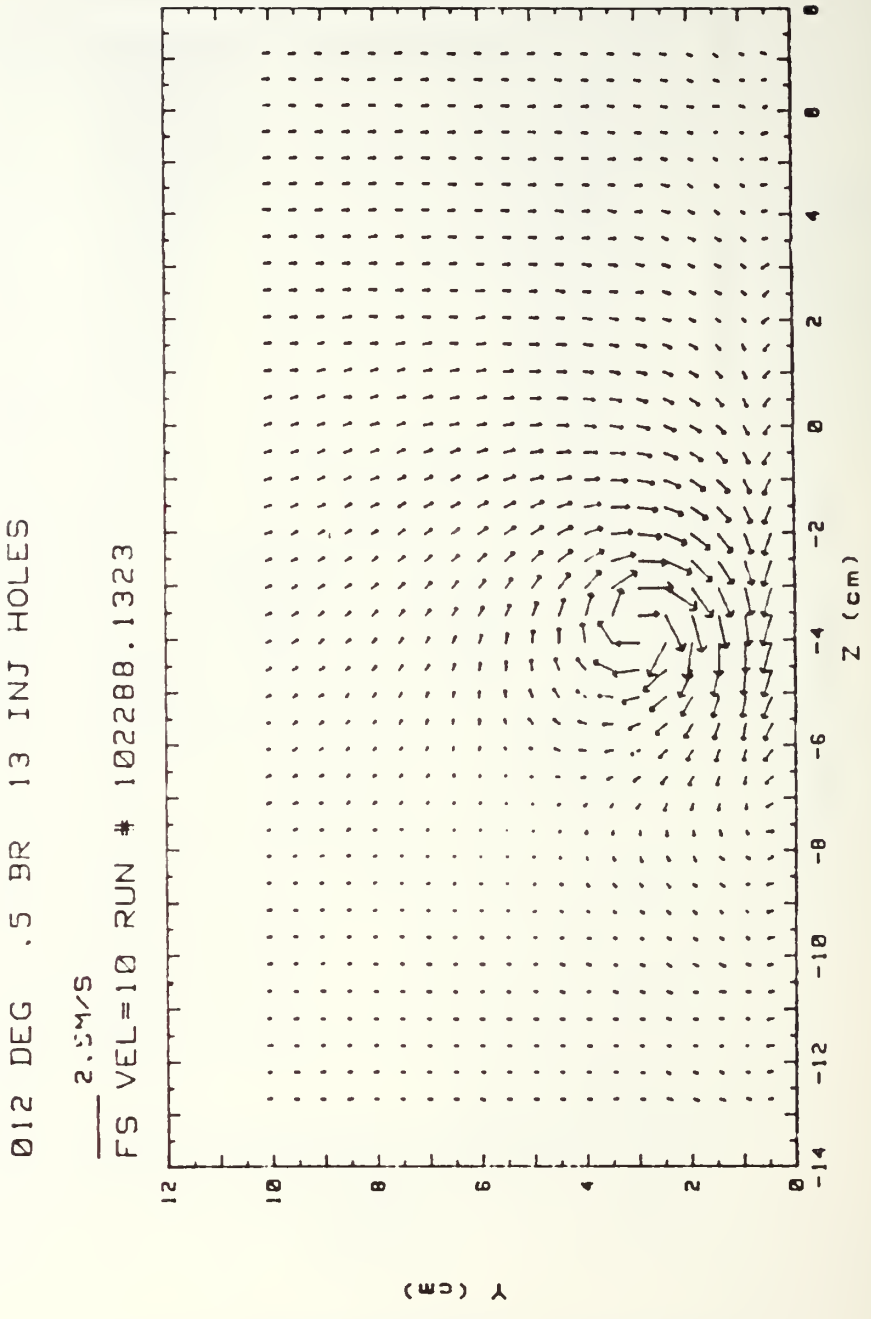

Figure 63. Secondary Flow Vectors, x/d=41.9 m=0.5, 13 Injection Holes, Γ=.088 m^2/s, S=1.86, Vortex x

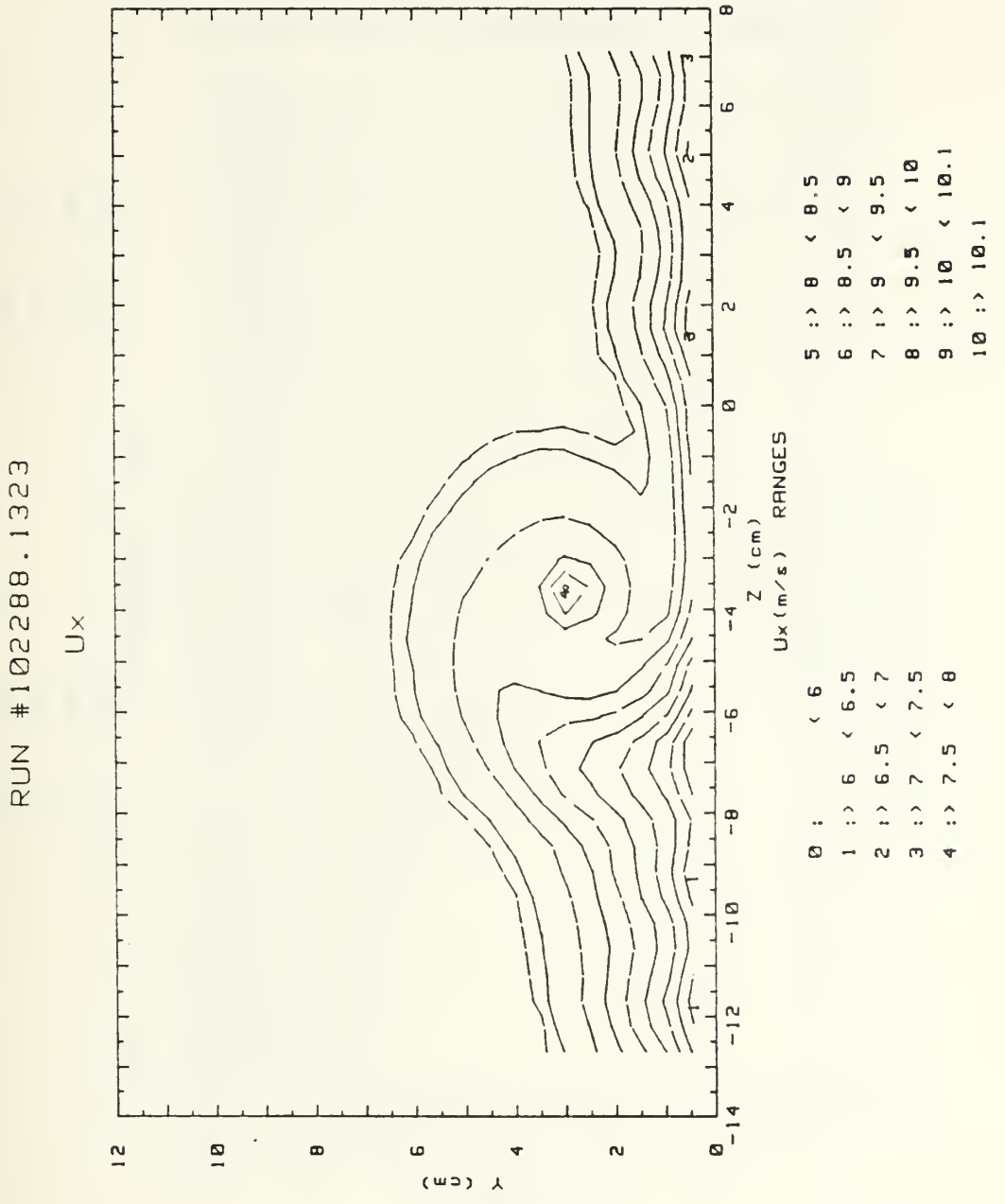

Figure 64. Streamwise Velocity Field, x/d=41.9 m=0.5, 13 Injection Holes, Γ=.088 m^2/s, S=1.86, Vortex x

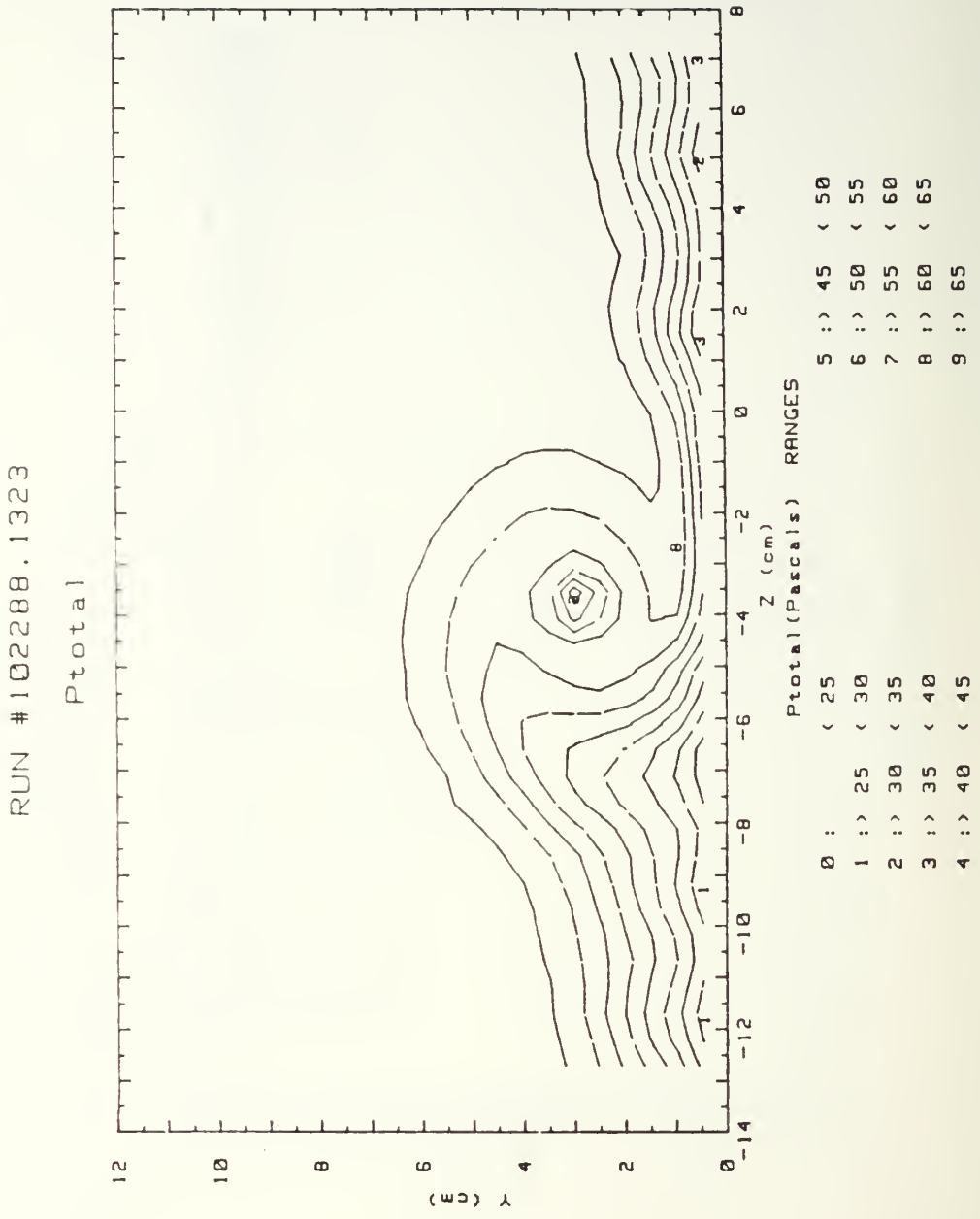

Figure 65. Total Pressure Field, x/d=41.9 m=0.5, 13 Injection Holes, Γ =.088 m^2/s, S=1.86, Vortex x

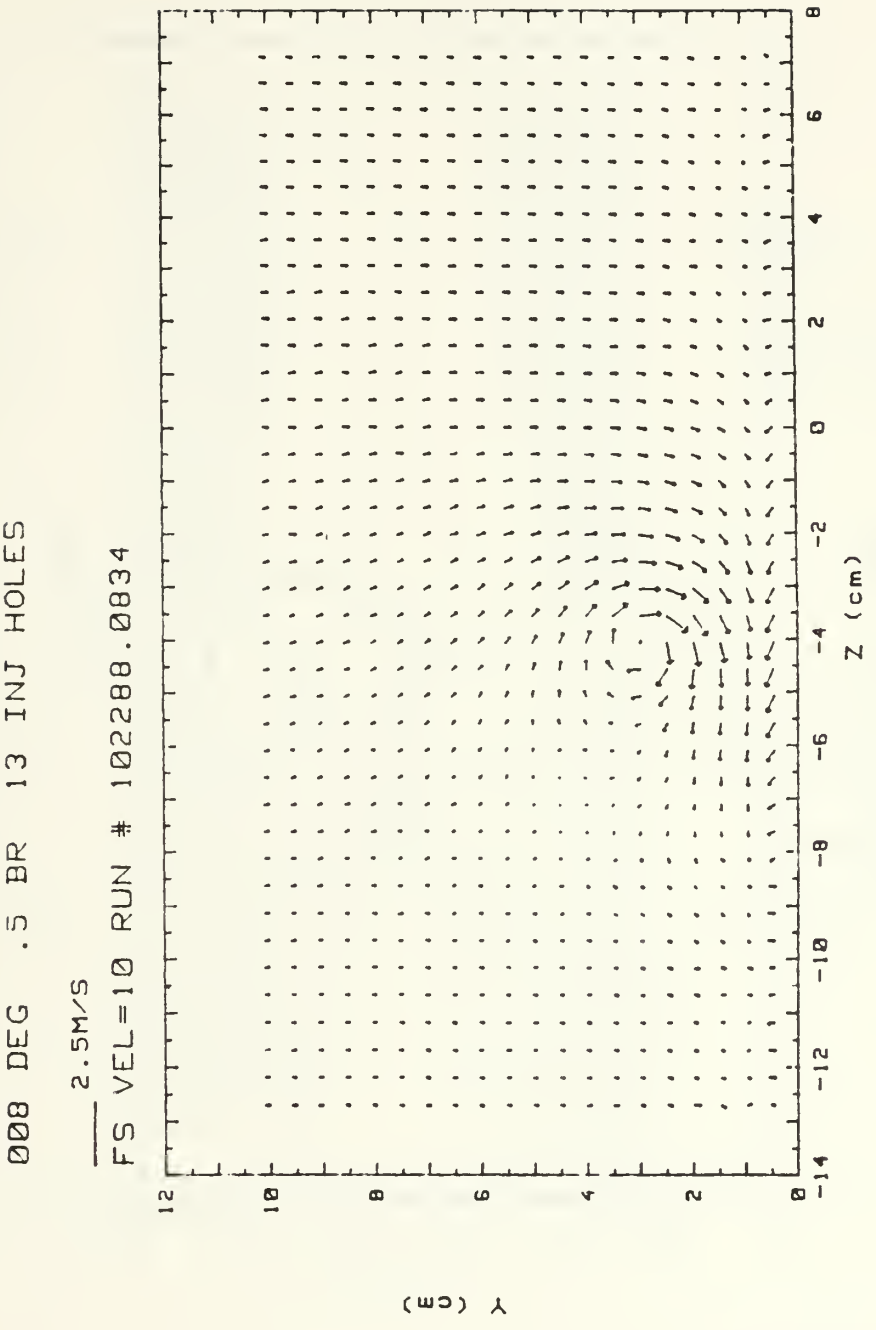

Figure 66. Secondary Flow Vectors, x/d=41.9 m=0.5, 13 Injection Holes Γ=.042 m^2/s, S=0.89, Vortex y

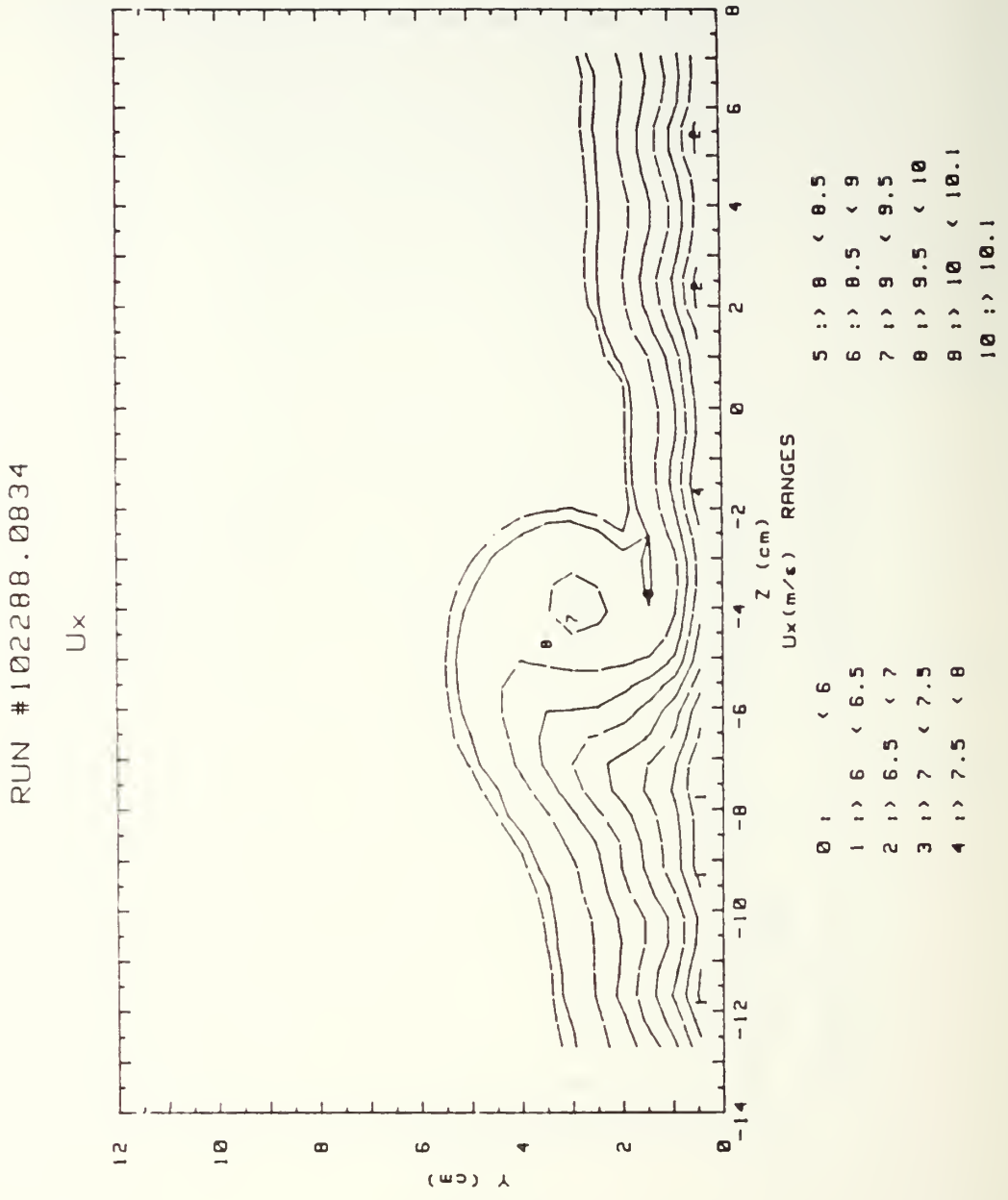

Figure 67. Streamwise Velocity Field, x/d=41.9 m=0.5, 13 Injection Holes, Γ=.042 m^2/s, S=0.89, Vortex y

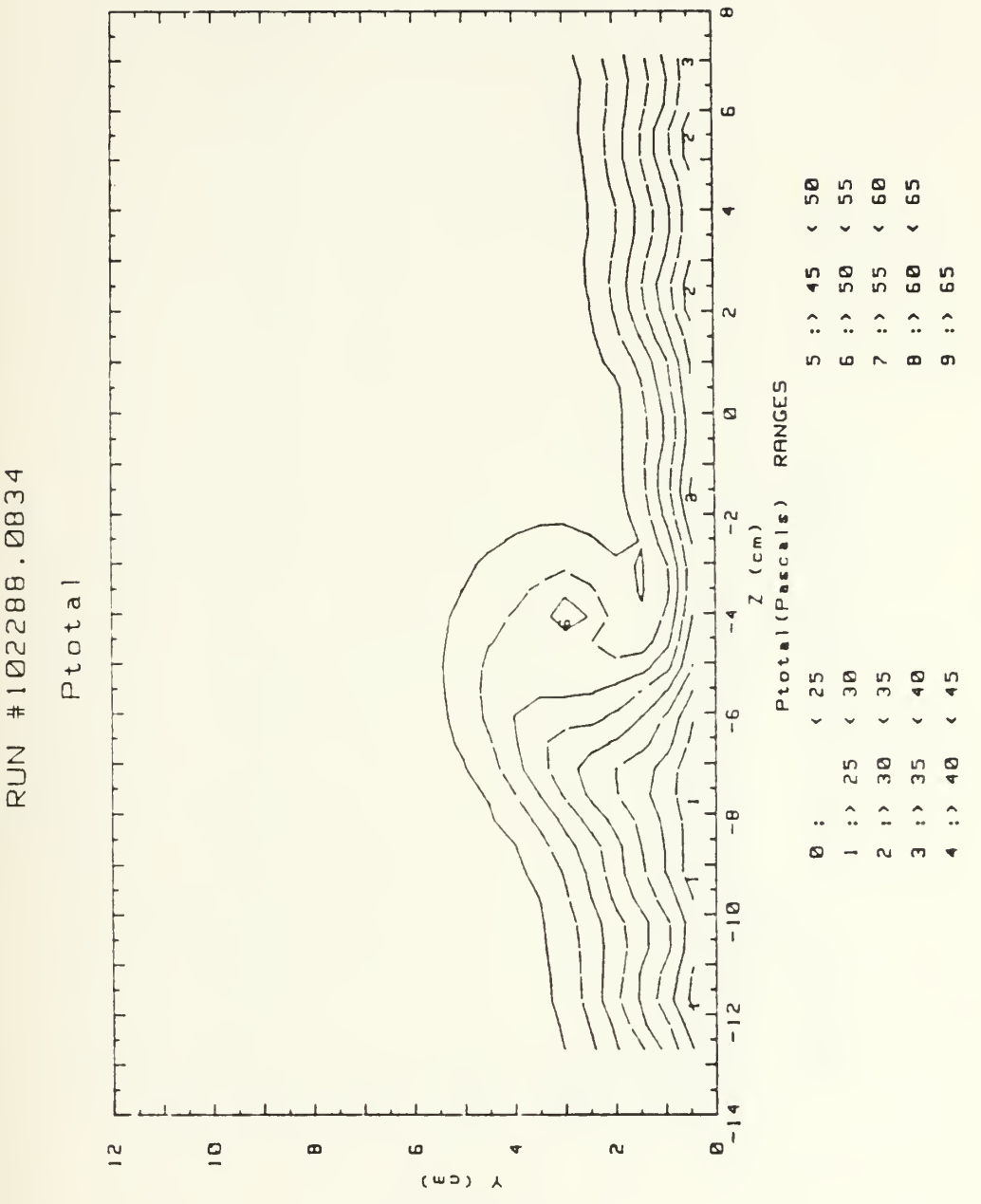

Figure 68. Total Pressure Field, x/d=41.9 m=0.5, 13 Injection Holes, Γ=.042 m^2/s, S=0.89, Vortex y

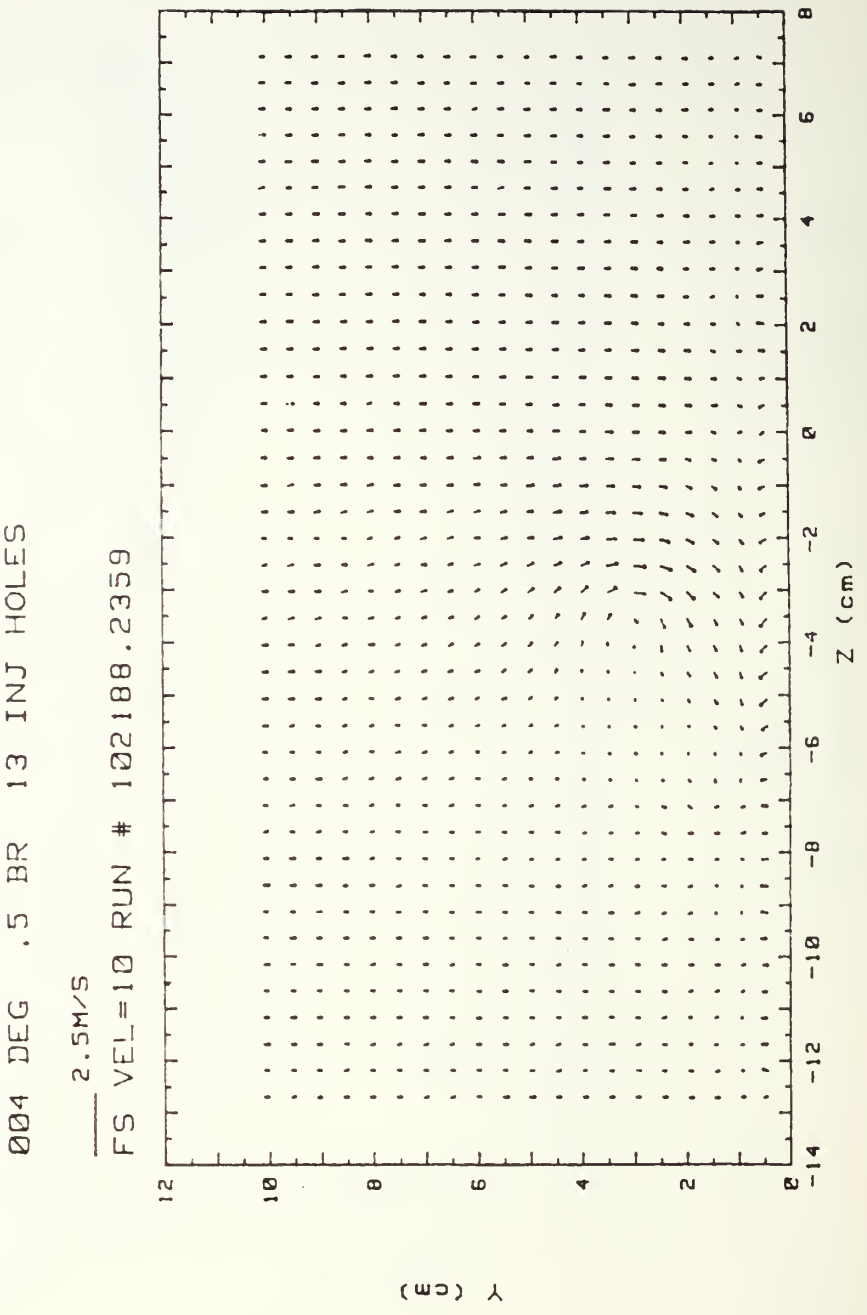

Figure 69. Secondary Flow Vectors, x/d=41.9 m=0.5, 13 Injection Holes, Γ =.008 m^2/s, S=0.17, Vortex z

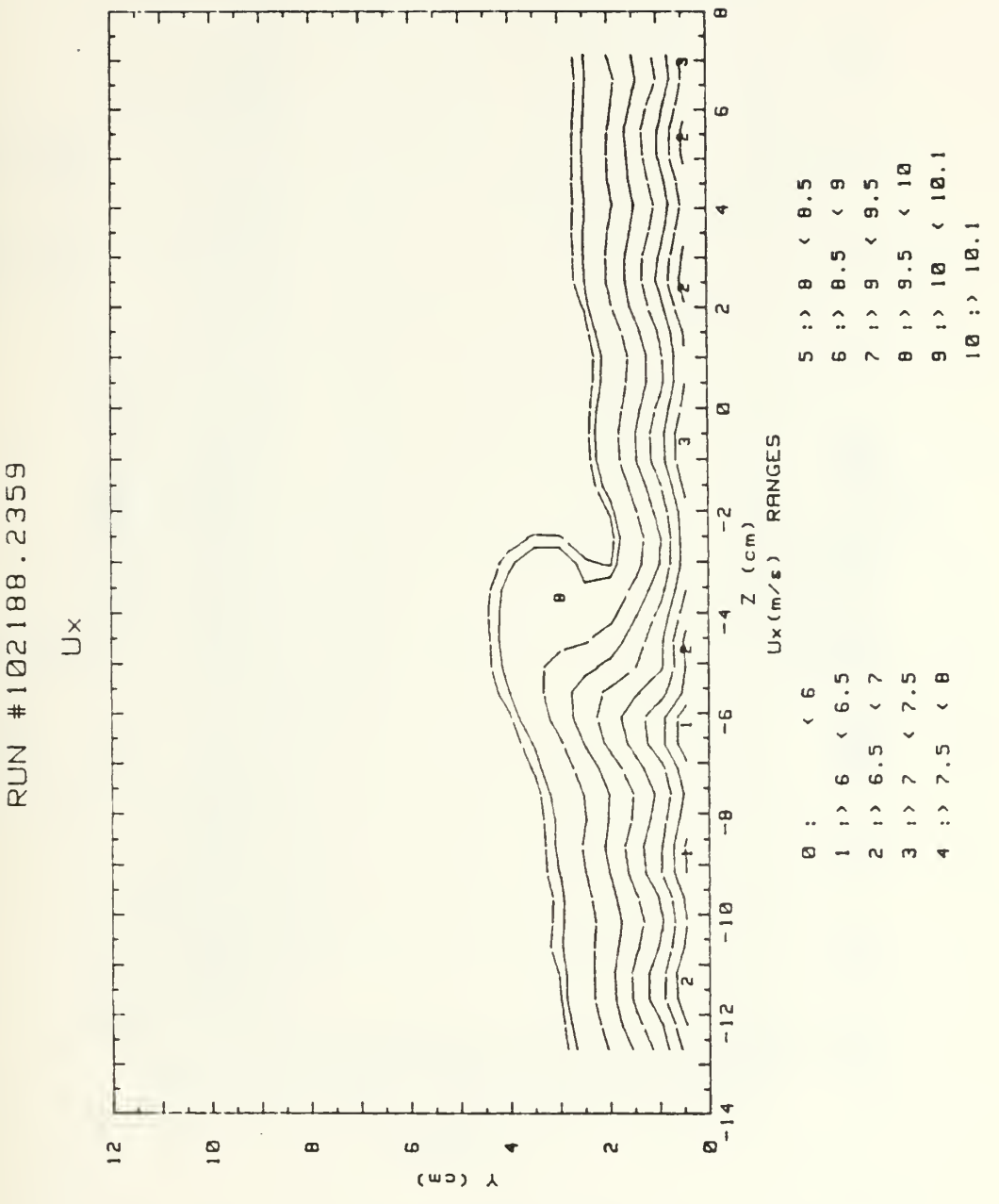

Figure 70. Streamwise Velocity Field, x/d=41.9 m=0.5, 13 Injection Holes, Γ=.008 m^2/s, S=0.17, Vortex z

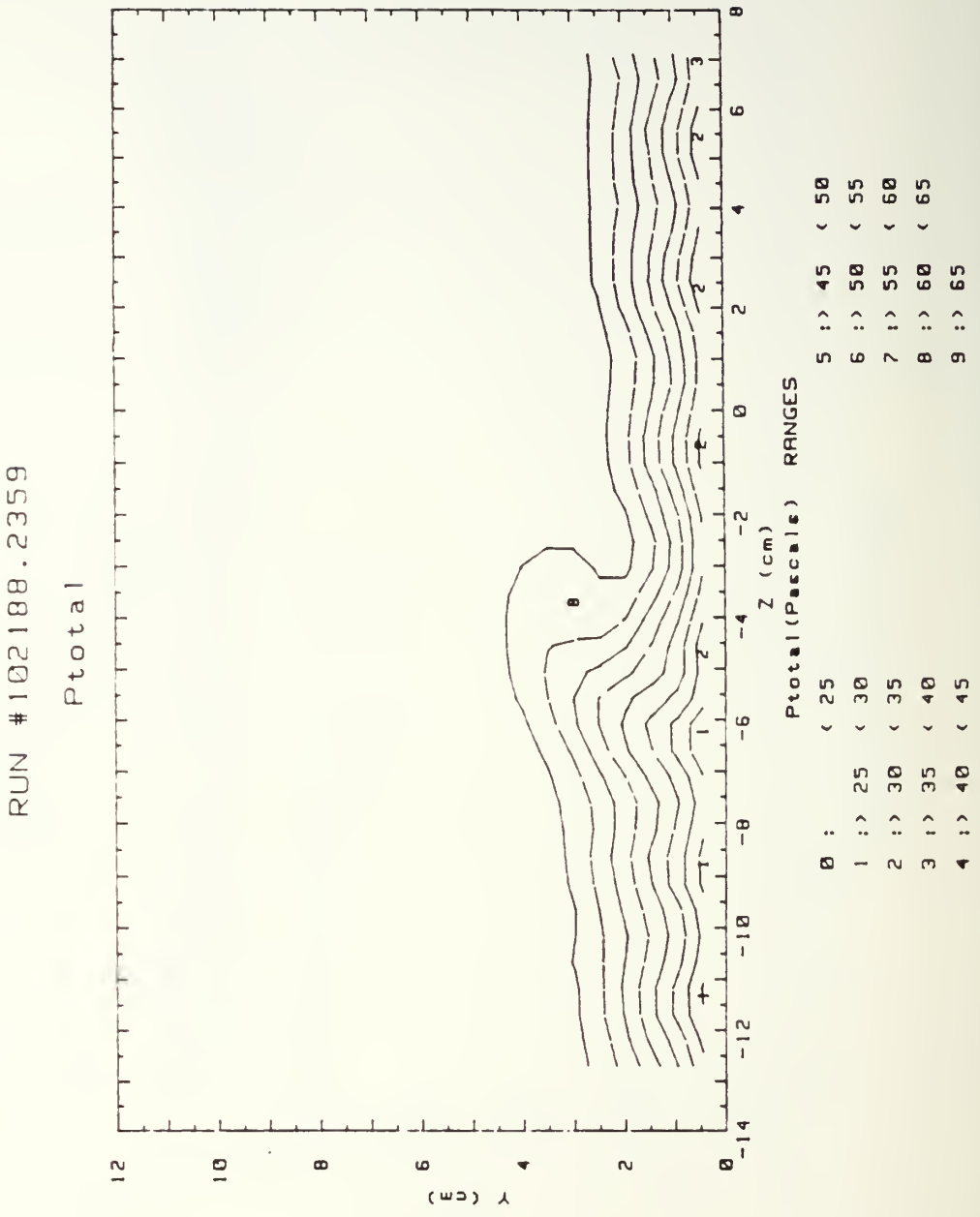

Figure 71. Total Pressure Field,
x/d=41.9 m=0.5, 13 Injection Holes,
Γ=.008 m^2/s, S=0.17, Vortex z

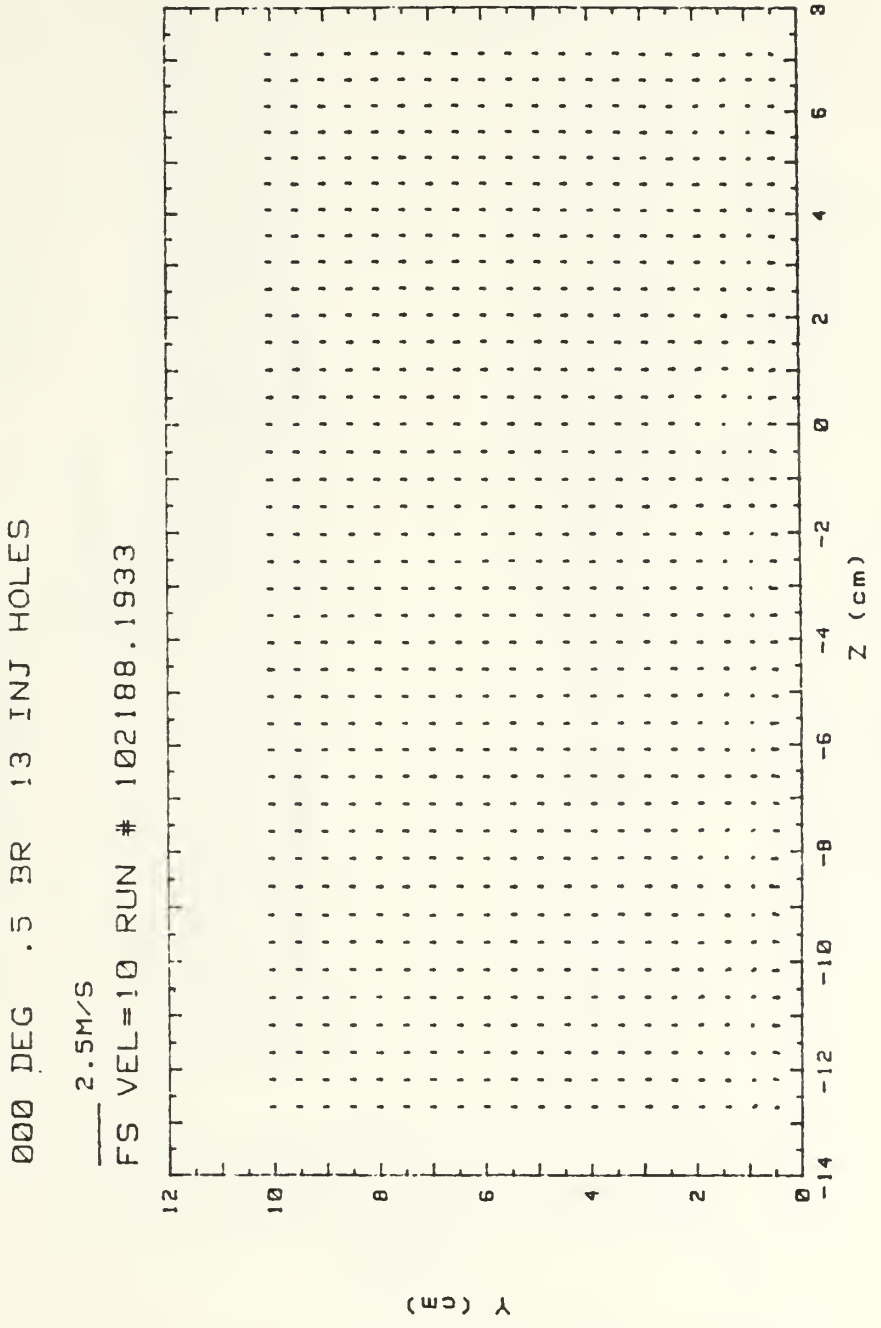

Figure 72. Secondary Flow Vectors, x/d=41.9 m=0.5, 13 Injection Holes, No Vortex, Film Cooled Turbulent Boundary Layer

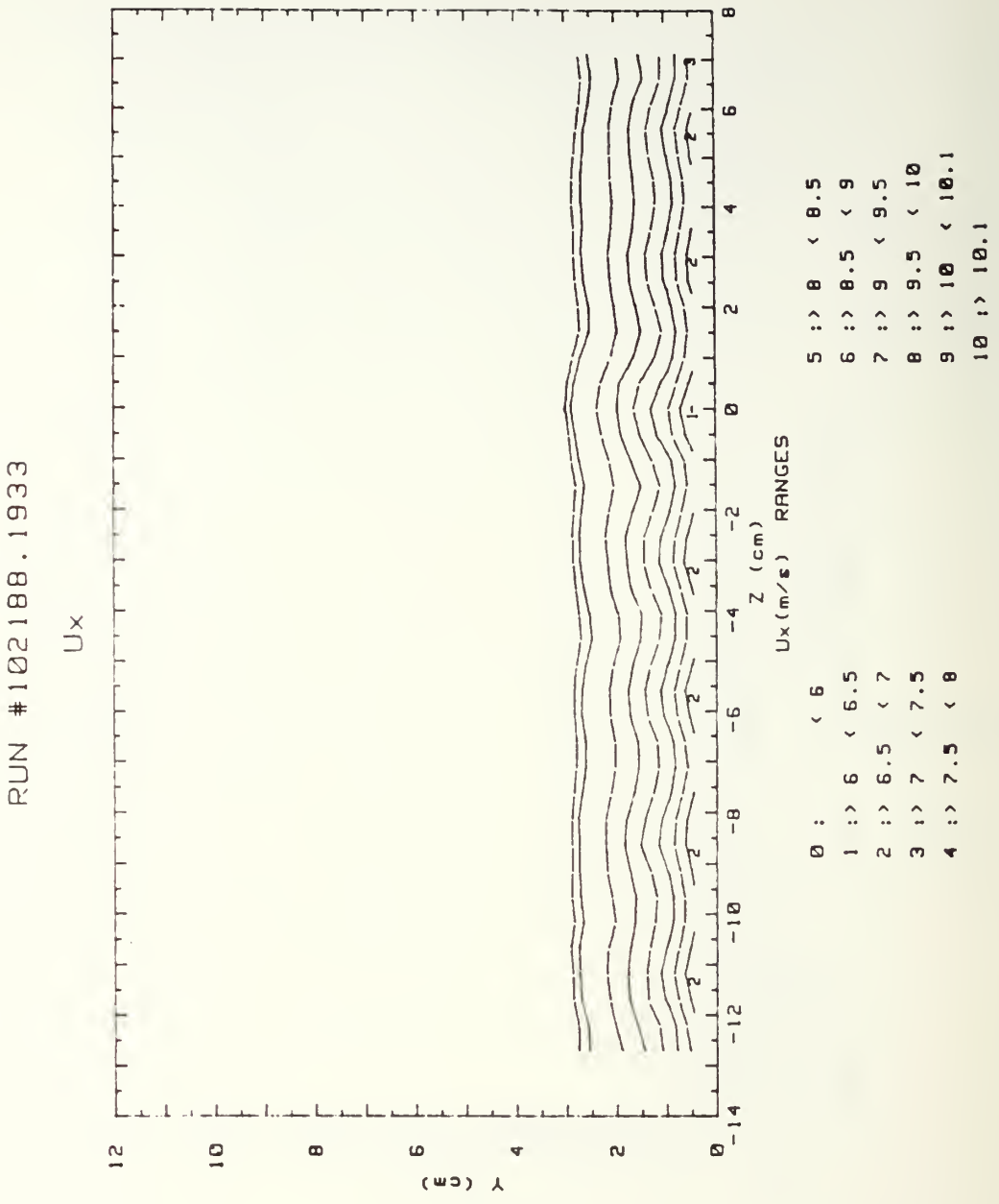

Figure 73. Streamwise Velocity Field, x/d=41.9 m=0.5, 13 Injection Holes, No Vortex, Film Cooled Turbulent Boundary Layer

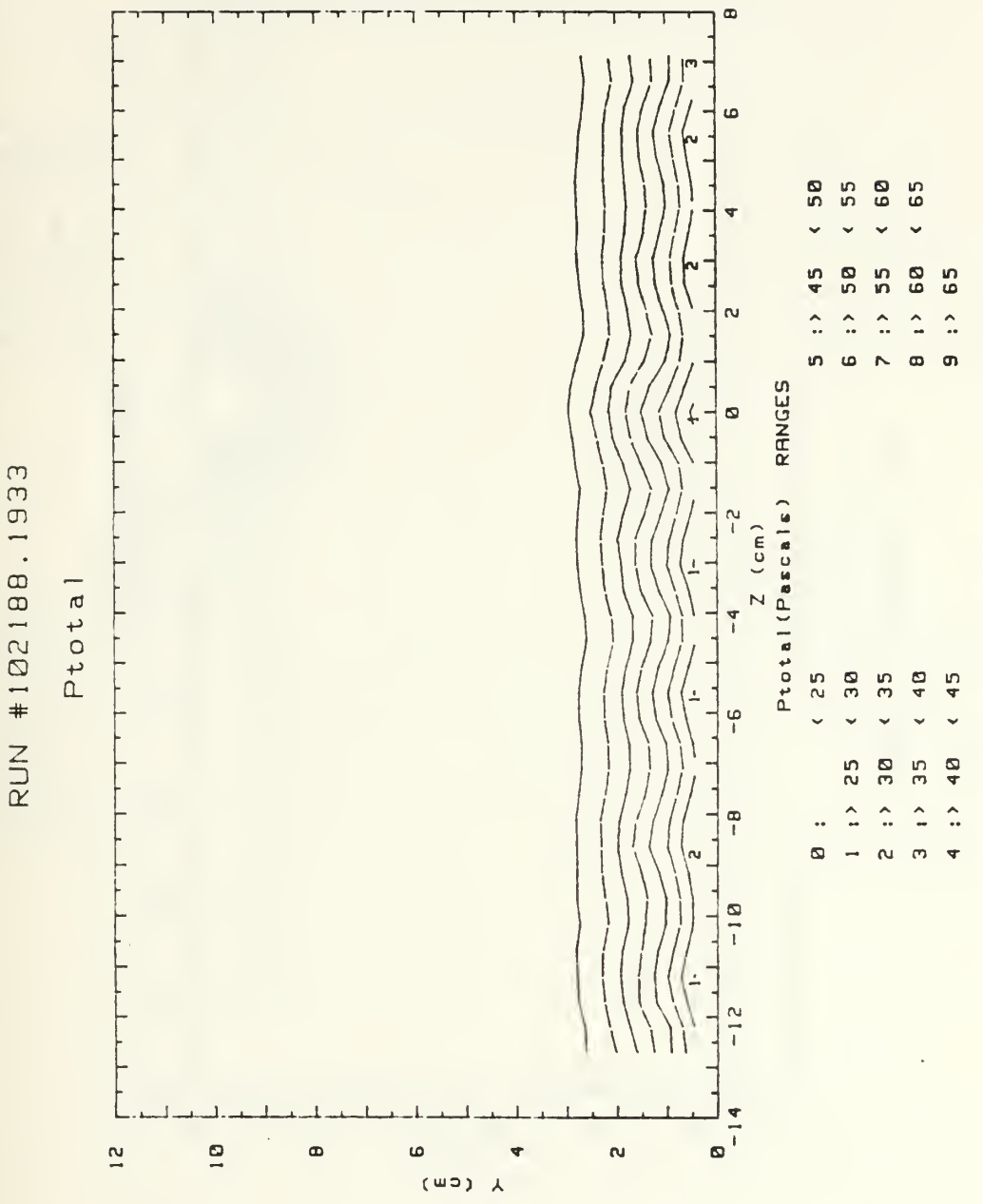

Figure 74. Total Pressure Field, x/d=41.9 m=0.5, 13 Injection Holes, No Vortex, Film Cooled Turbulent Boundary Layer

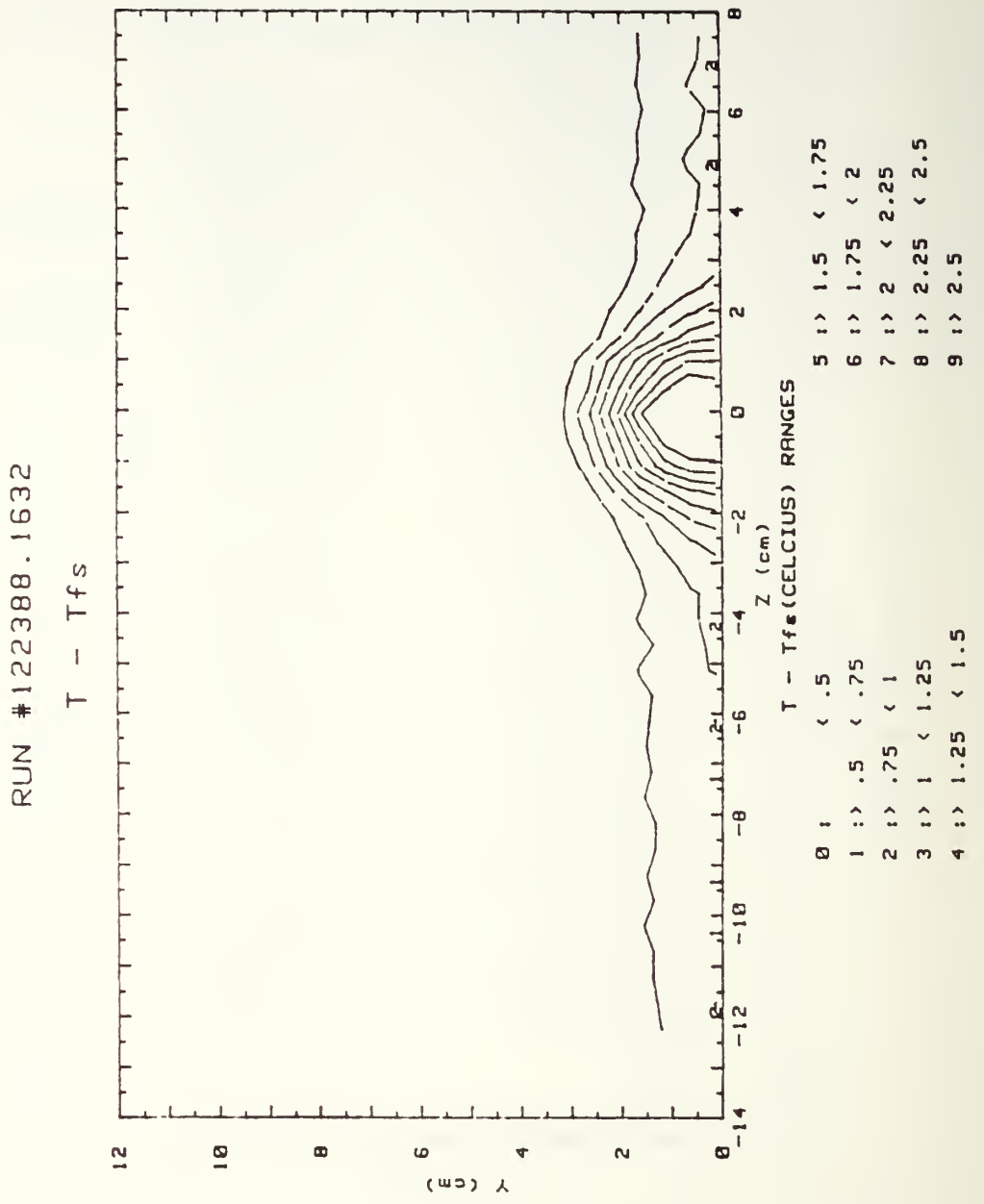

Figure 75. Local Temperature Distribution With Heated Injectant, No Wall Heating, x/d=41.9, m=0.5, Single Injection Hole, No Vortex

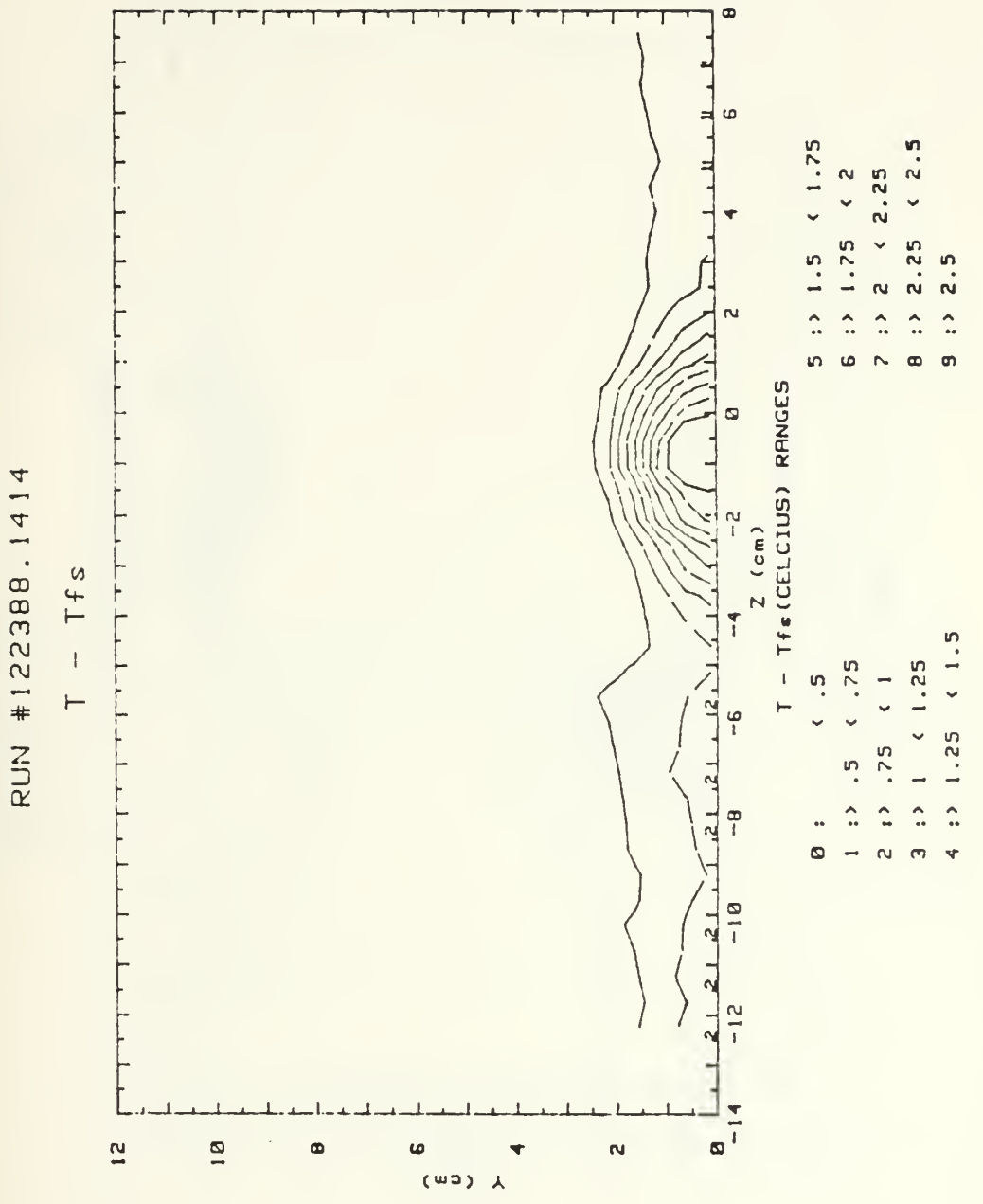

Figure 76. Local Temperature Distribution With Heated Injectant, No Wall Heating, x/d=41.9, m=0.5, Single Injection Hole Γ=.014 m^2/s, S=0.23, Vortex z

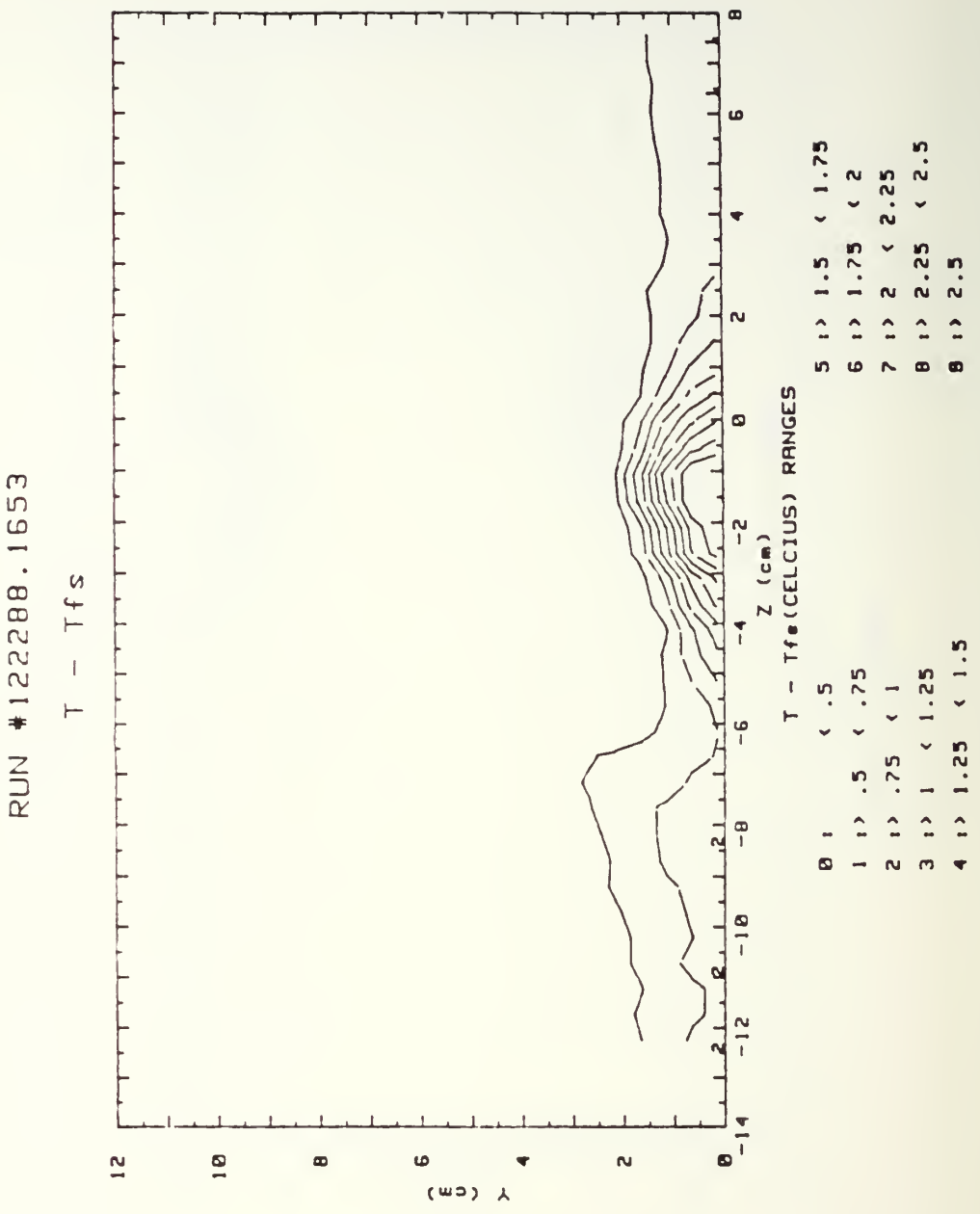

Figure 77. Local Temperature Distribution With Heated Injectant, No Wall Heating, x/d=41.9, m=0.5, Single Injection Hole Γ =.045 m^2/s, S=0.98, Vortex y

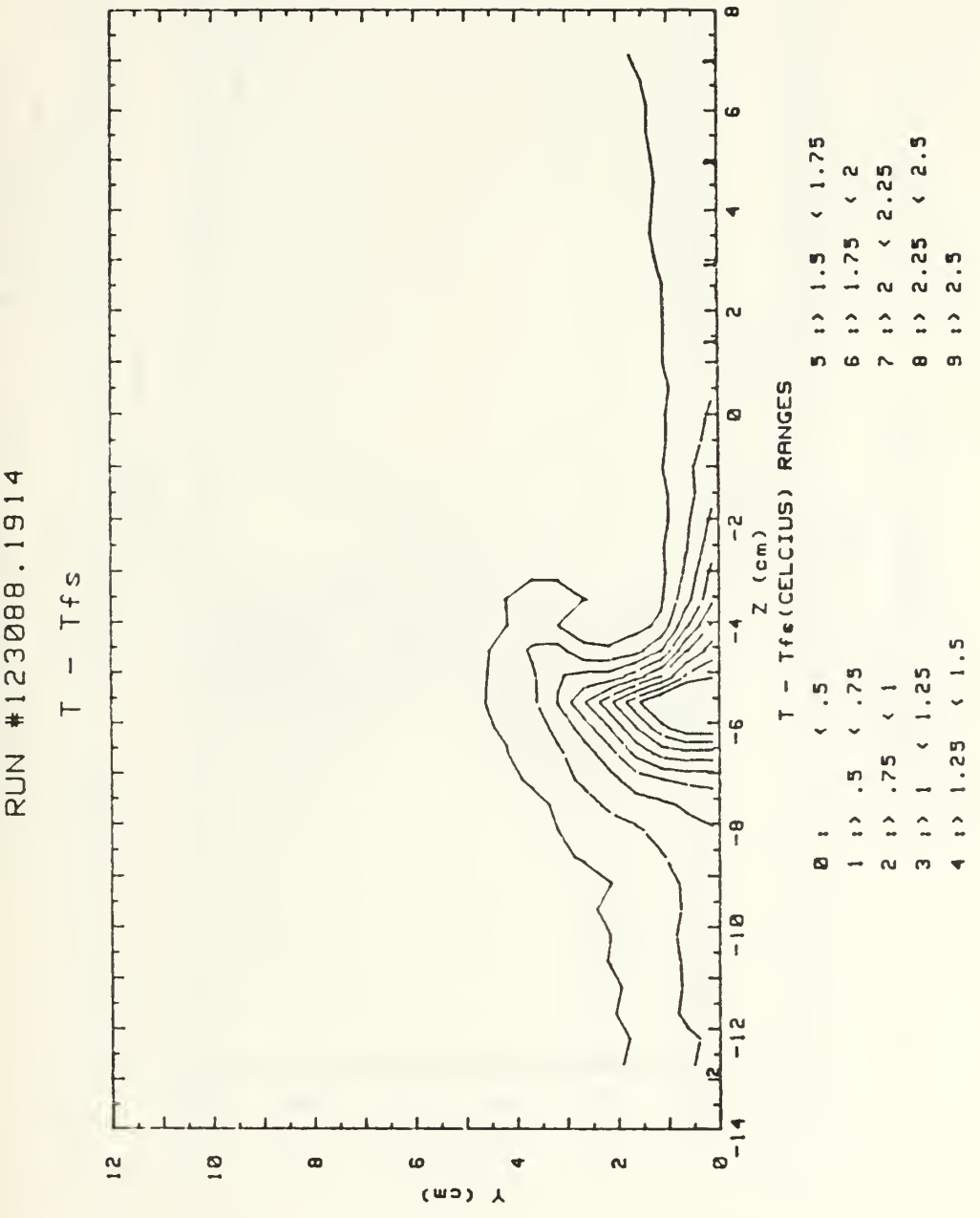

Figure 78. Local Temperature Distribution With Heated Injectant, No Wall Heating, x.d=41.9, m=0.5, Single Injection Hole Γ=.088 m^2/s, S=1.87, Vortex x

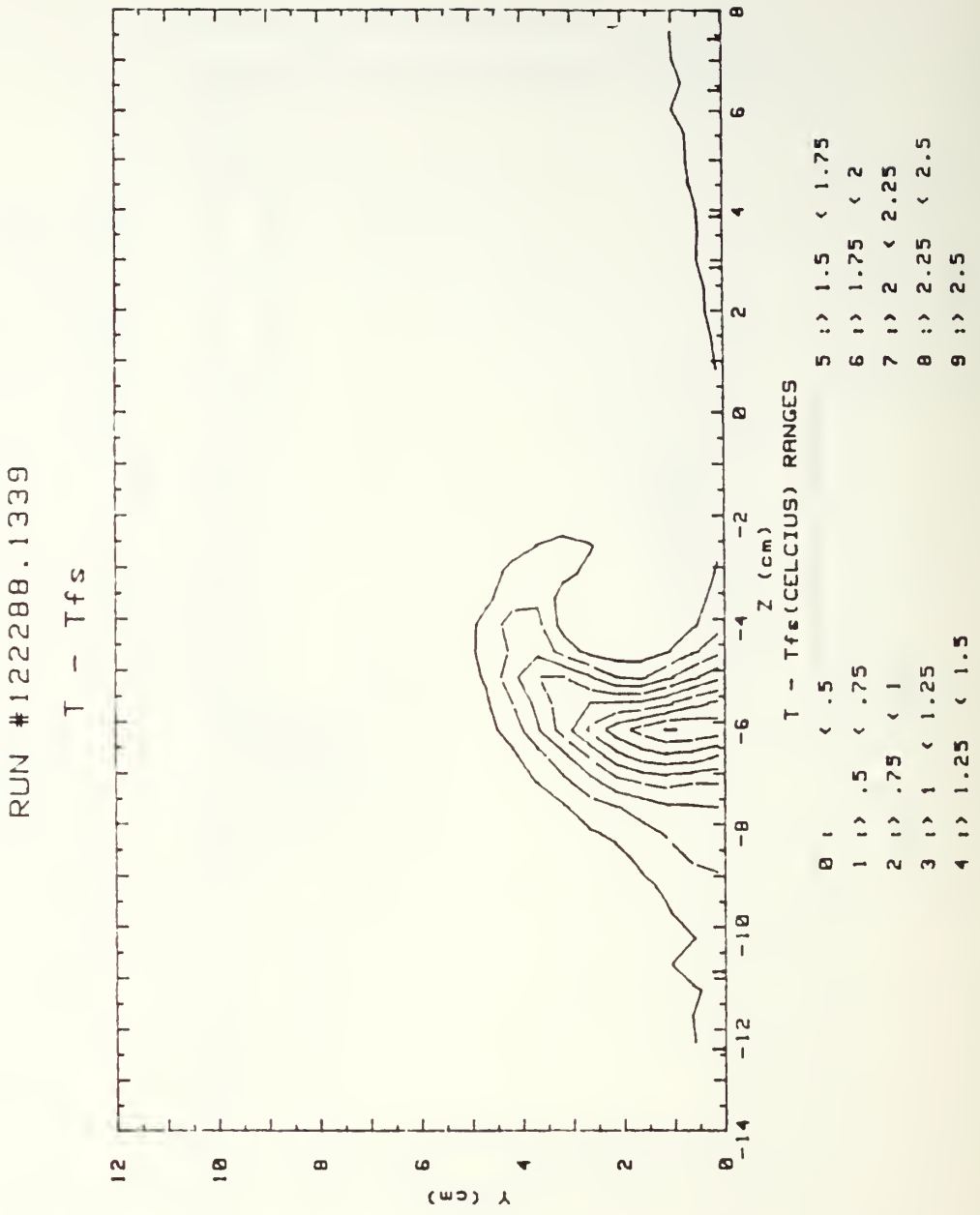

Figure 79. Local Temperature Distribution With Heated Injection, No Wall Heating, x/d=41.9, $\underline{m}$=0.5, Single Injection Hole Γ=.116 m^2/s, S=2.44, Vortex w

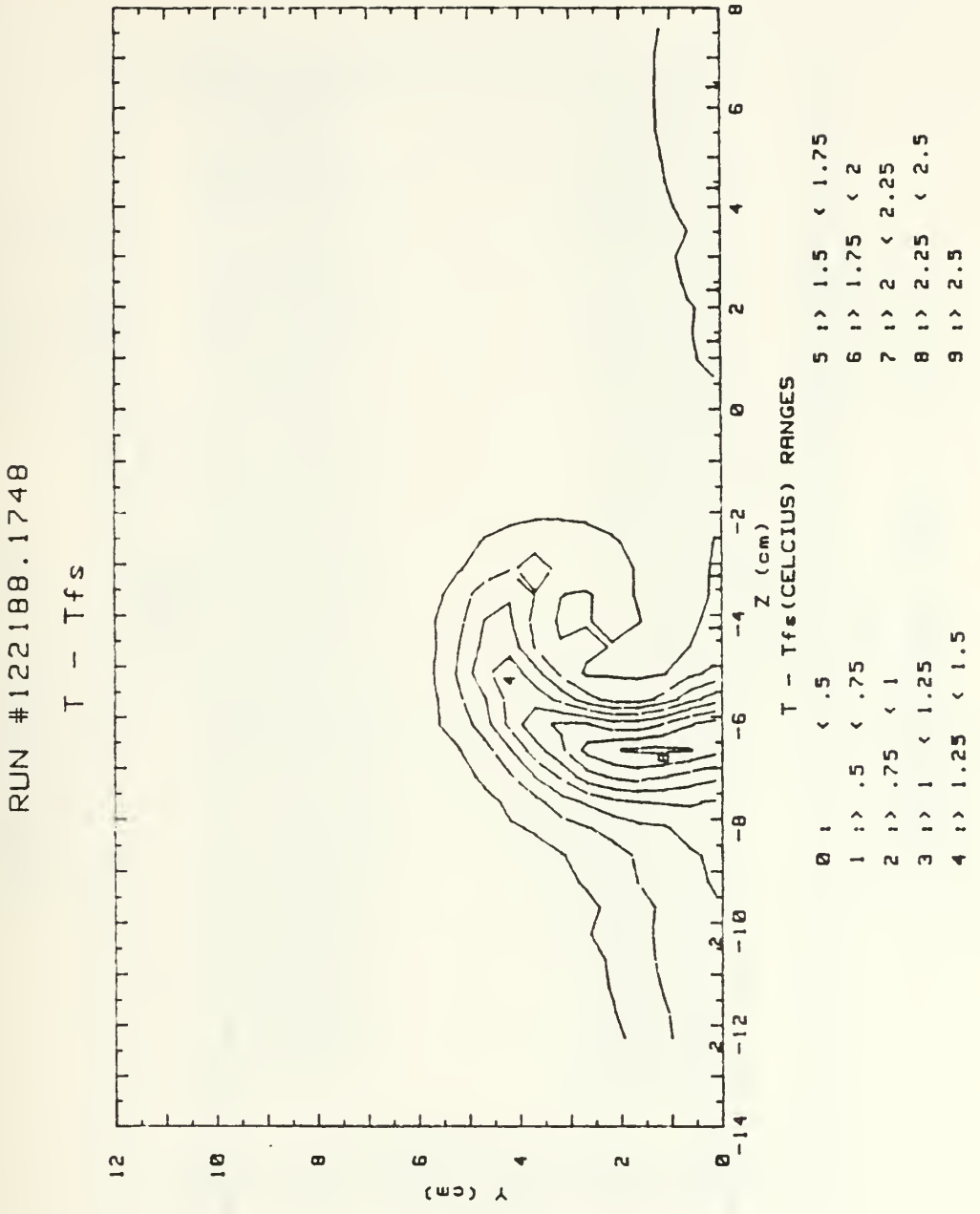

Figure 80. Local Temperature Distribution With Heated Injectant, No Wall Heating, x/d=41.9, $\bar{m}$=0.5, Single Injection Hole Γ=.145 m^2/s, S=2.99, Vortex r

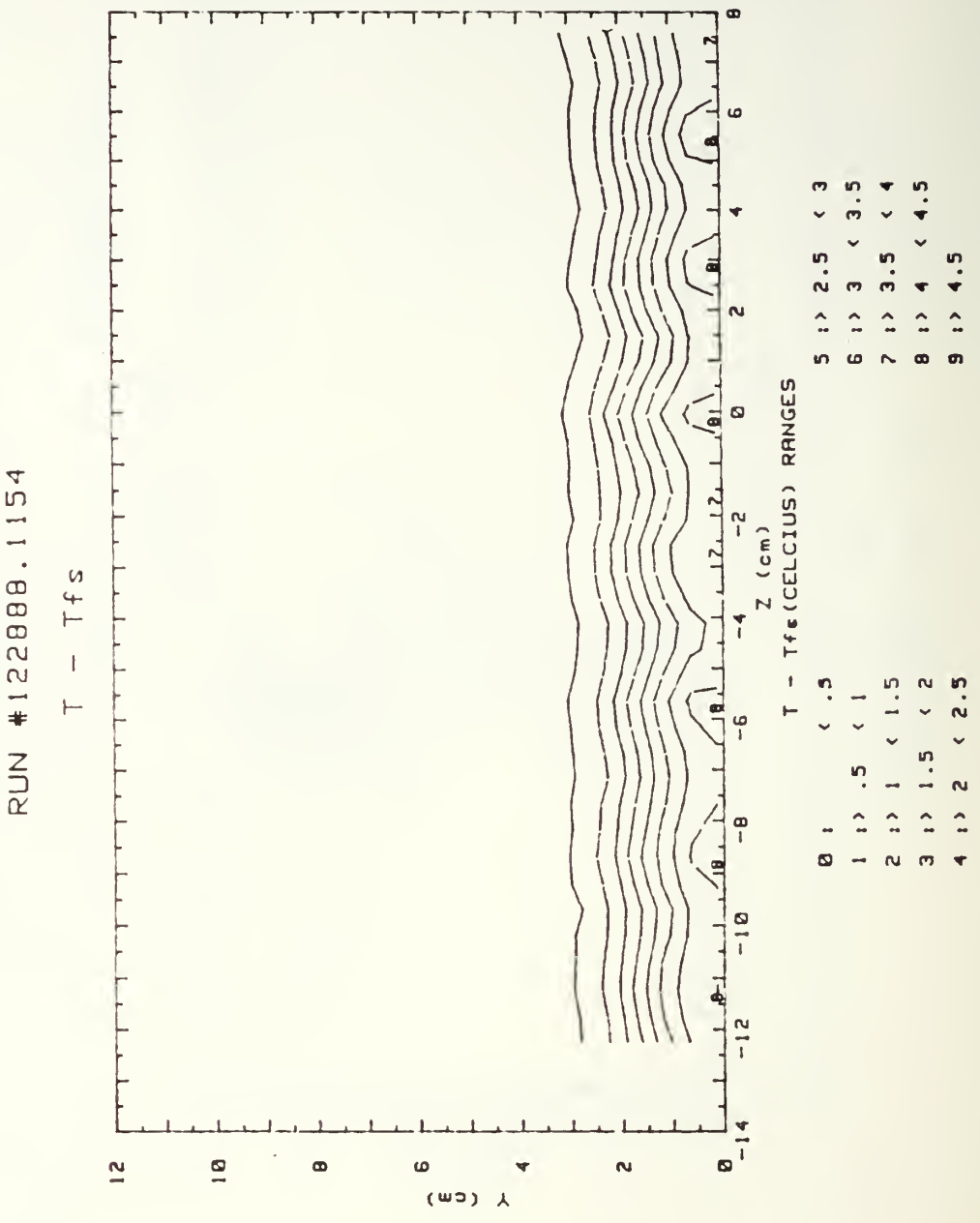

Figure 81. Local Temperature Distribution With Heated Injectant, No Wall Heating, No Vortex, x/d=41.9, m=0.5, 13 Injection Holes

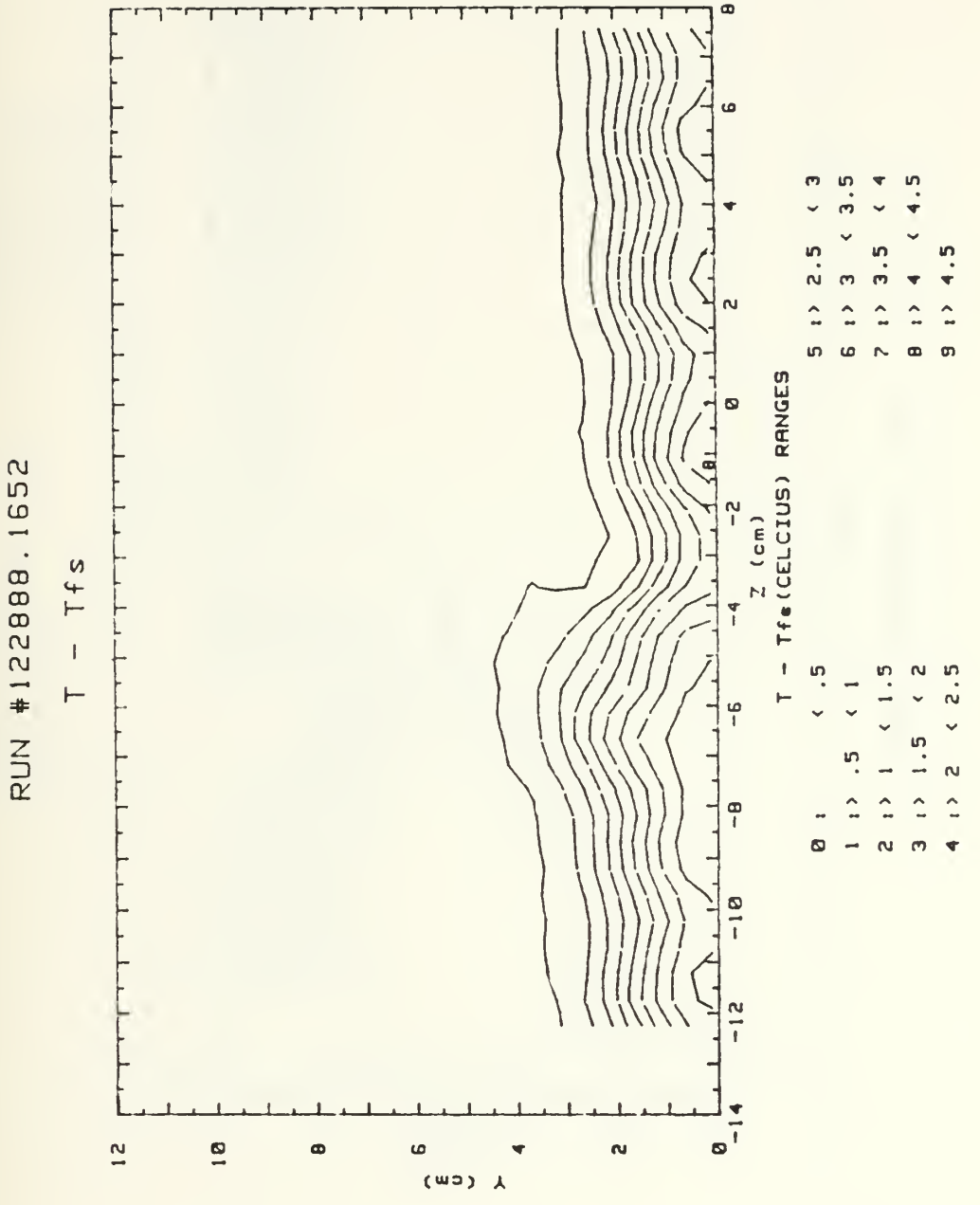

Figure 82. Local Temperature Distribution With Heated Injectant, No Wall Heating, x/d=41.9, m=0.5, 13 Injection Holes Γ=.014 m^2/s, S=0.23, Vortex z

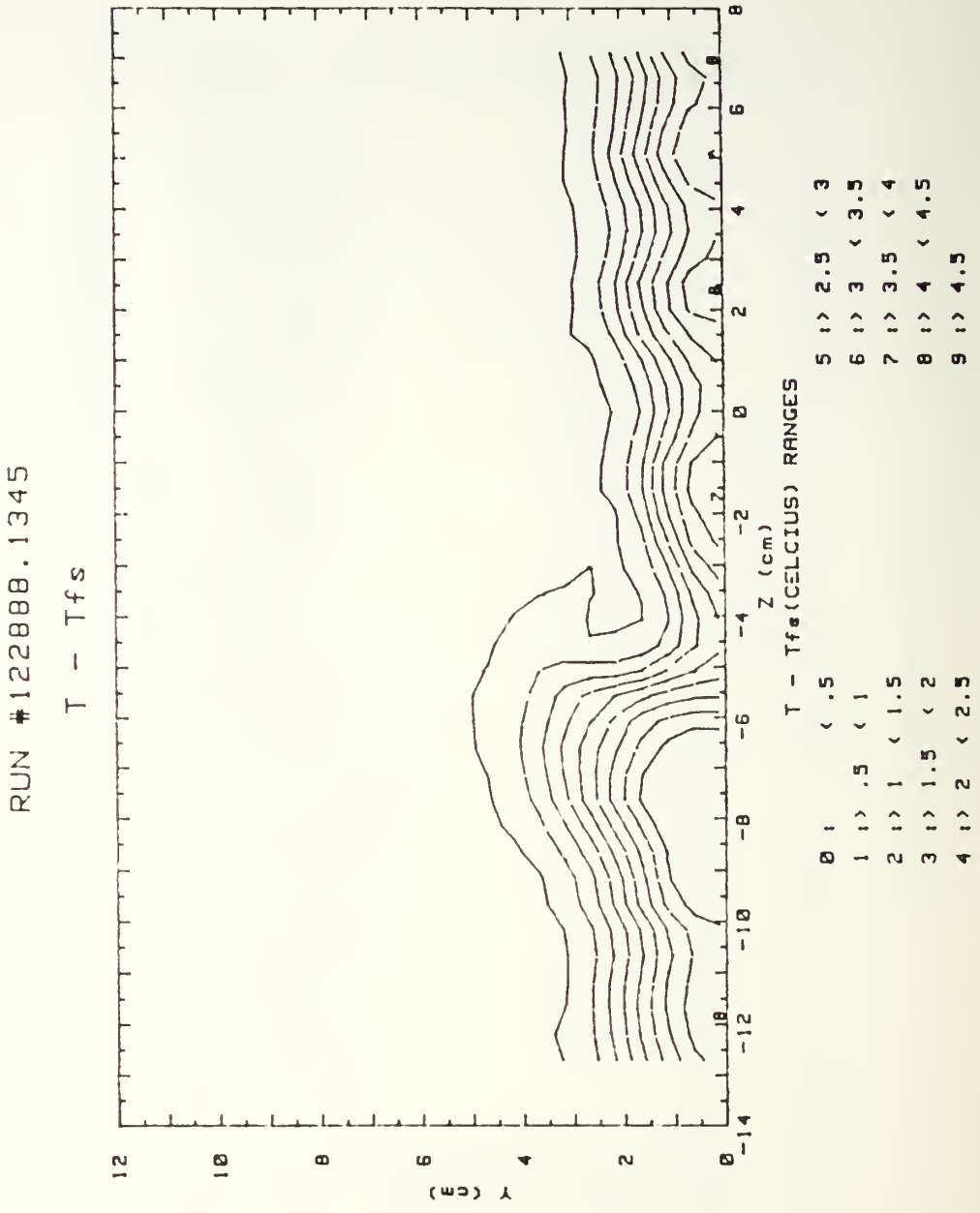

Figure 83. Local Temperature Distribution With Heated Injectant, No Wall Heating, x/d=41.9, $\underline{m}$=0.5, 13 Injection Holes Γ =.045 m^2/s, S-0.98, Vortex y

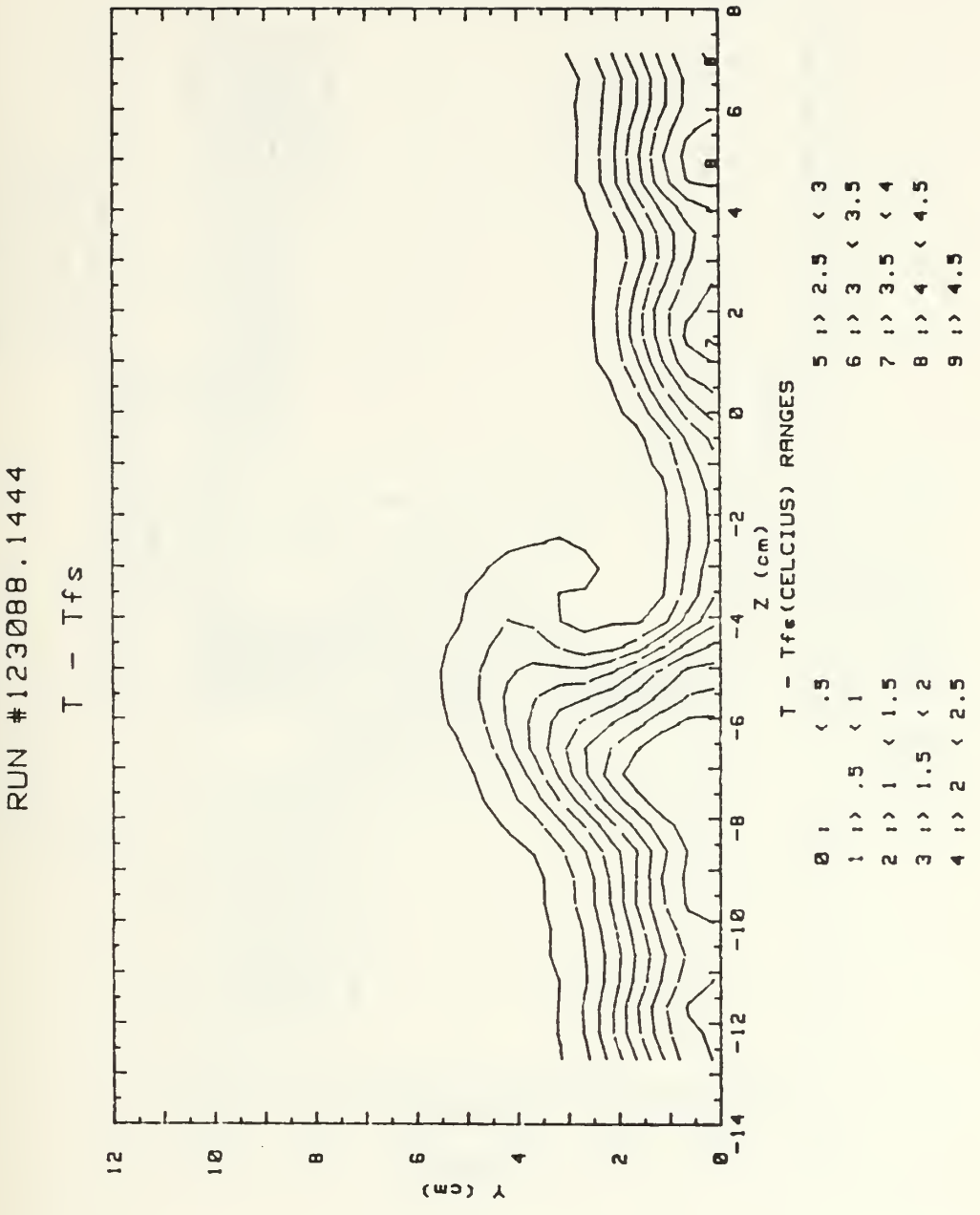

Figure 84. Local Temperature Distribution With Heated Injectant, No Wall Heating, x/d=41.9, m=0.5, 13 Injection Holes Γ =.088 m^2/s, S=1.87, Vortex x

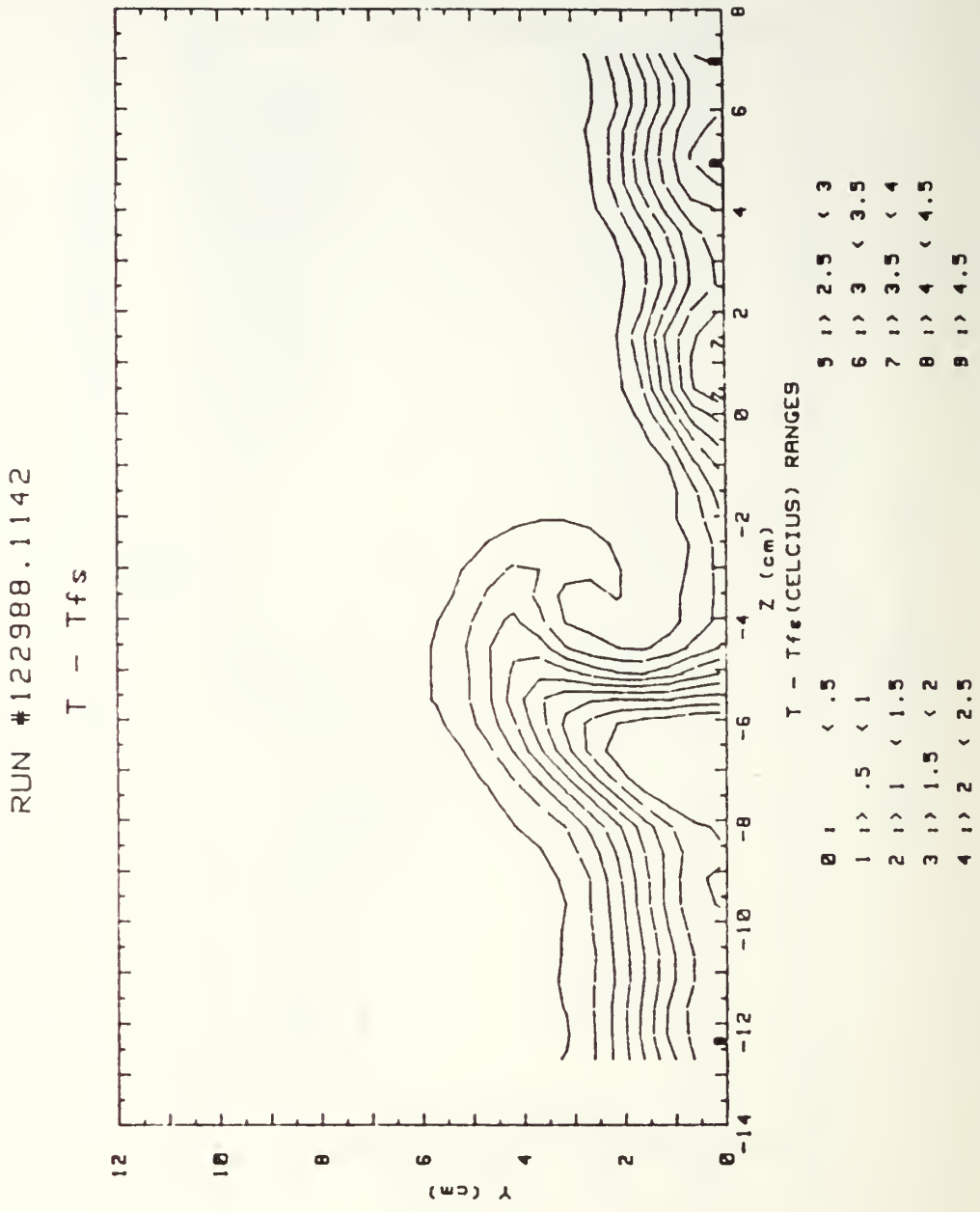

Figure 85. Local Temperature Distribution With Heated Injectant, No Wall Heating, x/d=41.9, m=0.5, 13 Injection Holes Γ=.116 m^2/s, S=2.44, Vortex w

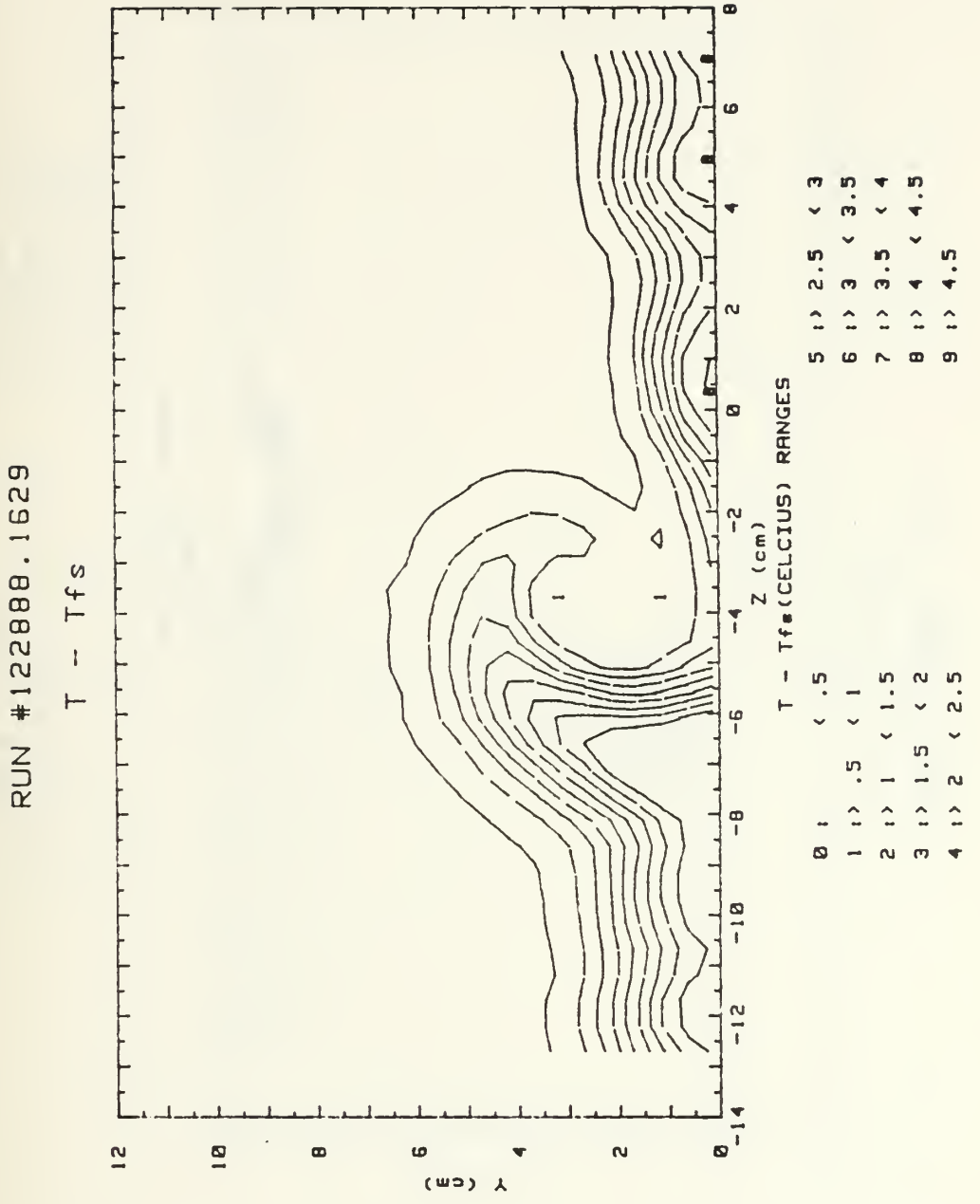

Figure 86. Local Temperature Distribution With Heated Injectant, No Wall Heating, x/d=41.9, $\bar{m}$=0.5, 13 Injection Holes Γ=.145 m^2/s, S=2.44, Vortex r

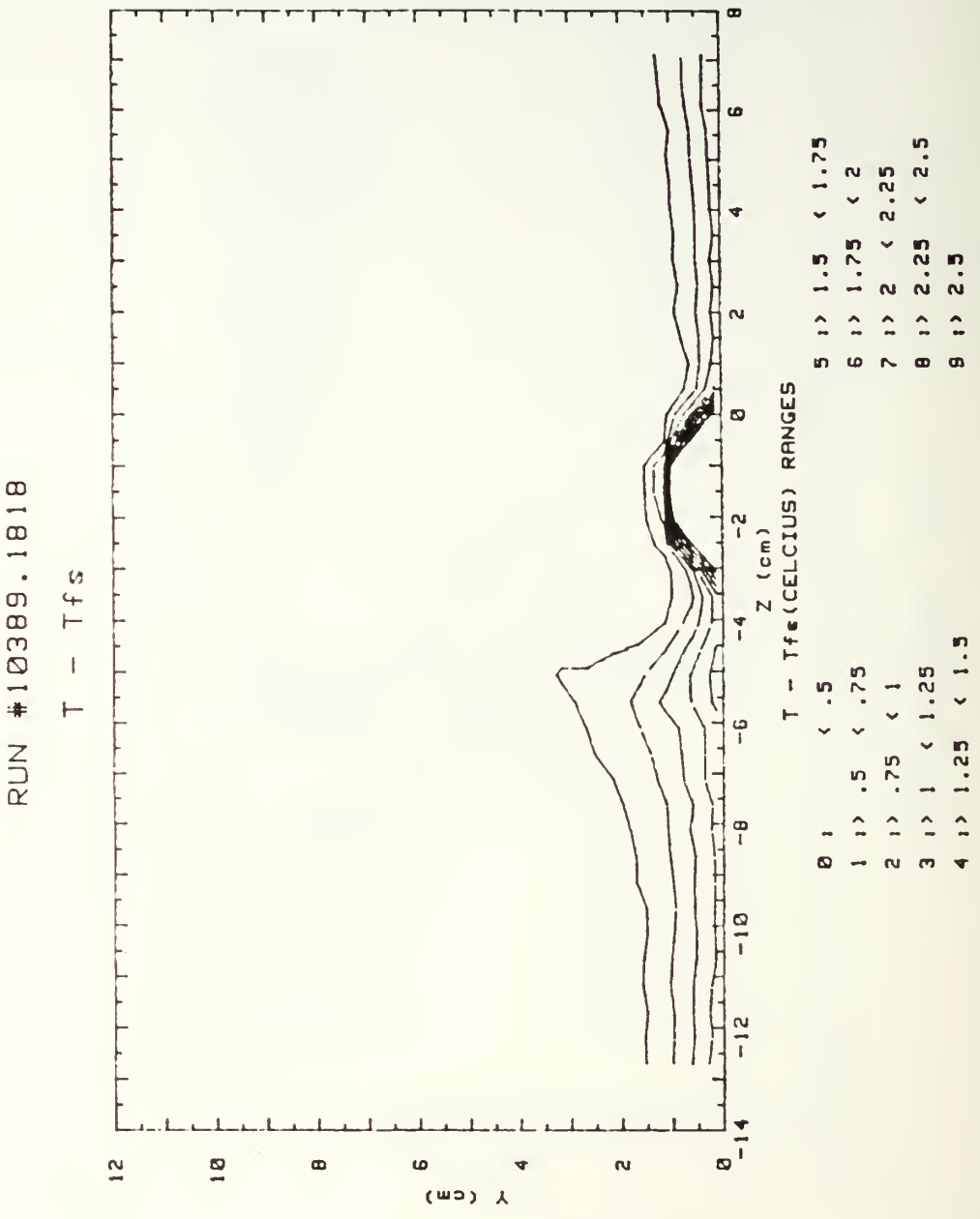

Figure 87. Local Temperature Distribution With Heated Injectant, No Wall Heating, x/d=5.2, m=0.5, Single Injection Hole Vortex w

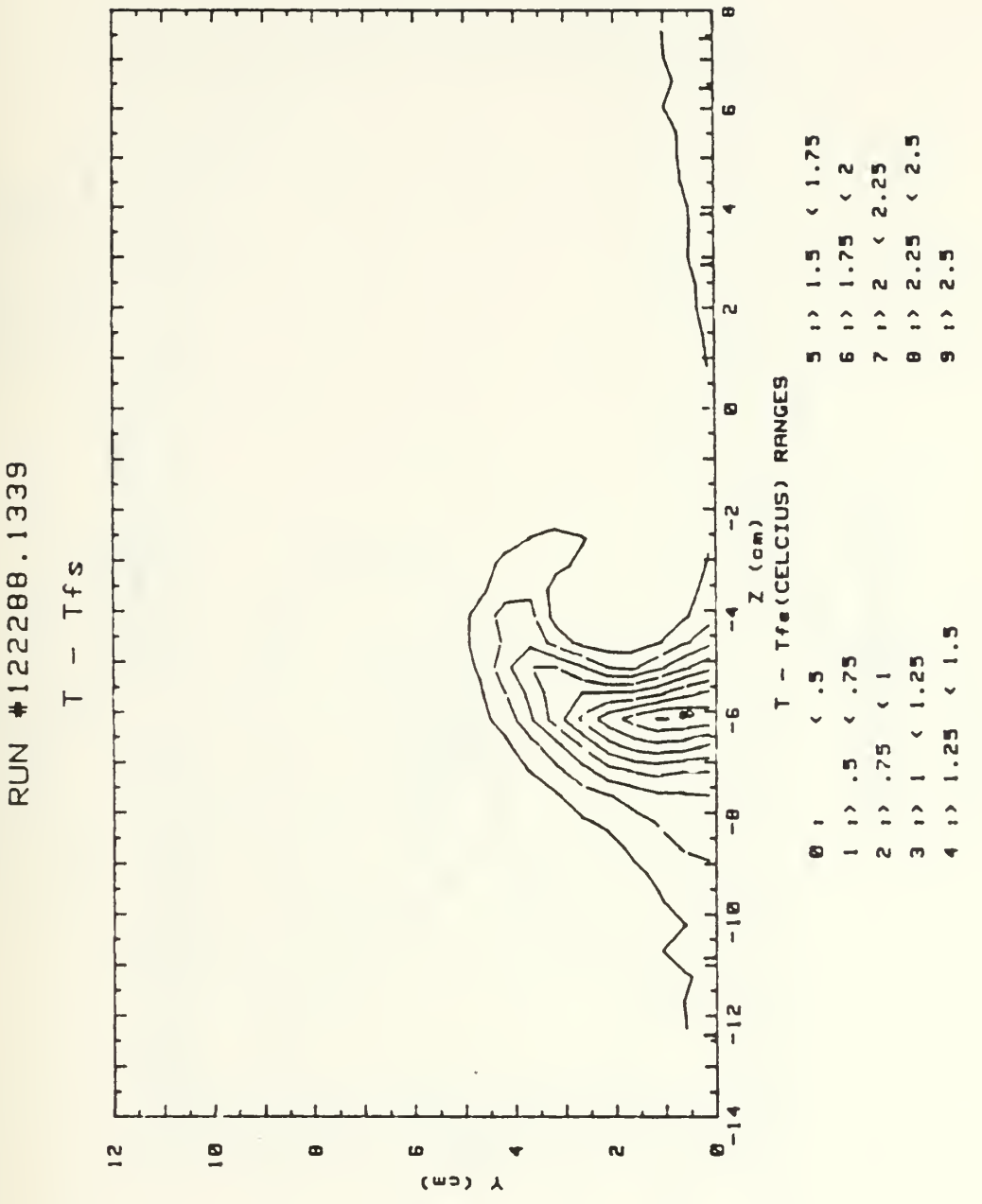

Figure 88. Local Temperature Distribution With Heated Injectant, No Wall Heating, x/d=41.9, m=0.5, Single Injection Hole Γ =.116 m^2/s, S=2.44, Vortex w

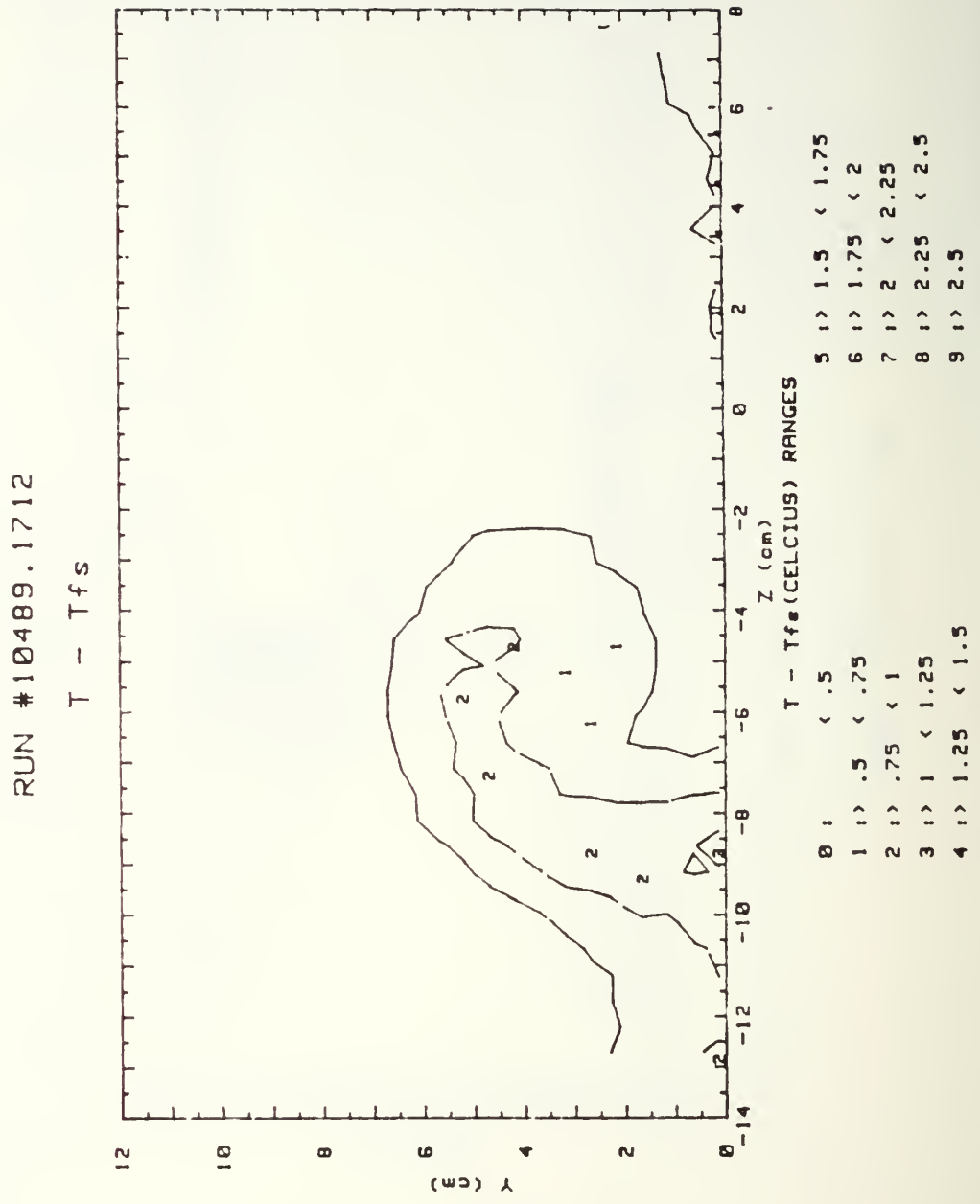

Figure 89. Local Temperature Distribution With Heated Injectant, No Wall Heating, x/d=82.9, m=0.5, Single Injection Hole Vortex w

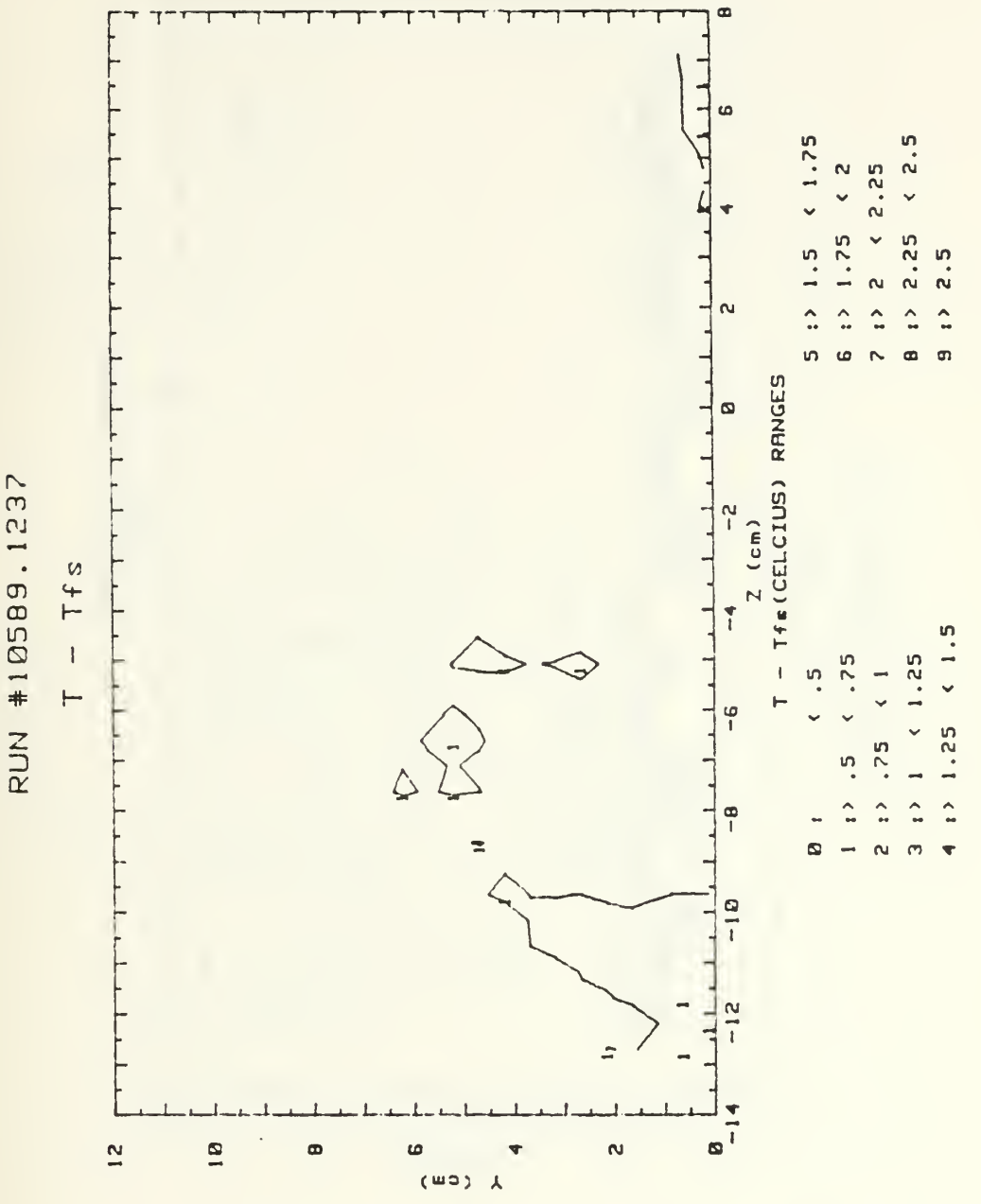

Figure 90. Local Temperature Distribution With Heated Injectant, No Wall Heating, x/d=109.2, m=0.5, Single Injection Hole Vortex w, Temp. Difference Range (.5 - 2.5) degrees

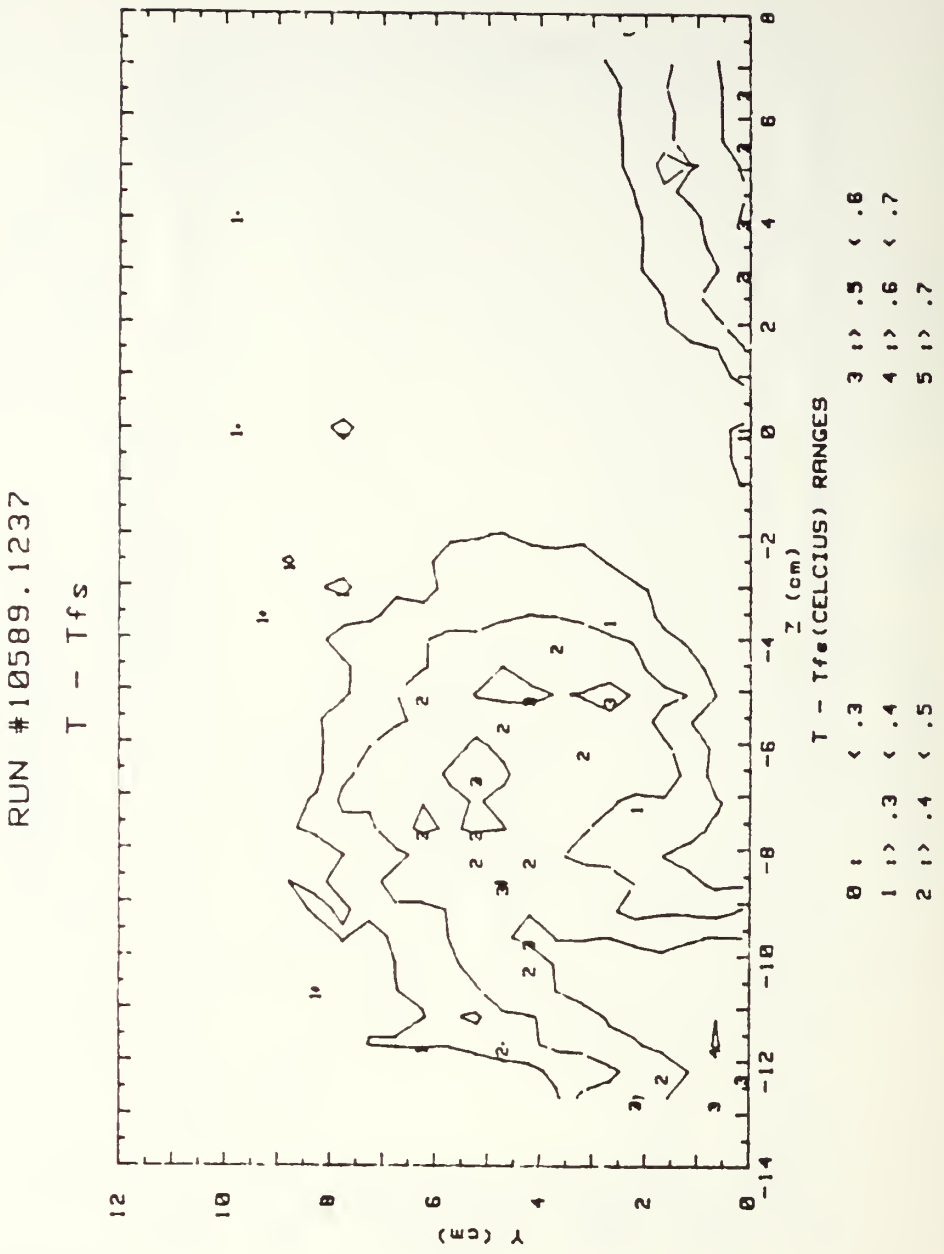

Figure 91. Local Temperature Distribution With Heated Injectant, No Wall Heating, x/d=109.2, m=0.5, Single Injection Hole Vortex w, Temp. Difference Range (.3 - .7) degrees

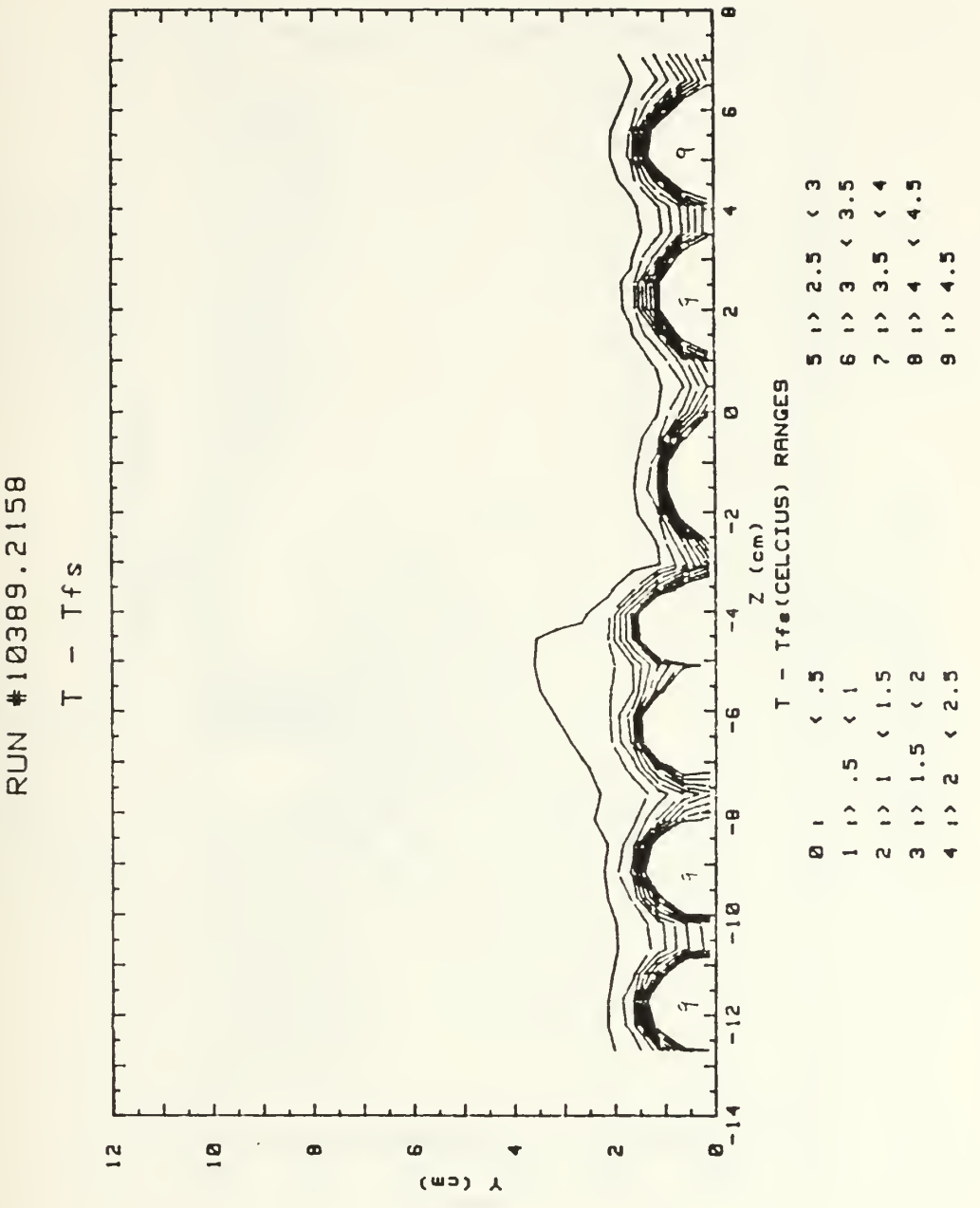

Figure 92. Local Temperature Distribution With Heated Injectant, No Wall Heating, x/d=5.2, m=0.5, 13 Injection Holes Vortex w

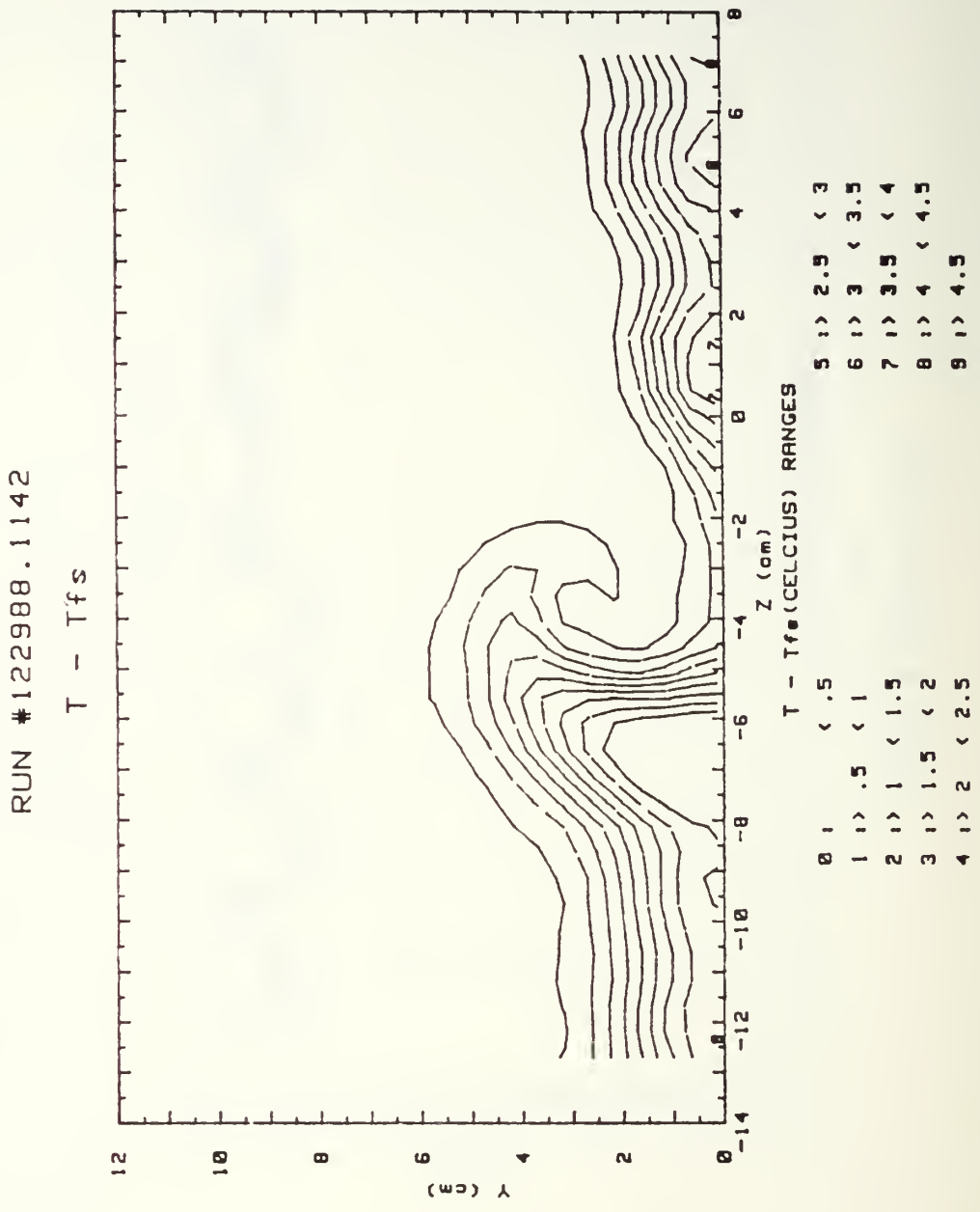

Figure 93. Local Temperature Distribution With Heated Injectant, No Wall Heating, x/d=41.9, $\bar{m}$=0.5, 13 Injection Holes Γ=.116 m^2/s, S=2.44, Vortex w

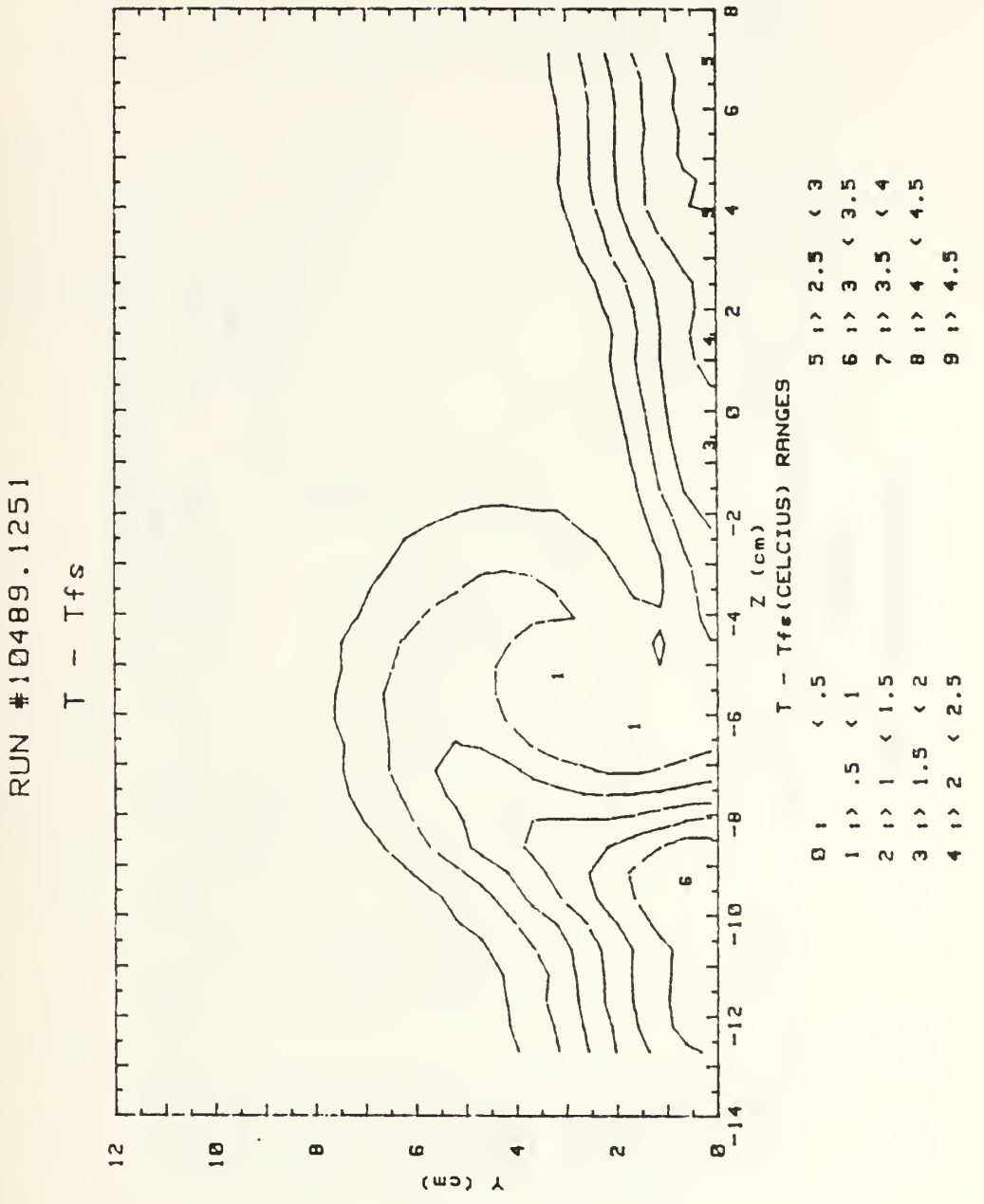

Figure 94. Local Temperature Distribution With Heated Injectant, No Wall Heating, x/d=82.9, m=0.5, 13 Injection Holes Vortex w

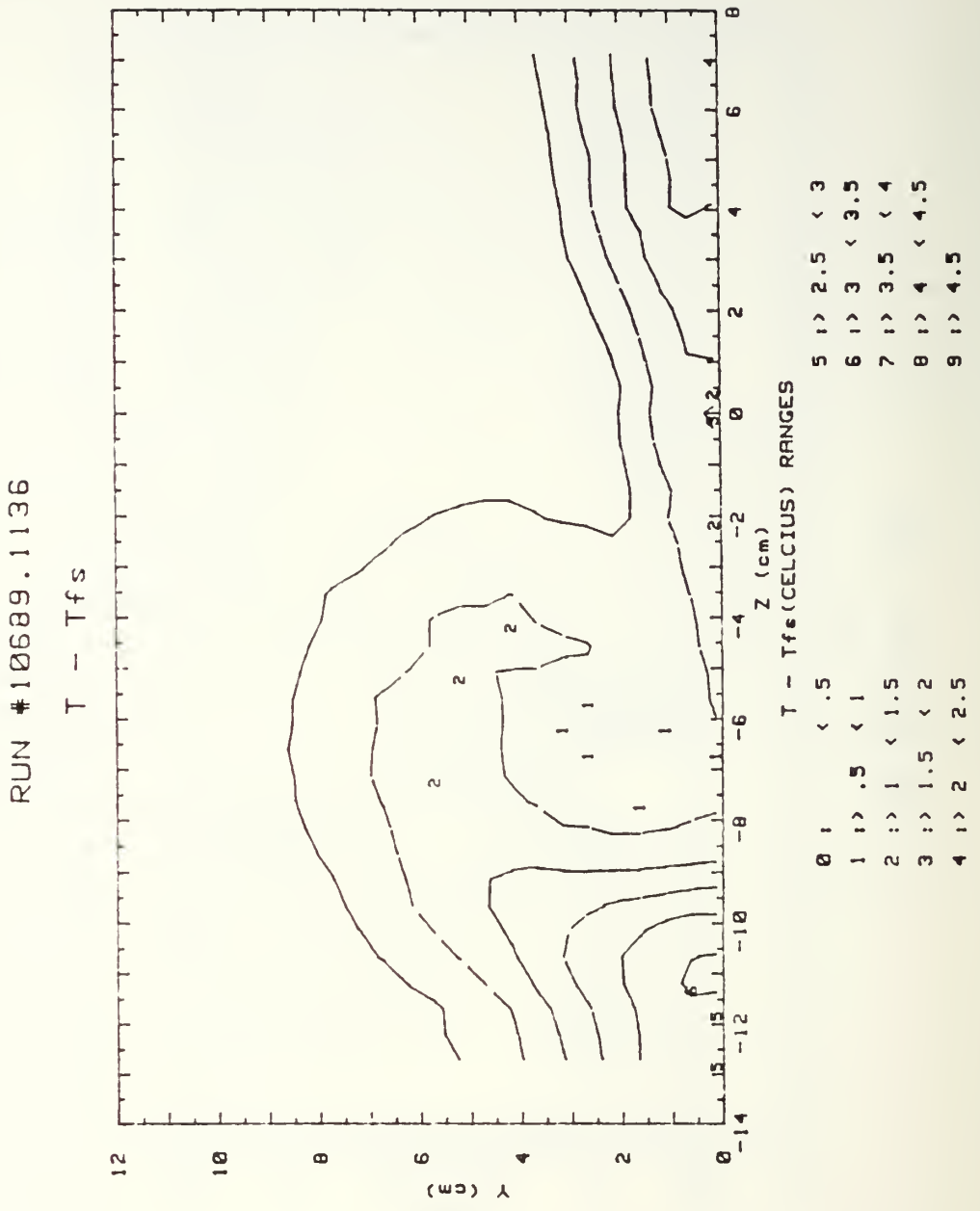

Figure 95. Local Temperature Distribution With Heated Injectant, No Wall Heating, x/d=109.2, m=0.5, 13 Injection Holes Vortex w

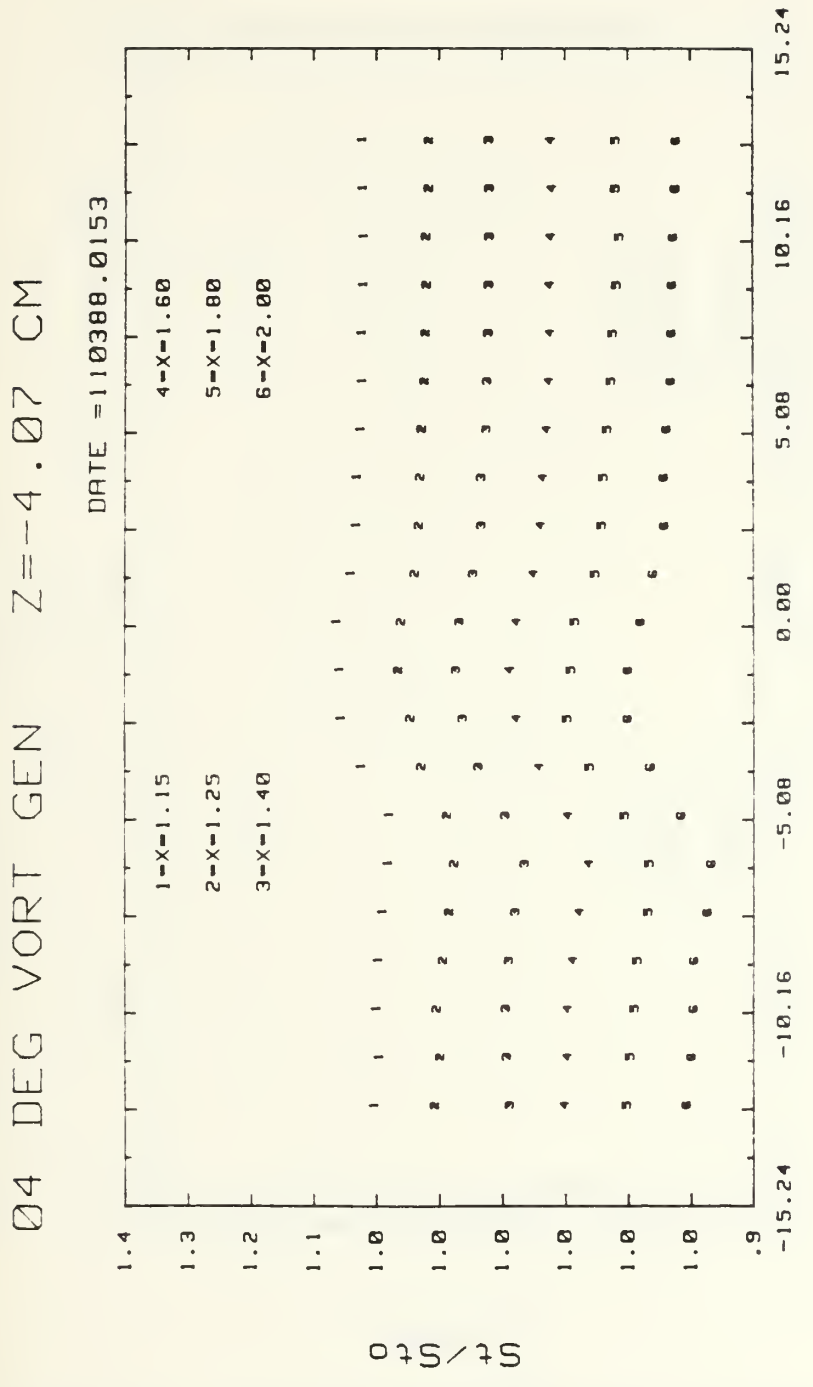

Figure 96. Local St/Sto Ratio Distribution With No Film Cooling, Embedded Vortex z

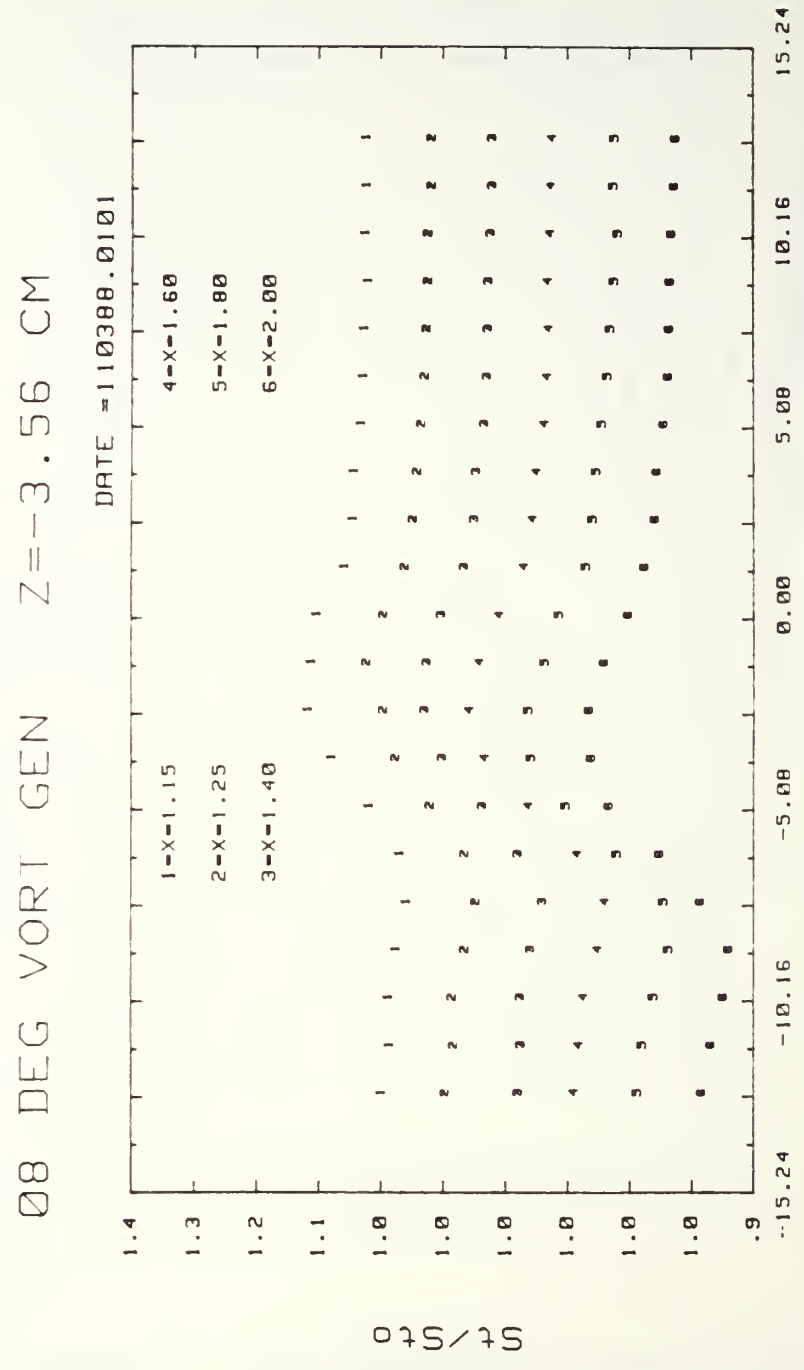

Figure 97. Local St/Sto Ratio Distribution With No Film Cooling, Embedded Vortex y

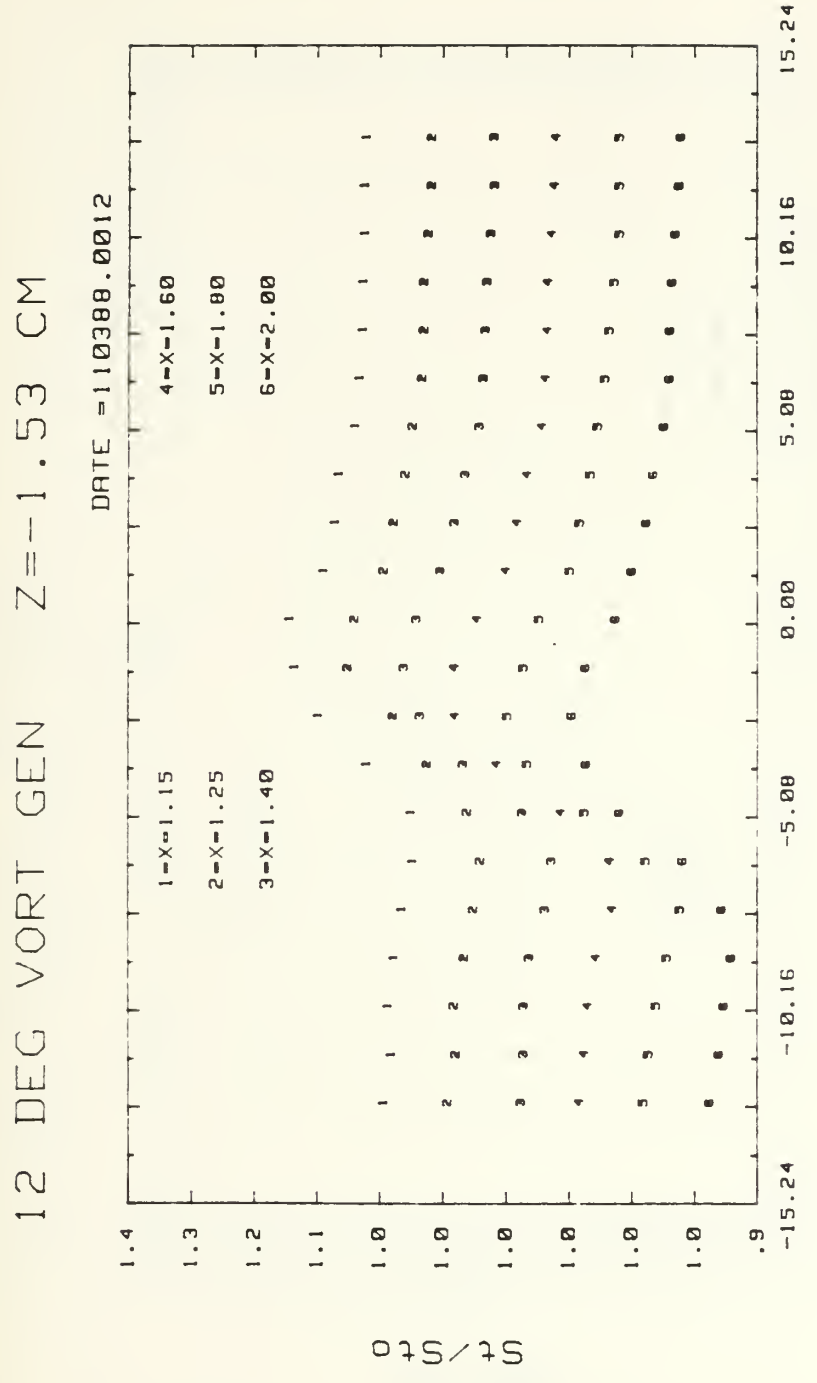

Figure 98. Local St/Sto Ratio Distribution With No Film Cooling, Embedded Vortex x

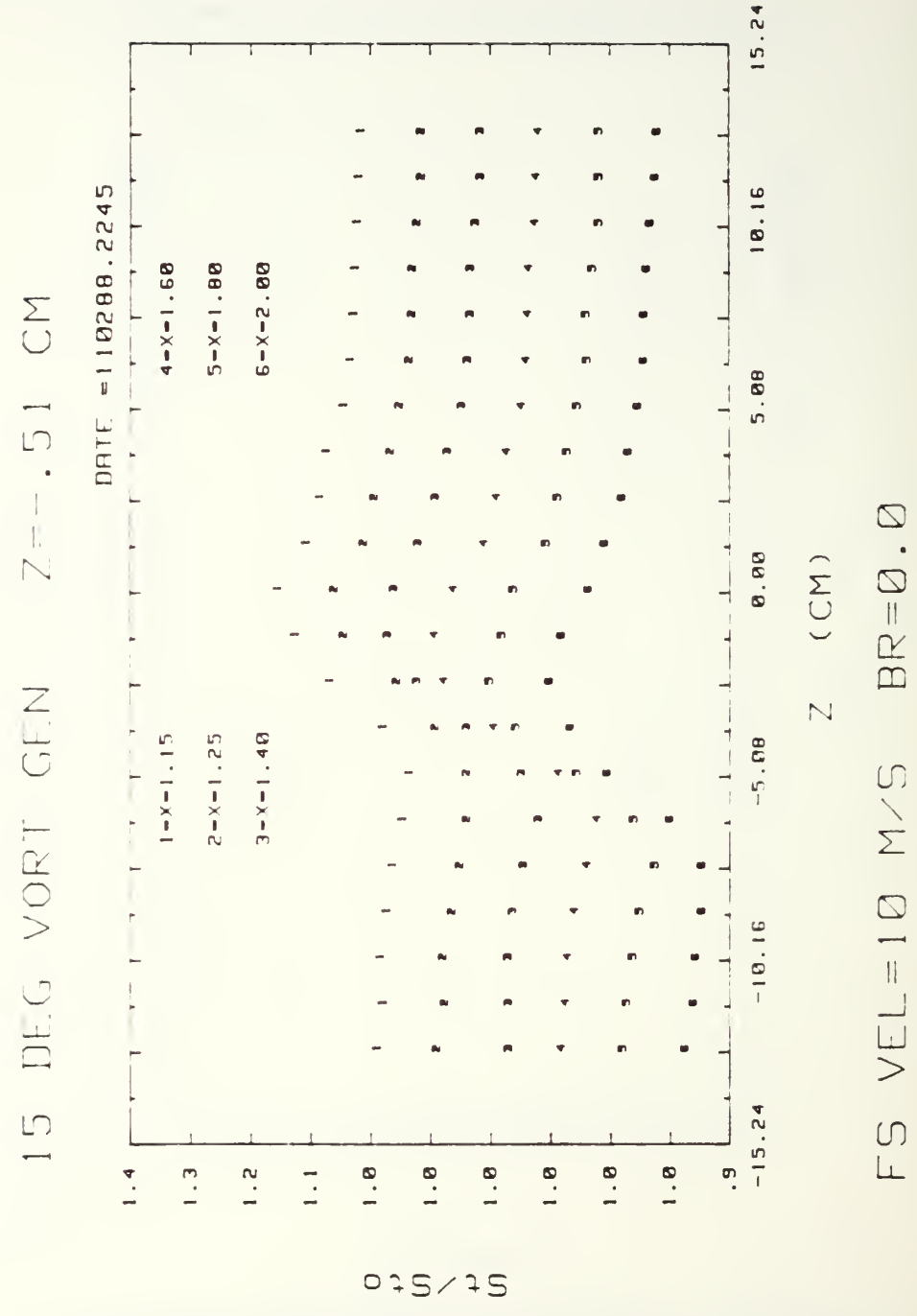

Figure 99. Local St/Sto Ratio Distribution With No Film Cooling, Embedded Vortex w

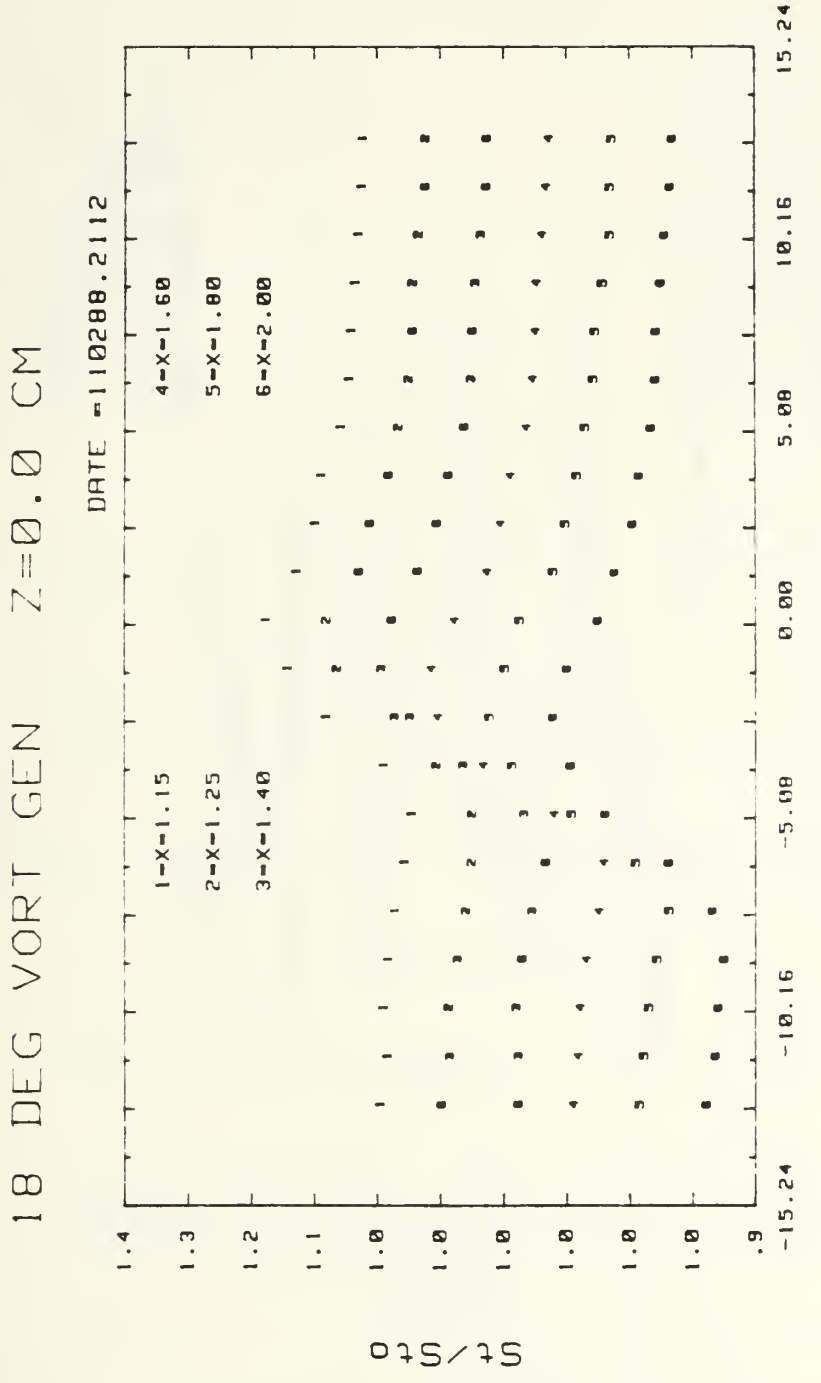

Figure 100. Local St/Sto Ratio Distribution With No Film Cooling, Embedded Vortex r

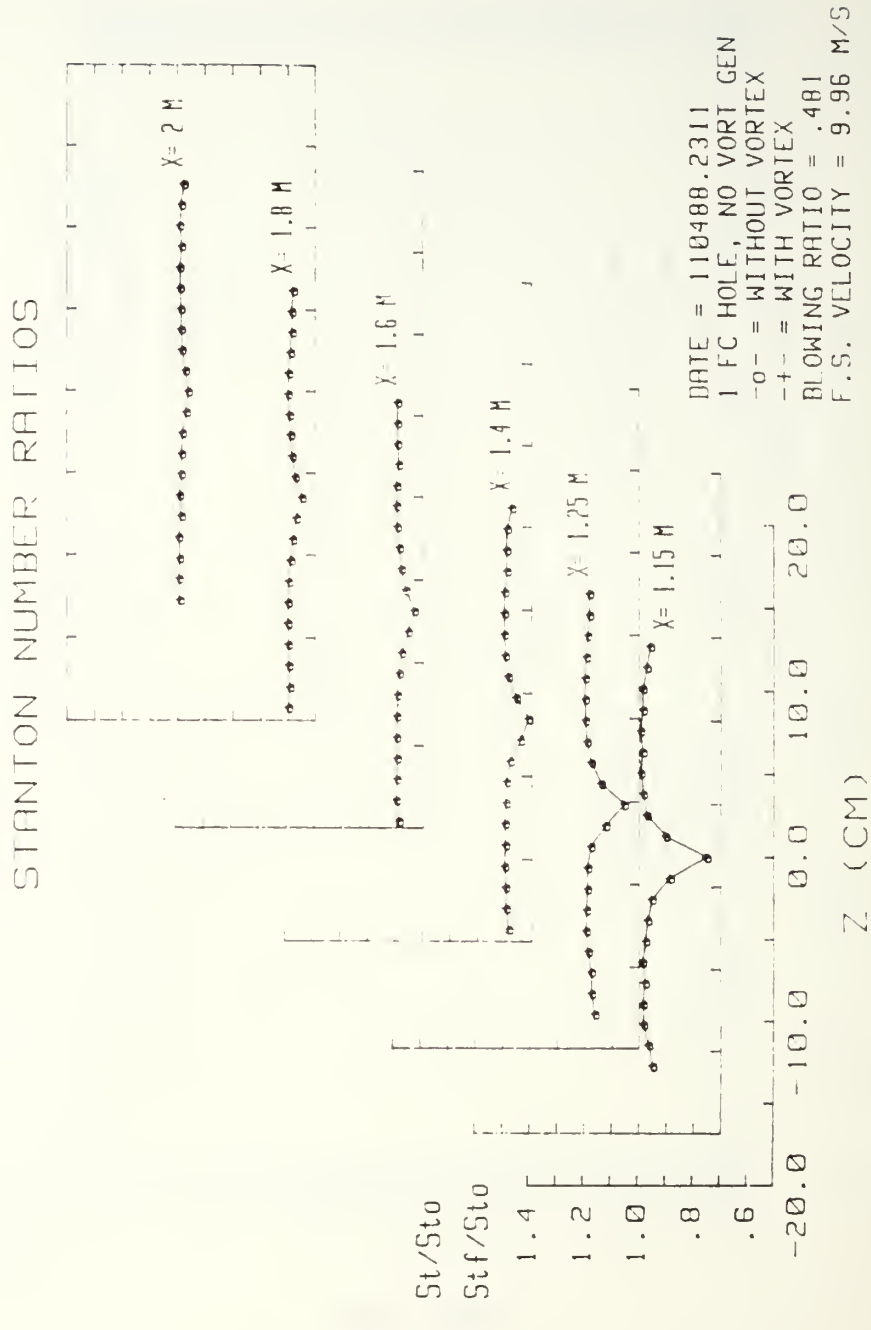

Figure 101. Local St/Sto and Stf/Sto Distributions With Film Cooling, m=0.5, Single Injection Hole Without Embedded Vortex

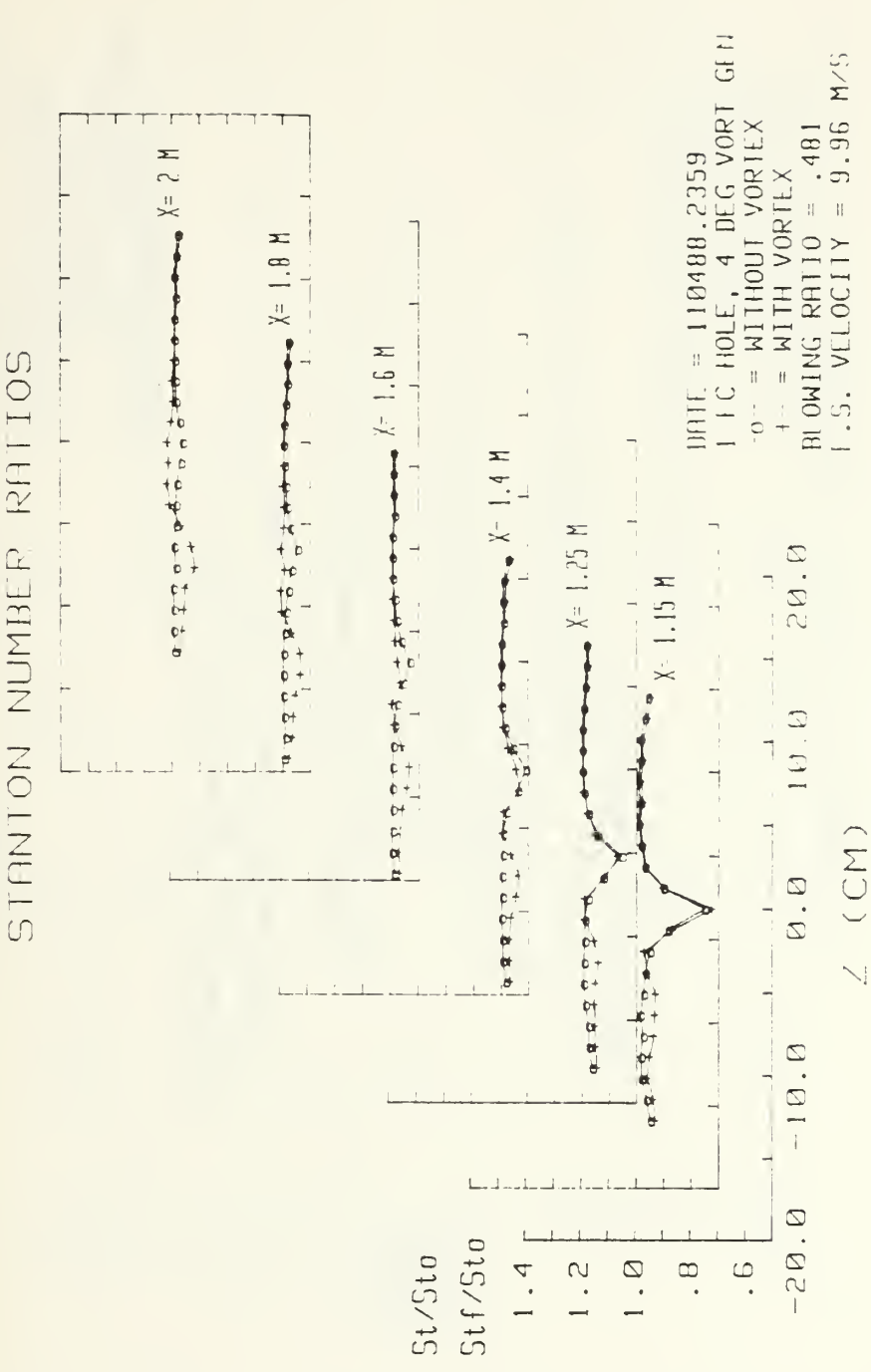

Figure 102. Local St/Sto and Stf/Sto Distributions With Film Cooling, m=0.5, Single Injection Hole With and Without Embedded Vortex z

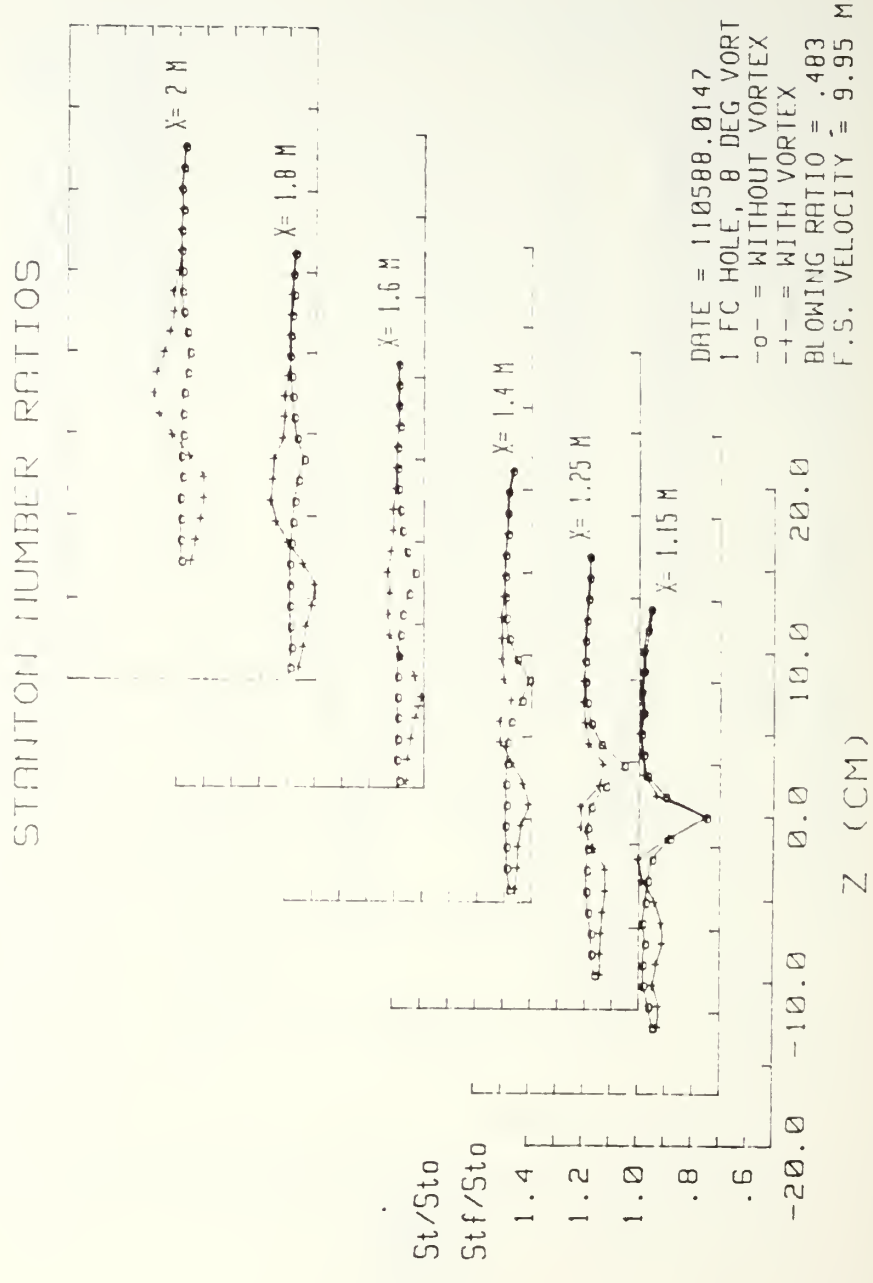

Figure 103. Local St/Sto and Stf/Sto Distributions With Film Cooling, m=0.5, Single Injection Hole With and Without Embedded Vortex y

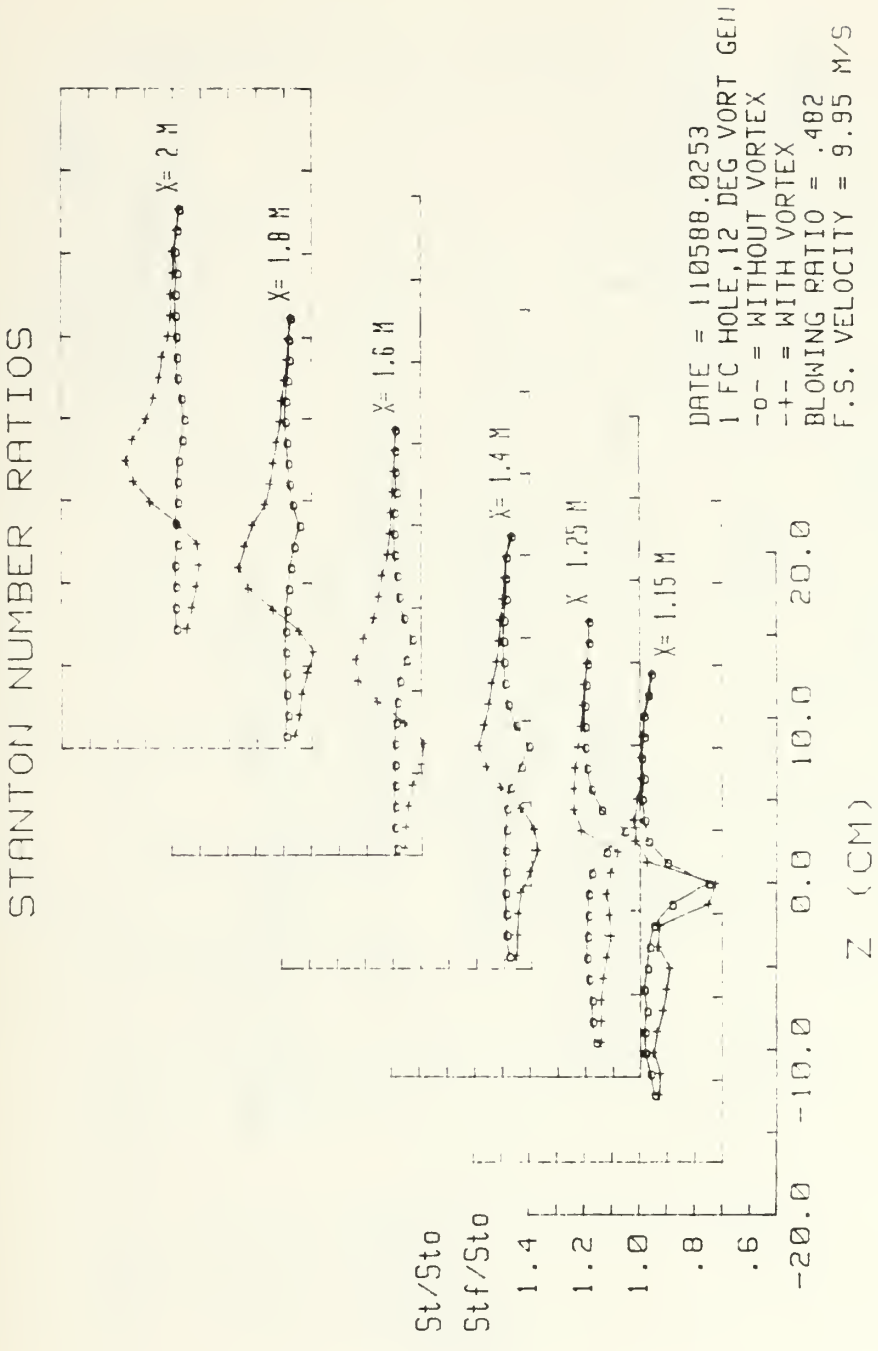

Figure 104. Local St/Sto and Staf/Sto Distributions With Film Cooling, m=0.5, Single Injection Hole With and Without Embedded Vortex x

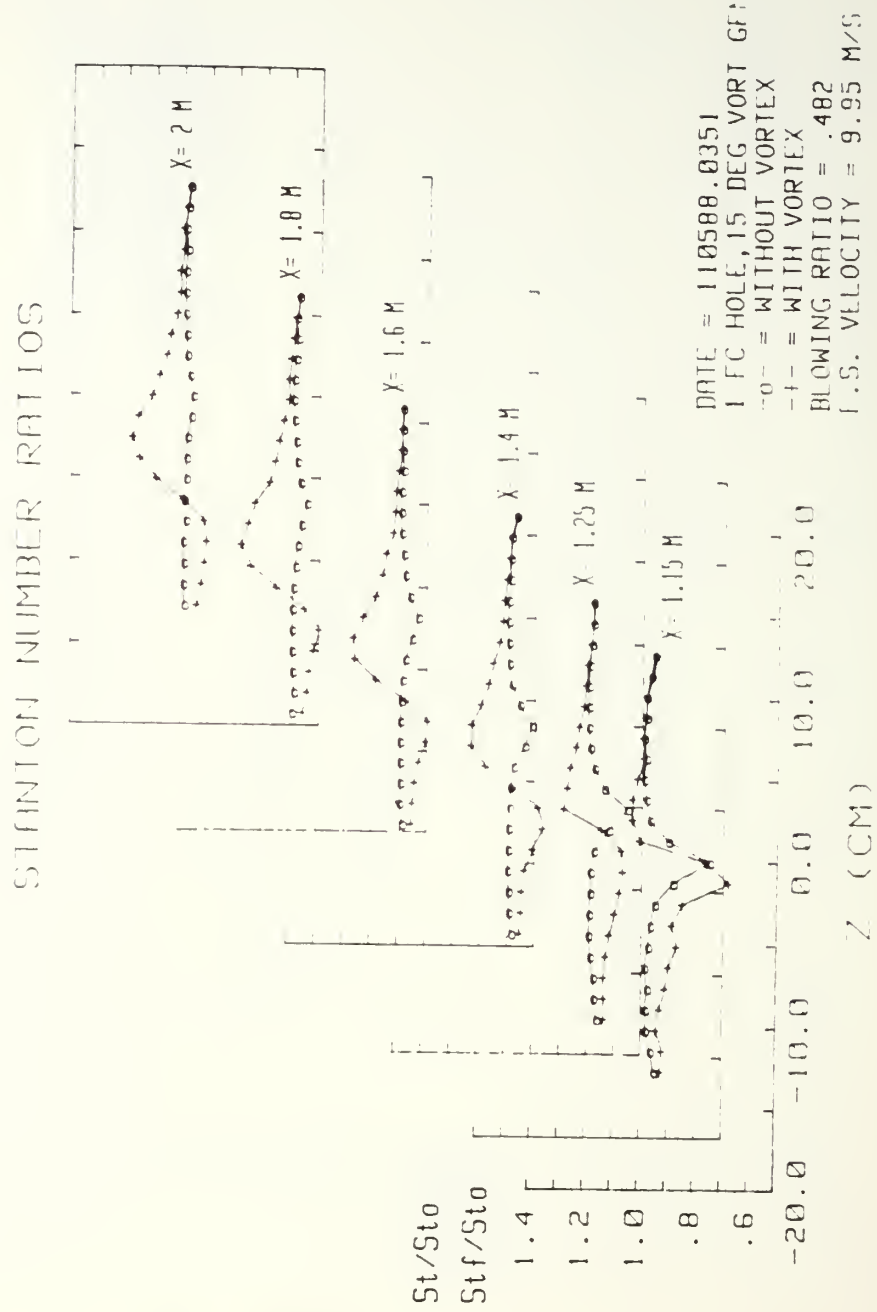

Figure 105. Local St/Sto and Stf/Sto Distributions With Film Cooling, m=0.5, Single Injection Hole With and Without Embedded Vortex w

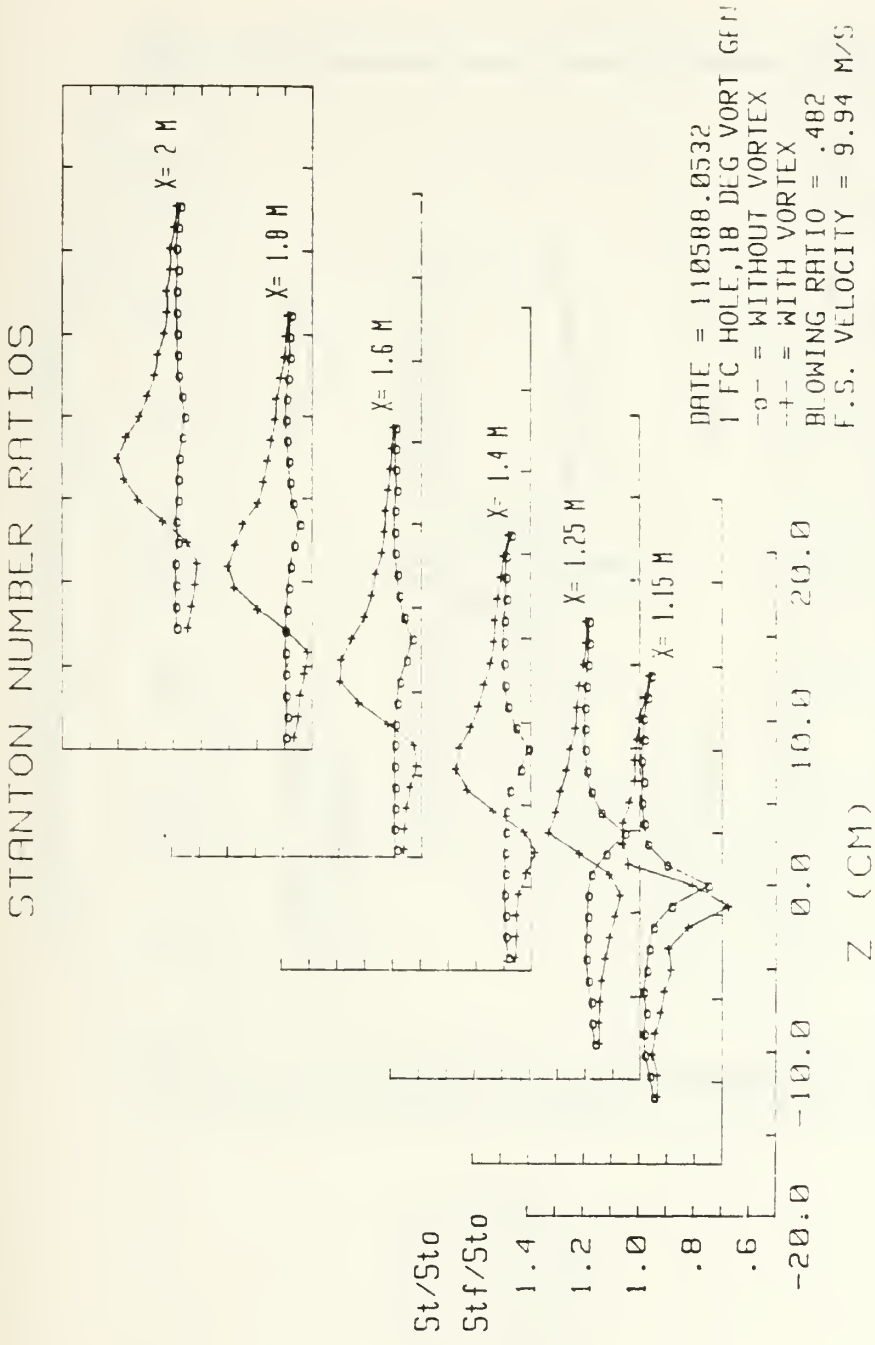

Figure 106. Local St/Sto and Stf/Sto Distributions With Film Cooling, m=0.5, Single Injection Hole With and Without Embedded Vortex r

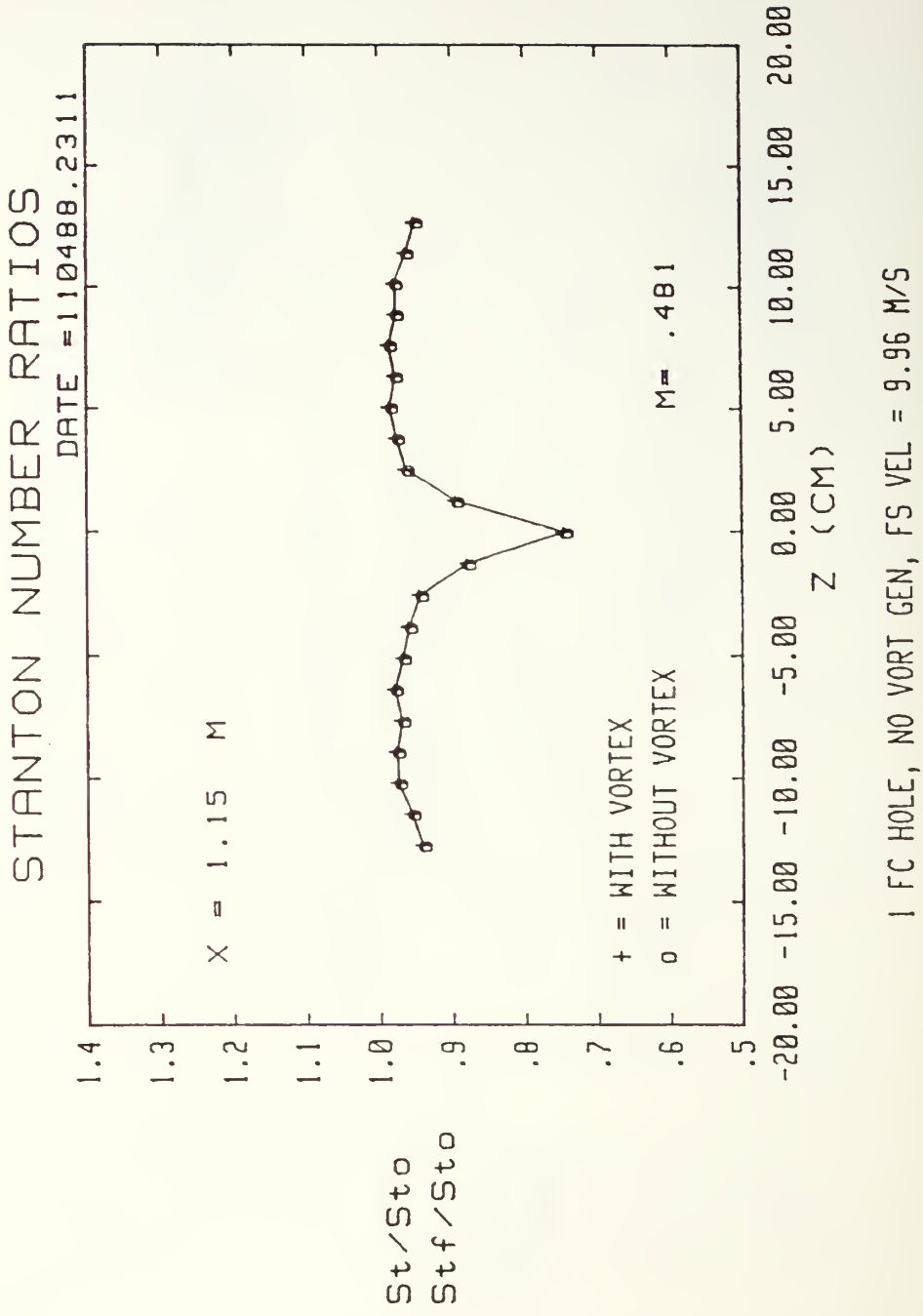

Figure 107. Spanwise Variation of St/Sto and Stf/Sto Ratios m=0.5, Single Injection Hole x/d=7.4, No Vortex

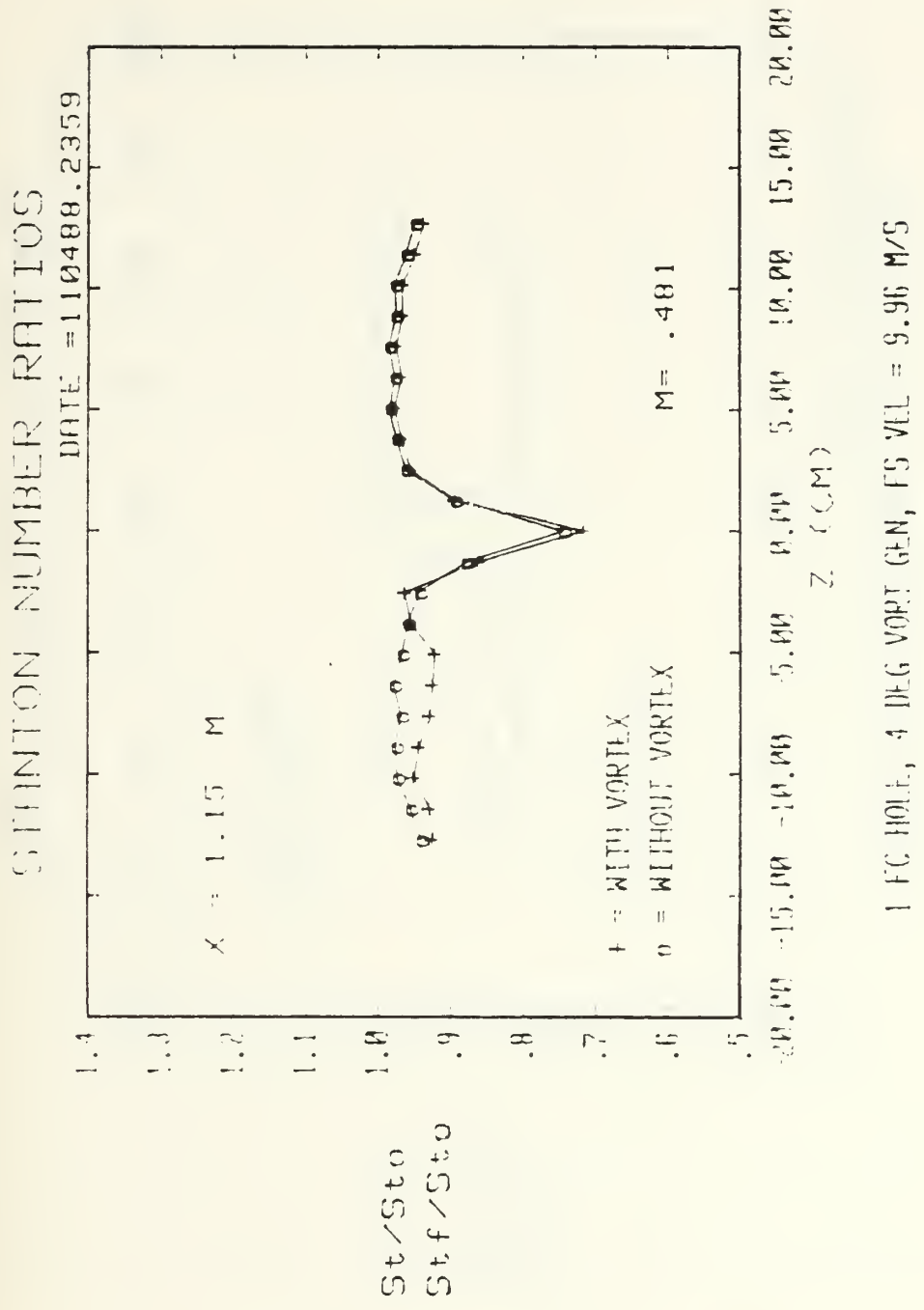

Figure 108. Spanwise Variation of St/Sto and Stf/Sto Ratios m=0.5, Single Injection Hole x/d=7.4, Vortex z

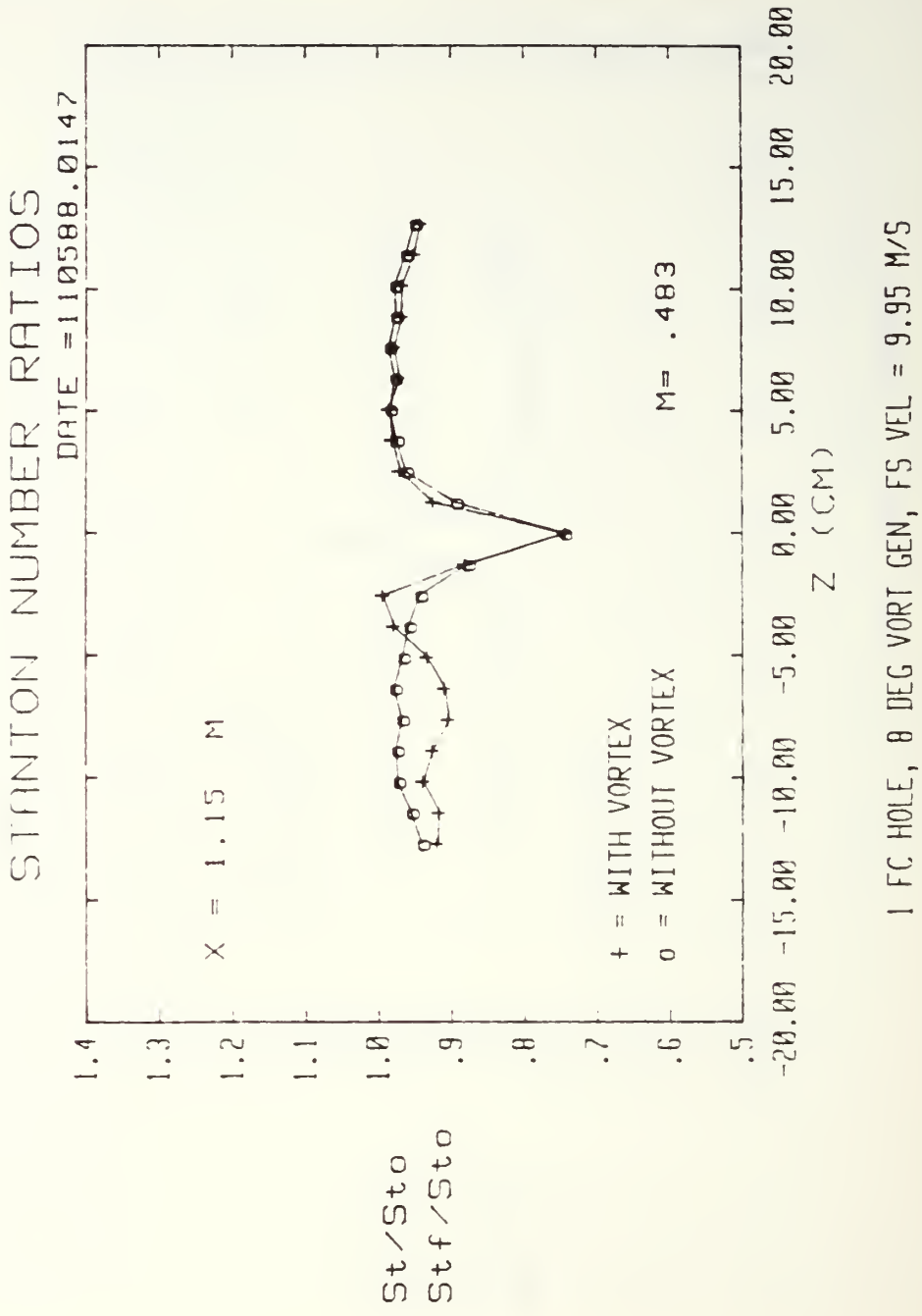

Figure 109. Spanwise Variation of St/Sto and Stf/Sto Ratios m=0.5, Single Injection Hole x/d=7.4, Vortex y

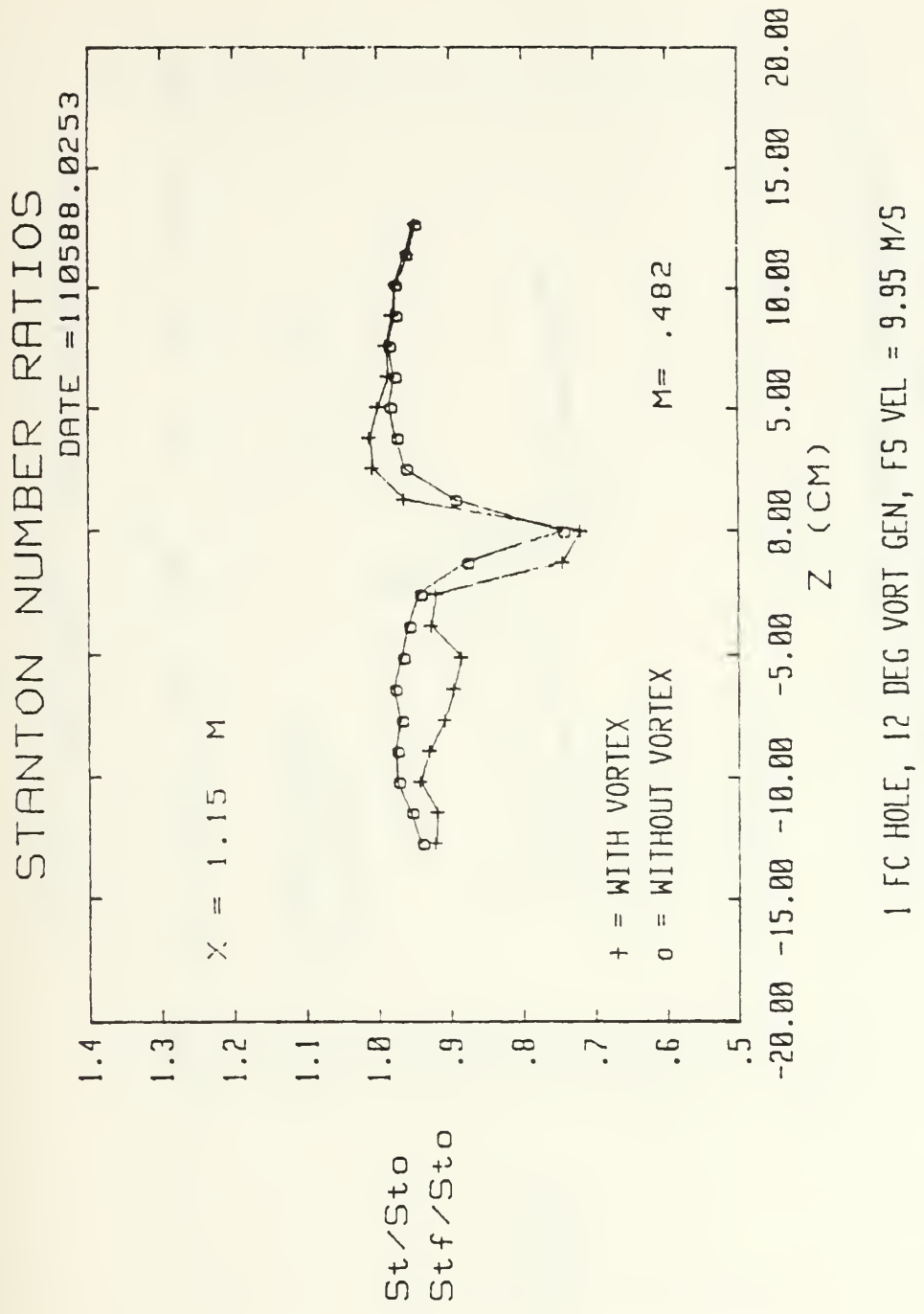

Figure 110. Spanwise Variation of St/Sto and Stf/Sto Ratios m=0.5, Single Injection Hole x/d=7.4, Vortex x

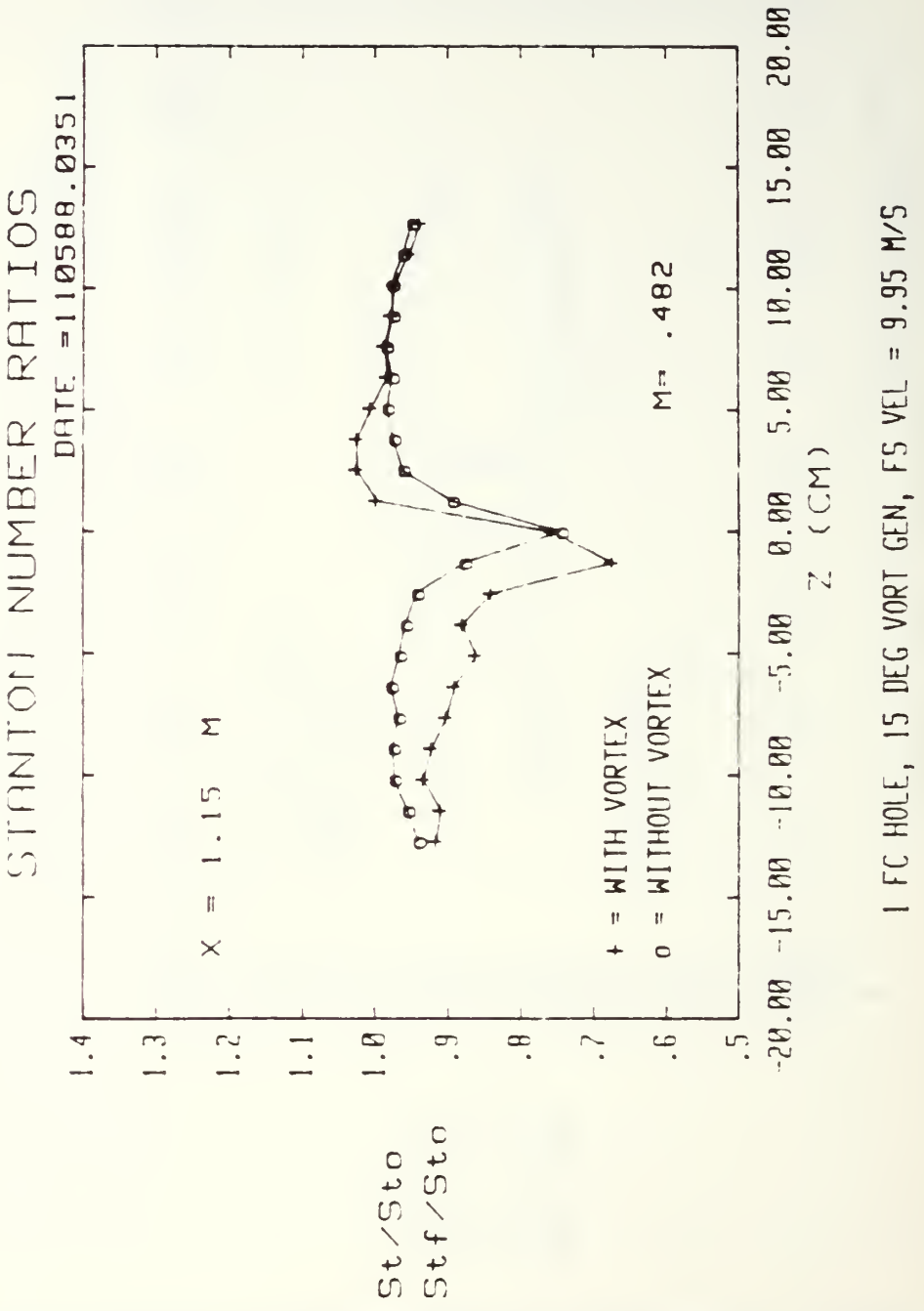

Figure 111. Spanwise Variation of St/Sto and Stf/Sto Ratios m=0.5, Single Injection Hole x/d=7.4, Vortex w

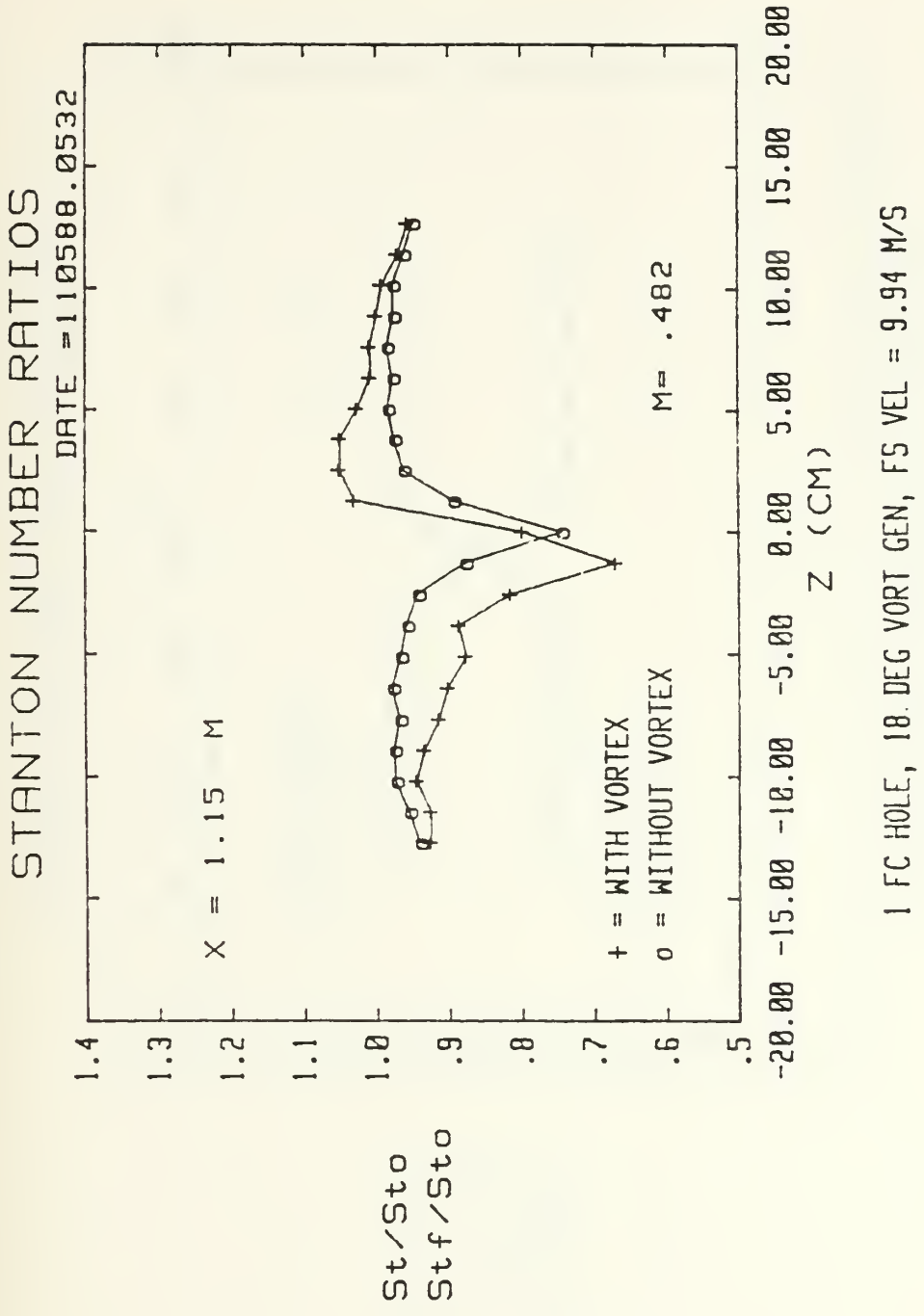

Figure 112. Spanwise Variation of St/Sto and Stf/Sto Ratios m=0.5, Single Injection Hole x/d=7.4, Vortex r

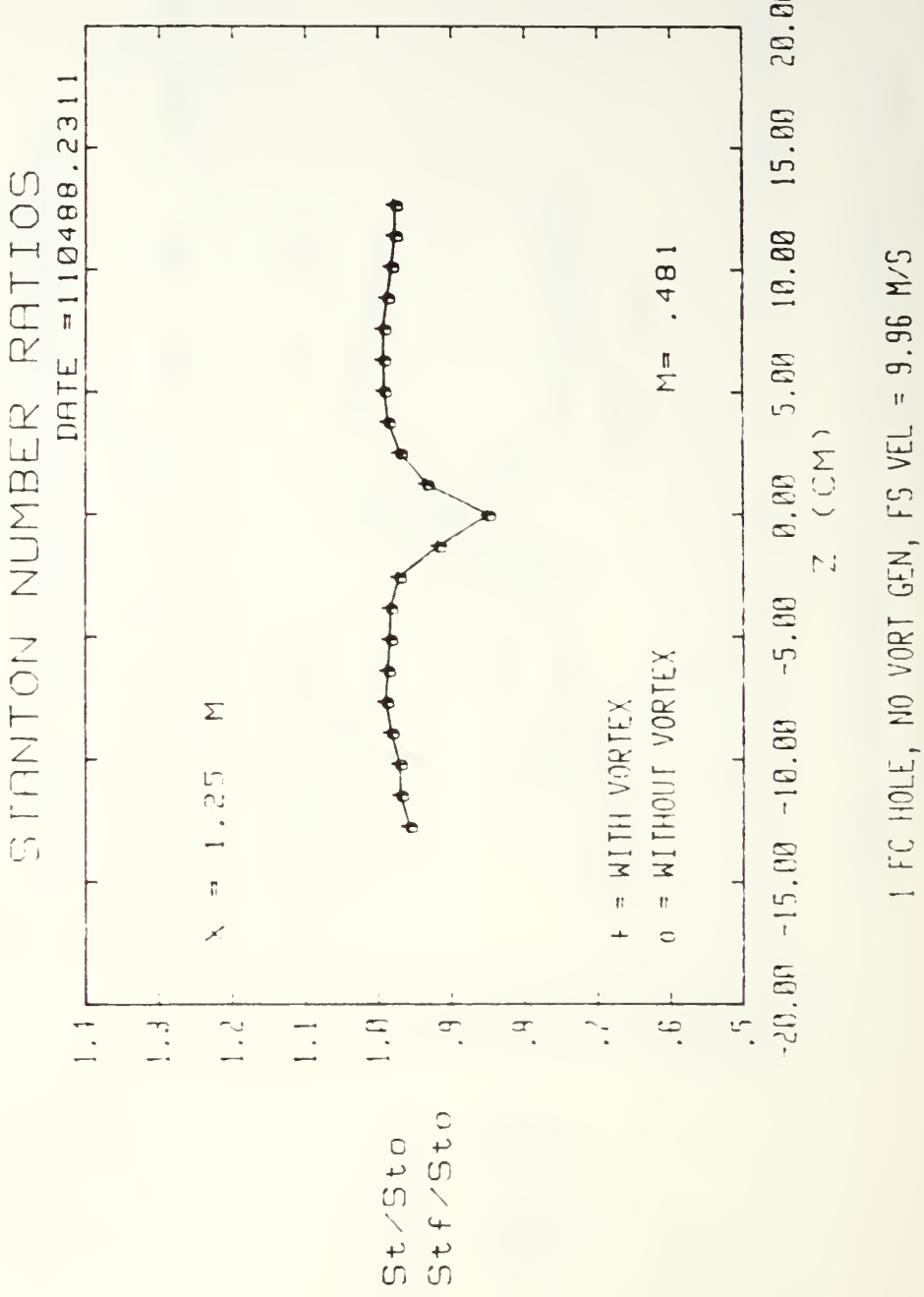

Figure 113. Spanwise Variation of St/Sto and Stf/Sto Ratios m=0.5, Single Injection Hole x/d=17.5, No Vortex

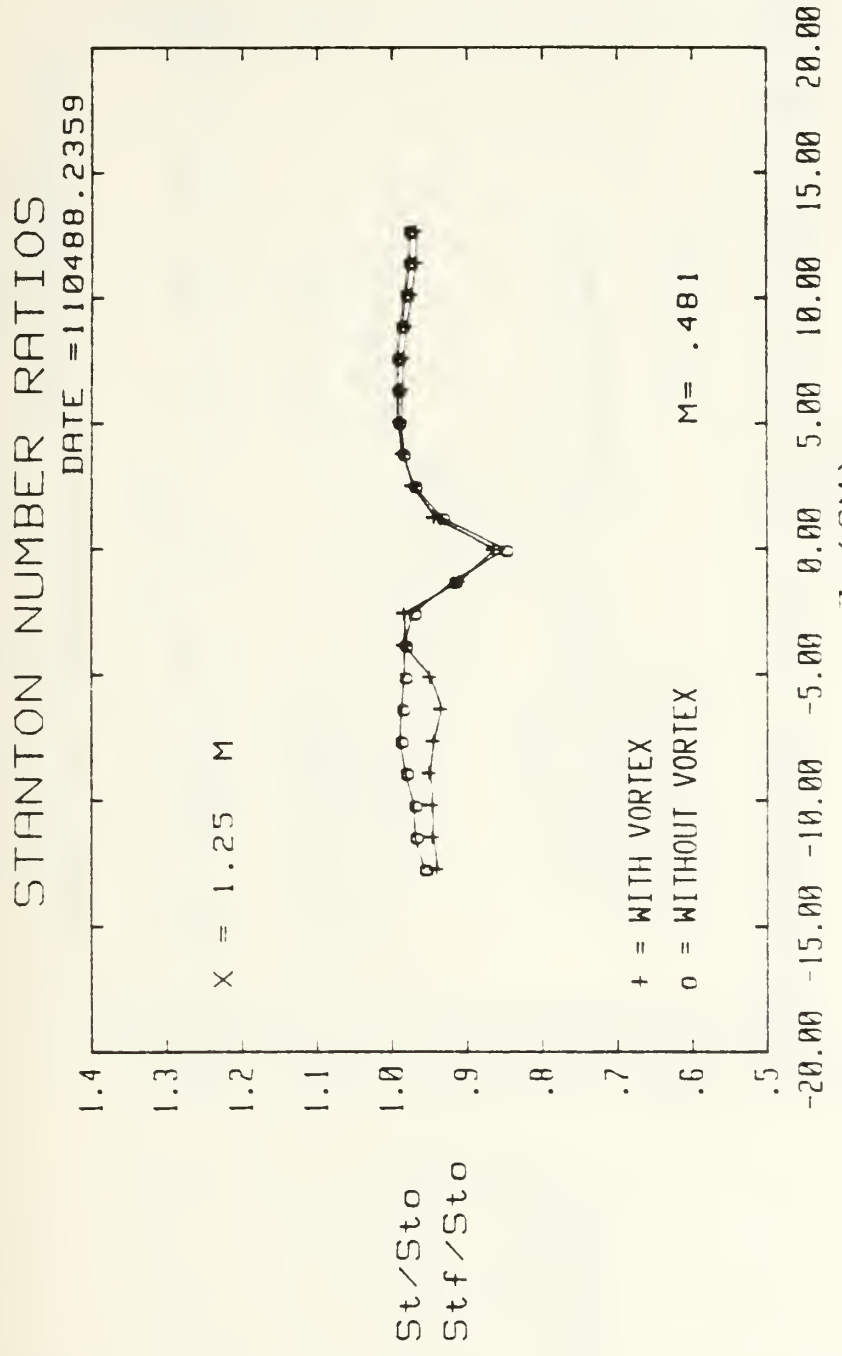

Figure 114. Spanwise Variation of St/Sto and Stf/Sto Ratios m=0.5, Single Injection Hole x/d=17.5, Vortex z

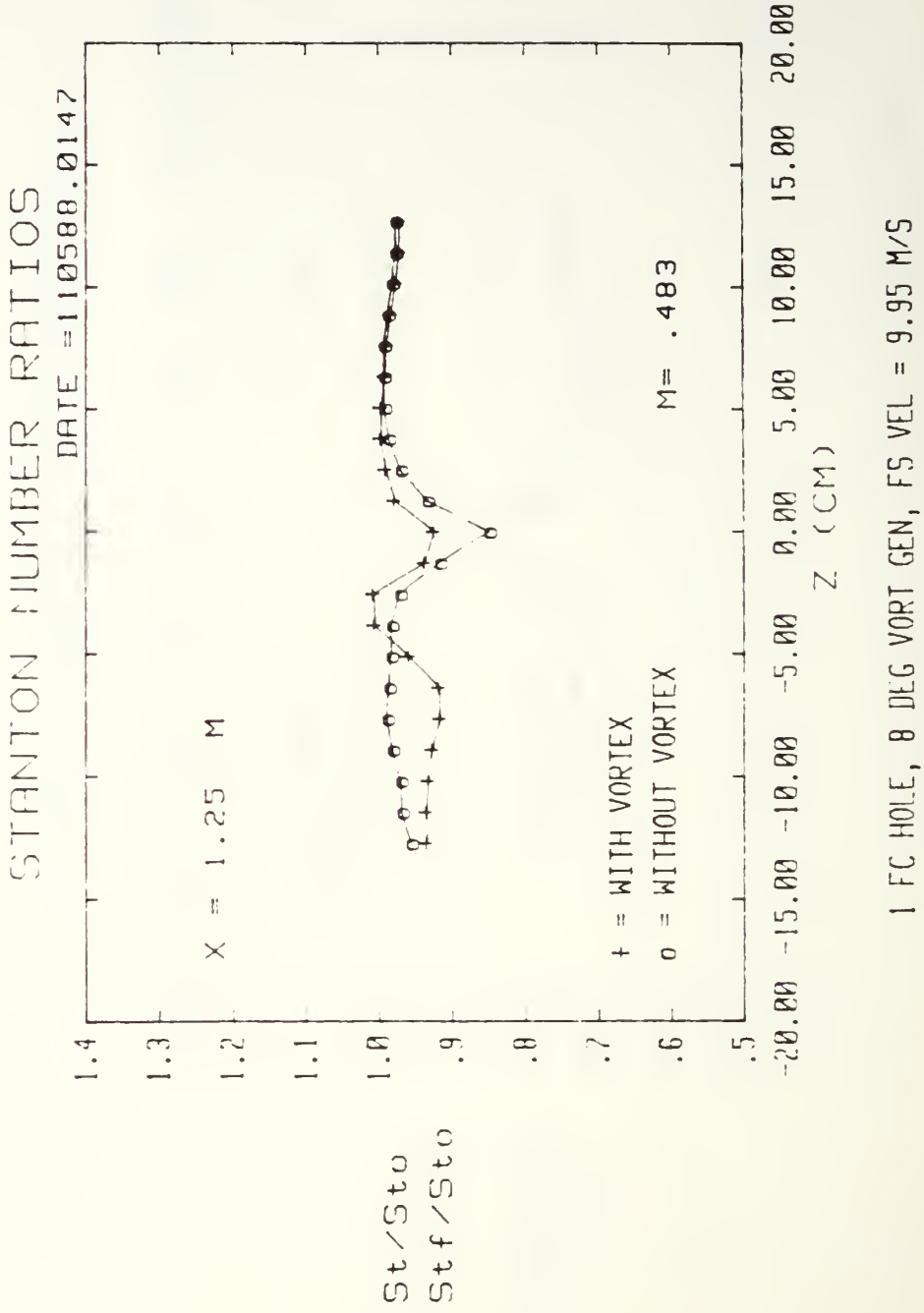

Figure 115. Spanwise Variation of St/Sto and Stf/Sto Ratios m=0.5, Single Injection Hole x/d=17.5, Vortex y

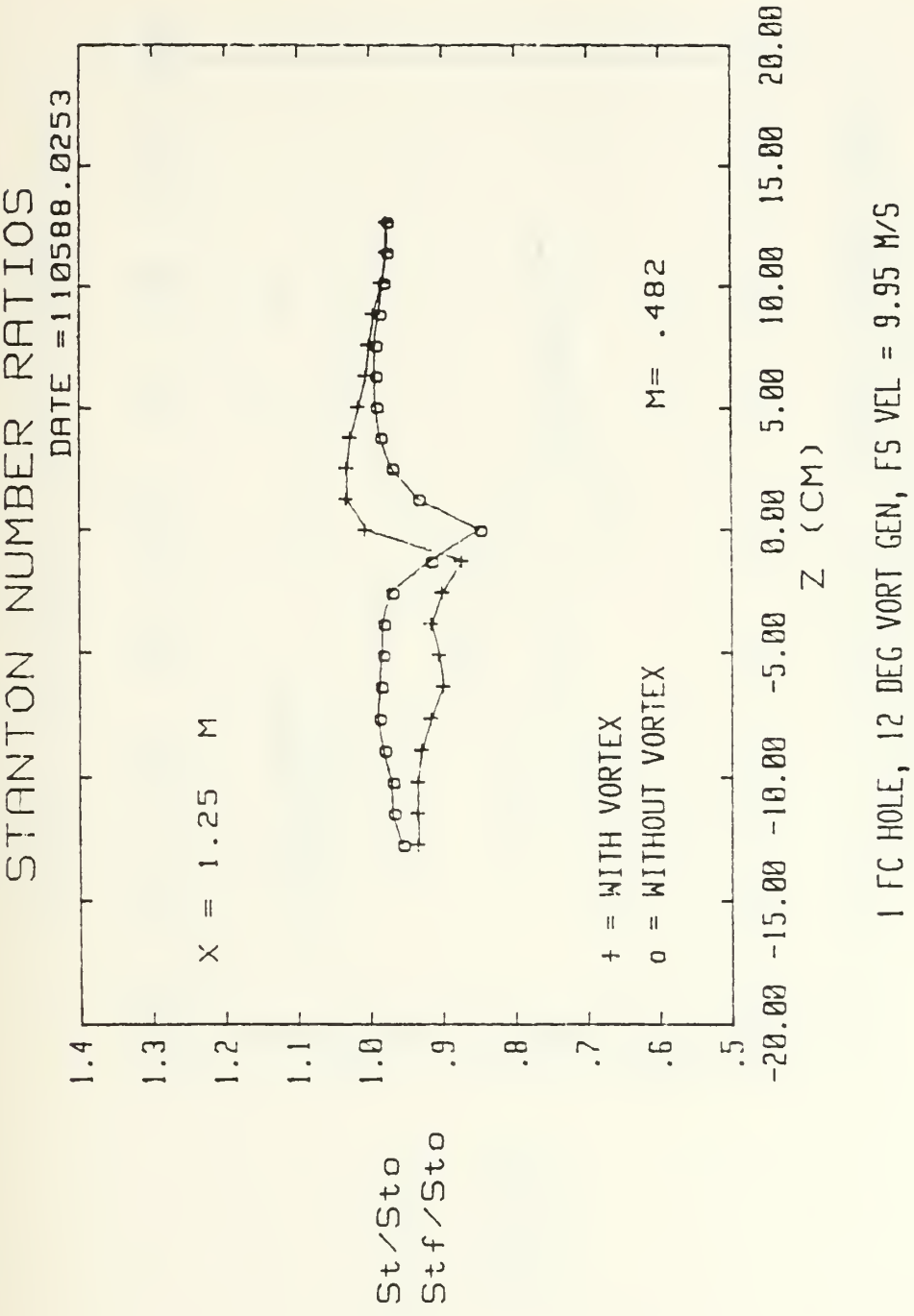

Figure 116. Spanwise Variation of St/Sto an Stf/Sto Ratios m=0.5, Single Injection Hole x/d=17.5, Vortex x

Figure 117. Spanwise Variation of St/Sto and Sto Ratios m=0.5, Single Injection Hole x/d=17.5, Vortex w

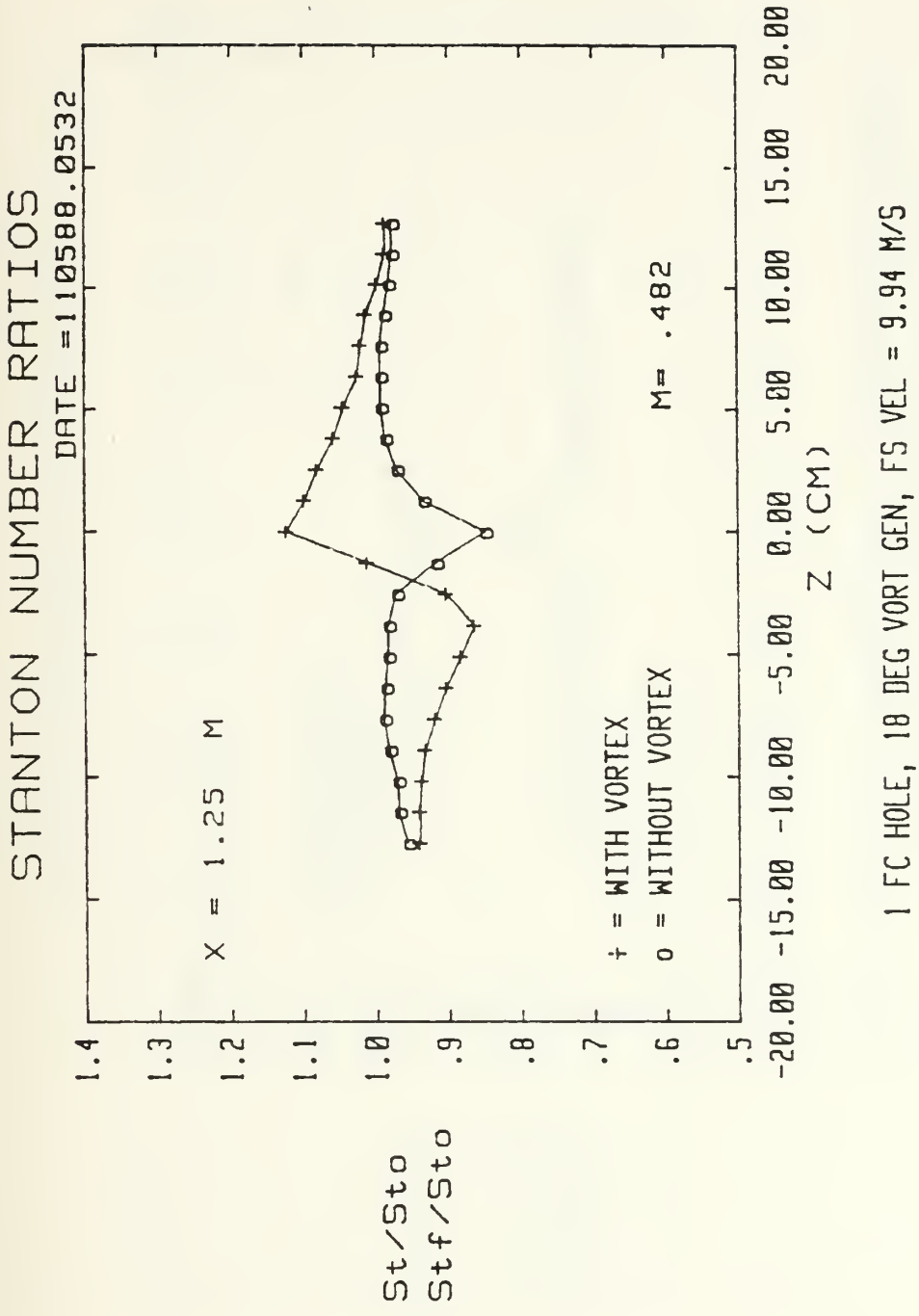

Figure 118. Spanwise Variation of St/Sto and Stf/Sto Ratios m=0.5, Single Injection Hole x/d=17.5, Vortex r

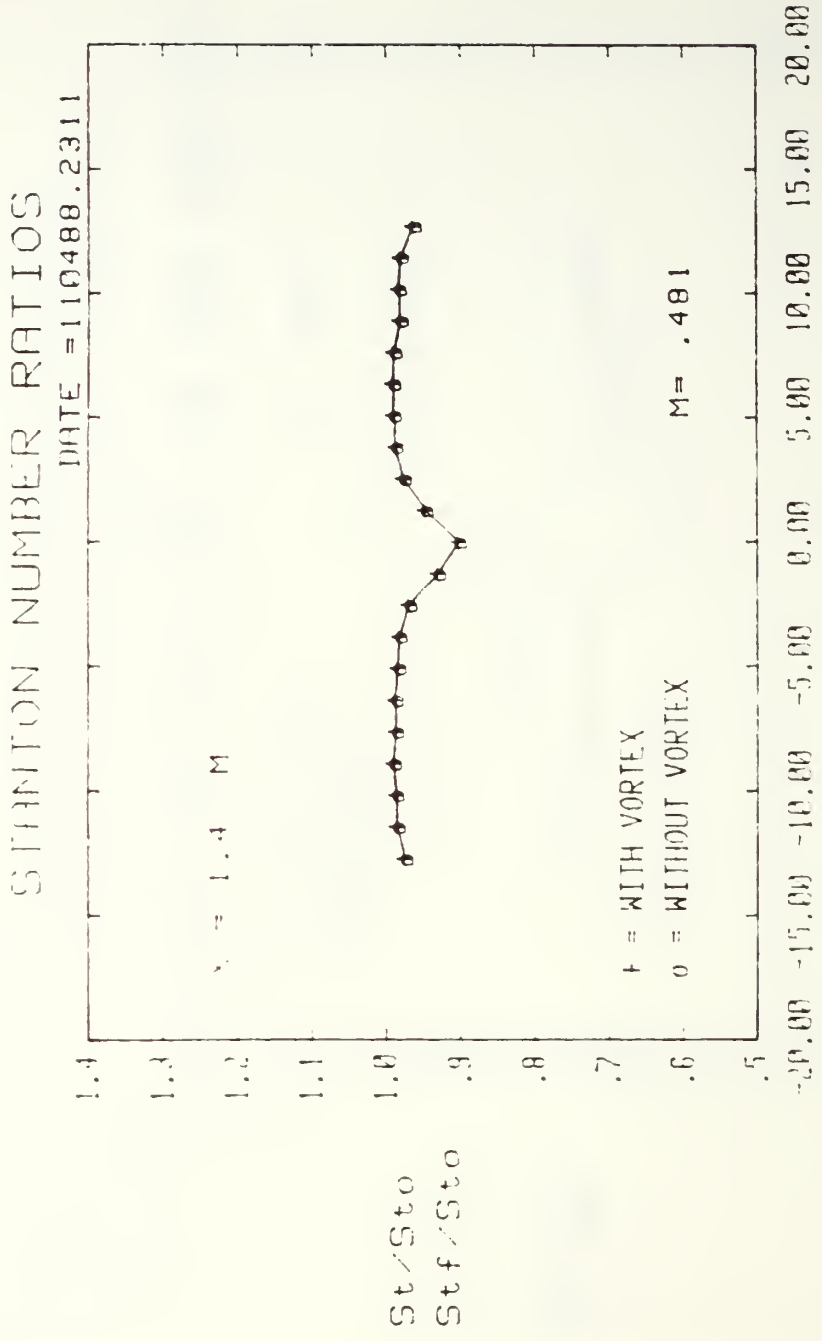

Figure 119. Spanwise Variation of St/Sto an Stf/Sto Ratios m=0.5, Single Injection Hole x/d=33.6, No Vortex

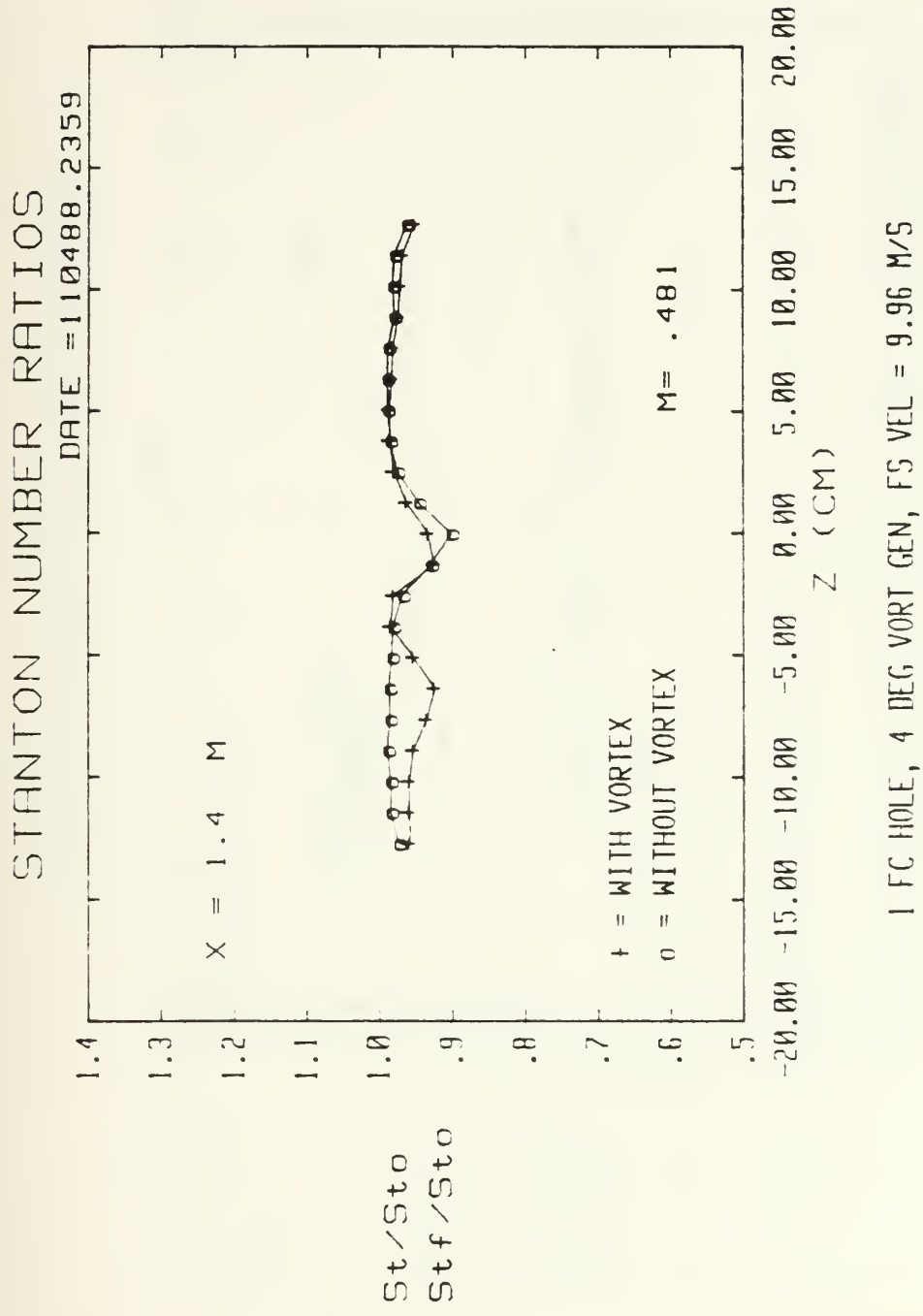

Figure 120. Spanwise Variation of St/Sto an Stf/Sto Ratios m=0.5, Single Injection Hole x/d=33.6, Vortex z

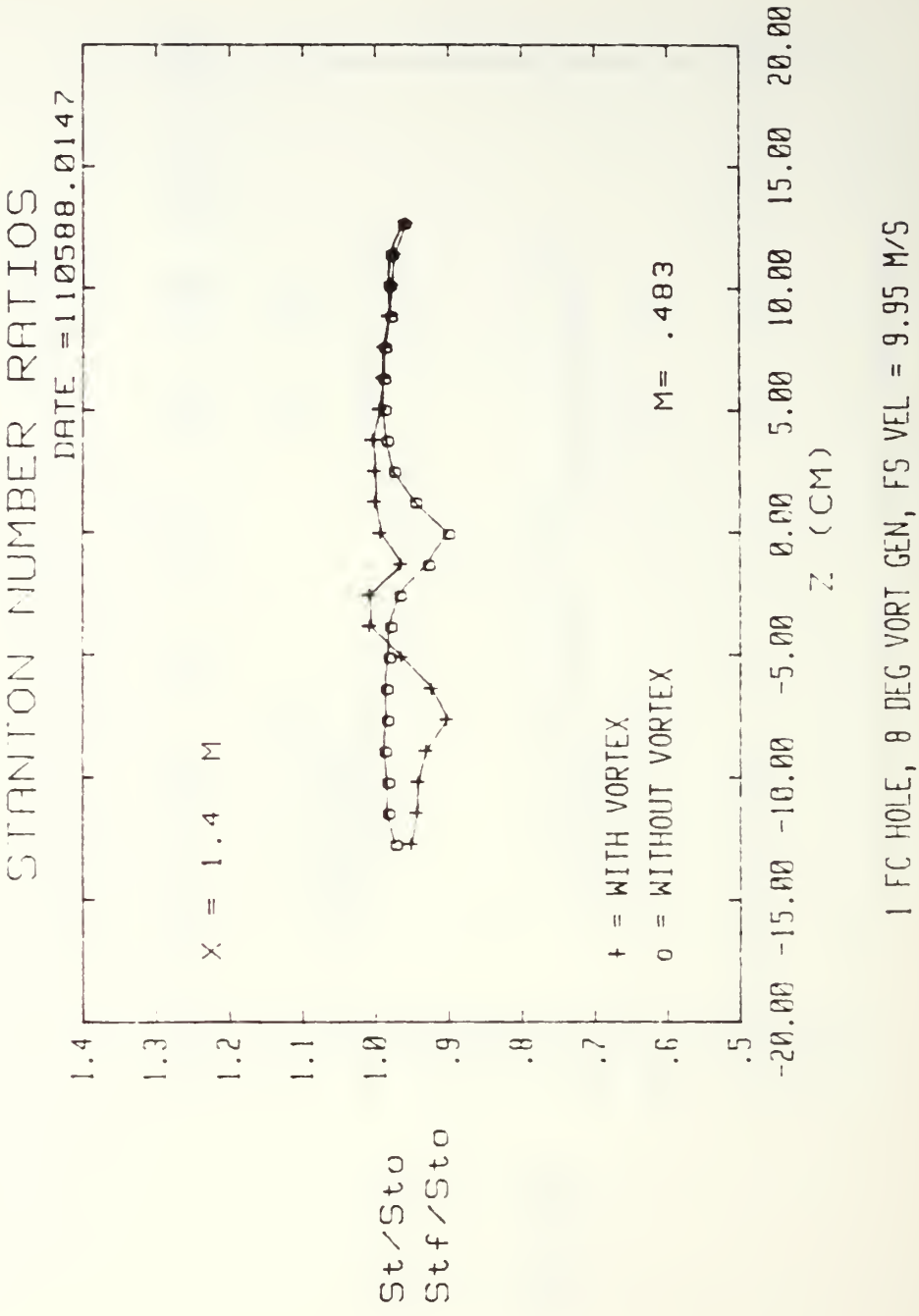

Figure 121. Spanwise Variation of St/Sto an Stf/Sto Ratios m=0.5, Single Injection Hole x/d=33.6, Vortex y

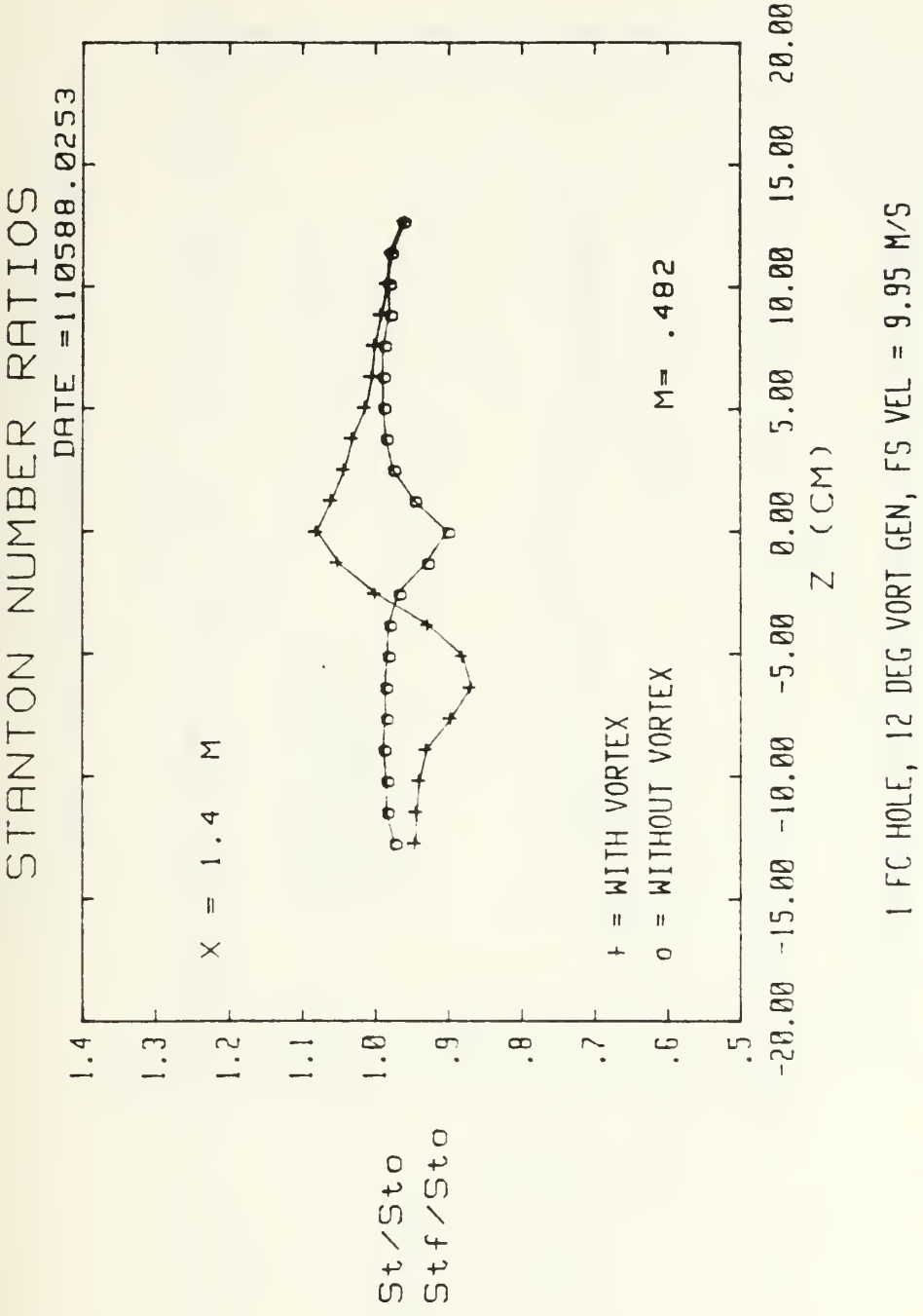

Figure 122. Spanwise Variation of St/Sto an Stf/Sto Ratios m=0.5, Single Injection Hole x/d=33.6, Vortex x

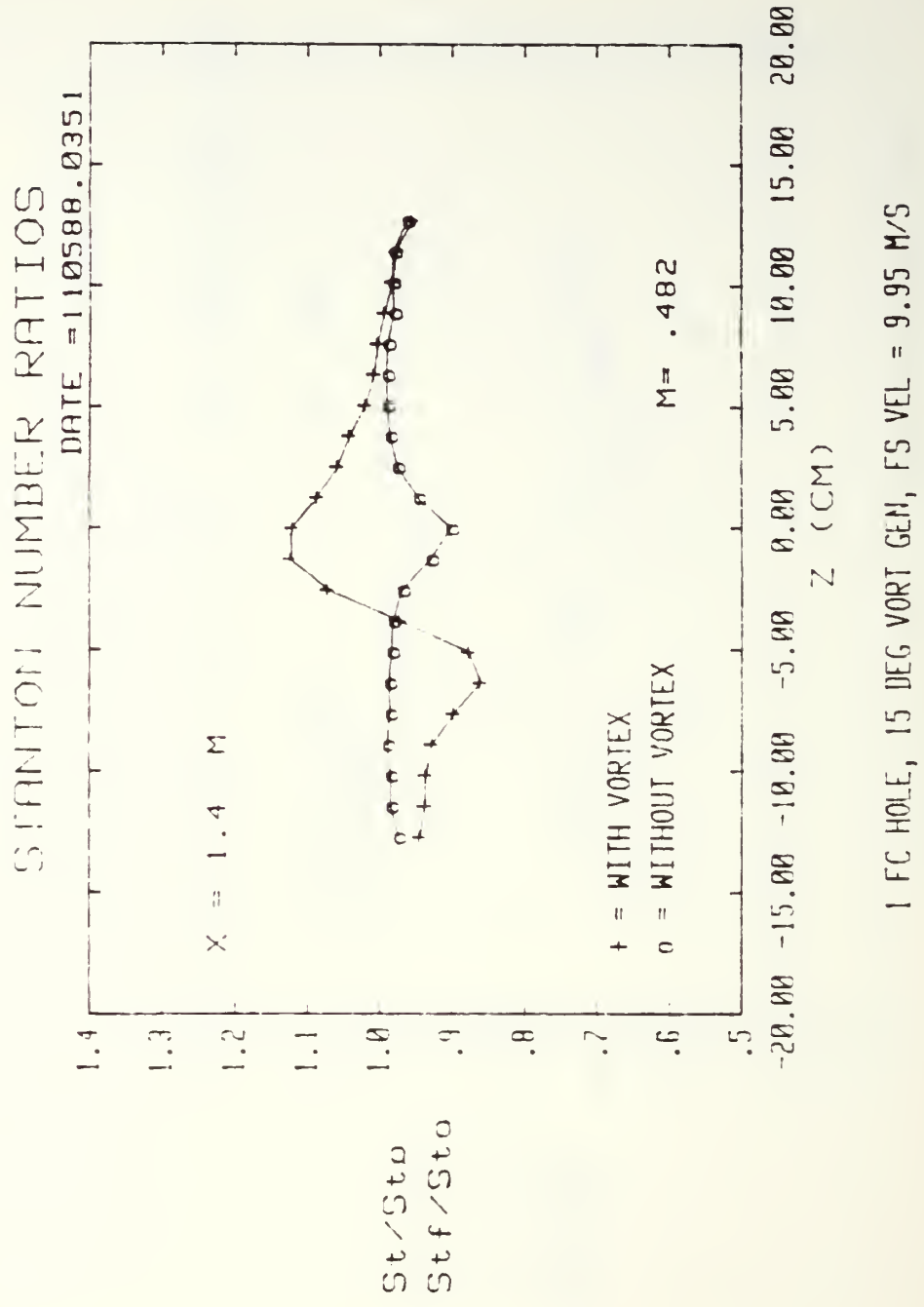

Figure 123. Spanwise Variation of St/Sto an Stf/Sto Ratios m=0.5, Single Injection Hole x/d=33.6, Vortex w

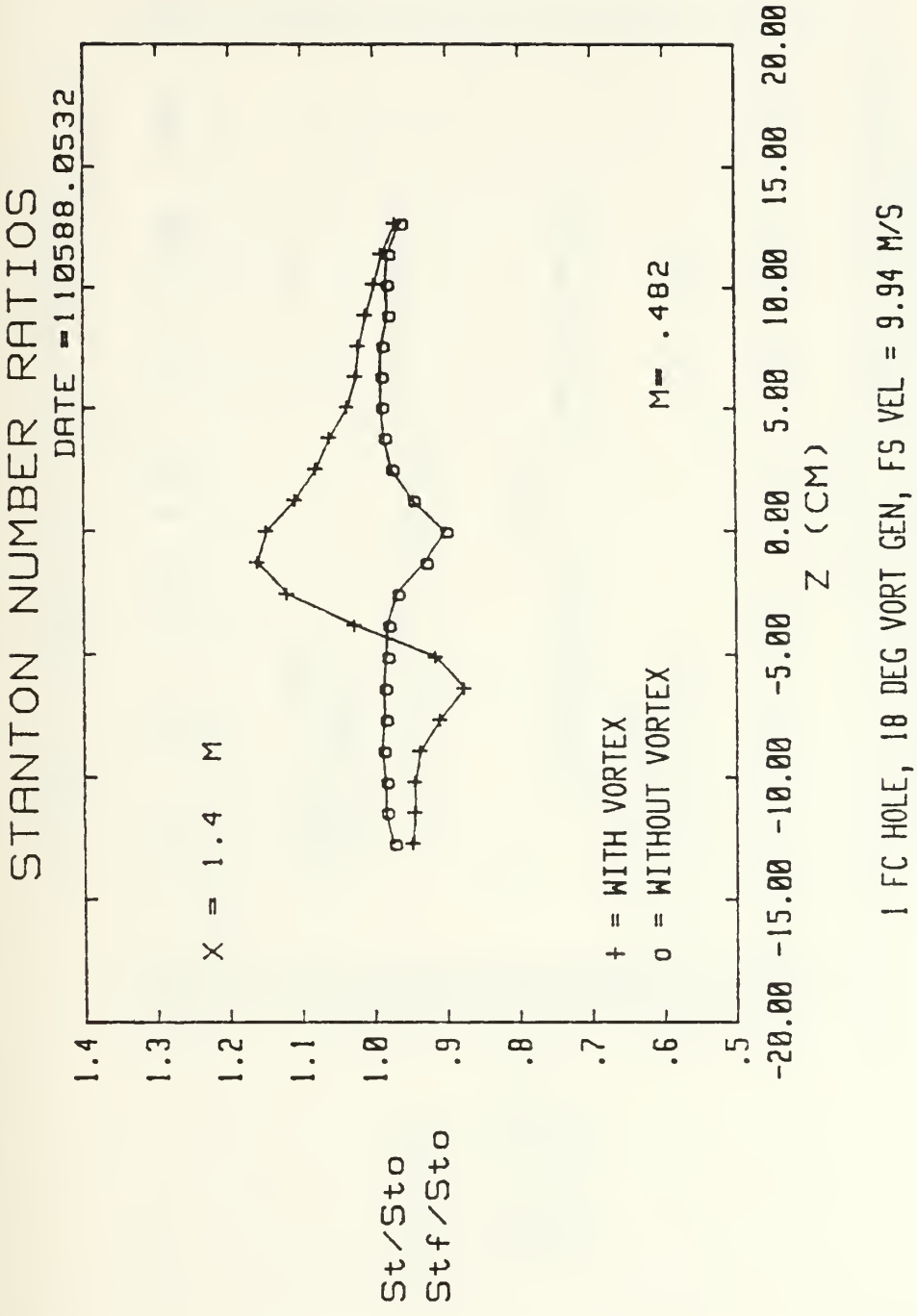

Figure 124. Spanwise Variation of St/Sto an Stf/Sto Ratios m=0.5, Single Injection Hole x/d=33.6, Vortex r

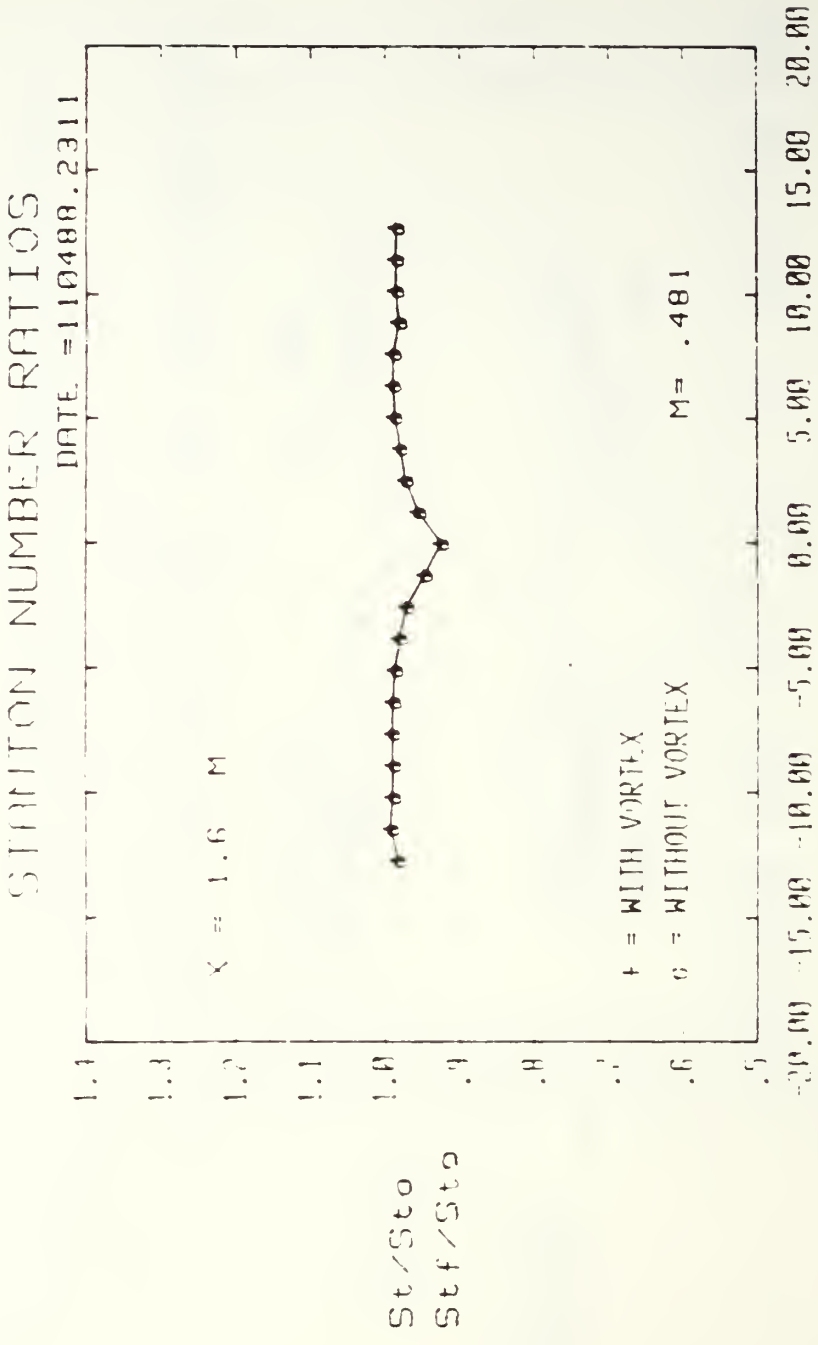

Figure 125. Spanwise Variation of St/Sto an Stf/Sto Ratios m=0.5, Single Injection Hole x/d=54.6, No Vortex

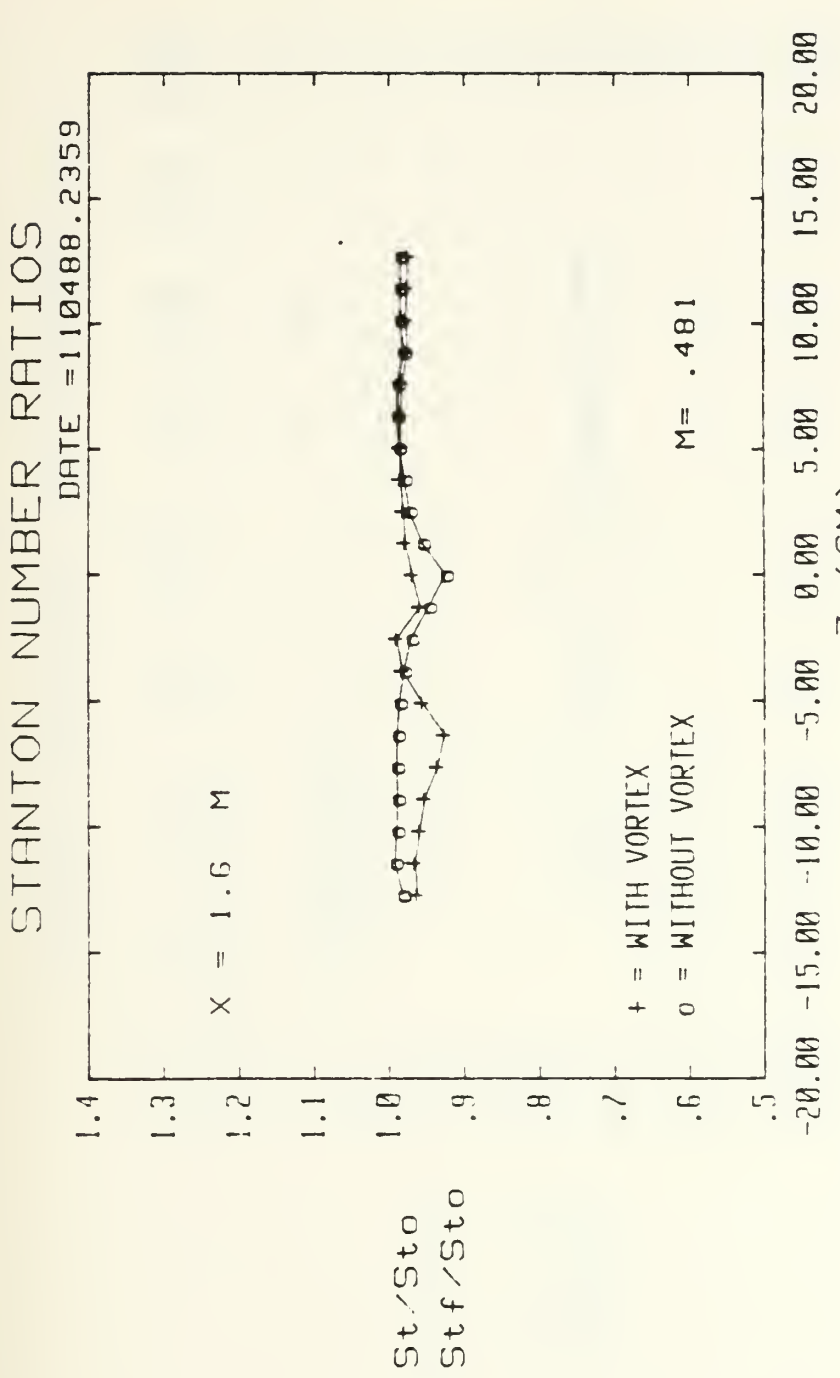

Figure 126. Spanwise Variation of St/Sto an Stf/Sto Ratios m=0.5, Single Injection Hole x/d=54.6, Vortex z

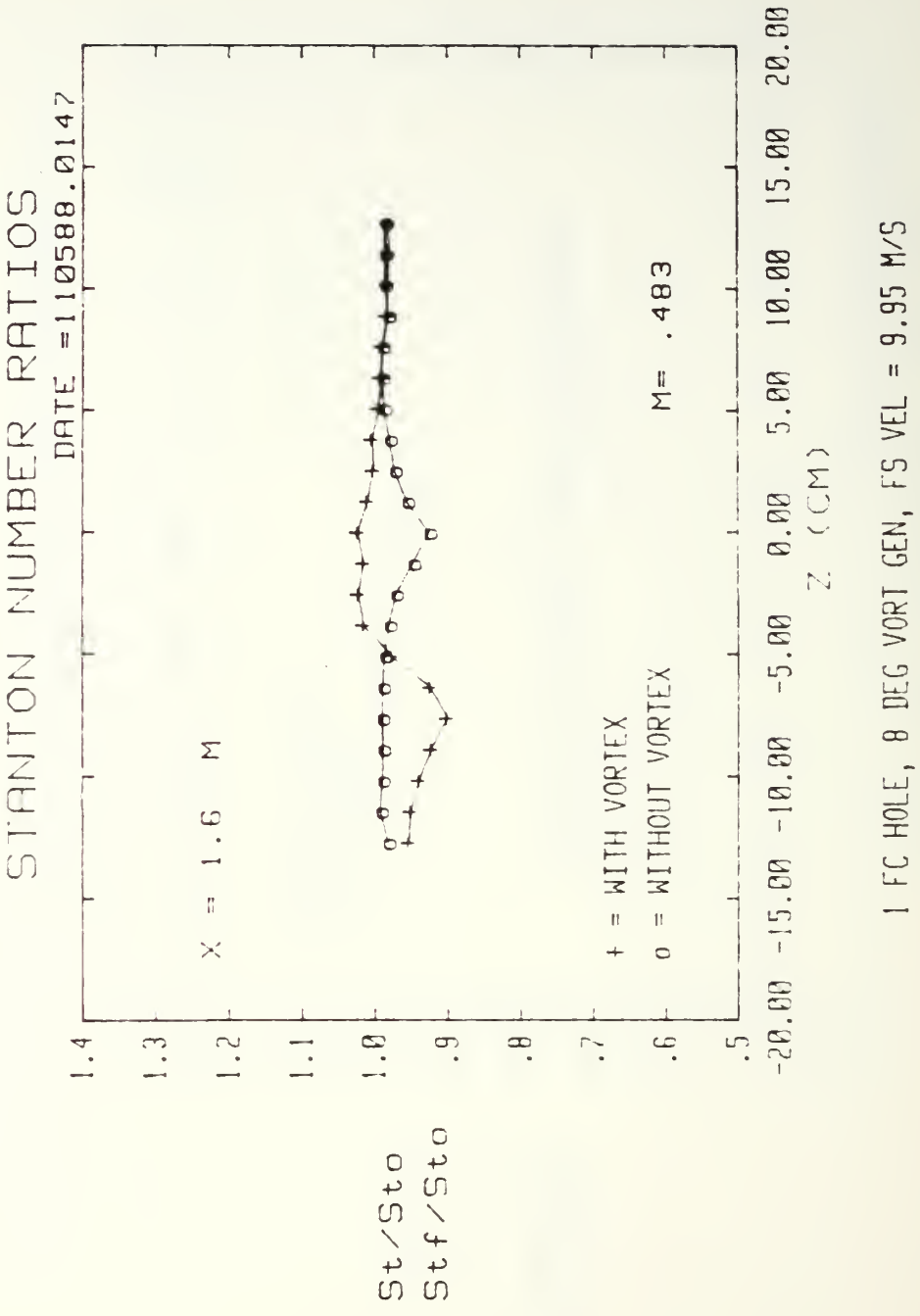

Figure 127. Spanwise Variation of St/Sto an Stf/Sto Ratios m=0.5, Single Injection Hole x/d=54.6, Vortex y

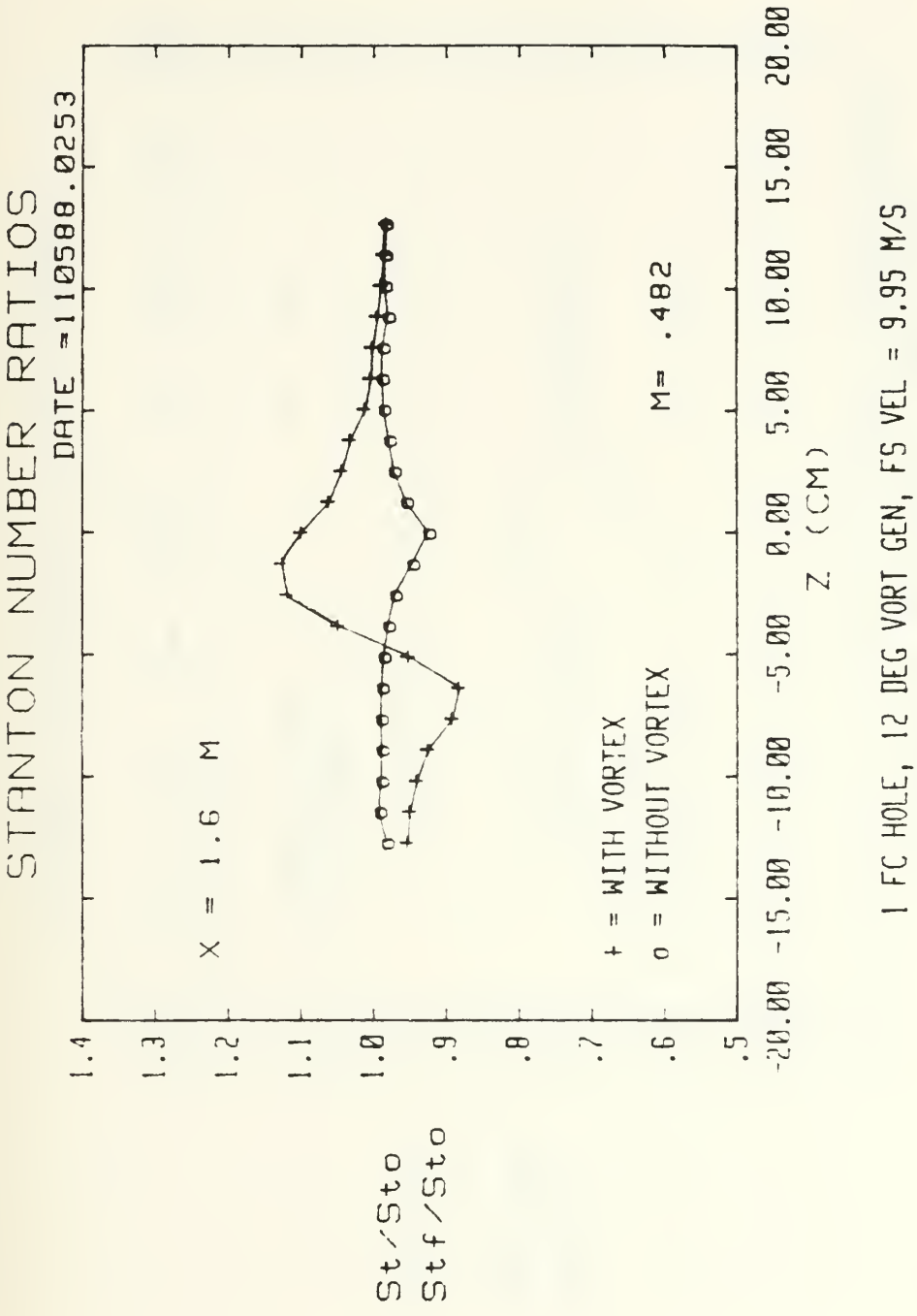

Figure 128. Spanwise Variation of St/Sto an Stf/Sto Ratios m=0.5, Single Injection Hole x/d=54.6, Vortex x

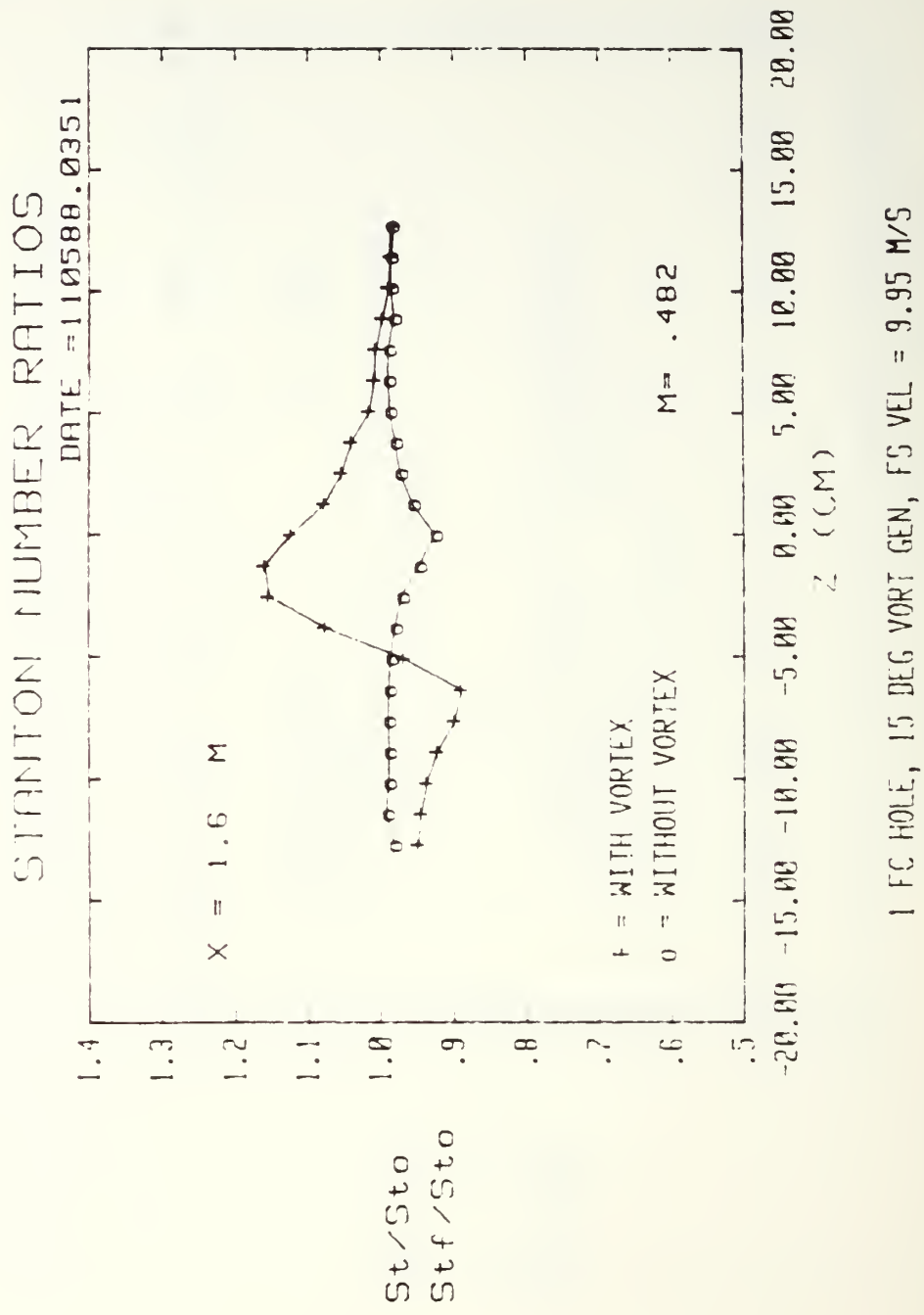

Figure 129. Spanwise Variation of St/Sto an Stf/Sto Ratios m=0.5, Single Injection Hole x/d=54.6, Vortex w

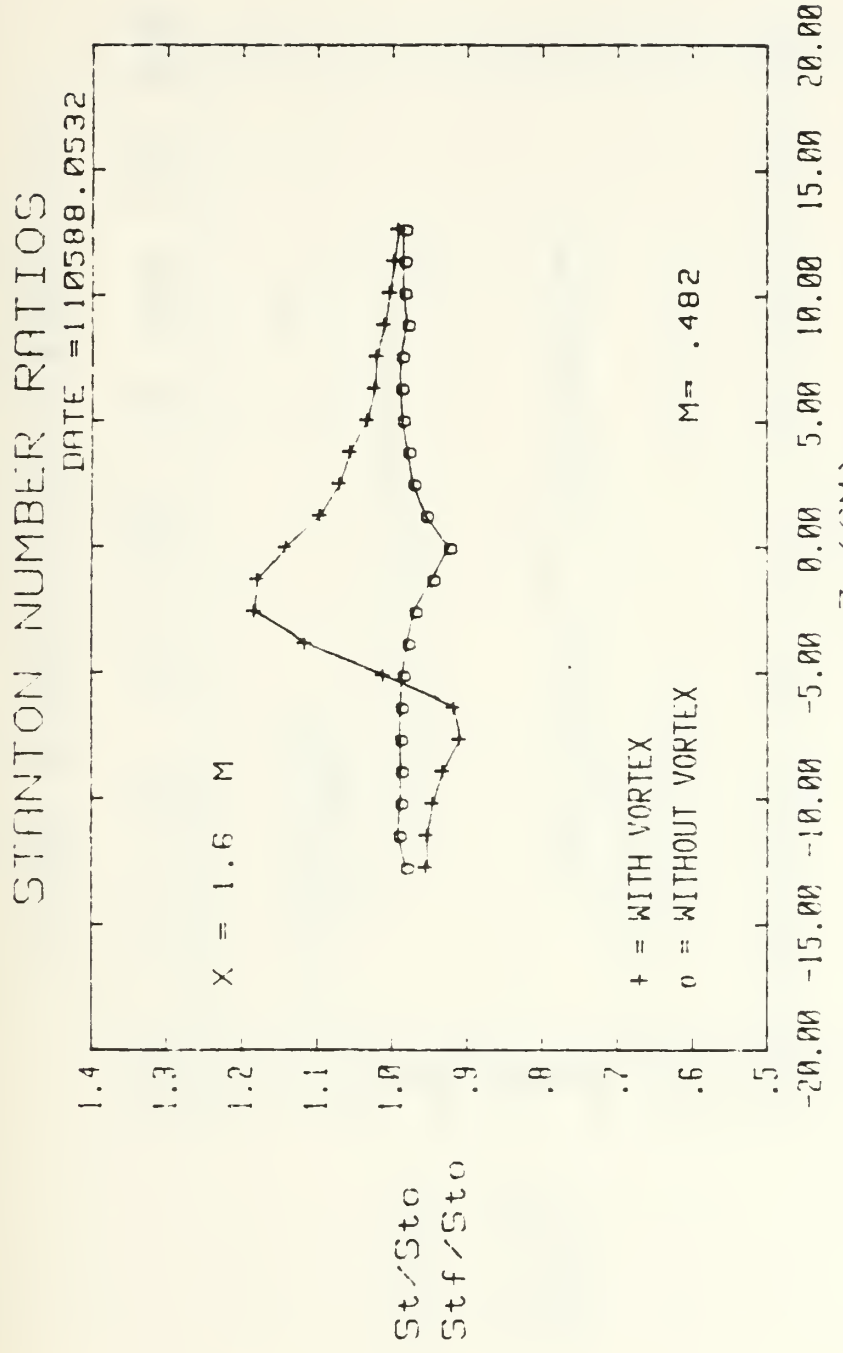

Figure 130. Spanwise Variation of St/Sto an Stf/Sto Ratios m=0.5, Single Injection Hole x/d=54.6, Vortex r

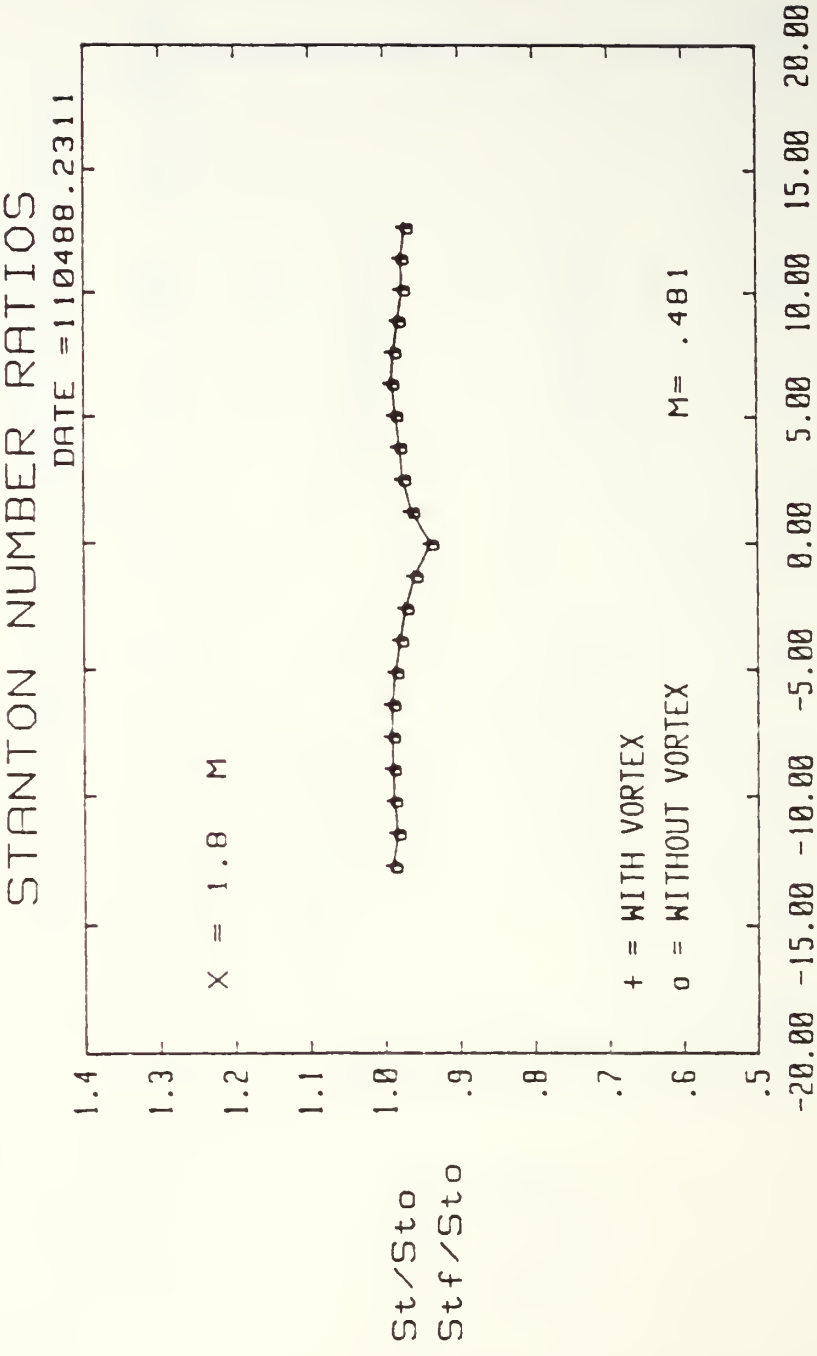

Figure 131. Spanwise Variation of St/Sto an Stf/Sto Ratios m=0.5, Single Injection Hole x/d=75.6, No Vortex

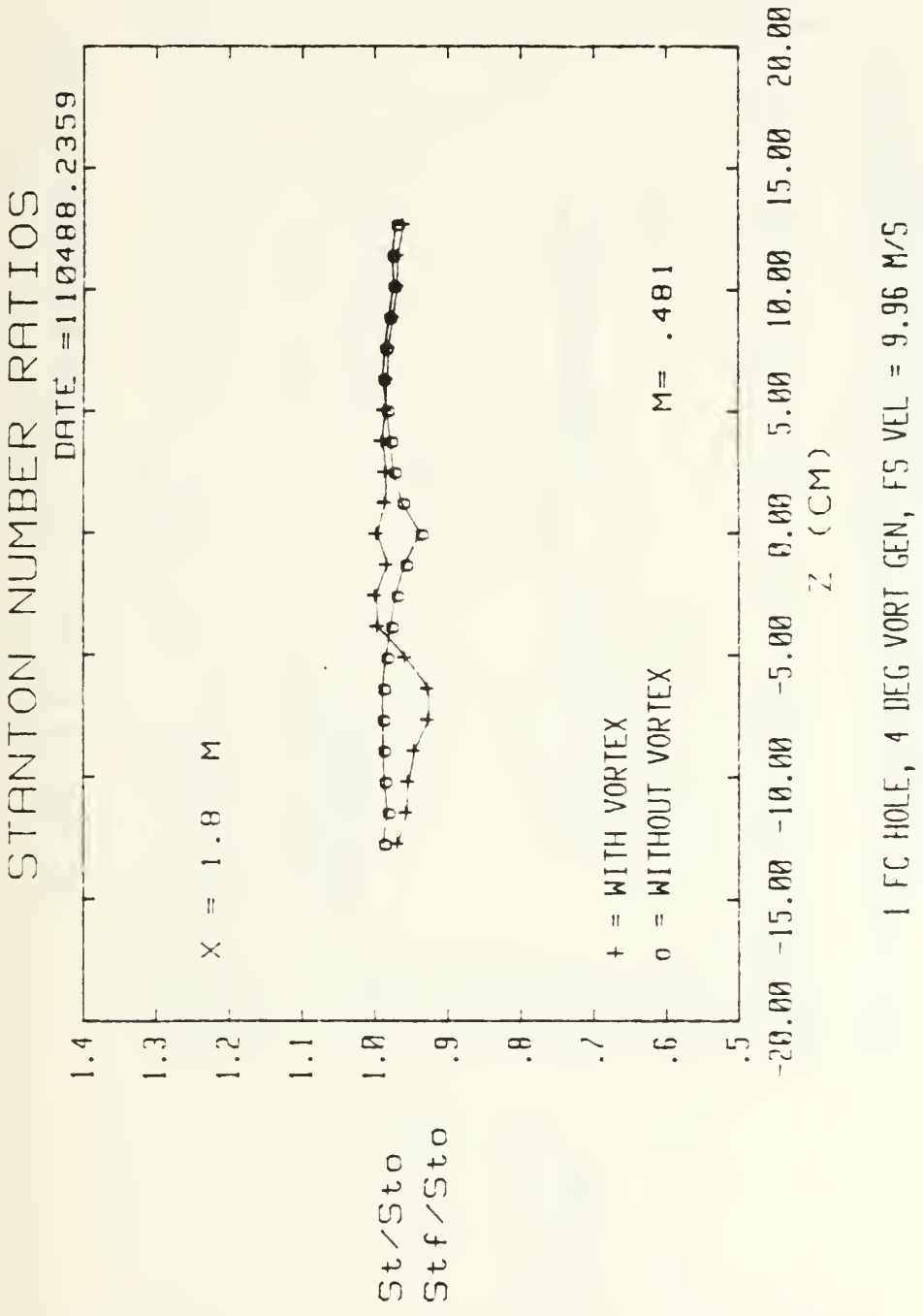

Figure 132. Spanwise Variation of St/Sto an Stf/Sto Ratios m=0.5, Single Injection Hole x/d=75.6, Vortex z

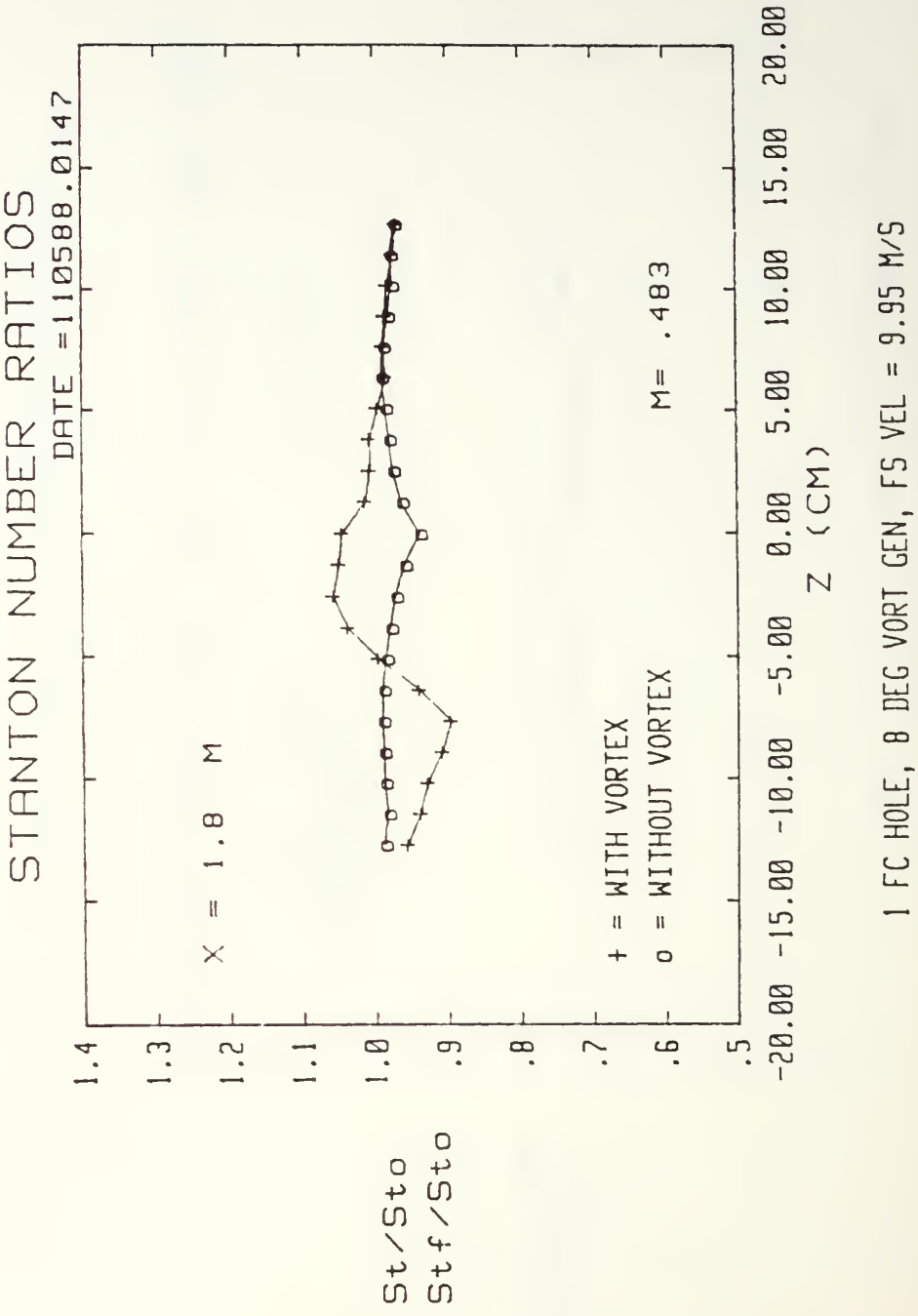

Figure 133. Spanwise Variation of St/Sto an Stf/Sto Ratios m=0.5, Single Injection Hole x/d=75.6, Vortex y

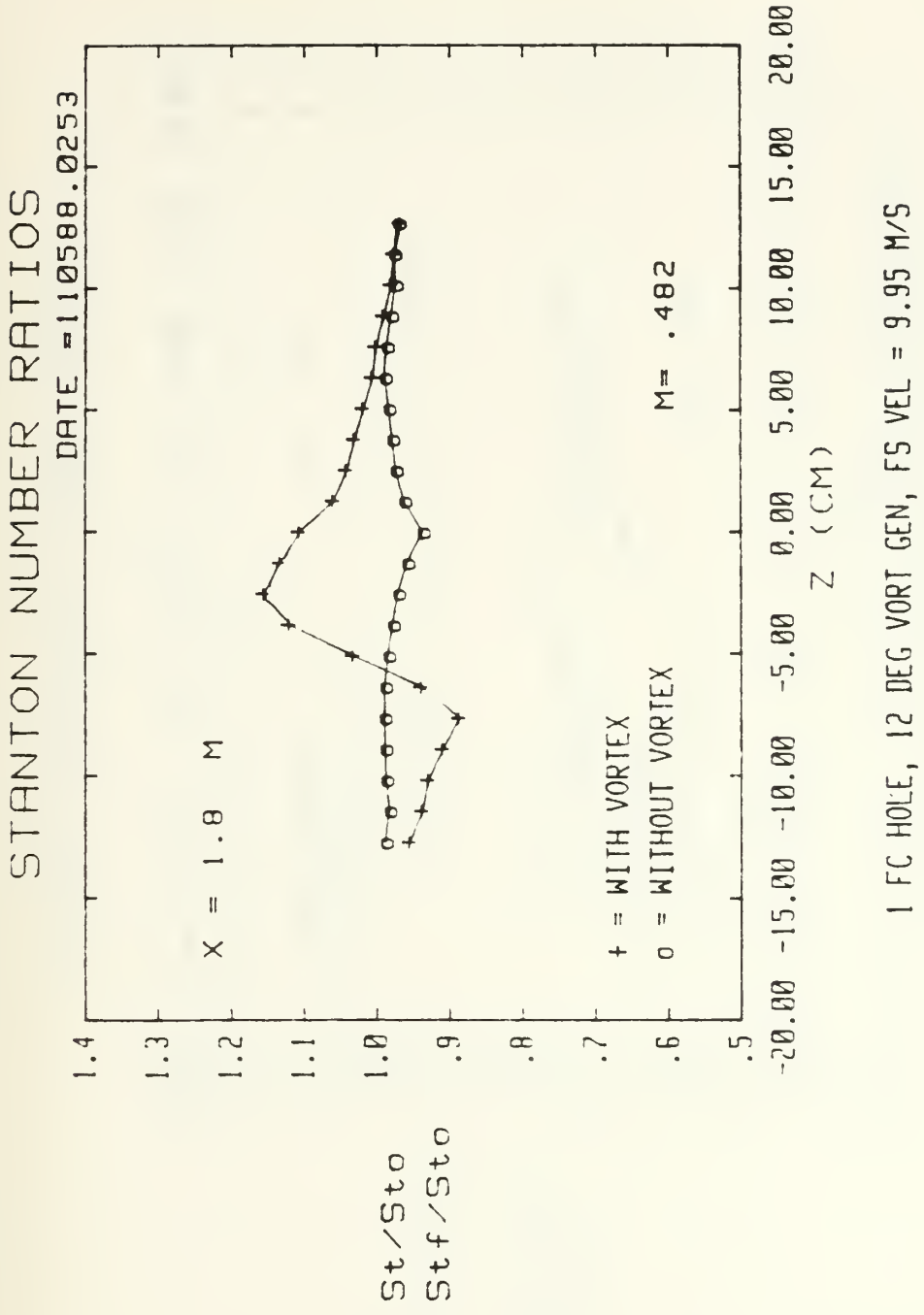

Figure 134. Spanwise Variation of St/Sto an Stf/Sto Ratios m=0.5, Single Injection Hole x/d=75.6, Vortex x

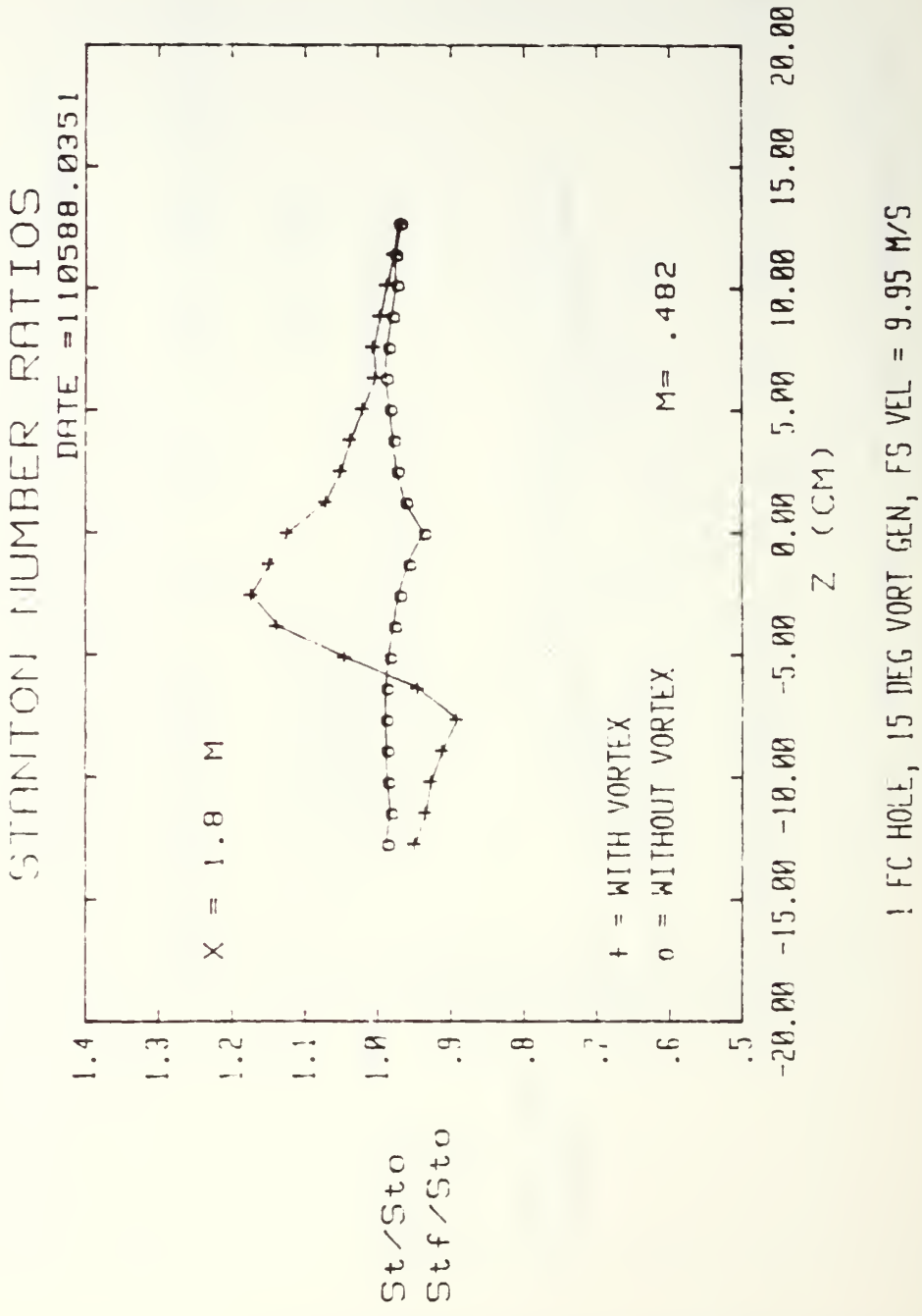

Figure 135. Spanwise Variation of St/Sto an Stf/Sto Ratios m=0.5, Single Injection Hole x/d=75.6, Vortex w

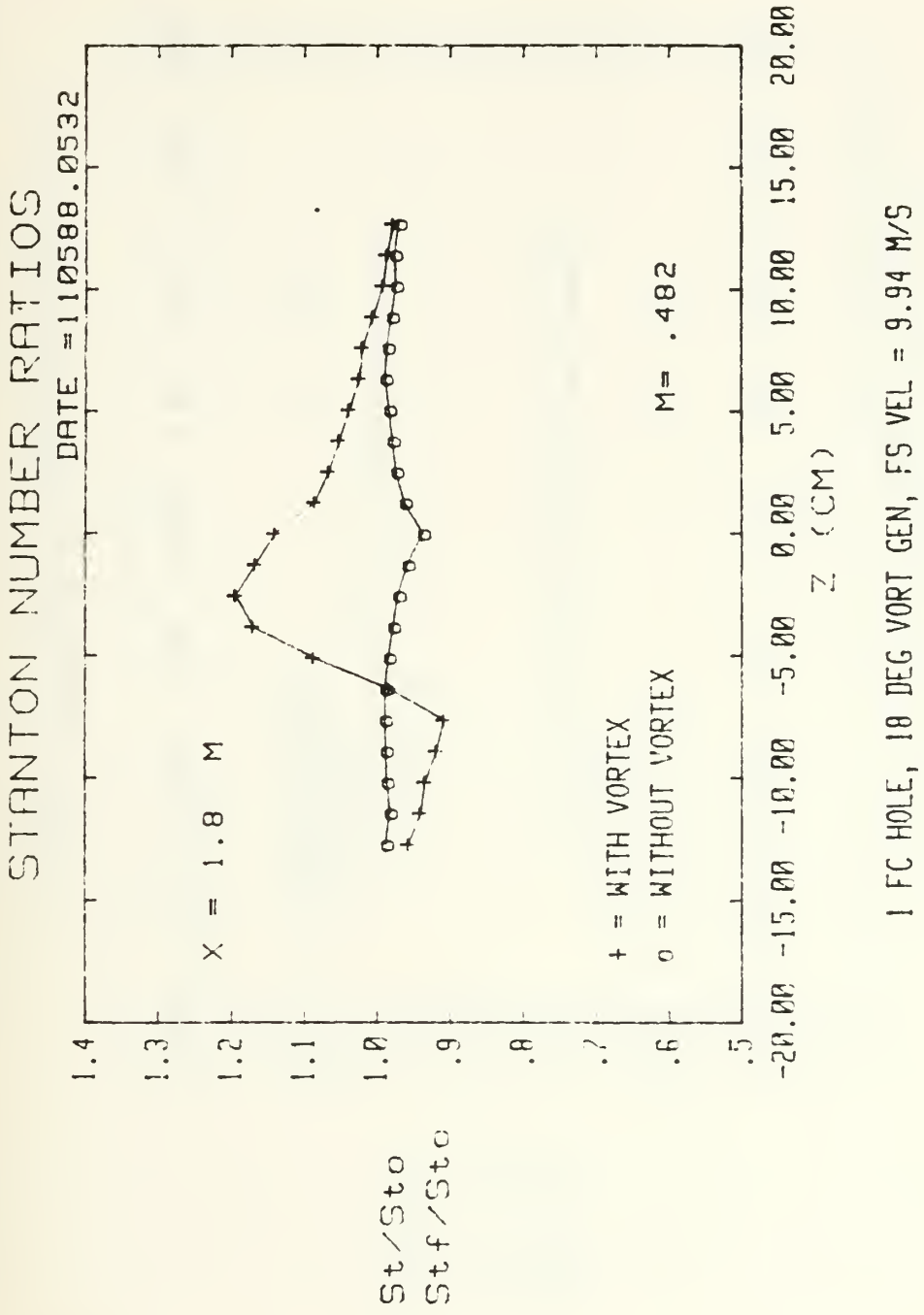

Figure 136. Spanwise Variation of St/Sto an Stf/Sto Ratios m=0.5, Single Injection Hole x/d=75.6, Vortex r

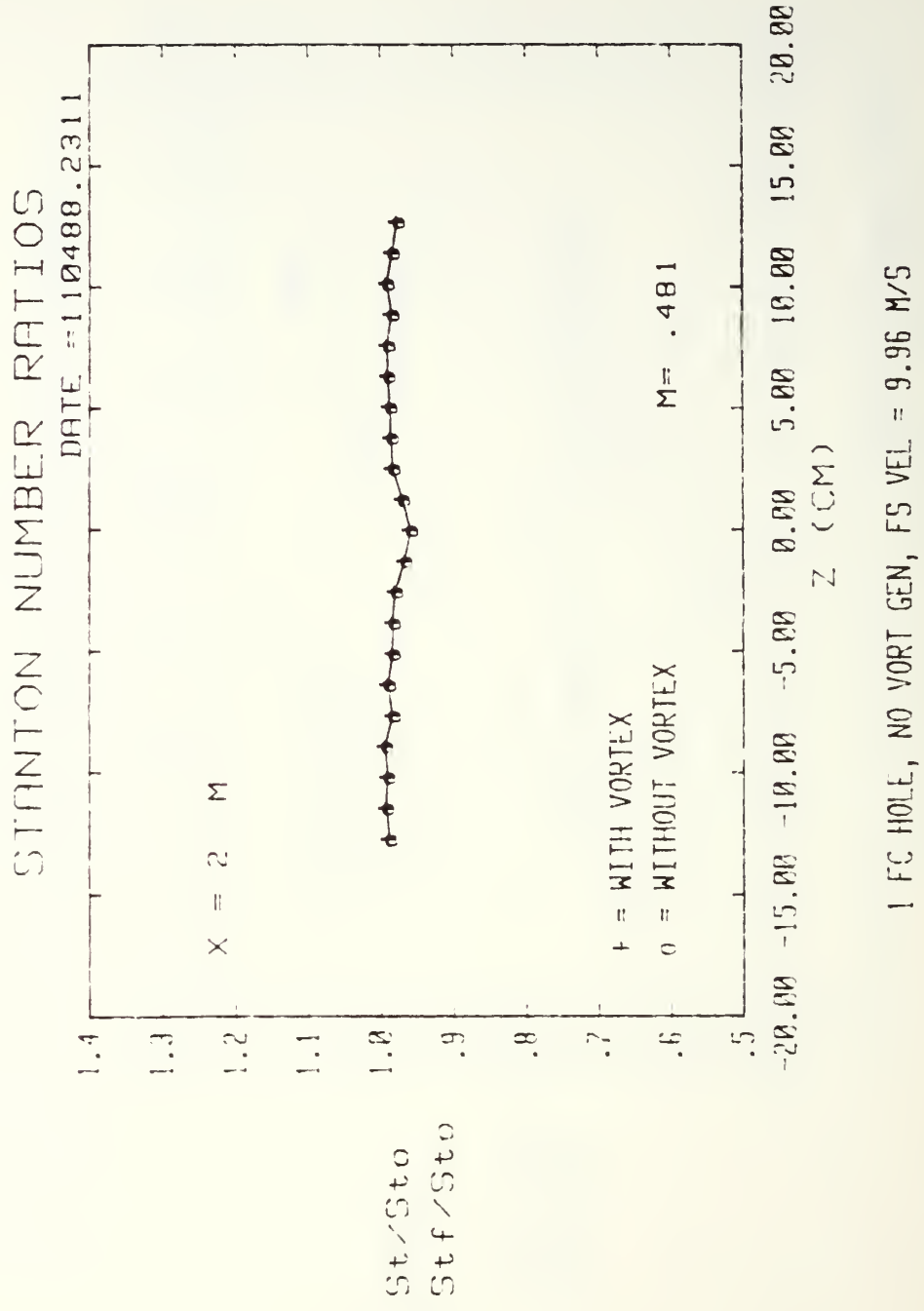

Figure 137. Spanwise Variation of St/Sto an Stf/Sto Ratios m=0.5, Single Injection Hole x/d=96.6, No Vortex

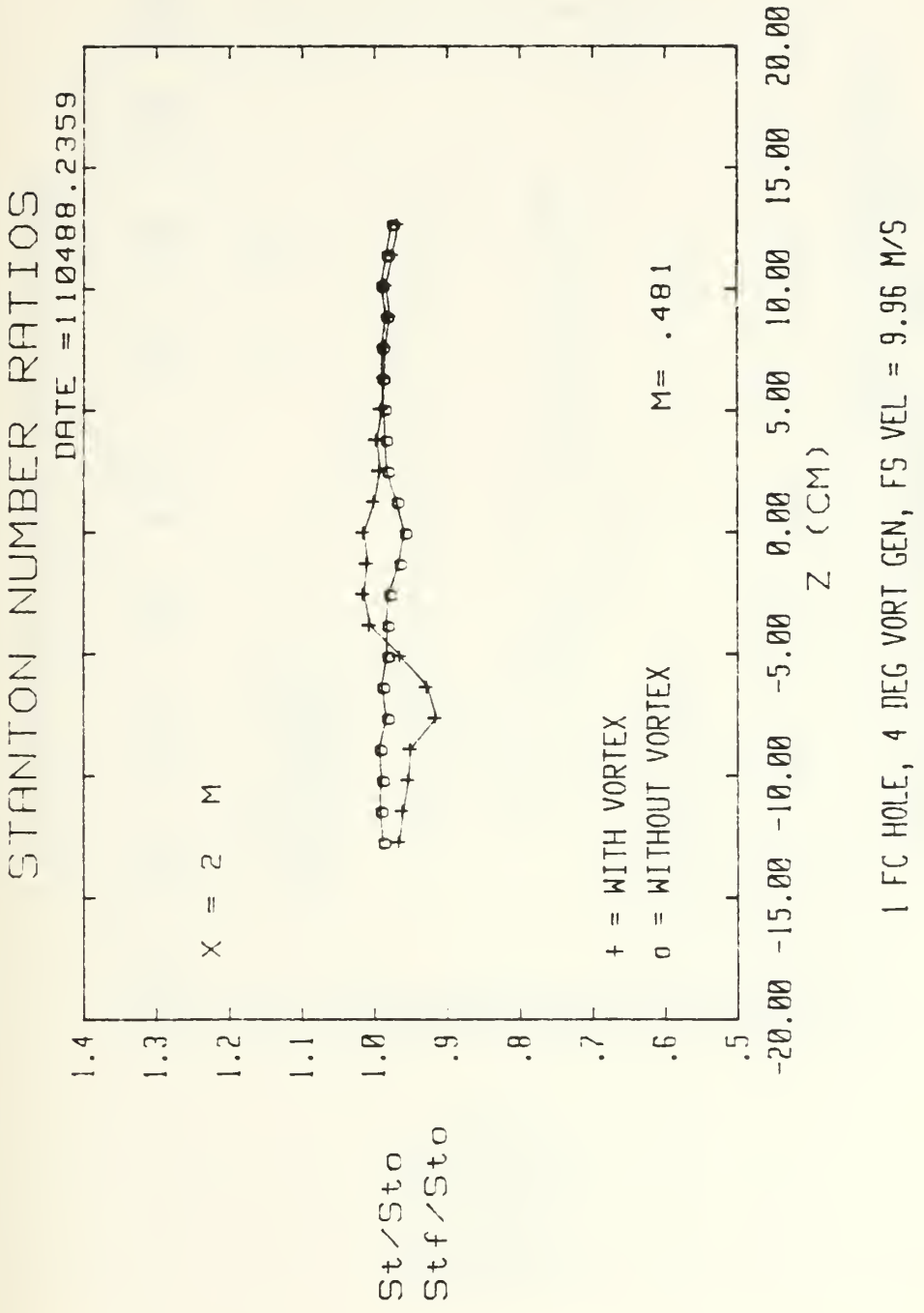

Figure 138. Spanwise Variation of St/Sto an Stf/Sto Ratios m=0.5, Single Injection Hole x/d=96.6, Vortex z

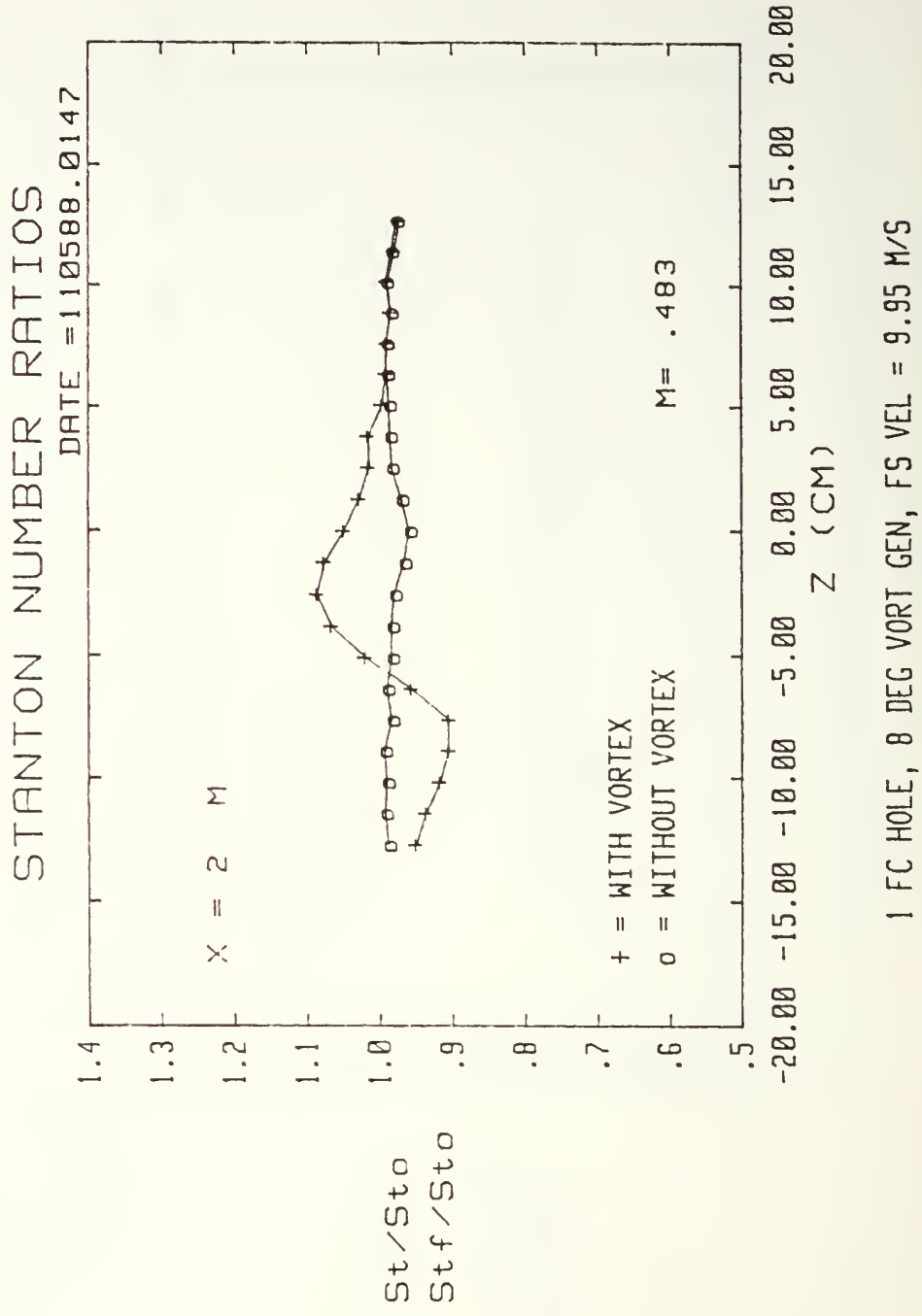

Figure 139. Spanwise Variation of St/Sto an Stf/Sto Ratios m=0.5, Single Injection Hole x/d=96.6, Vortex y

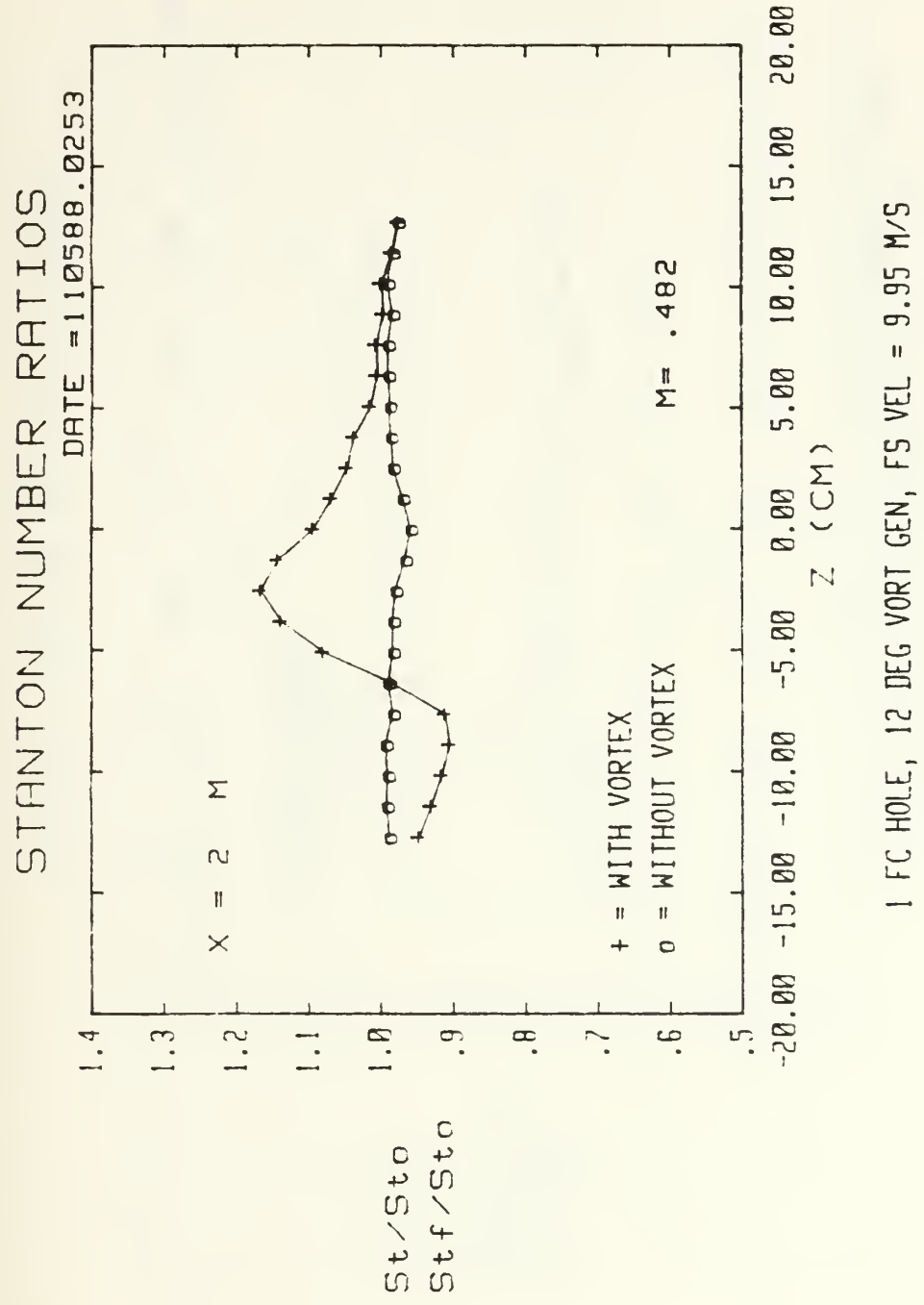

Figure 140. Spanwise Variation of St/Sto an Stf/Sto Ratios m=0.5, Single Injection Hole x/d=96.6, Vortex x

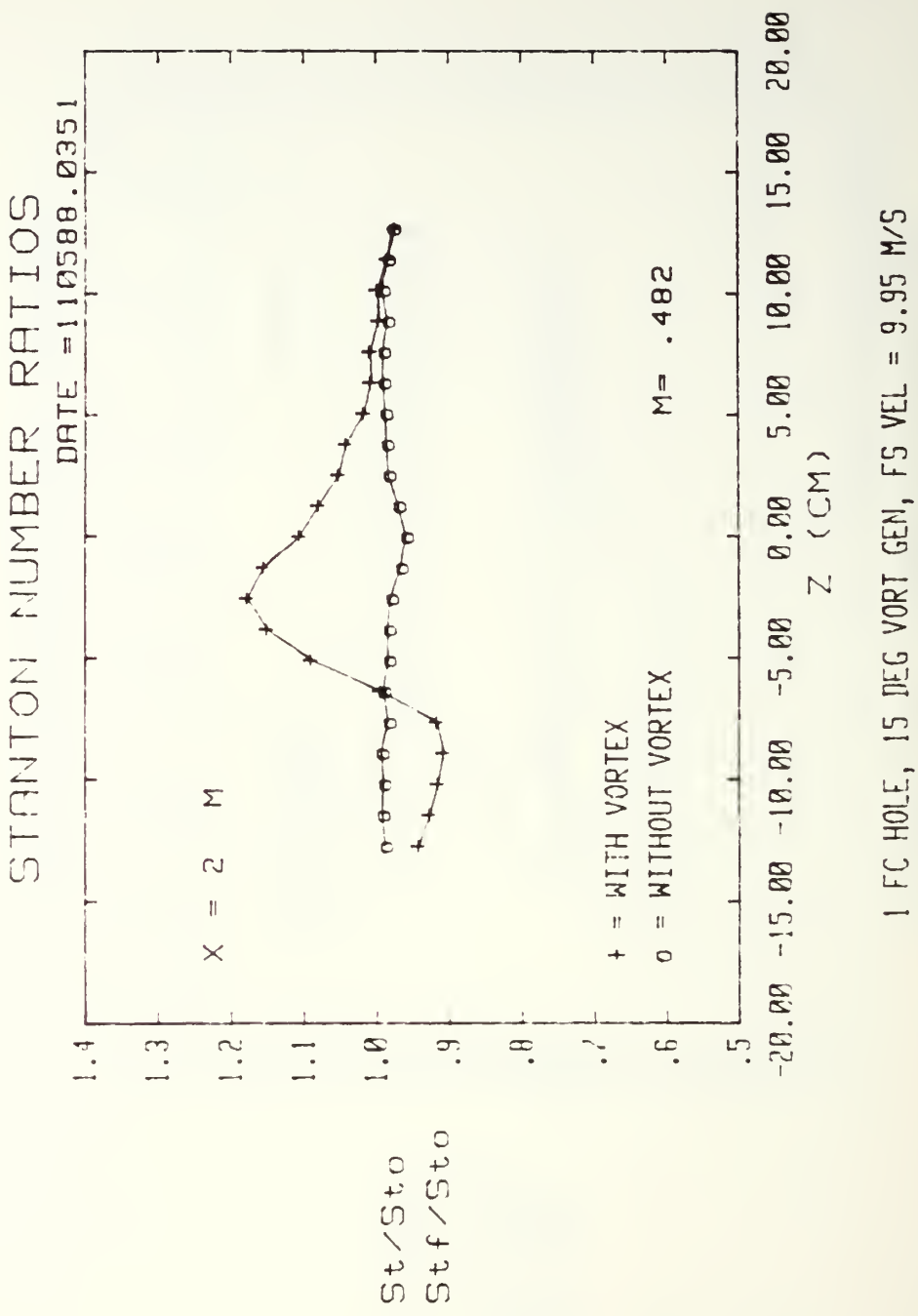

Figure 141. Spanwise Variation of St/Sto an Stf/Sto Ratios m=0.5, Single Injection Hole x/d=96.6, Vortex w

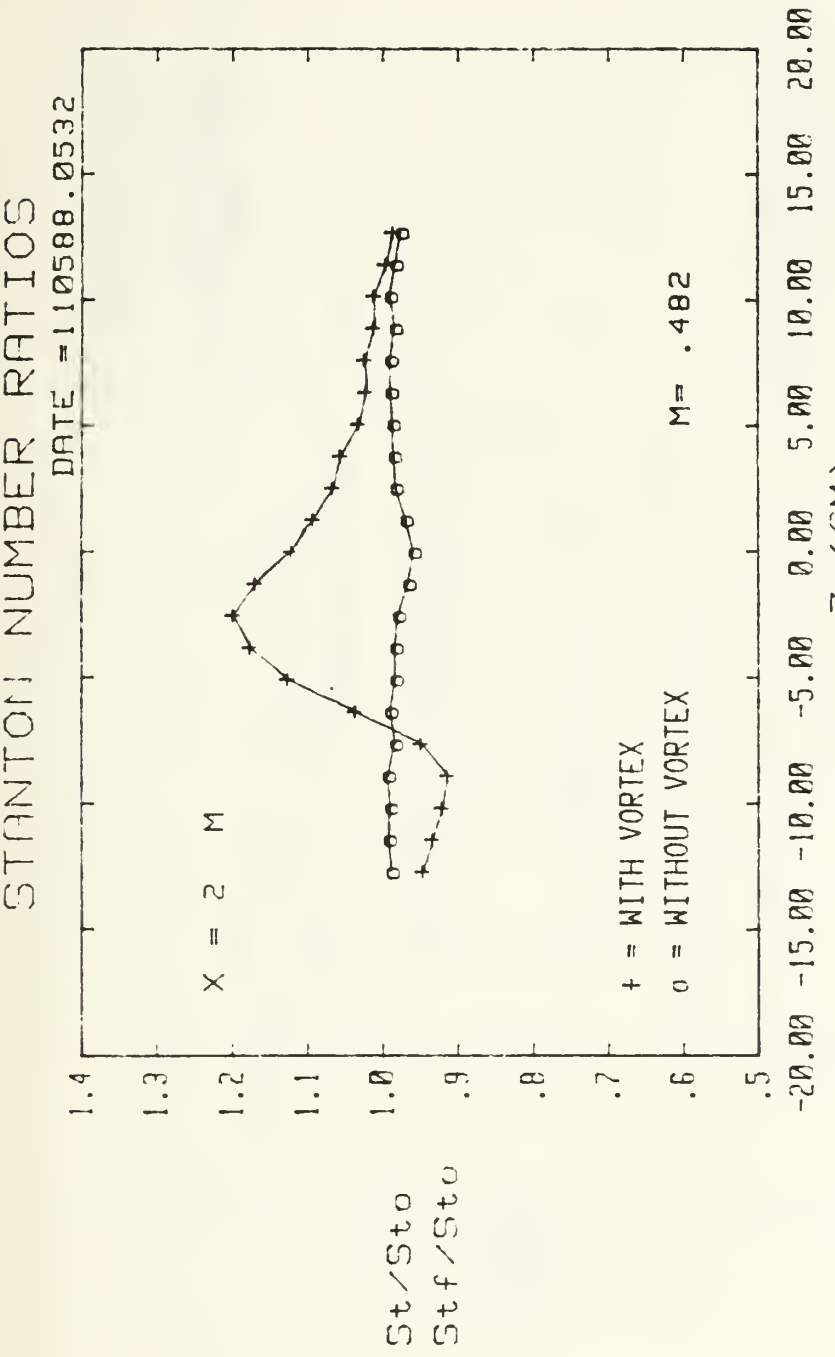

Figure 142. Spanwise Variation of St/Sto an Stf/Sto Ratios m=0.5, Single Injection Hole x/d=96.6, Vortex r

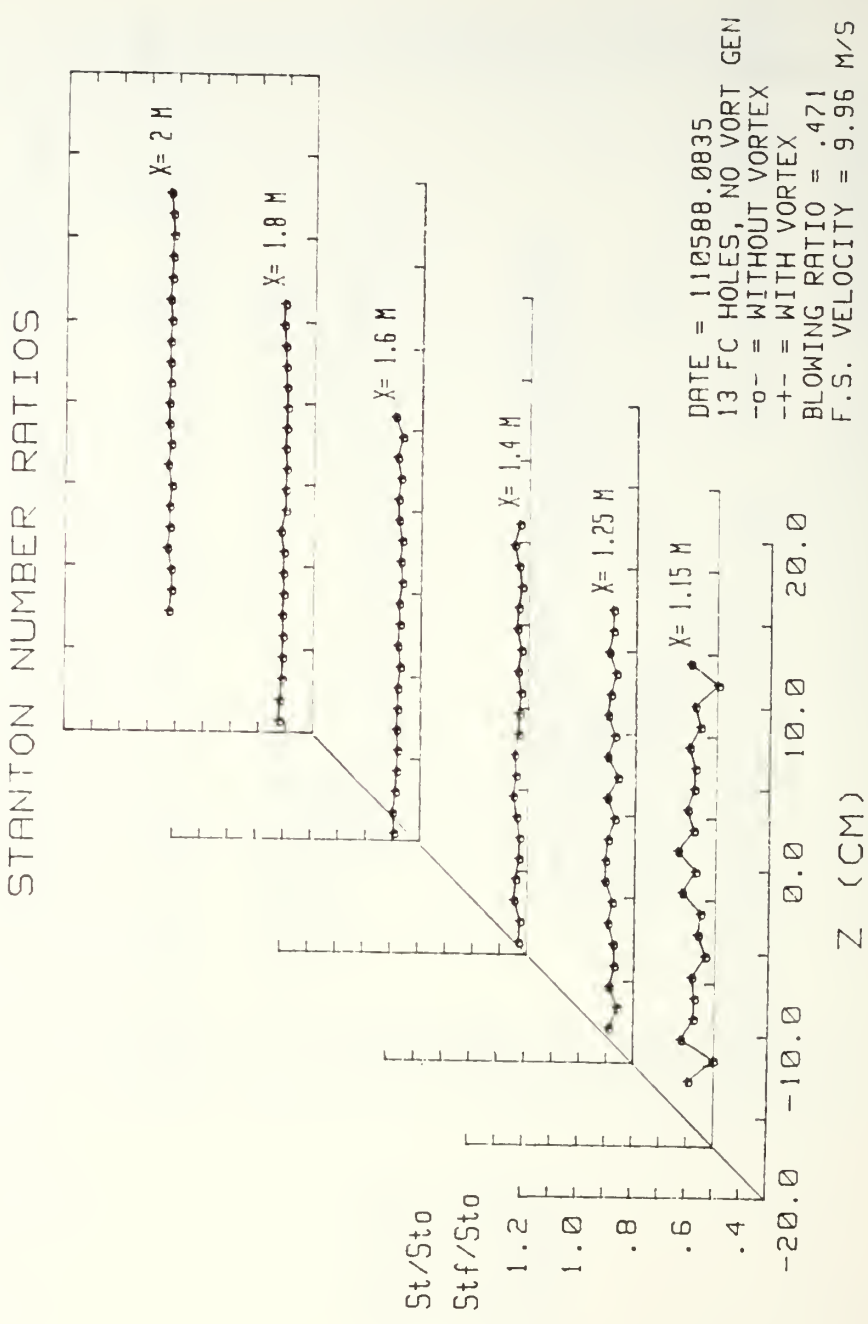

Figure 143. Local St/Sto and Stf/Sto Distributions With Film Cooling, m=0.5, 13 Injection Holes Without Embedded Vortex

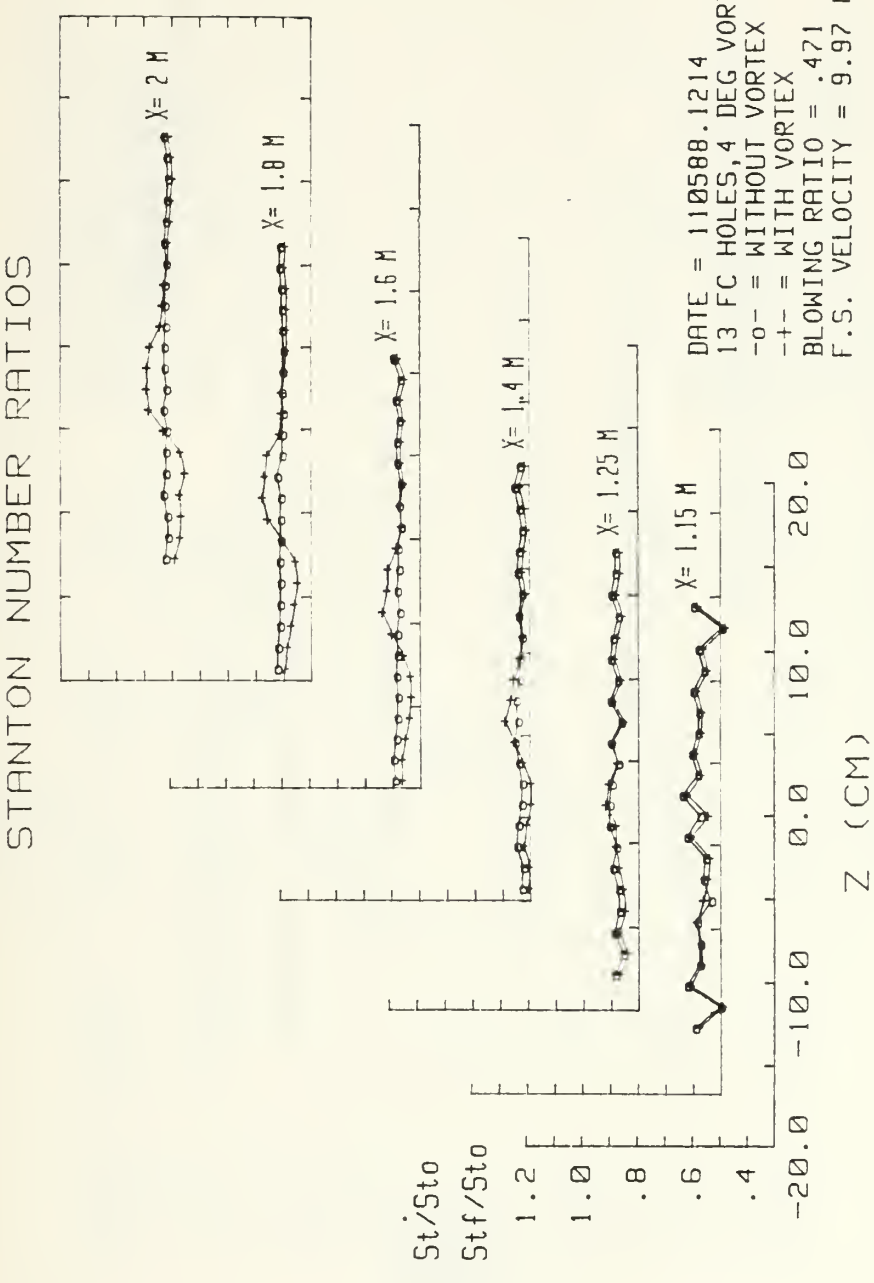

Figure 144. Local St/Sto and Stf/Sto Distributions With Film Cooling, m=0.5, 13 Injection Holes With and Without Embedded Vortex z

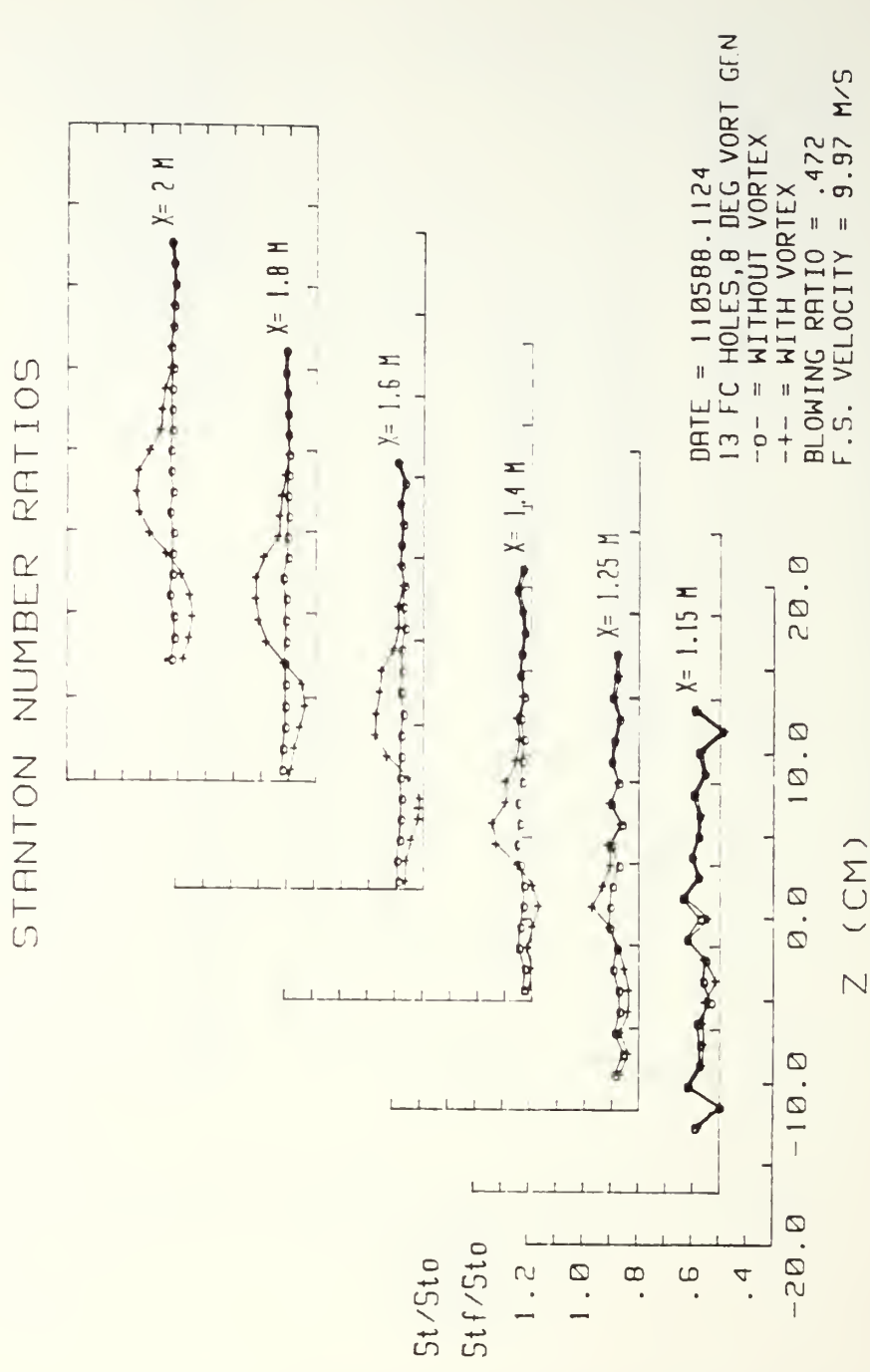

Figure 145. Local St/Sto and Stf/Sto Distributions With Film Cooling, m=0.5, 13 Injection Holes With and Without Embedded Vortex y

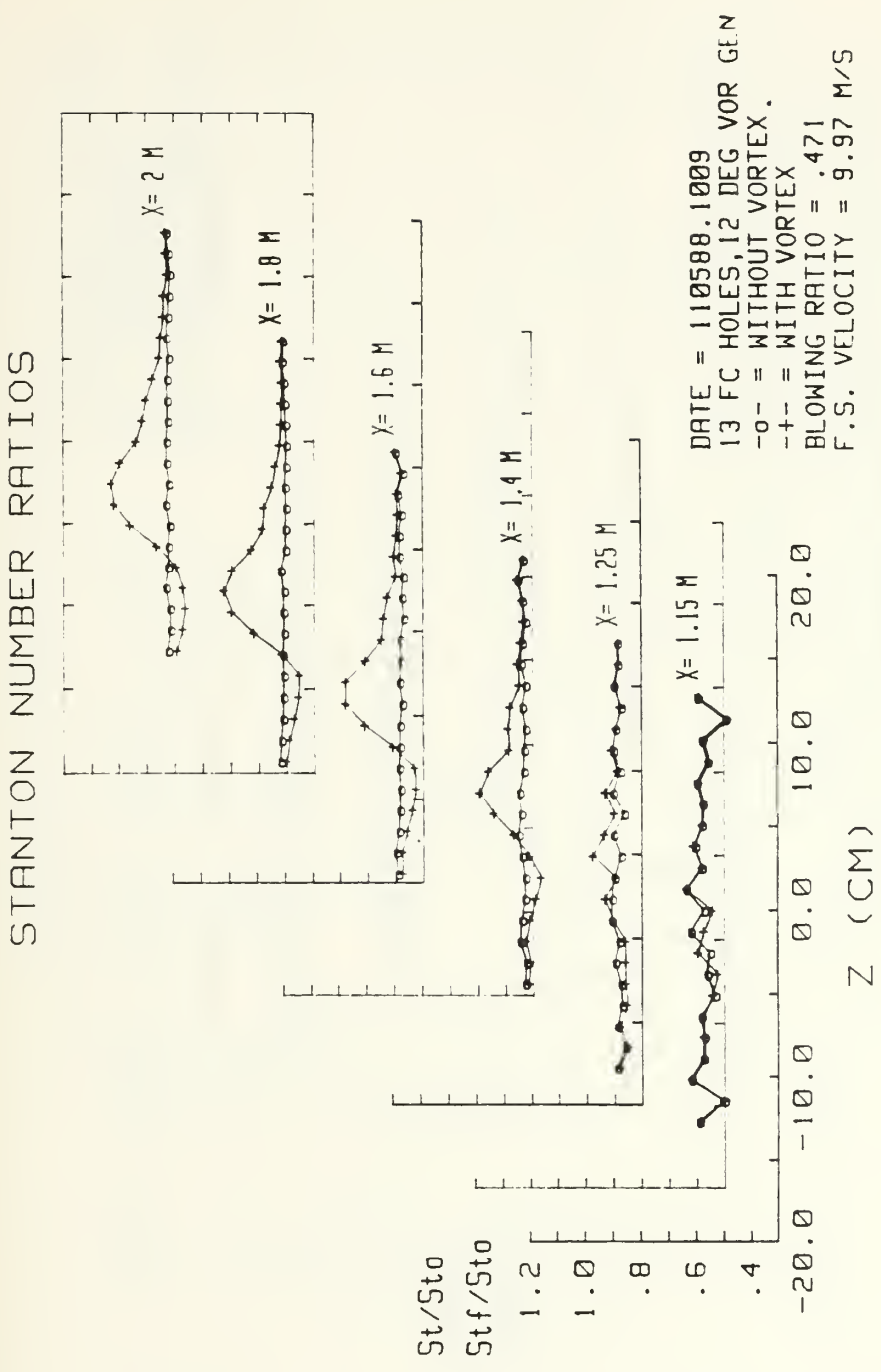

Figure 146. Local St/Sto and Stf/Sto Distributions With Film Cooling, m=0.5, 13 Injection Holes With and Without Embedded Vortex x

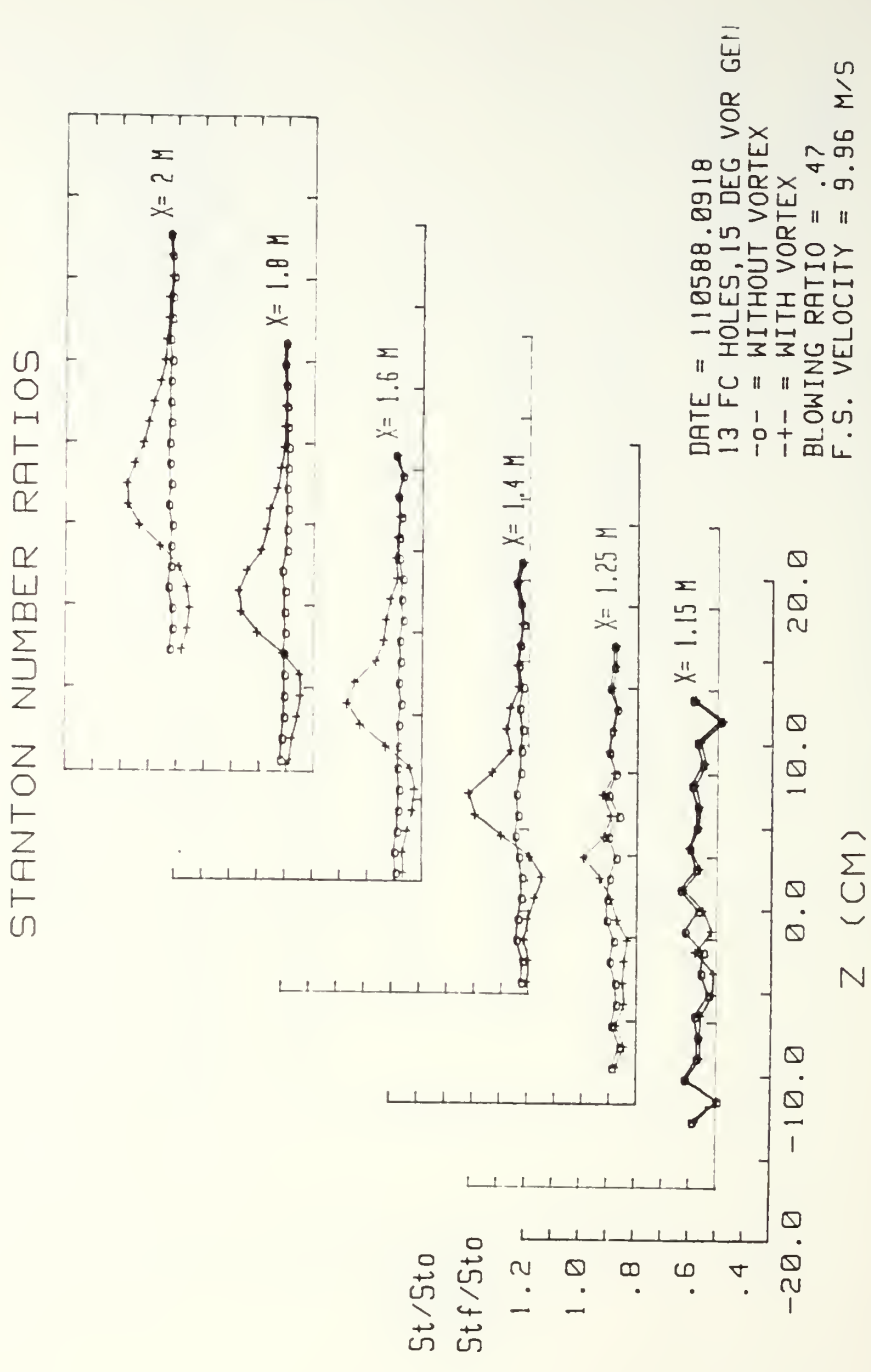

Figure 147. Local St/Sto and Stf/Sto Distributions With Film Cooling, m=0.5, 13 Injection Holes With and Without Embedded Vortex w

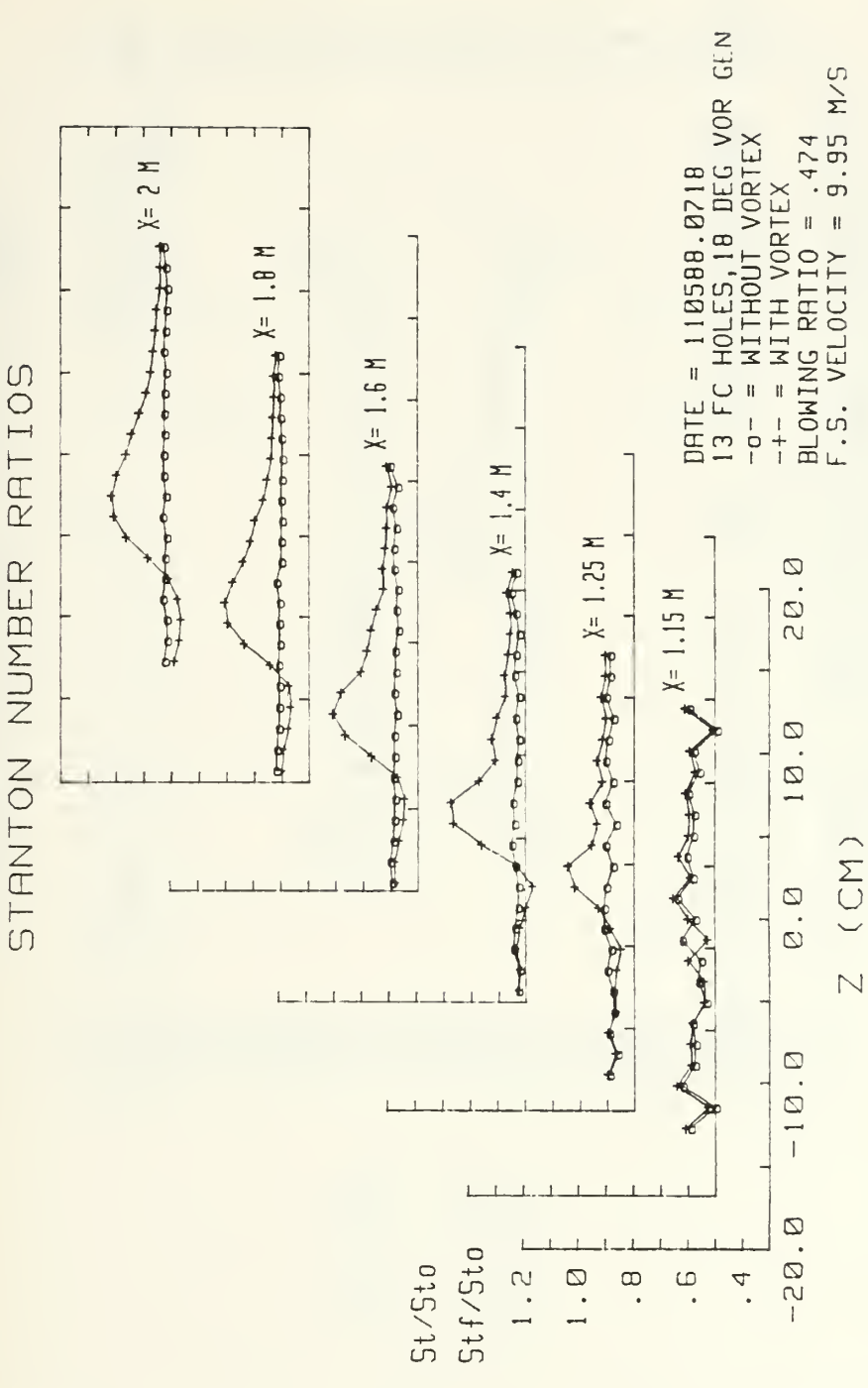

Figure 148. Local St/Sto and Stf/Sto Distributions With Film Cooling, m=0.5, 13 Injection Holes With and Without Embedded Vortex r

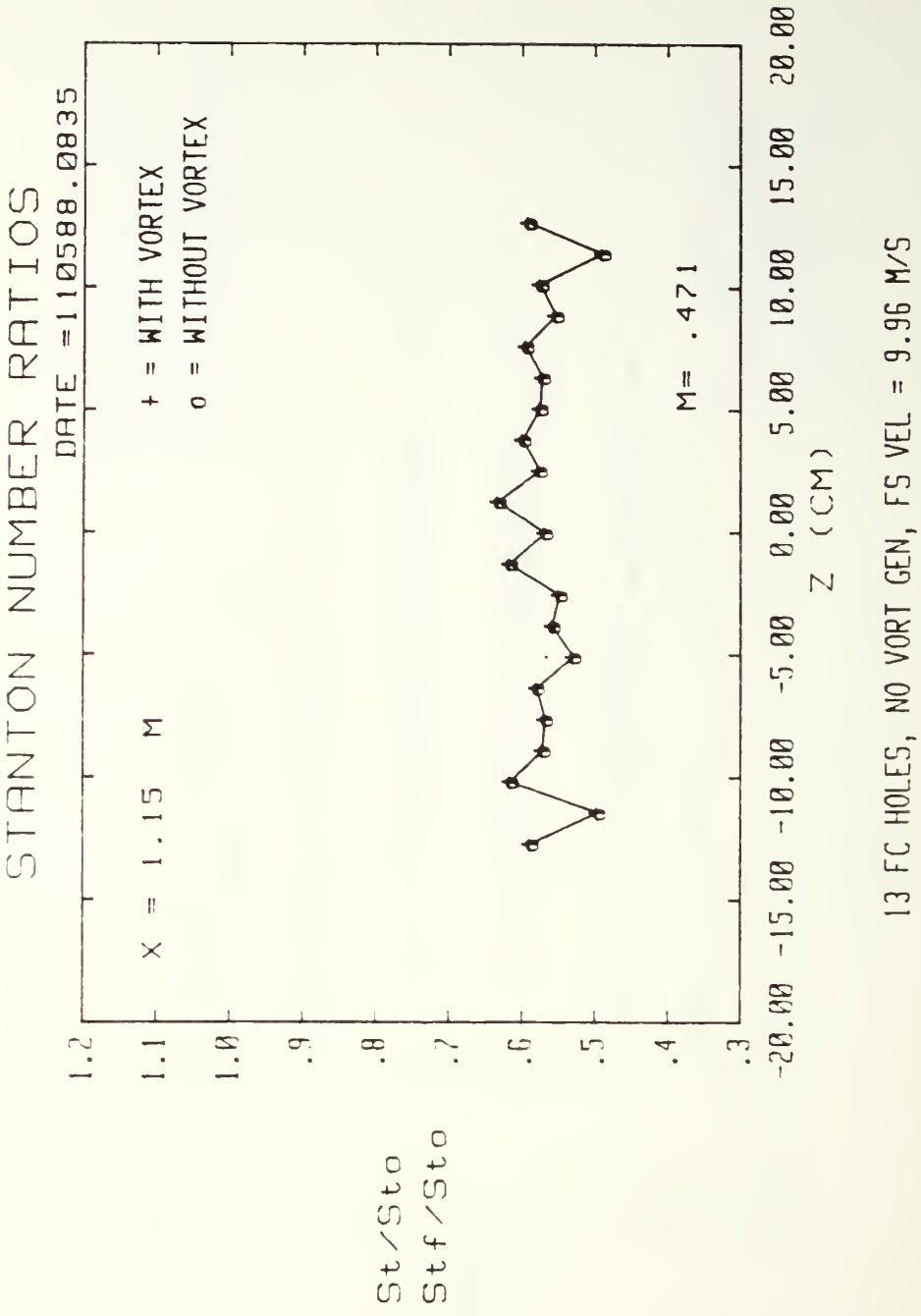

Figure 149. Spanwise Variation of St/Sto and Stf/Sto Ratios m=0.5, 13 Injection Holes x/d=7.4, No Vortex

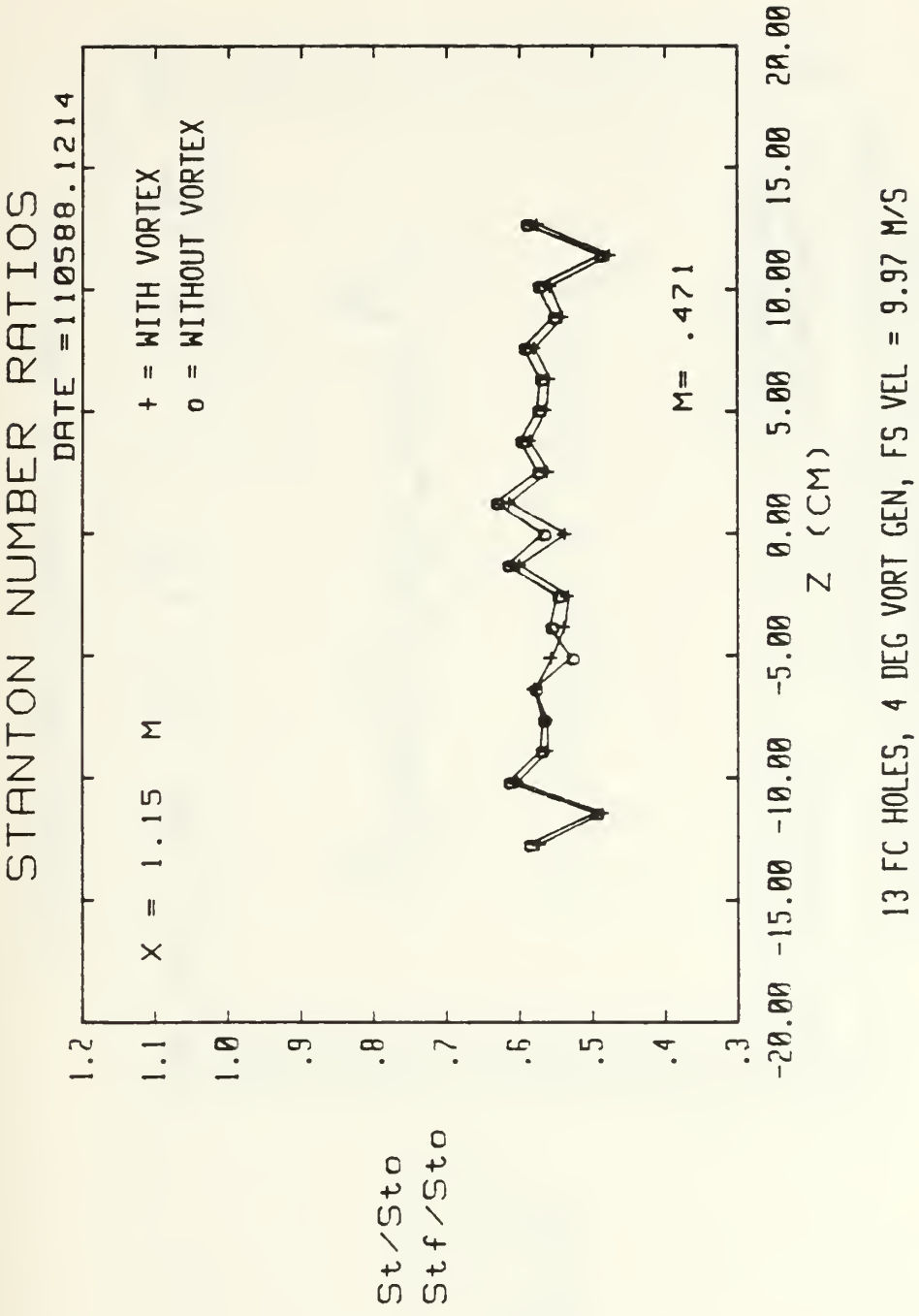

Figure 150. Spanwise Variation of St/Sto and Stf/Sto Ratios m=0.5, 13 Injection Holes x/d=7.4, Vortex z

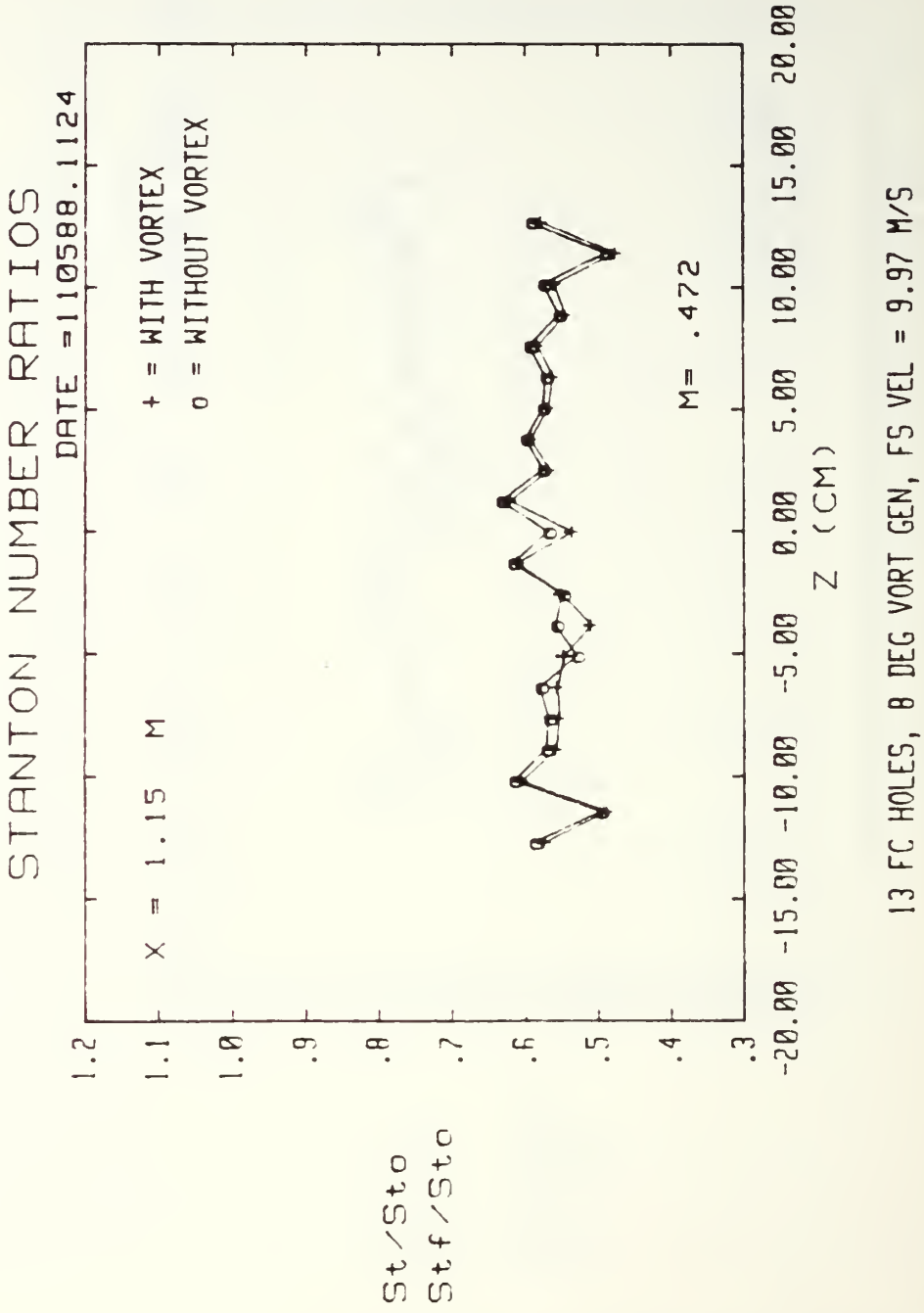

Figure 151. Spanwise Variation of St/Sto and Stf/Sto Ratios m=0.5, 13 Injection Holes x/d=7.4, Vortex y

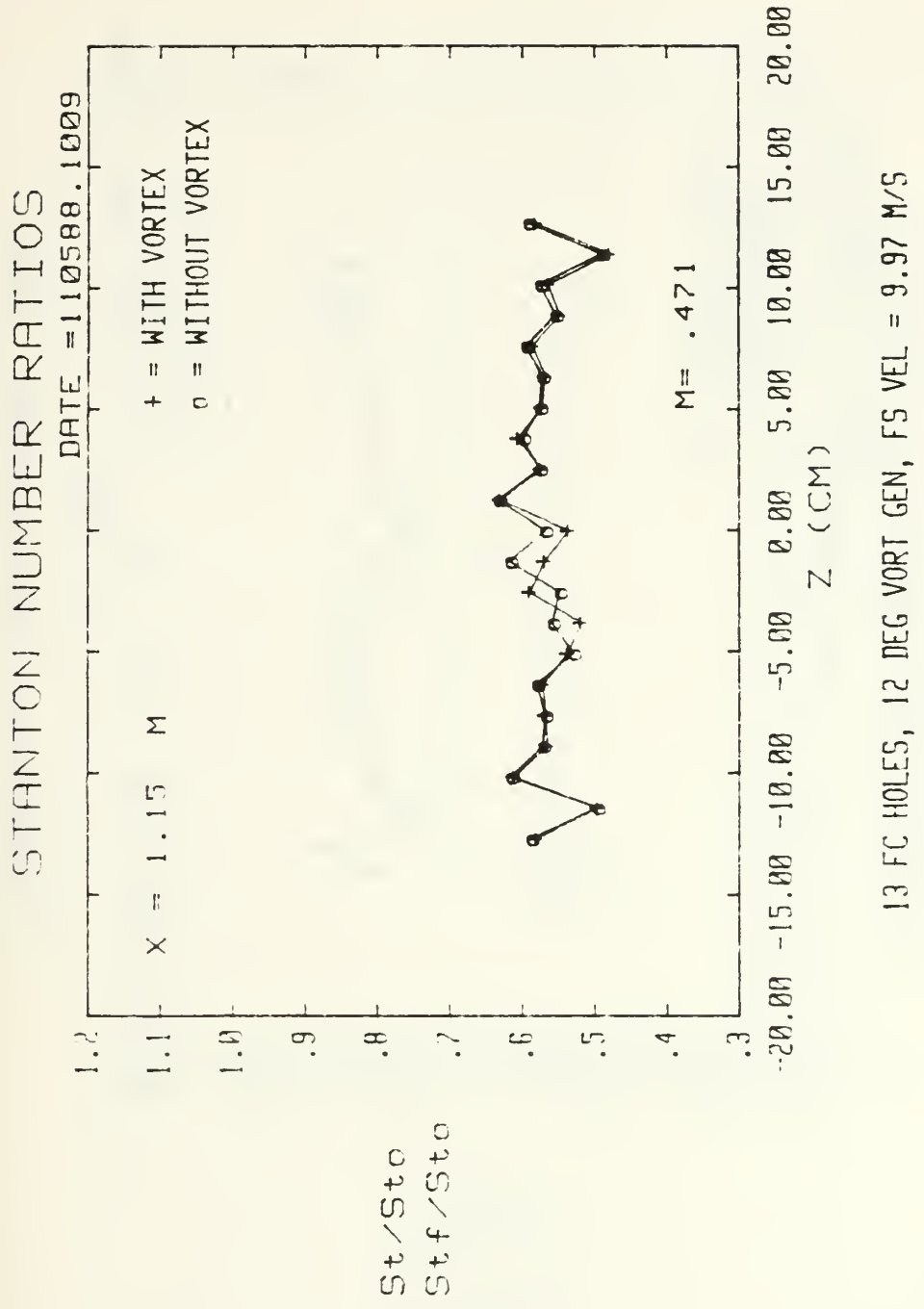

Figure 152. Spanwise Variation of St/Sto and Stf/Sto Ratios m=0.5, 13 Injection Holes x/d=7.4, Vortex x

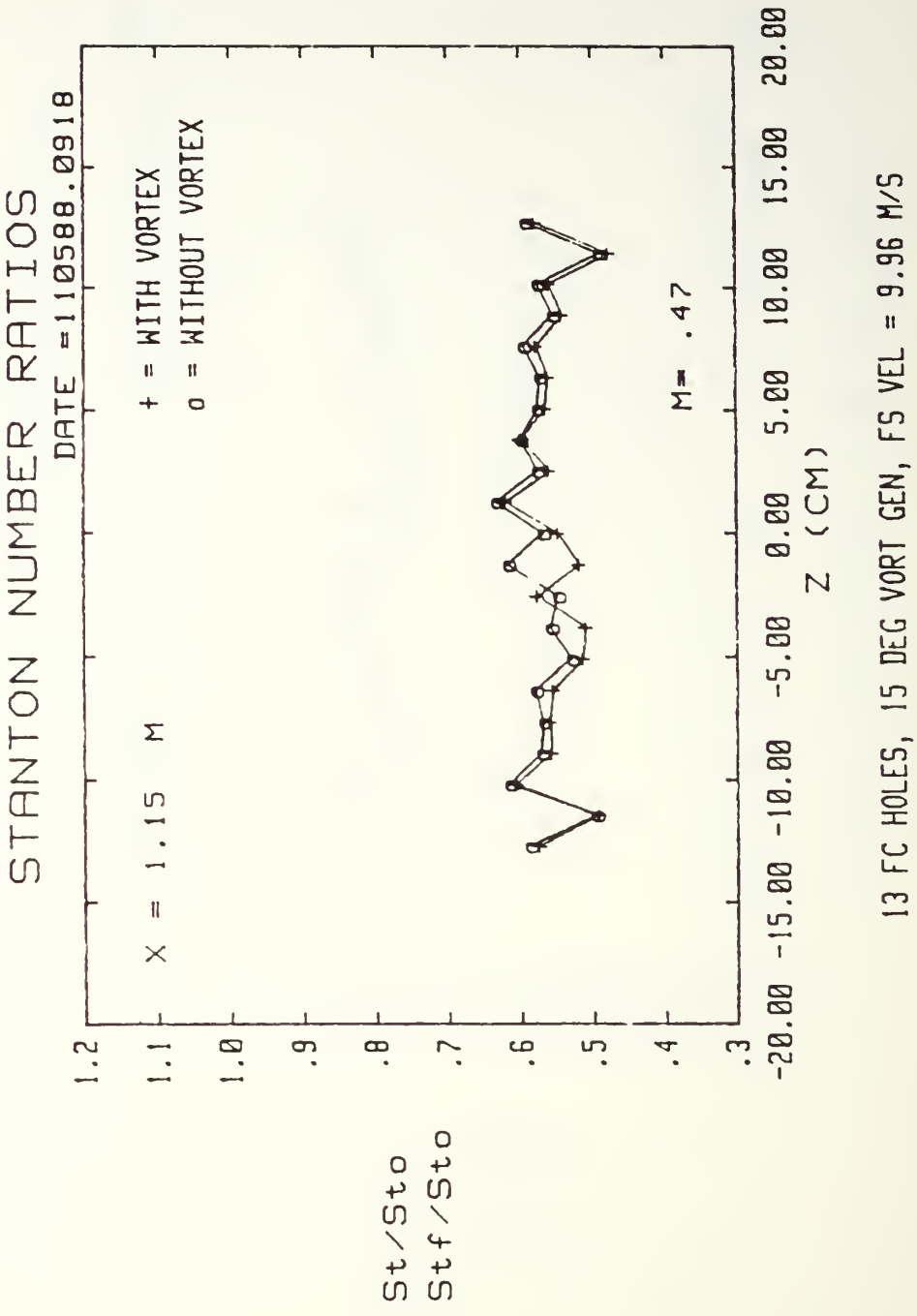

Figure 153. Spanwise Variation of St/Sto and Stf/Sto Ratios m=0.5, 13 Injection Holes x/d=7.4, Vortex w

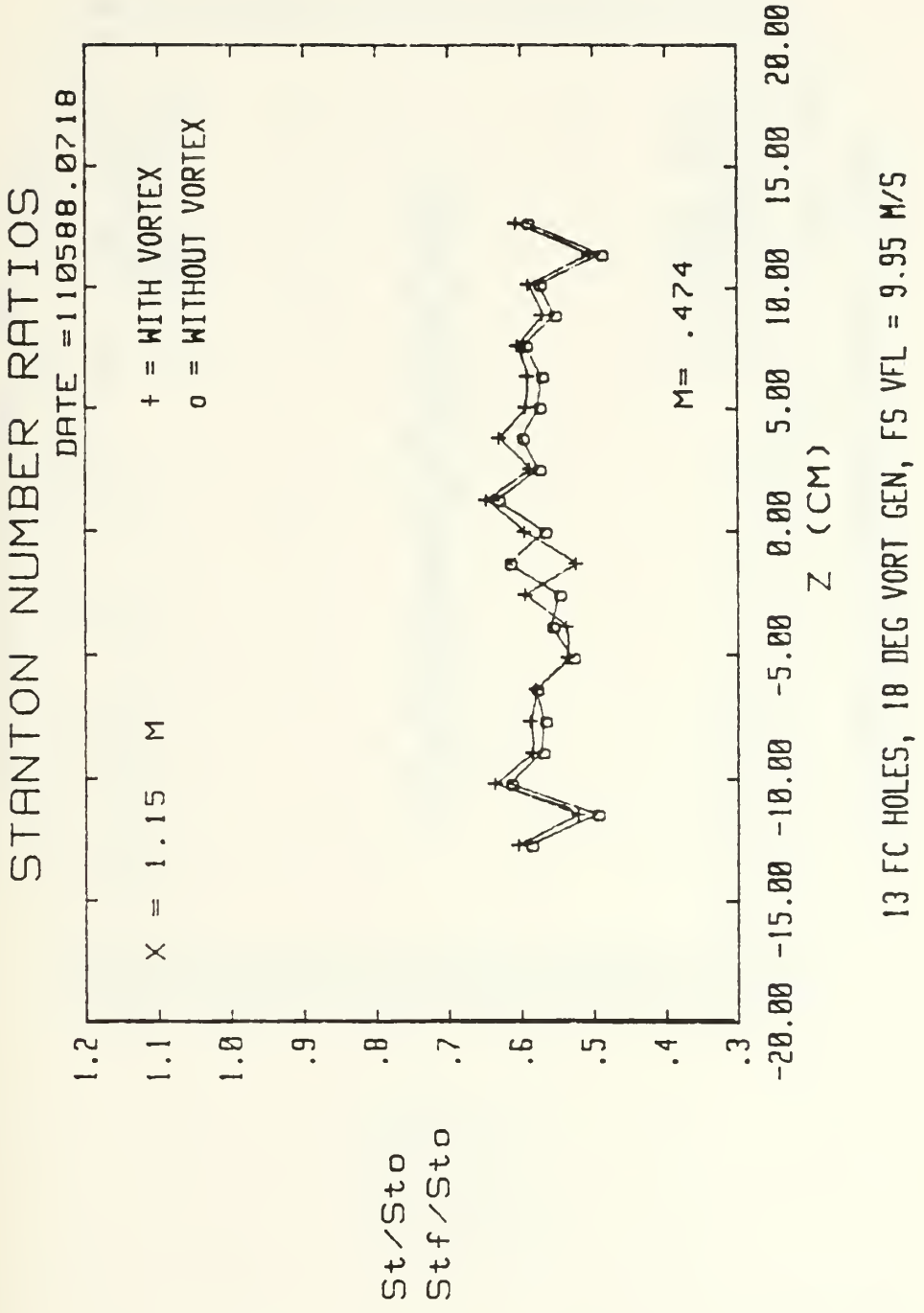

Figure 154. Spanwise Variation of St/Sto and Stf/Sto Ratios m=0.5, 13 Injection Holes x/d=7.4, Vortex r

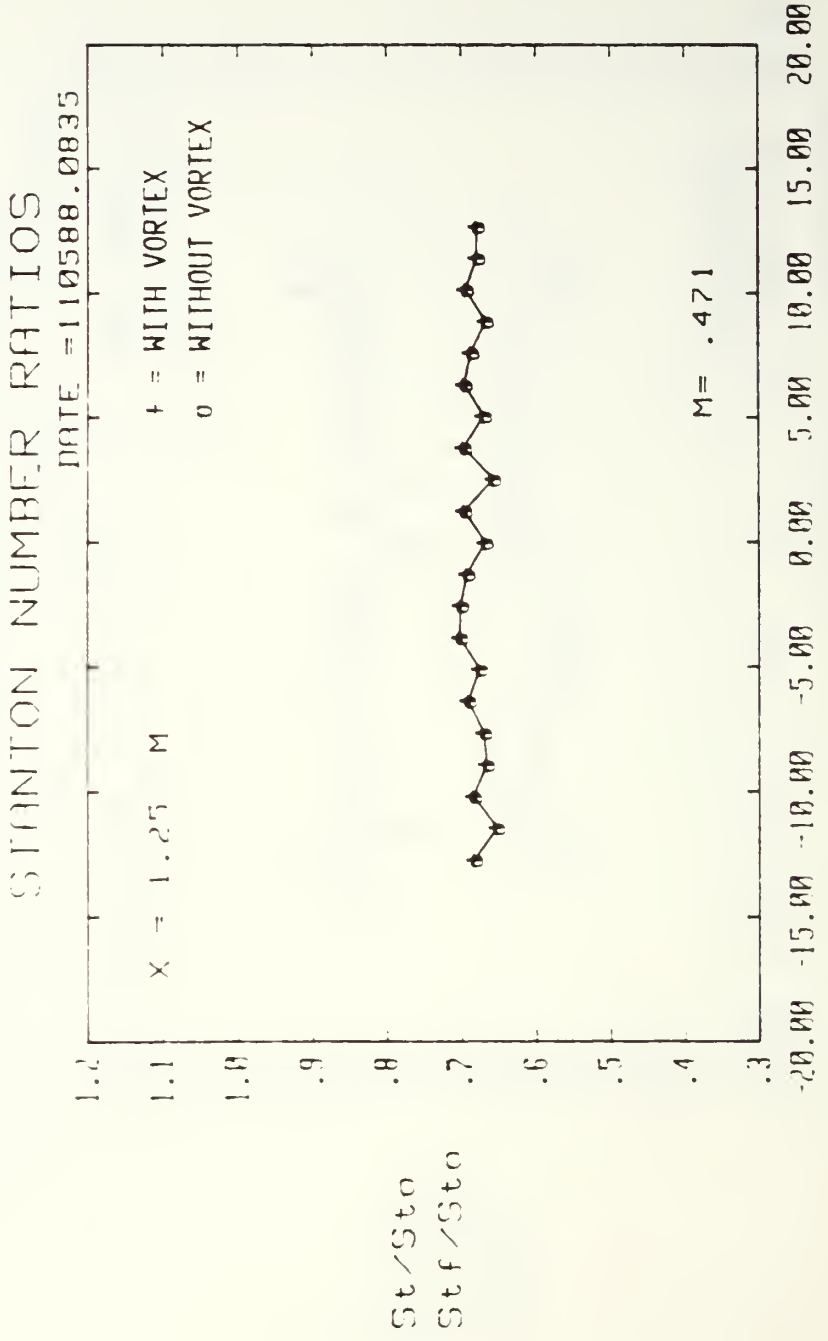

Figure 155. Spanwise Variation of St/Sto and Stf/Sto Ratios m=0.5, 13 Injection Holes x/d=17.5, No Vortex

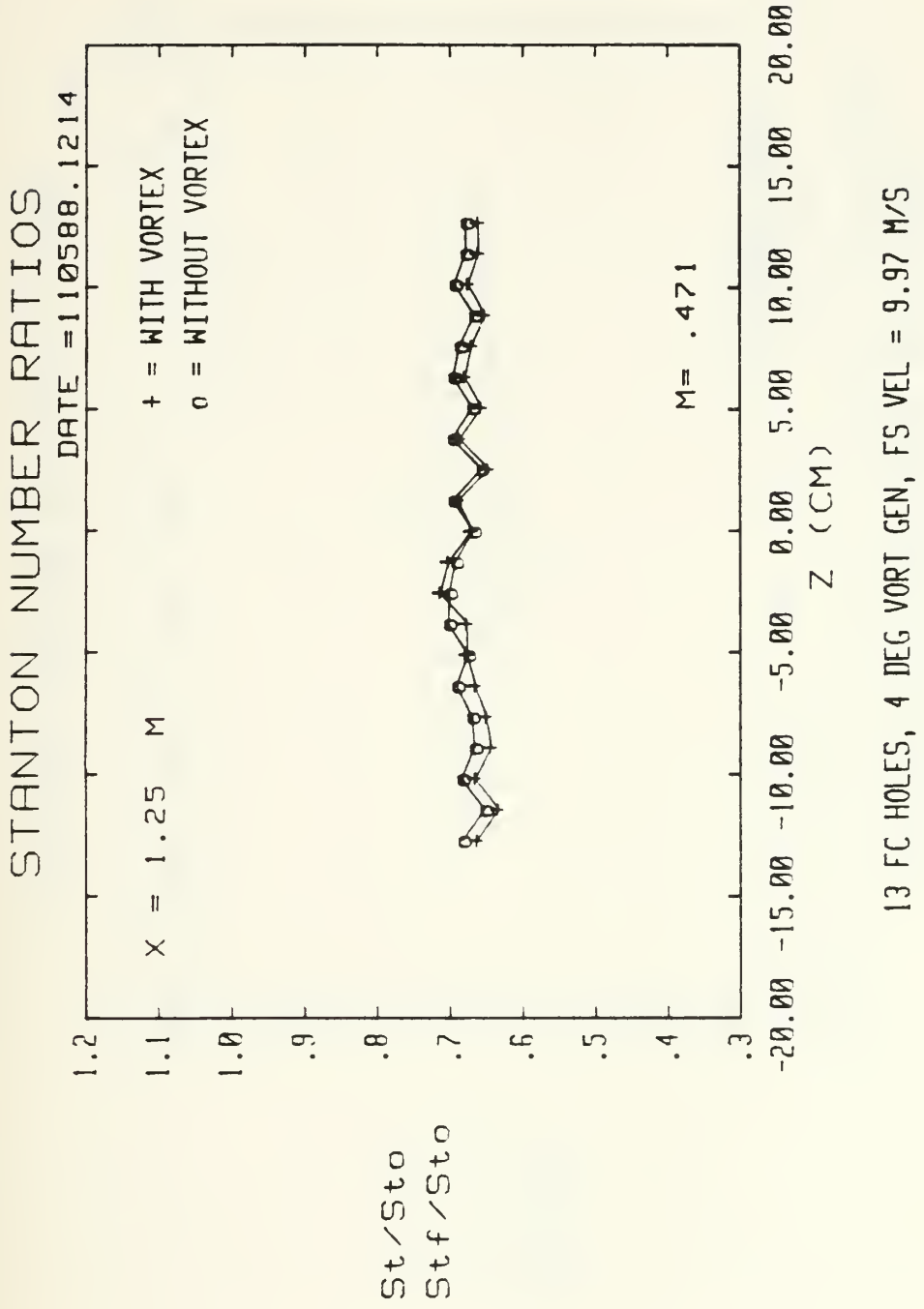

Figure 156. Spanwise Variation of St/Sto and Stf/Sto Ratios m=0.5, 13 Injection Holes x/d=17.5, Vortex z

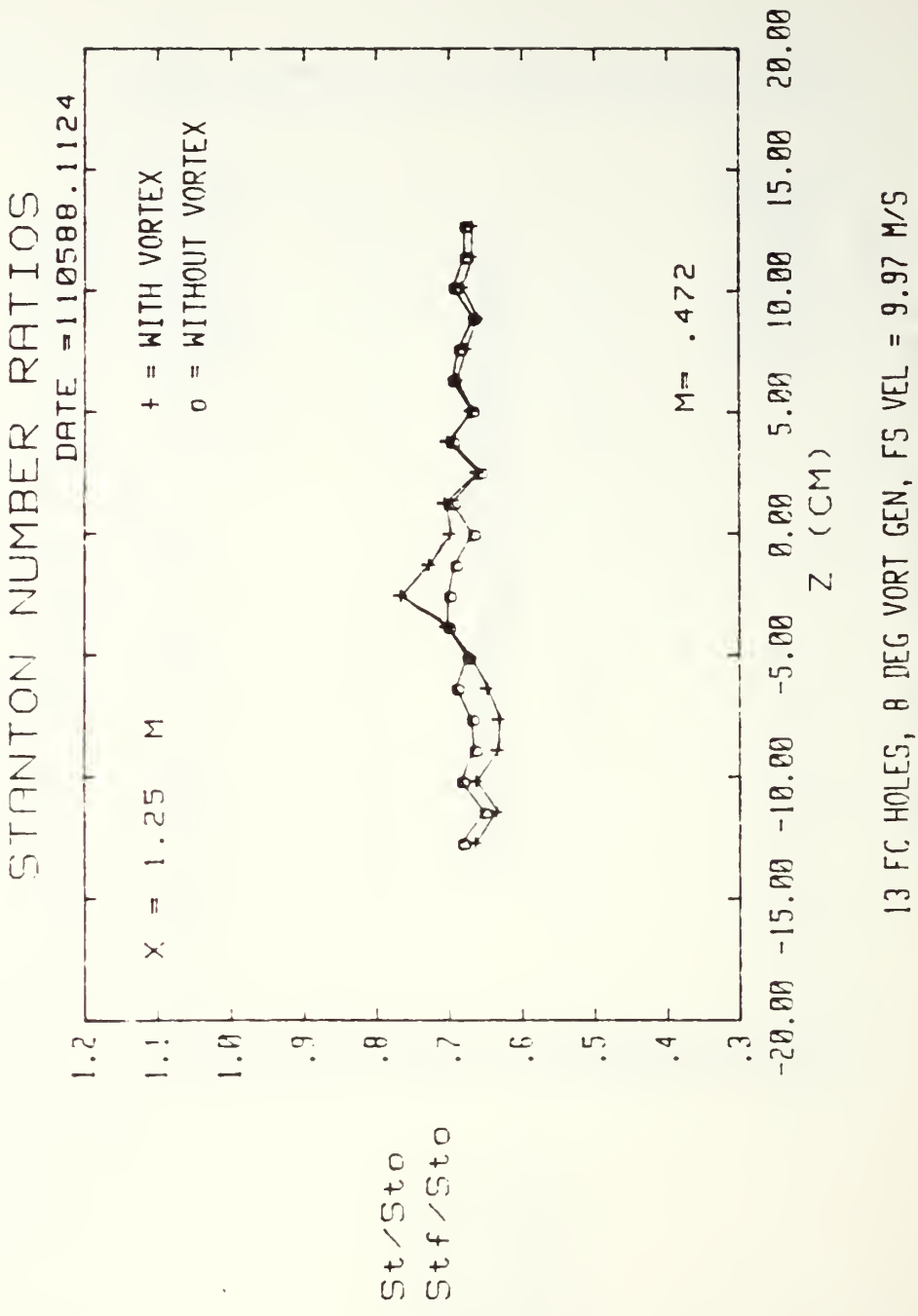

Figure 157. Spanwise Variation of St/Sto and Stf/Sto Ratios m=0.5, 13 Injection Holes x/d=17.5, Vortex y

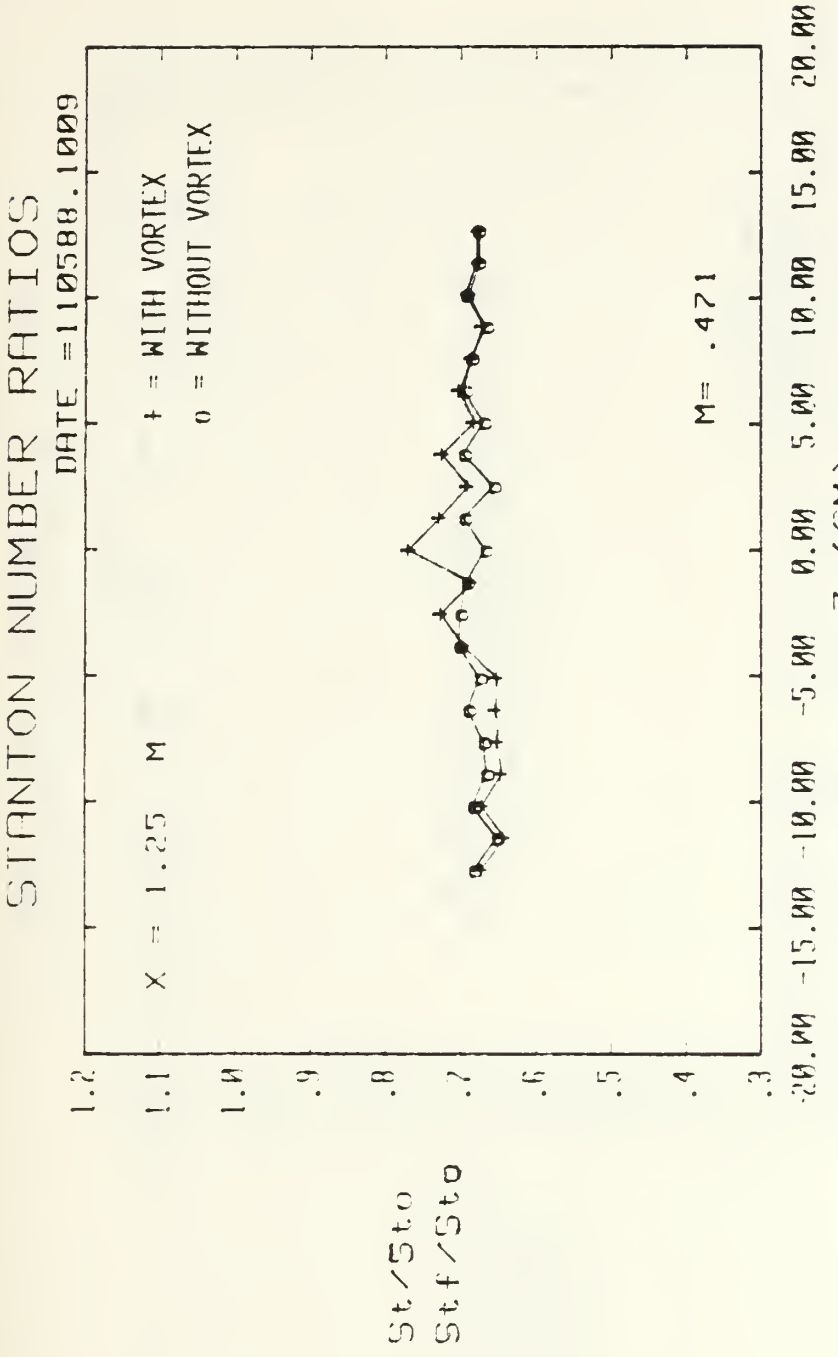

Figure 158. Spanwise Variation of St/Sto and Stf/Sto Ratios m=0.5, 13 Injection Holes x/d=17.5, Vortex x

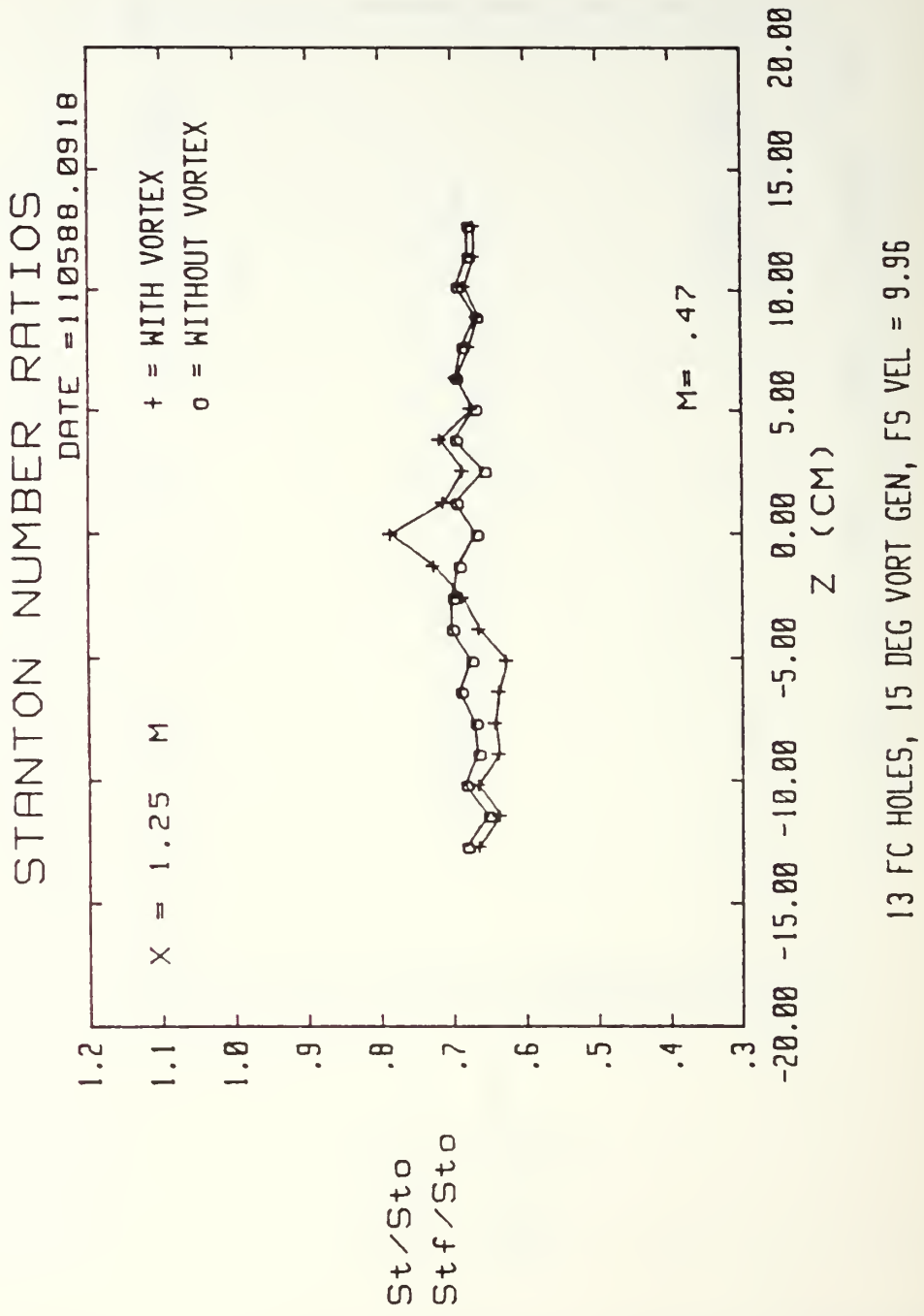

Figure 159. Spanwise Variation of St/Sto and Stf/Sto Ratios m=0.5, 13 Injection Holes x/d=17.5, Vortex w

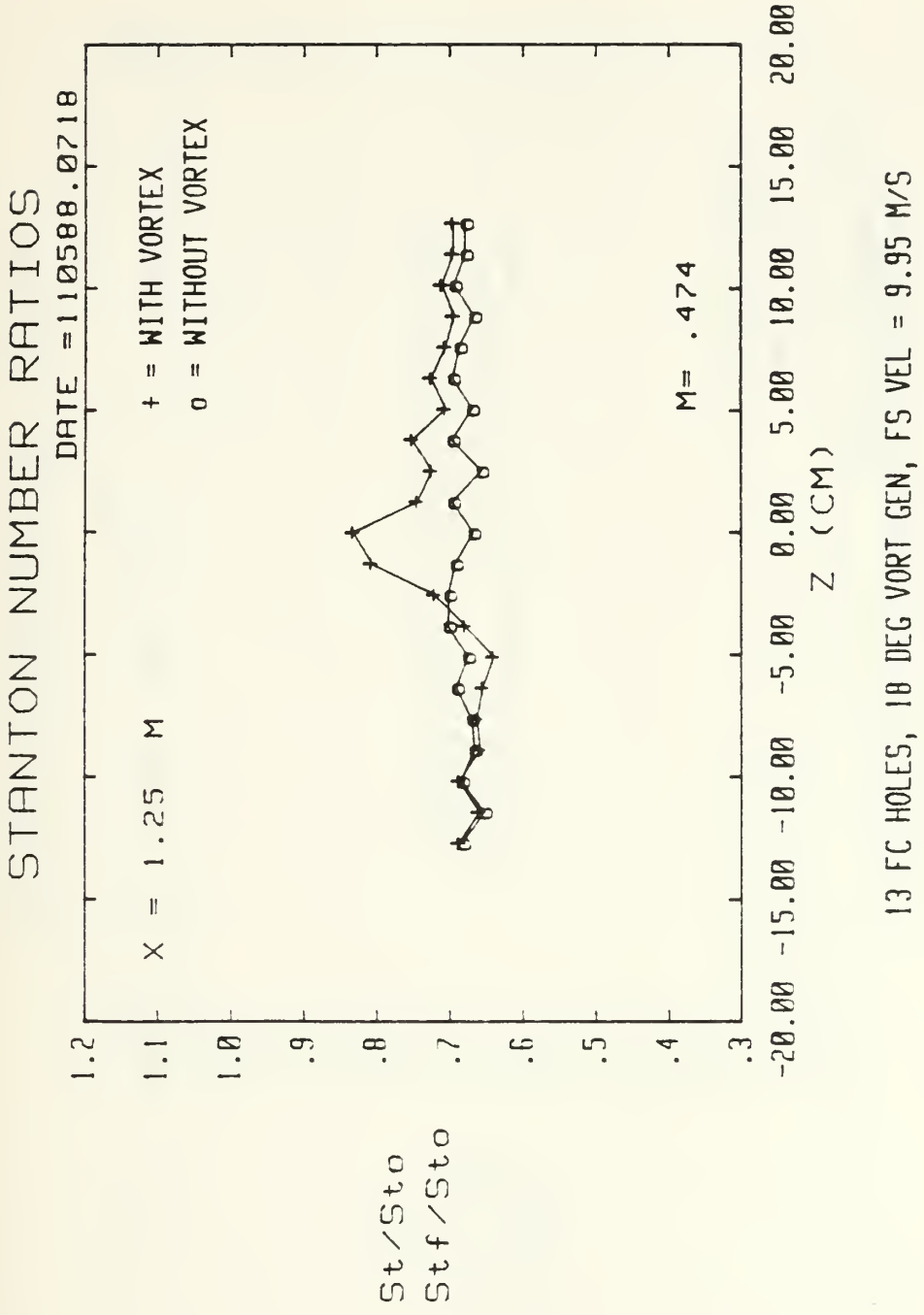

Figure 160. Spanwise Variation of St/Sto and Stf/Sto Ratios m=0.5, 13 Injection Holes x/d=17.5, Vortex r

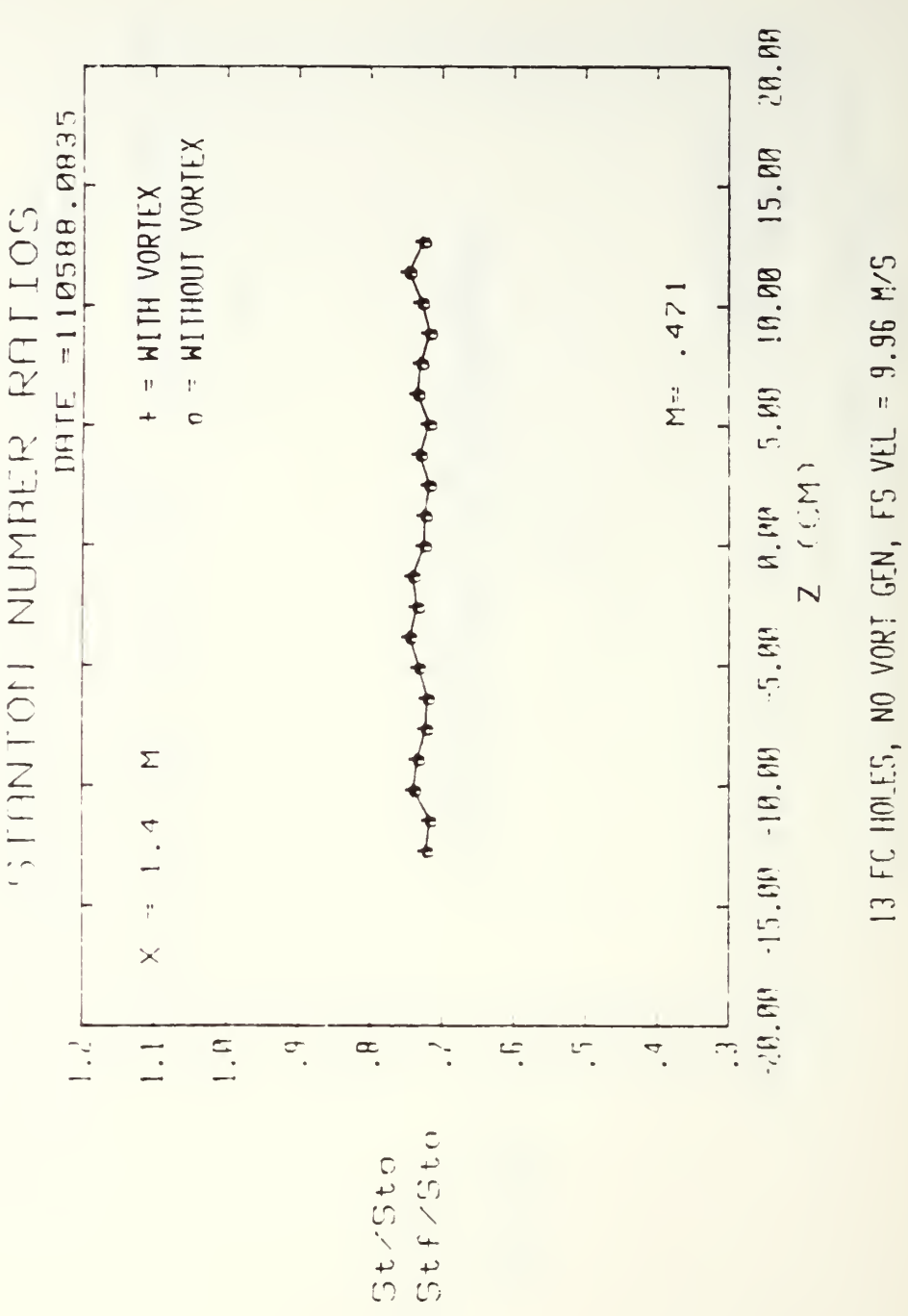

Figure 161. Spanwise Variation of St/Sto and Stf/Sto Ratios m=0.5, 13 Injection Holes x/d=33.6, No Vortex

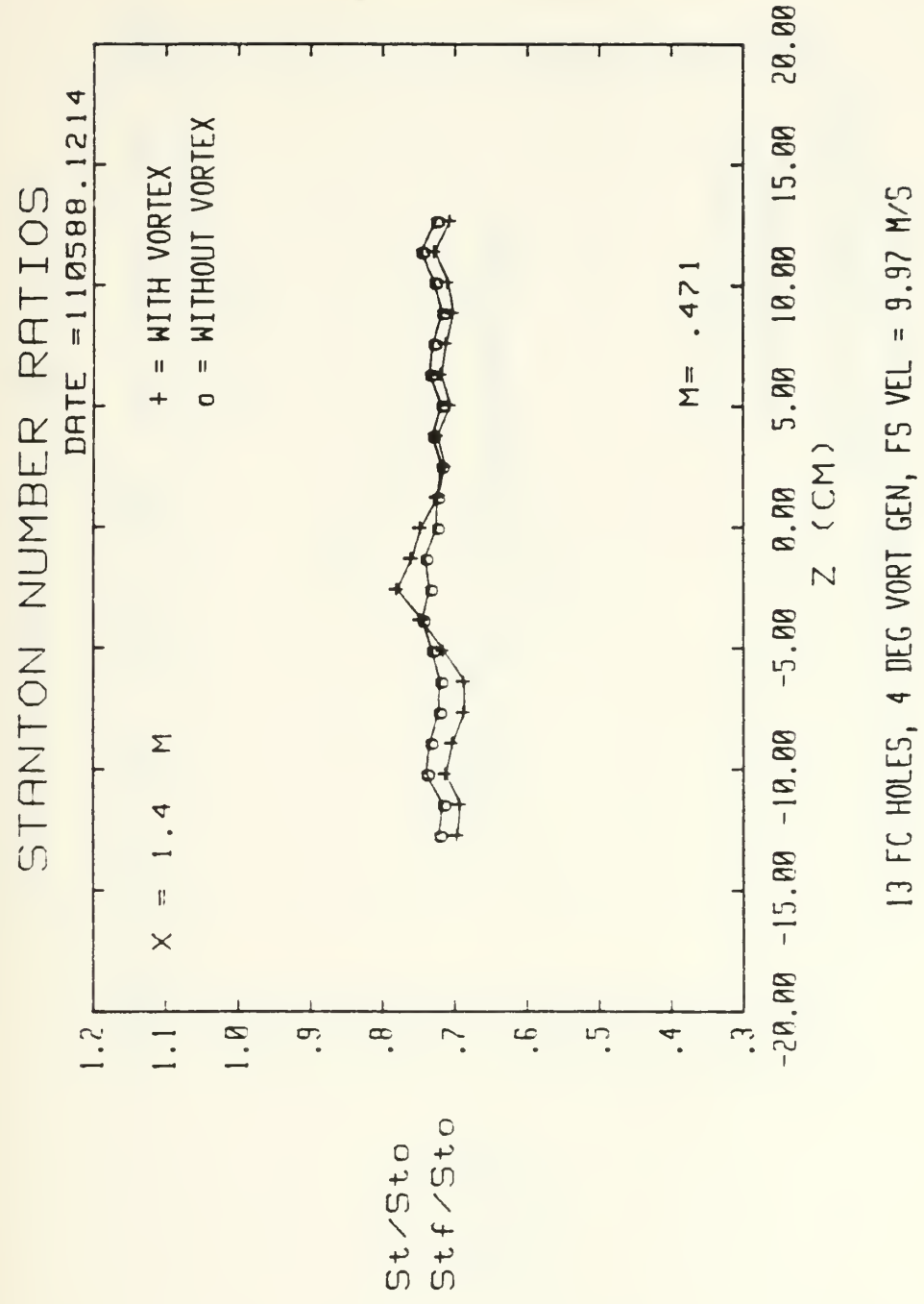

Figure 162. Spanwise Variation of St/Sto and Stf/Sto Ratios m=0.5, 13 Injection Holes x/d=33.6, Vortex z

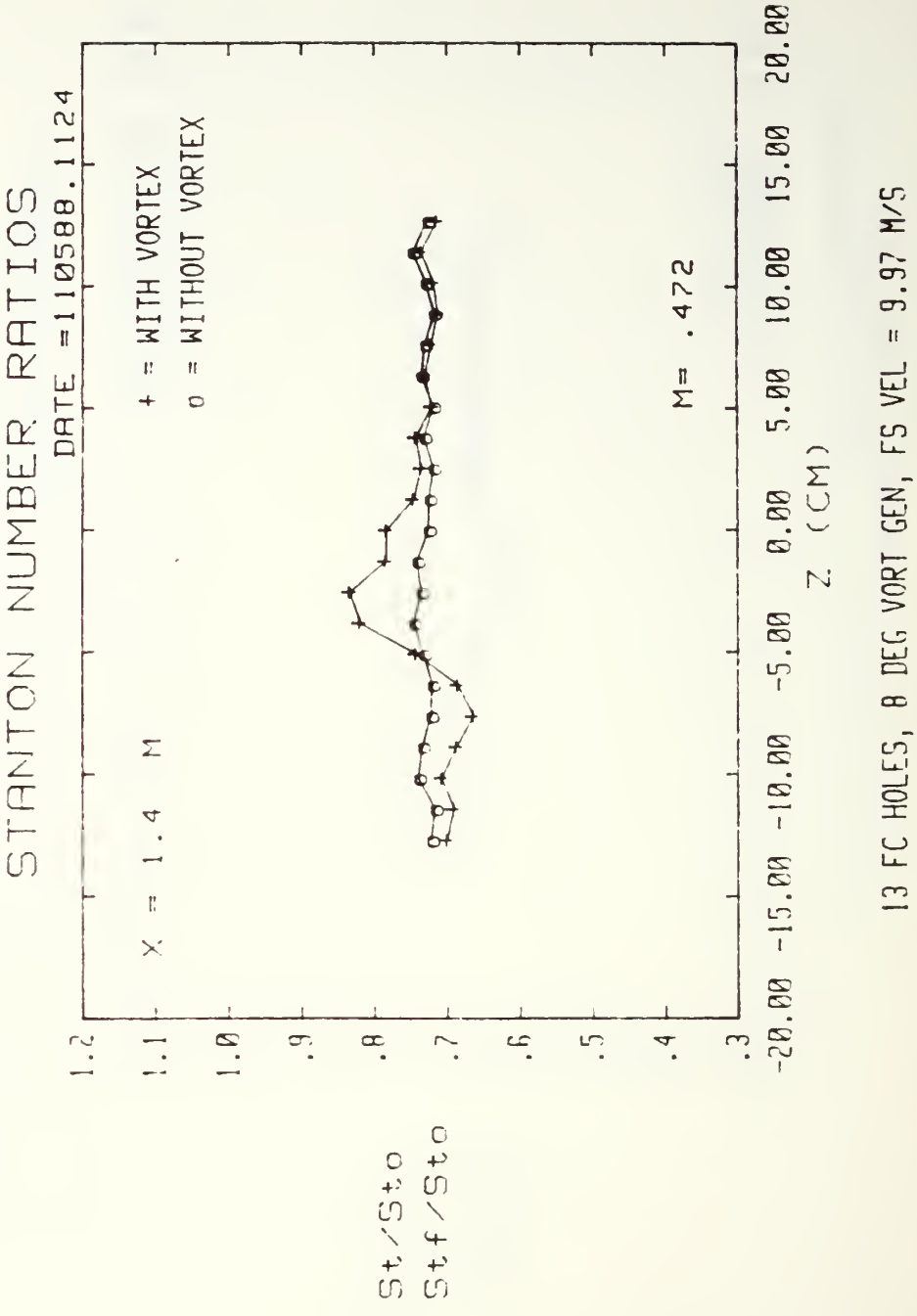

Figure 163. Spanwise Variation of St/Sto and Stf/Sto Ratios m=0.5, 13 Injection Holes x/d=33.6, Vortex y

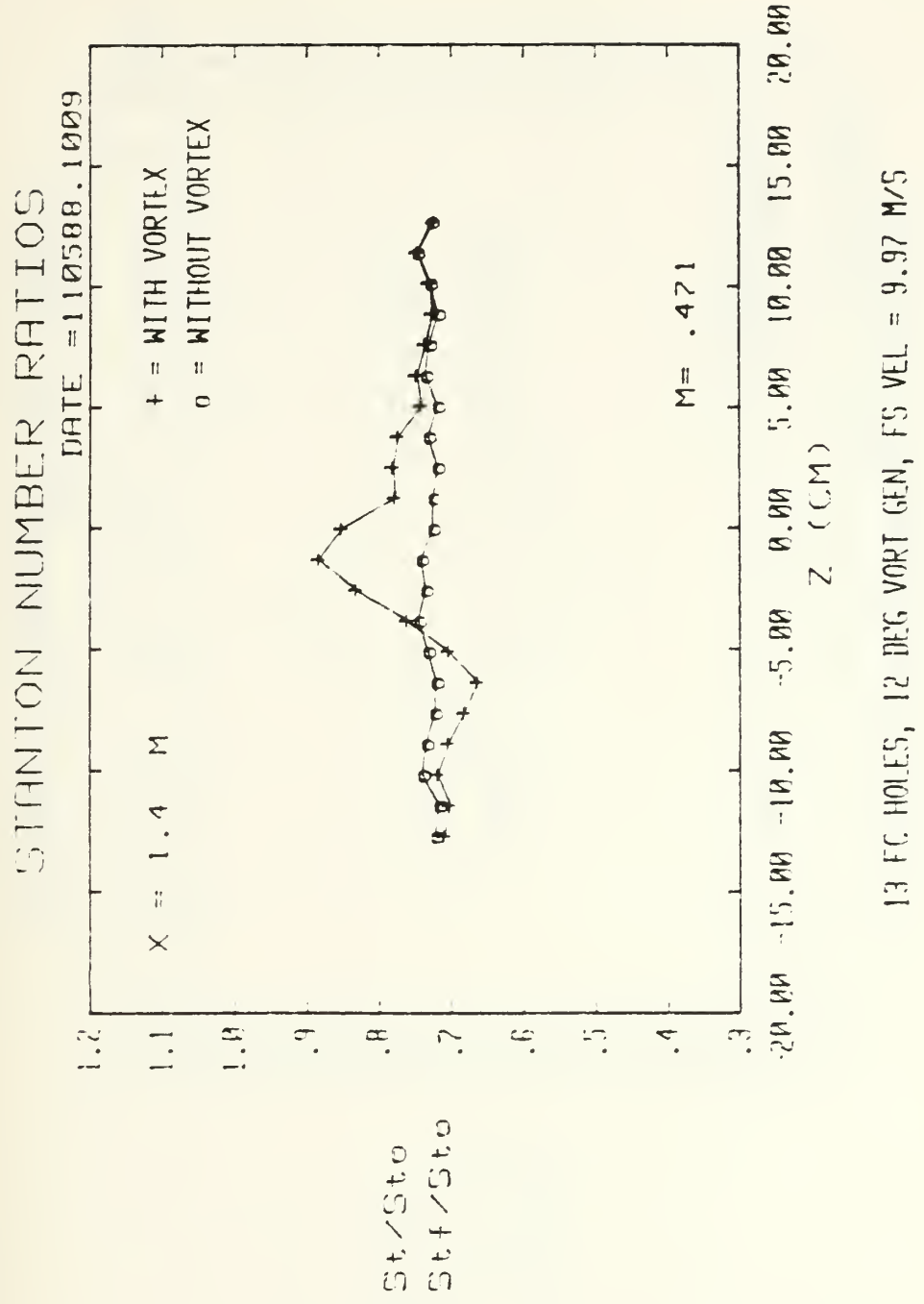

Figure 164. Spanwise Variation of St/Sto and Stf/Sto Ratios m=0.5, 13 Injection Holes x/d=33.6, Vortex x

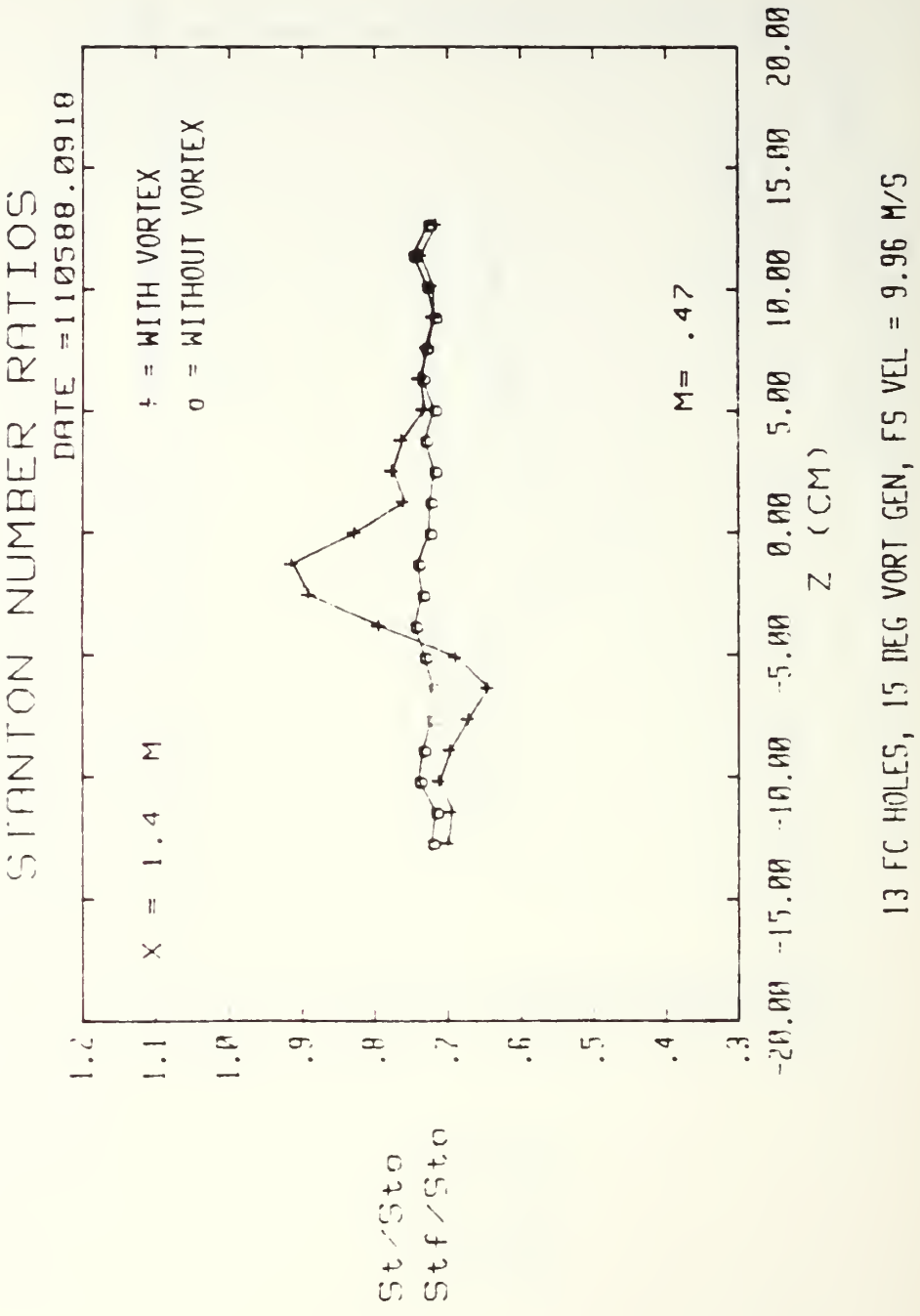

Figure 165. Spanwise Variation of St/Sto and Stf/Sto Ratios m=0.5, 13 Injection Holes x/d=33.6, Vortex w

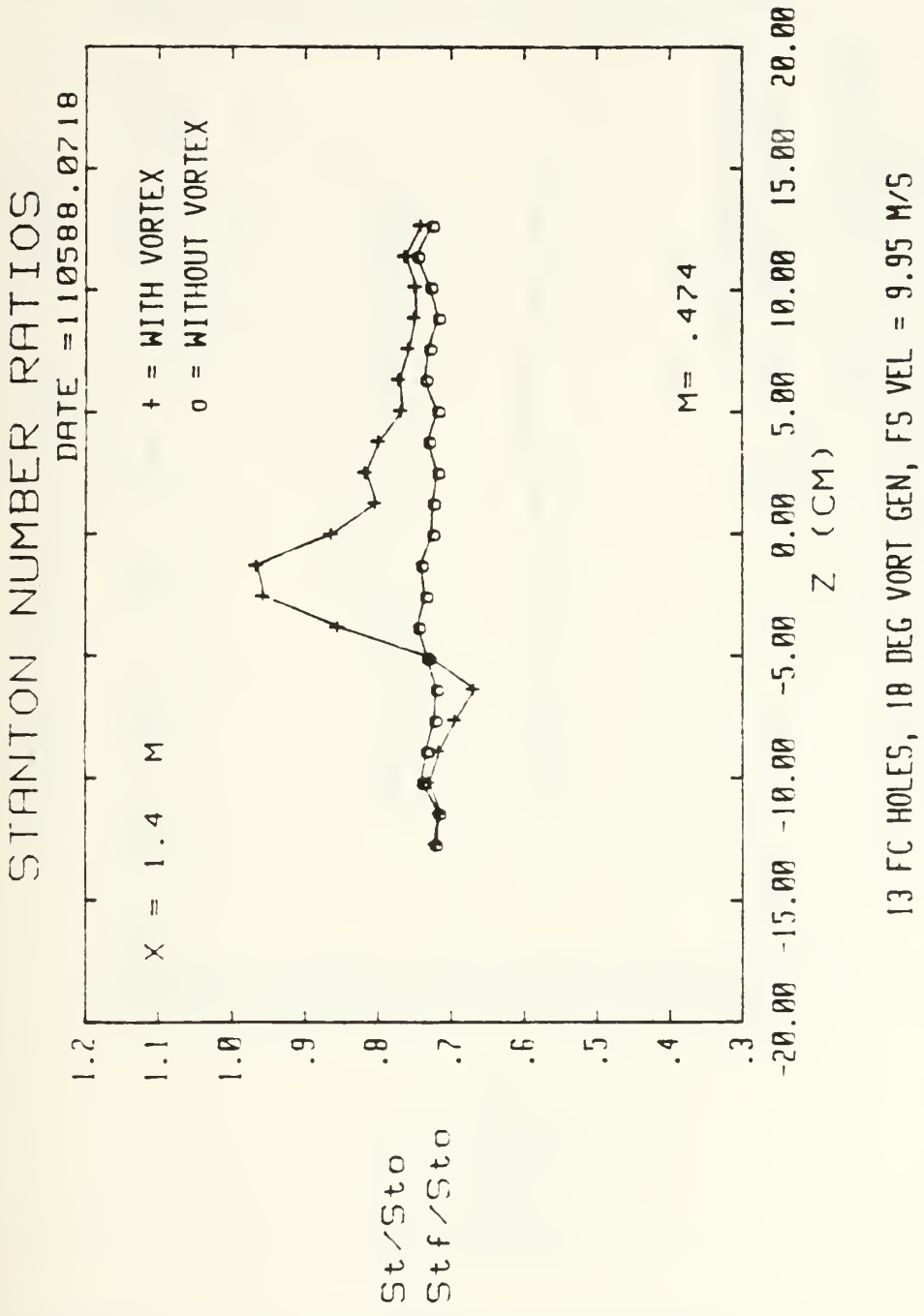

Figure 166. Spanwise Variation of St/Sto and Stf/Sto Ratios m=0.5, 13 Injection Holes x/d=33.6, Vortex r

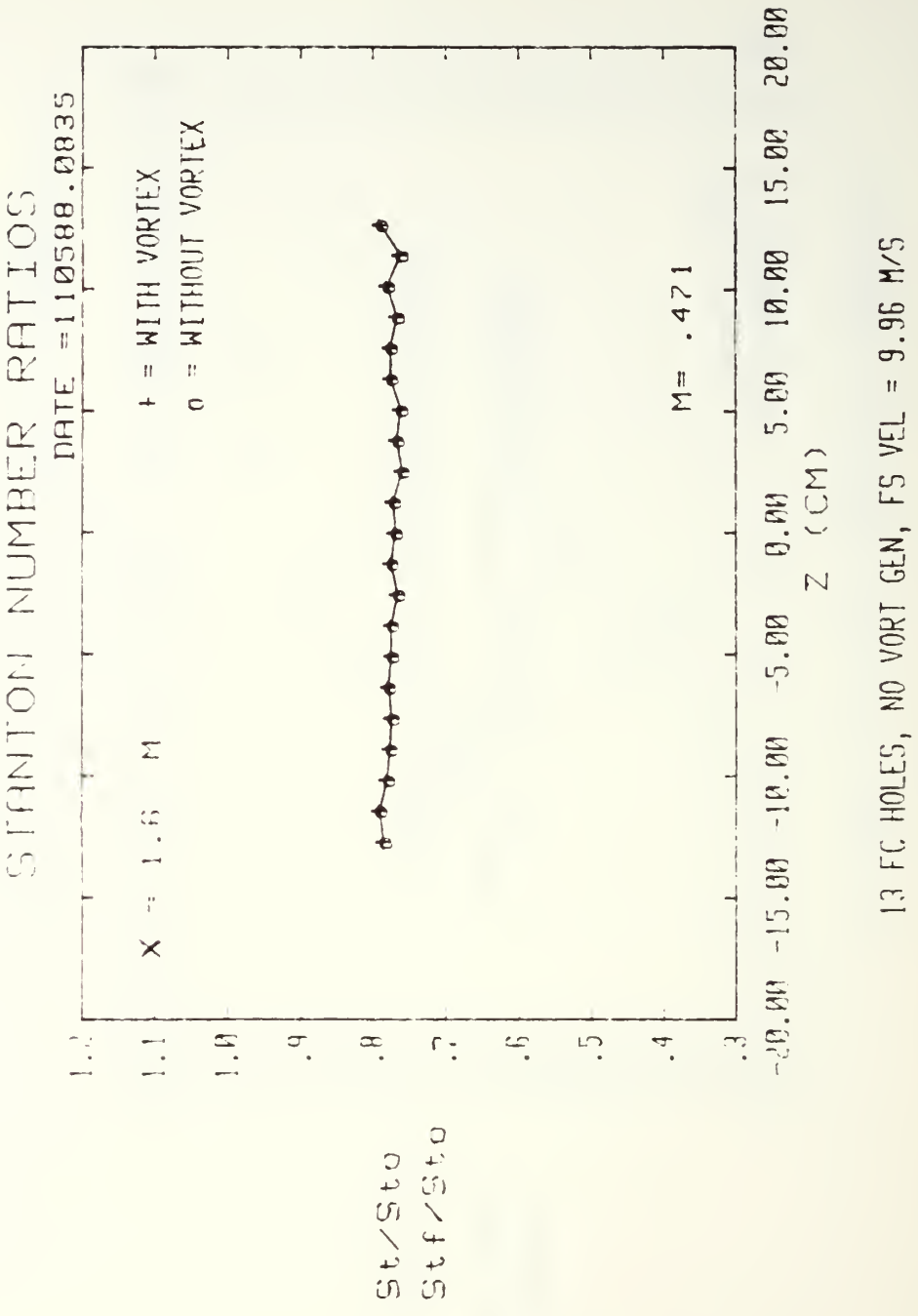

Figure 167. Spanwise Variation of St/Sto and Stf/Sto Ratios m=0.5, 13 Injection Holes x/d=54.6, No Vortex

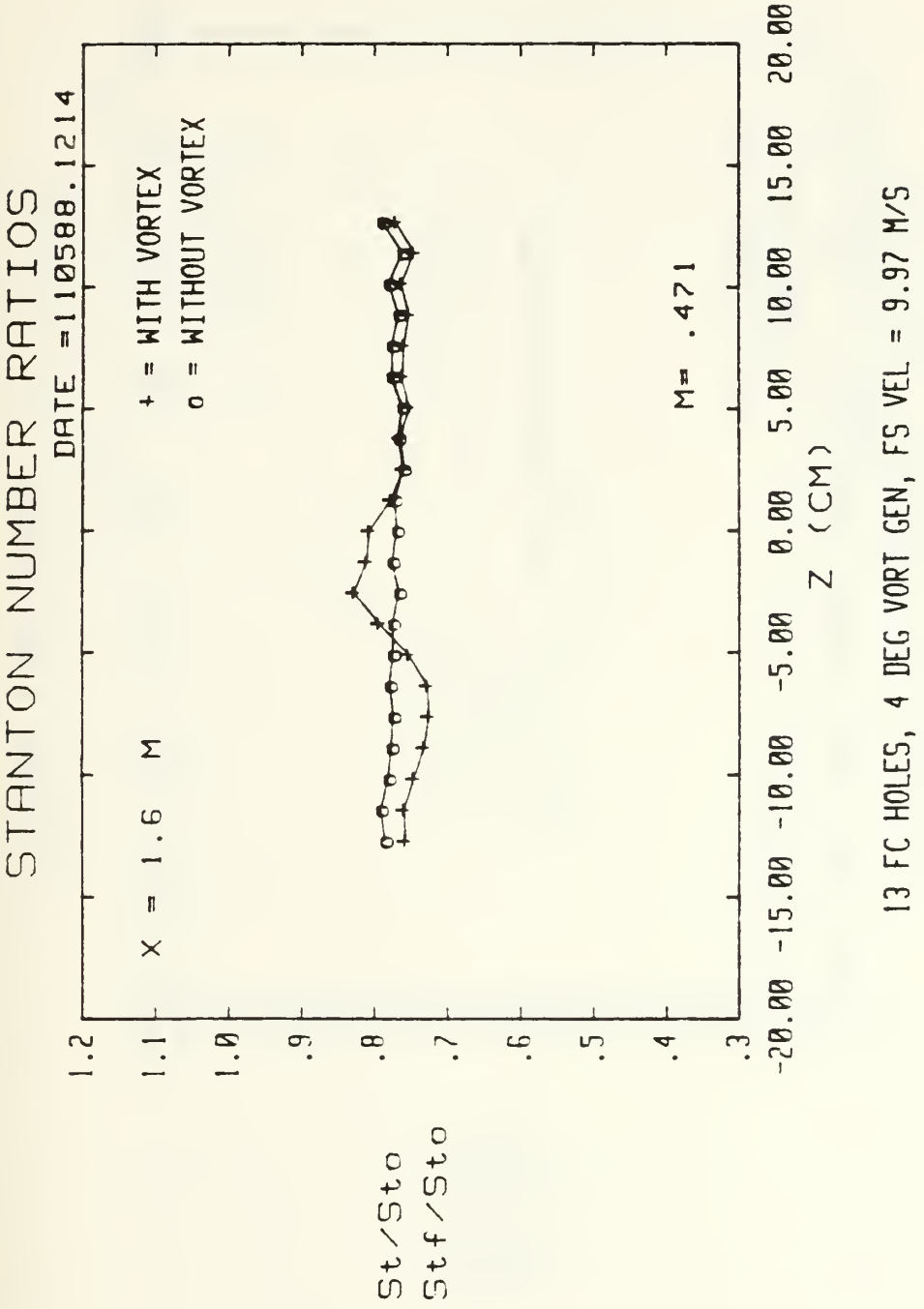

Figure 168. Spanwise Variation of St/Sto and Stf/Sto Ratios m=0.5, 13 Injection Holes x/d=54.6, Vortex z

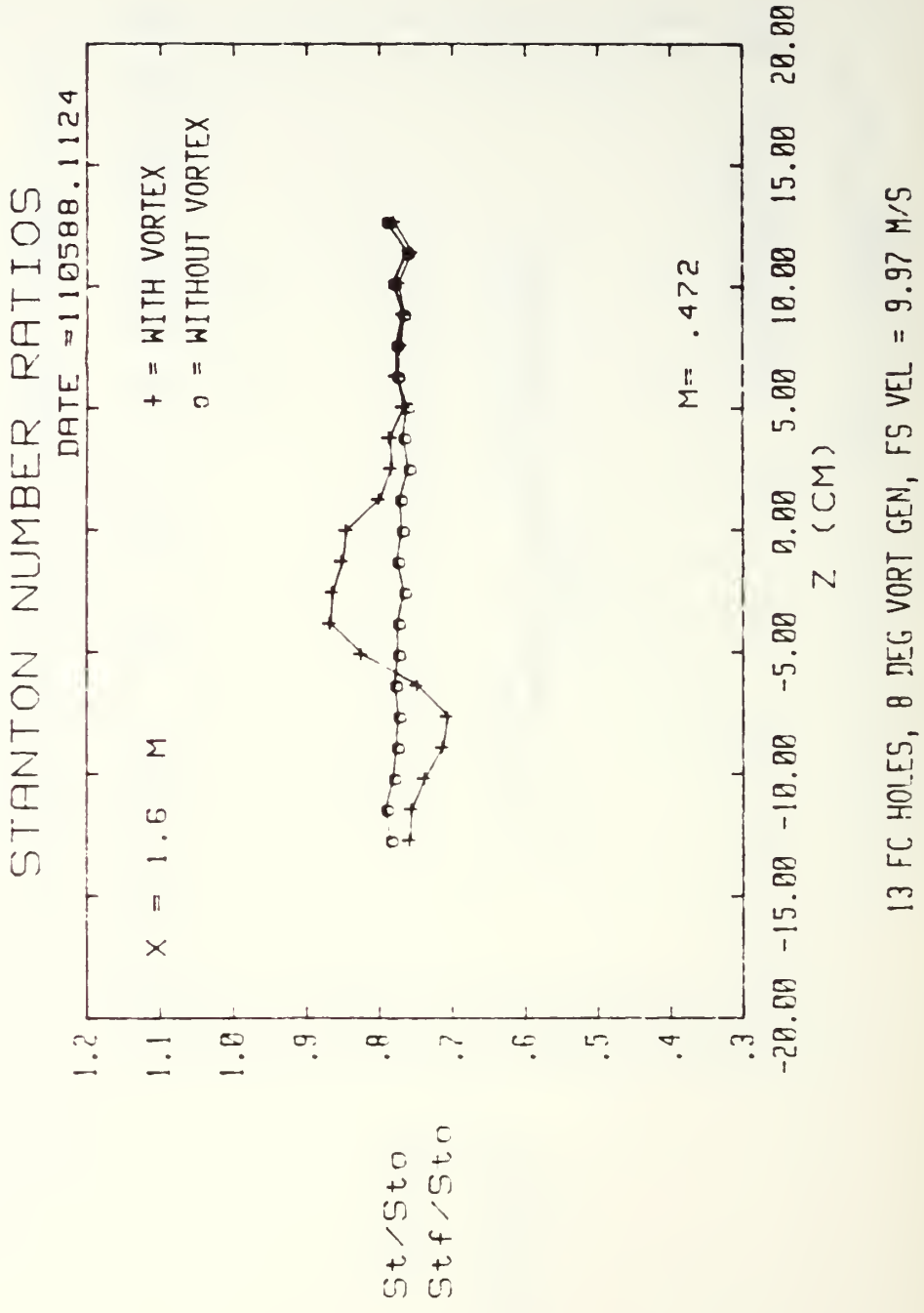

Figure 169. Spanwise Variation of St/Sto and Stf/Sto Ratios m=0.5, 13 Injection Holes x/d=54.6, Vortex y

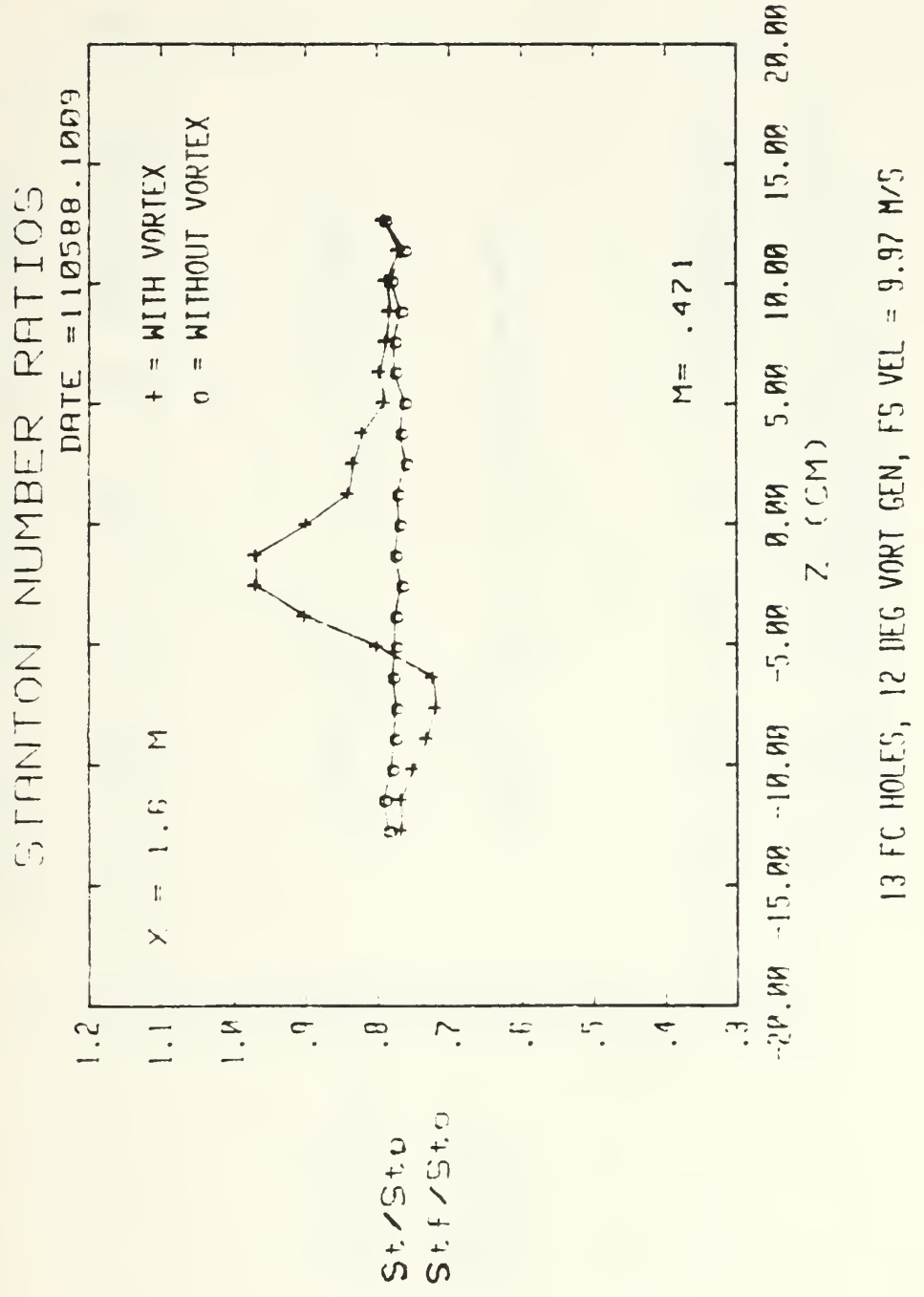

Figure 170. Spanwise Variation of St/Sto and Stf/Sto Ratios m=0.5, 13 Injection Holes x/d=54.6, Vortex x

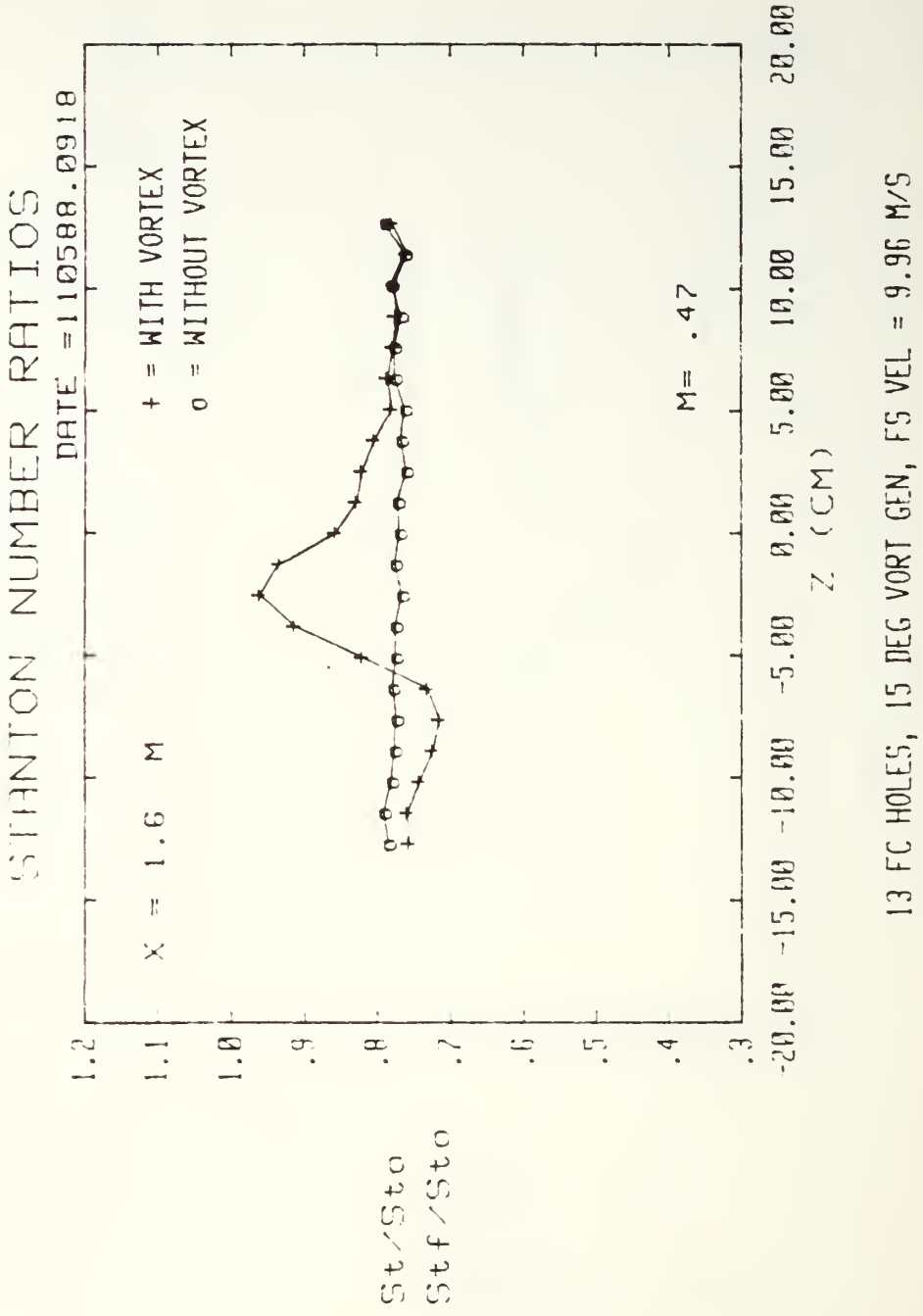

Figure 171. Spanwise Variation of St/Sto and Stf/Sto Ratios m=0.5, 13 Injection Holes x/d=54.6, Vortex w

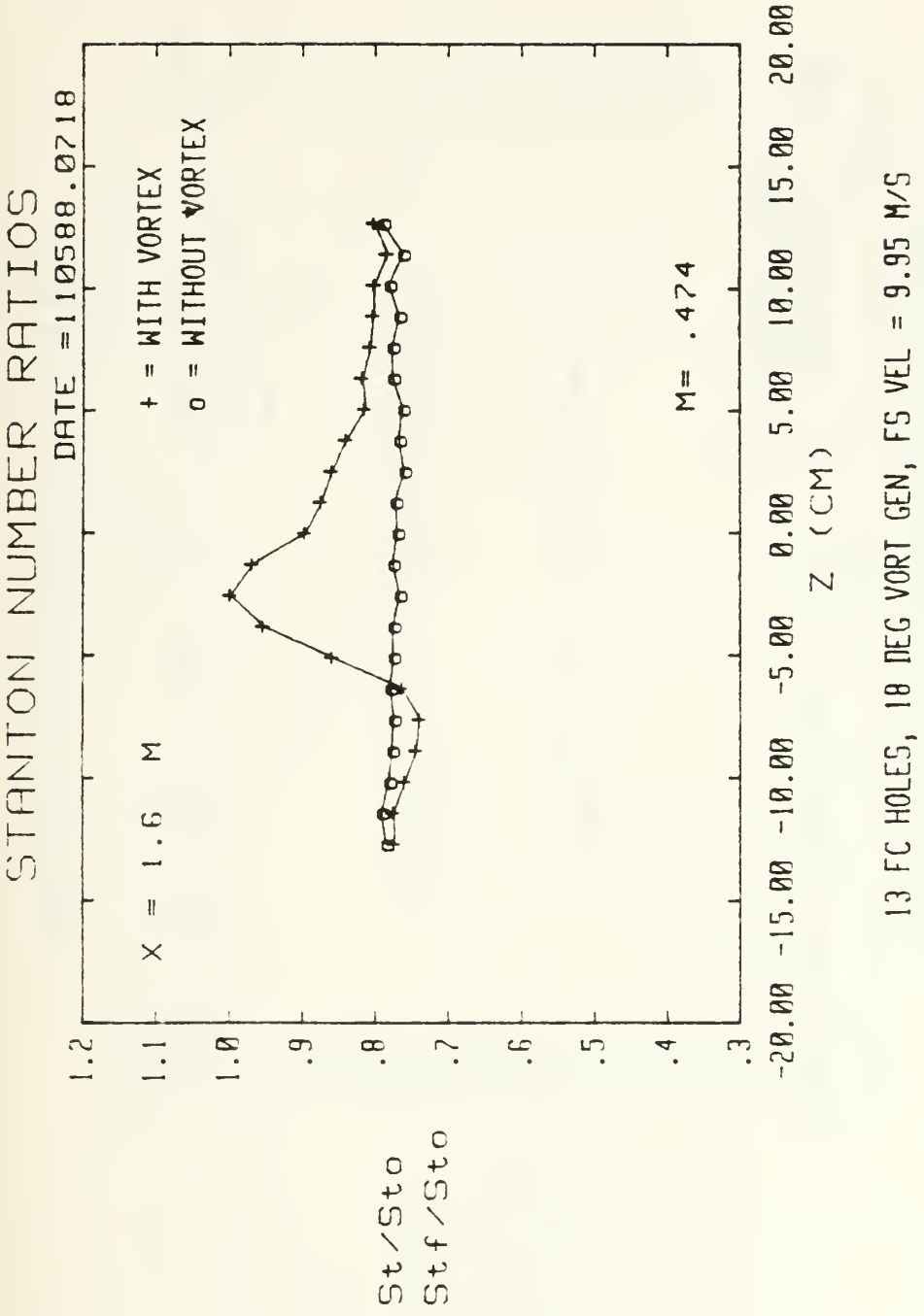

Figure 172. Spanwise Variation of St/Sto and Stf/Sto Ratios m=0.5, 13 Injection Holes x/d=54.6, Vortex r

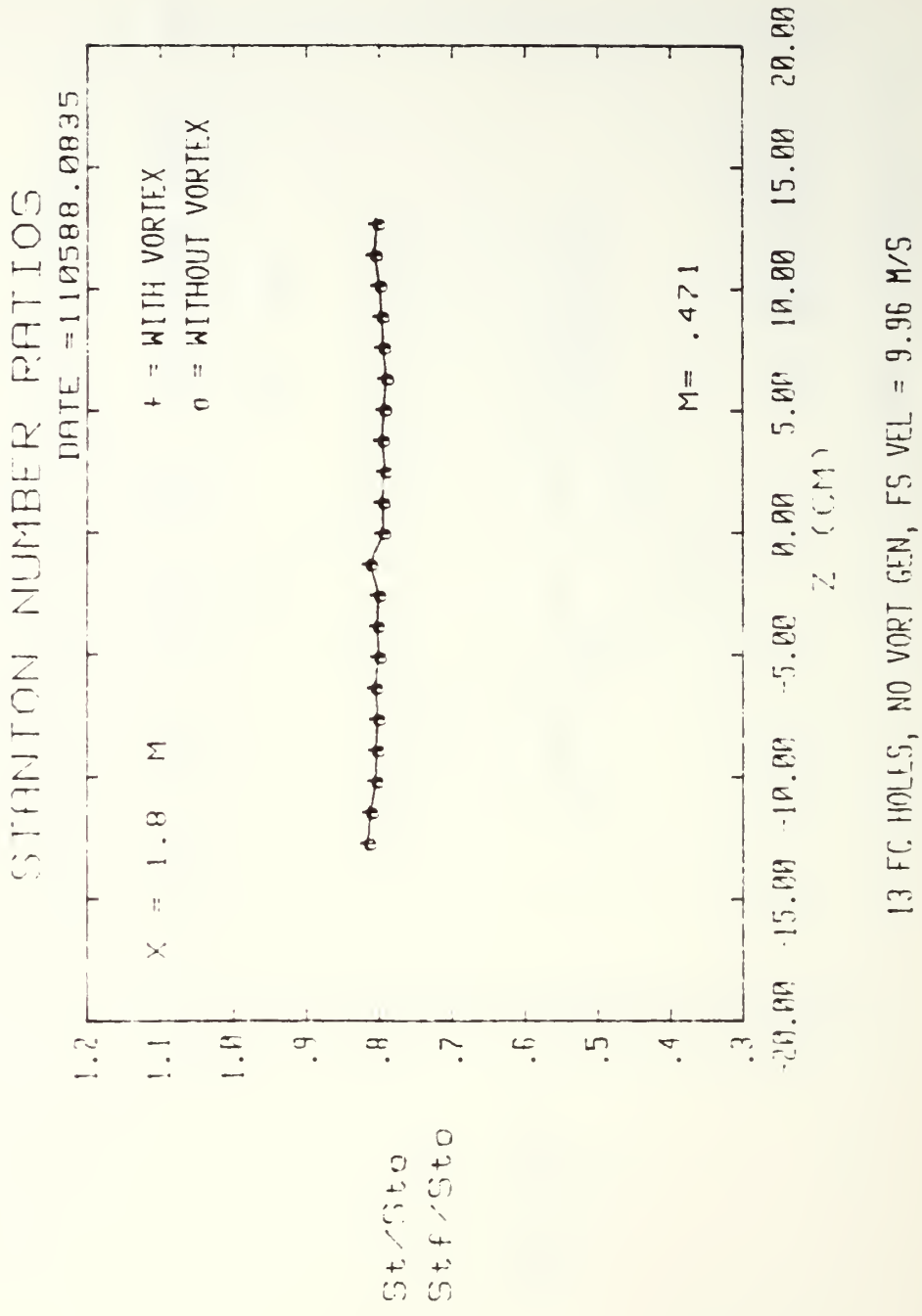

Figure 173. Spanwise Variation of St/Sto and Stf/Sto Ratios m=0.5, 13 Injection Holes x/d=75.6, No Vortex

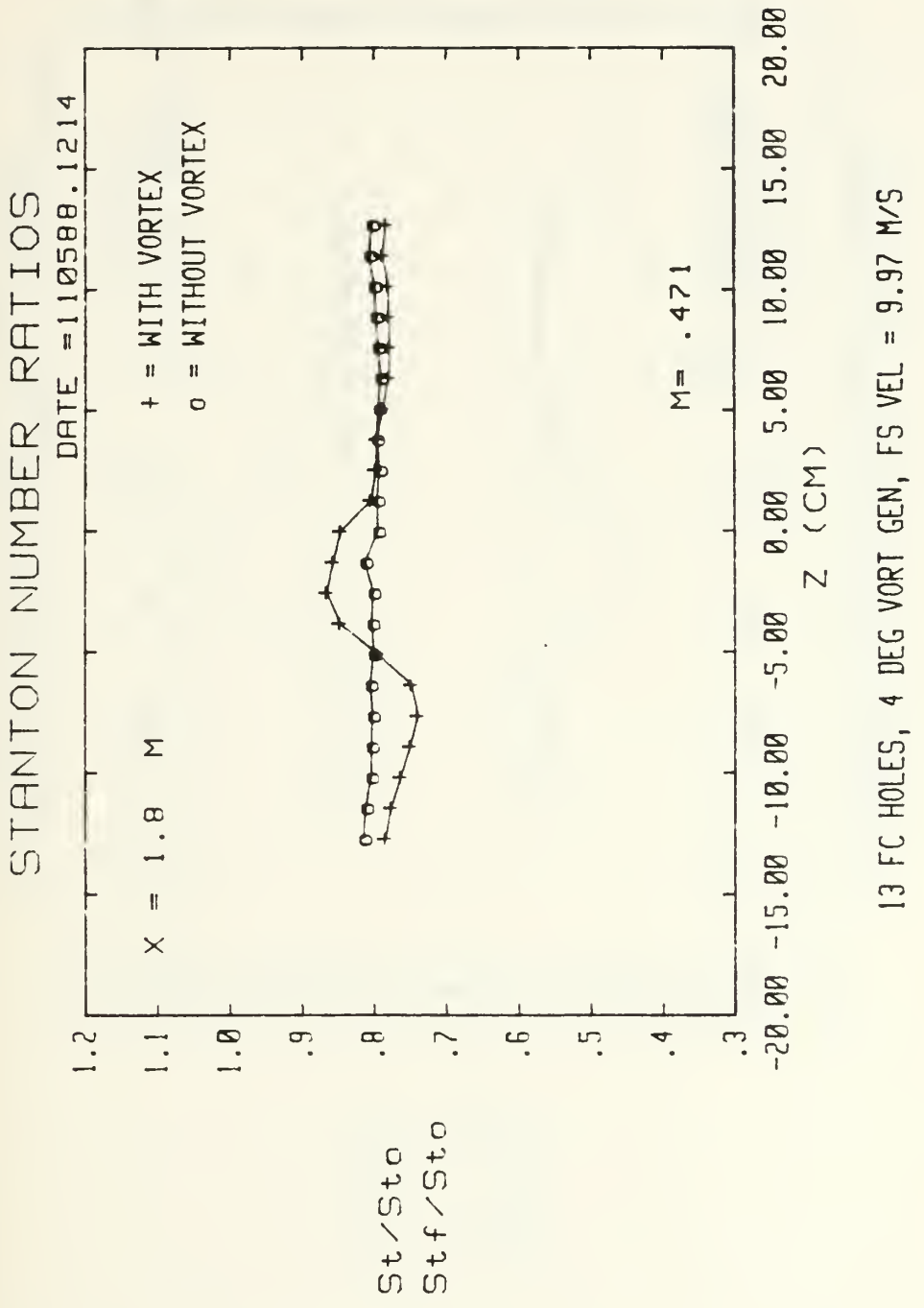

Figure 174. Spanwise Variation of St/Sto and Stf/Sto Ratios m=0.5, 13 Injection Holes x/d=75.6, Vortex z

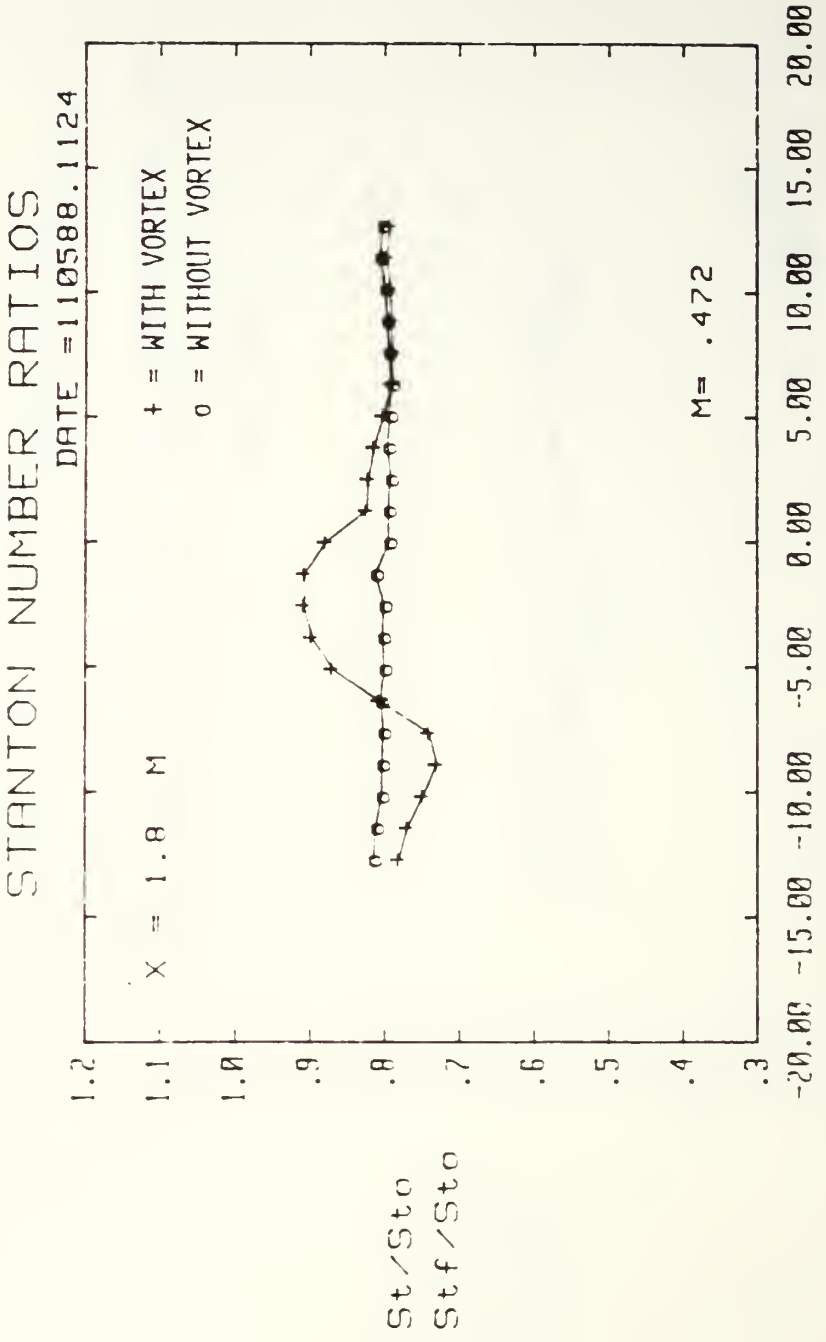

Figure 175. Spanwise Variation of St/Sto and Stf/Sto Ratios m=0.5, 13 Injection Holes x/d=75.6, Vortex y

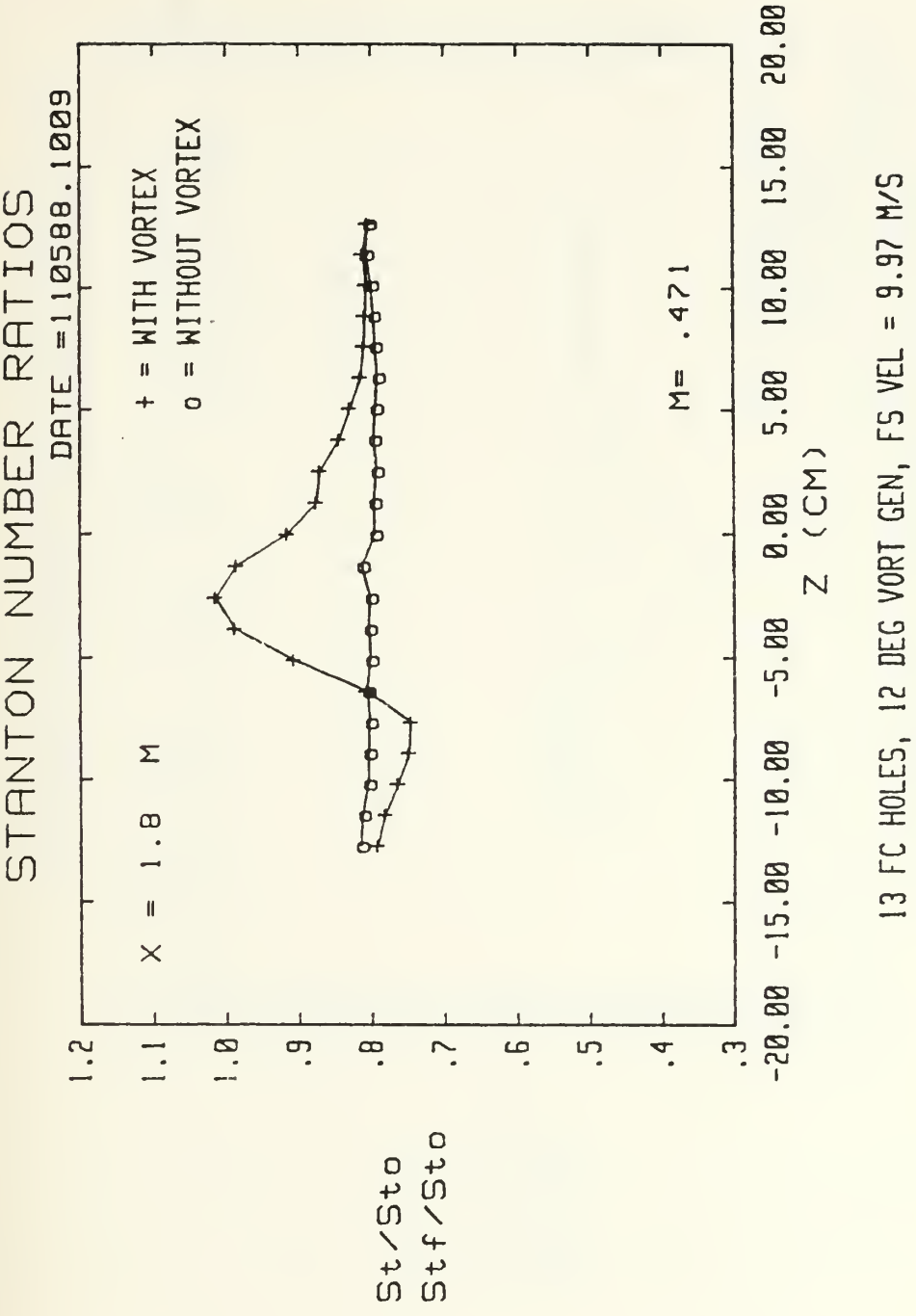

Figure 176. Spanwise Variation of St/Sto and Stf/Sto Ratios m=0.5, 13 Injection Holes x/d=75.6, Vortex x

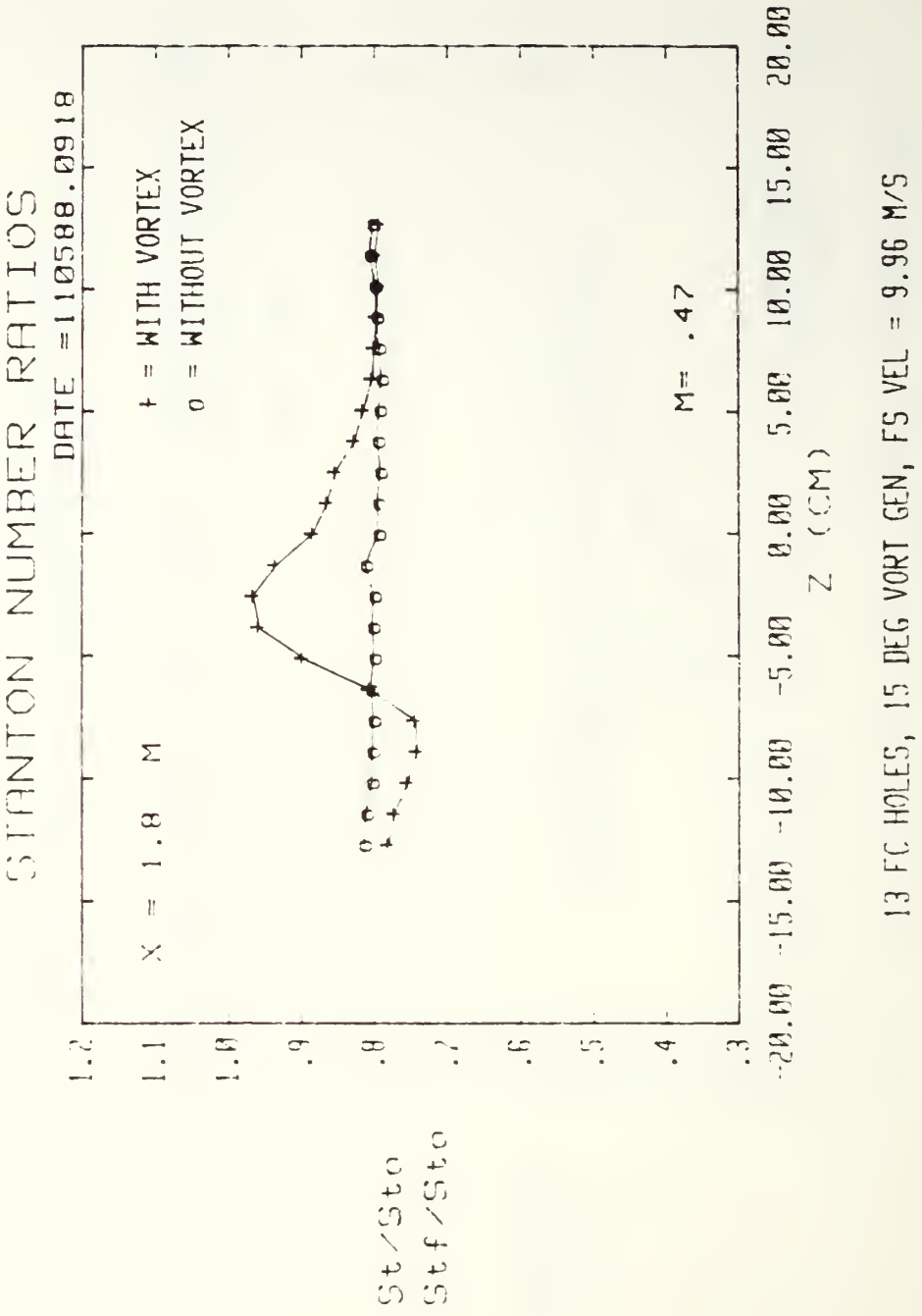

Figure 177. Spanwise Variation of St/Sto and Stf/Sto Ratios m=0.5, 13 Injection Holes x/d=75.6, Vortex w

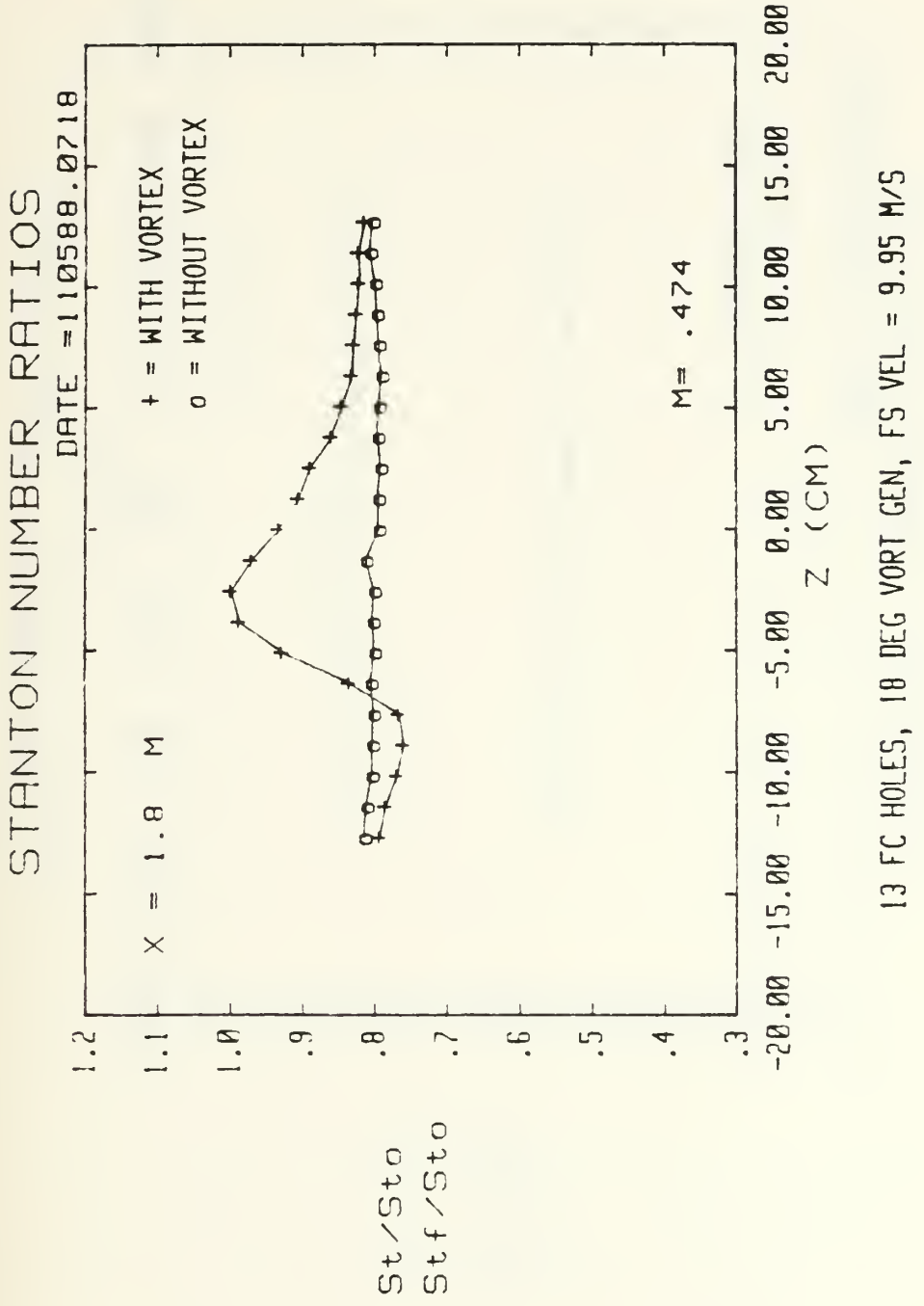

Figure 178. Spanwise Variation of St/Sto and Stf/Sto Ratios m=0.5, 13 Injection Holes x/d=75.6, Vortex r

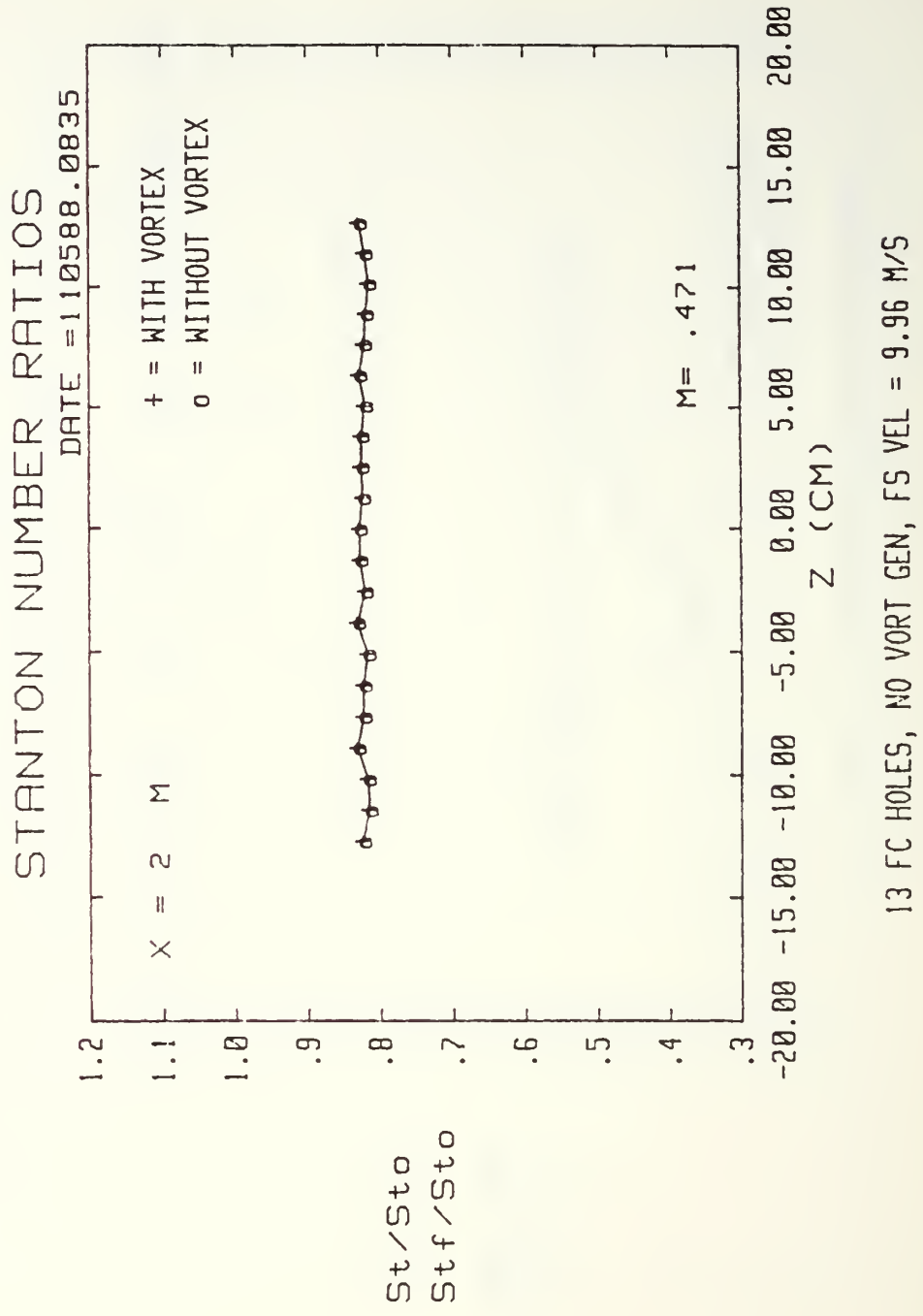

Figure 179. Spanwise Variation of St/Sto and Stf/Sto Ratios m=0.5, 13 Injection Holes x/d=96.6, No Vortex

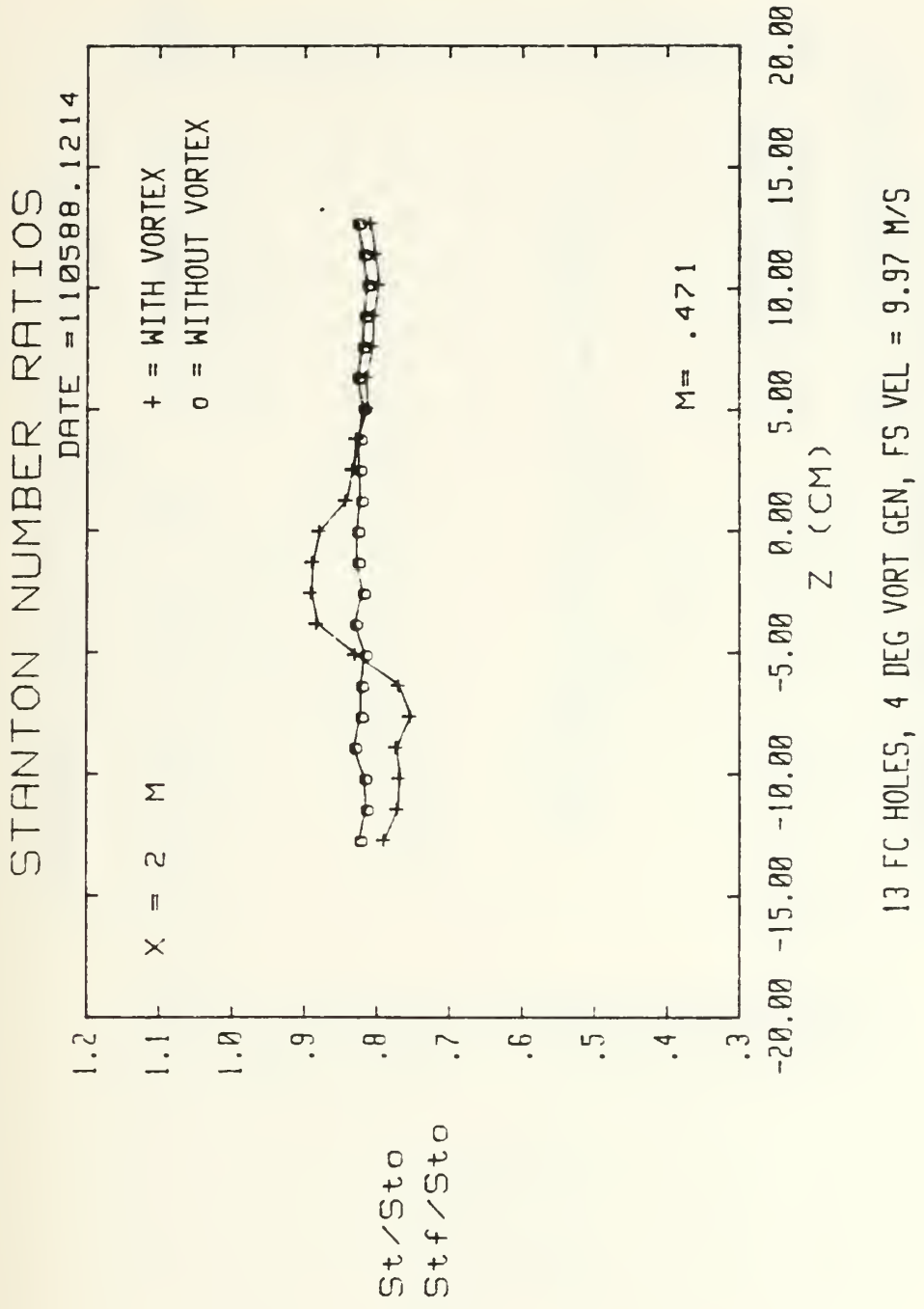

Figure 180. Spanwise Variation of St/Sto and Stf/Sto Ratios m=0.5, 13 Injection Holes x/d=96.6, Vortex z

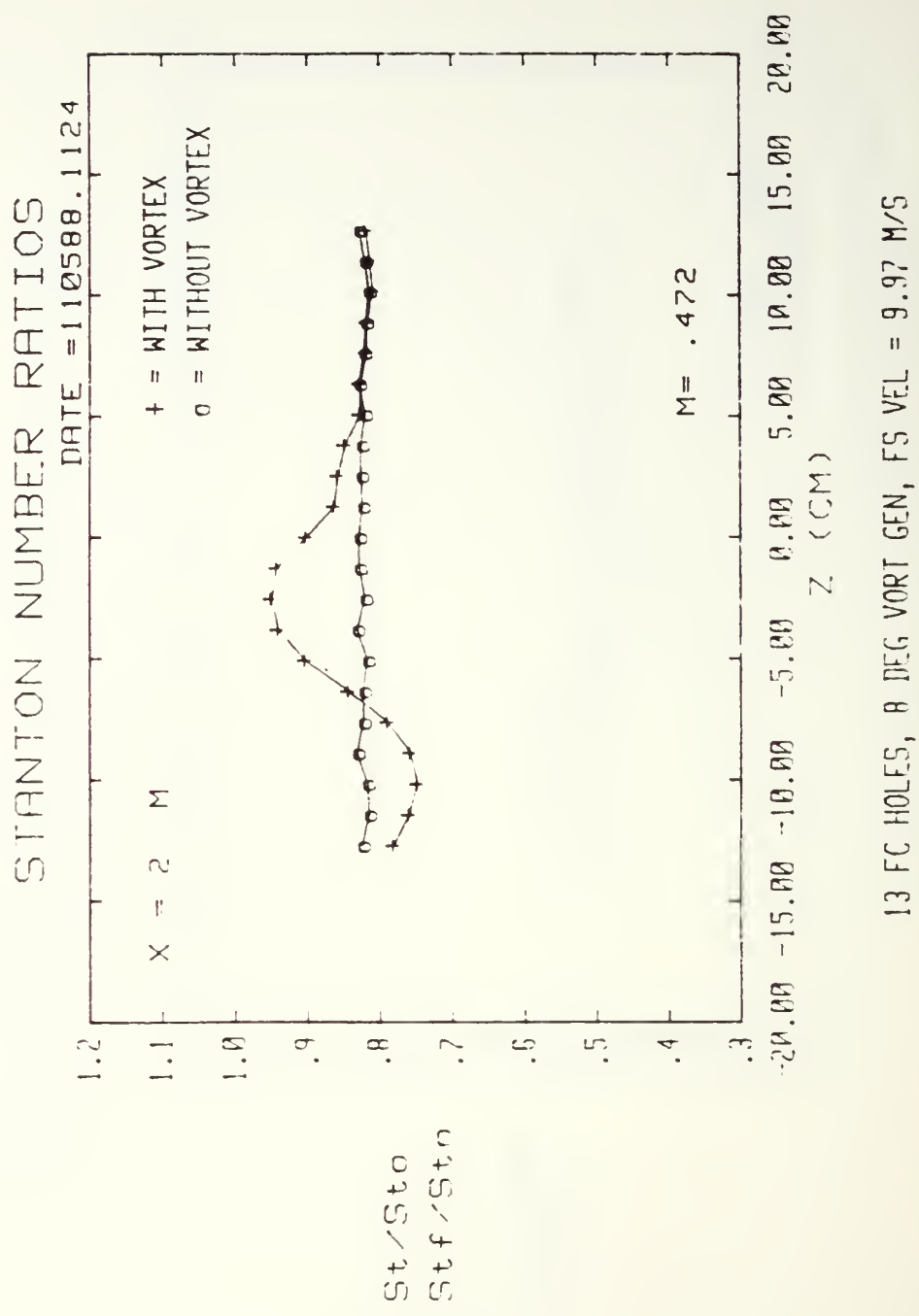

Figure 181. Spanwise Variation of St/Sto and Stf/Sto Ratios m=0.5, 13 Injection Holes x/d=96.6, Vortex y

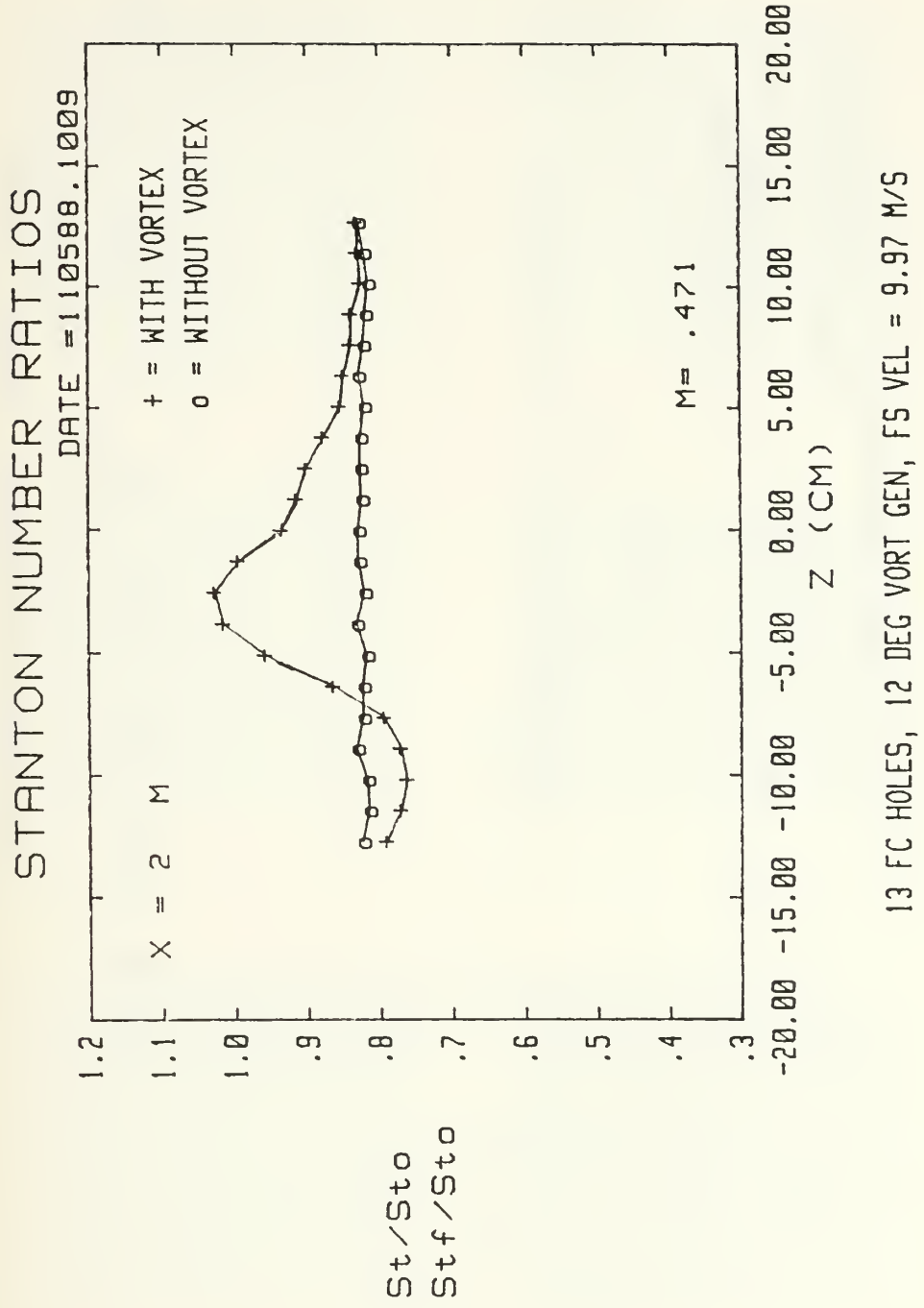

Figure 182. Spanwise Variation of St/Sto and Stf/Sto Ratios m=0.5, 13 Injection Holes x/d=96.6, Vortex x

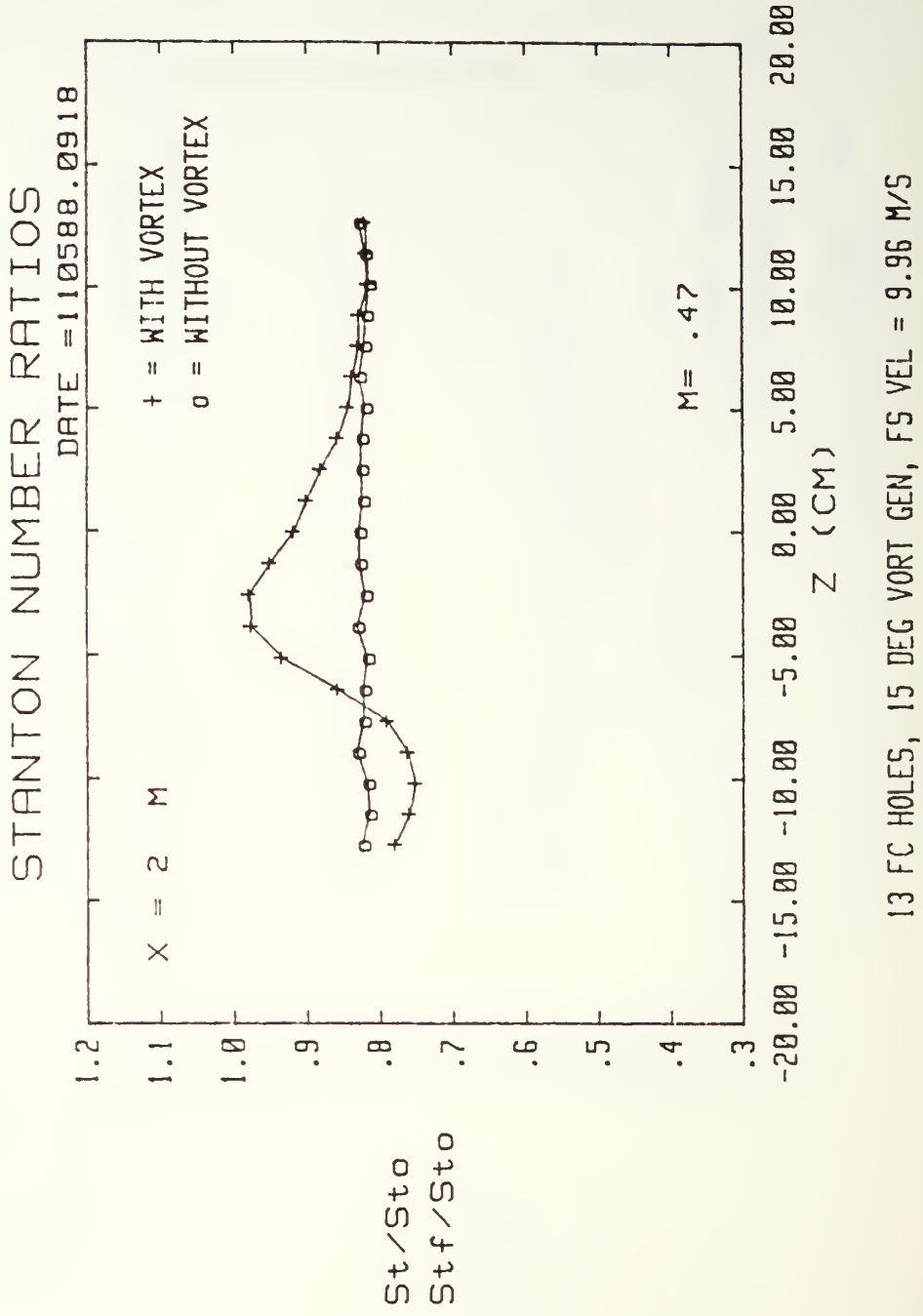

Figure 183. Spanwise Variation of St/Sto and Stf/Sto Ratios m=0.5, 13 Injection Holes x/d=96.6, Vortex w

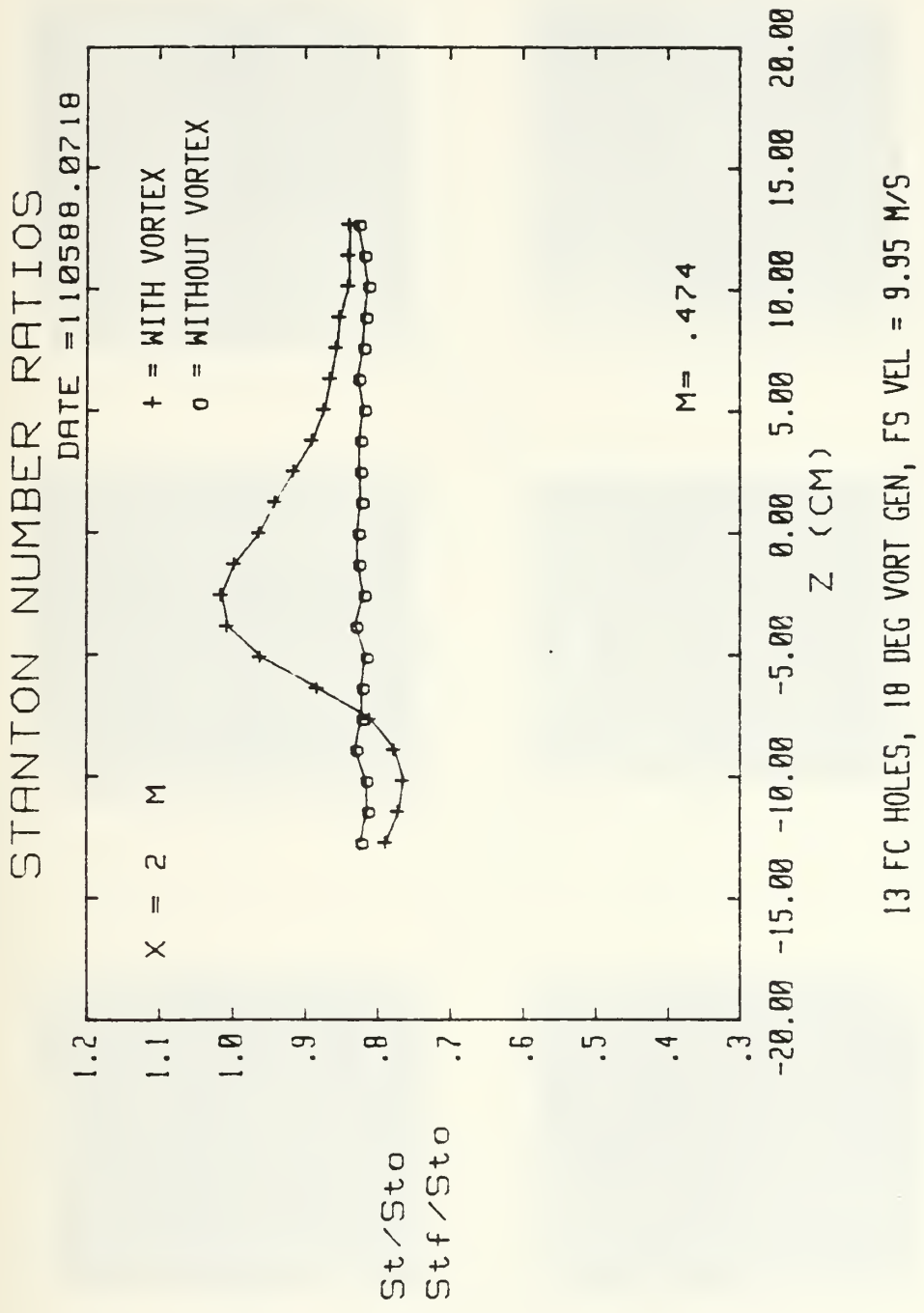

Figure 184. Spanwise Variation of St/Sto and Stf/Sto Ratios m=0.5, 13 Injection Holes x/d=96.6, Vortex r

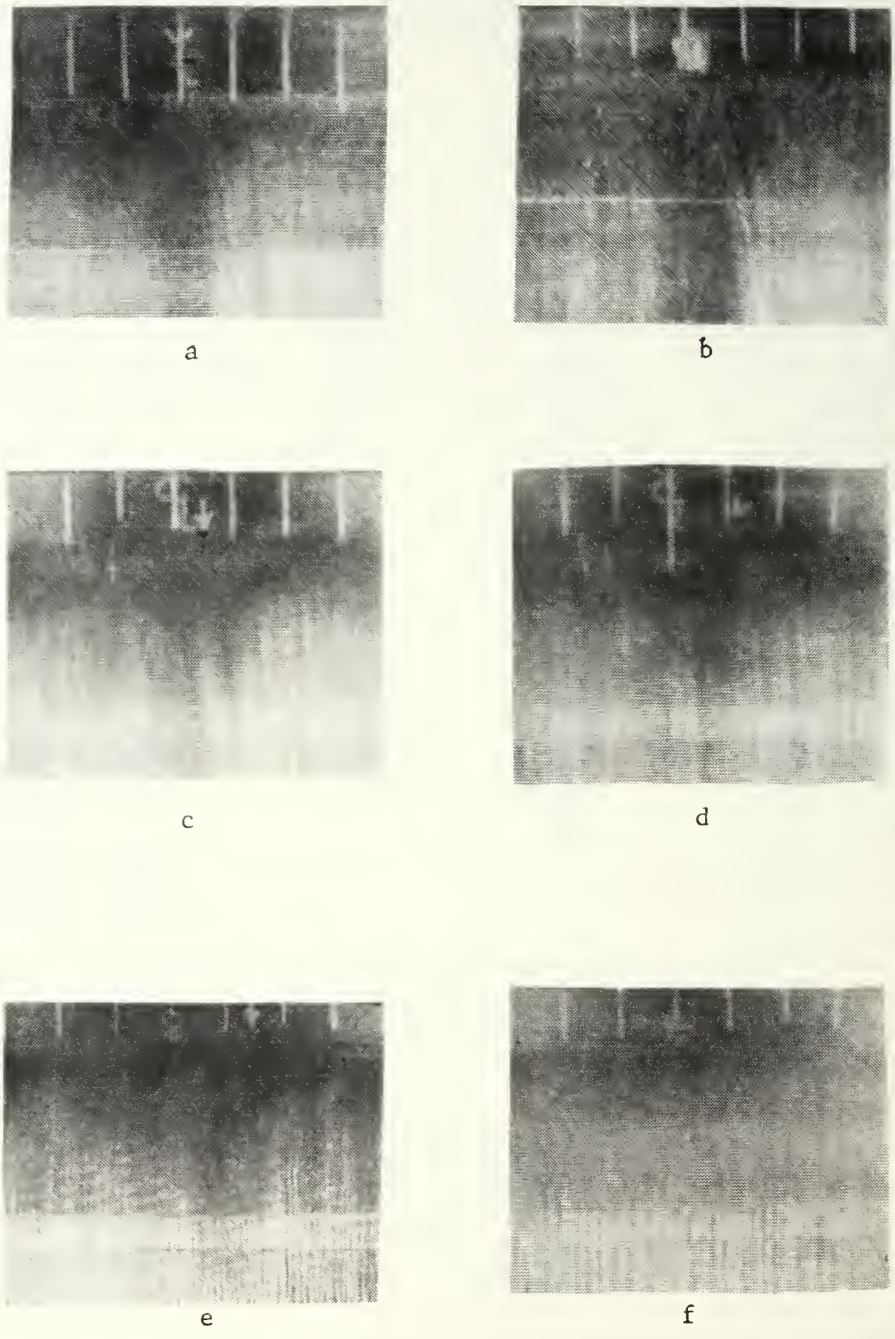

Figure 185. Surface Flow Patterns: 13 Injection Holes

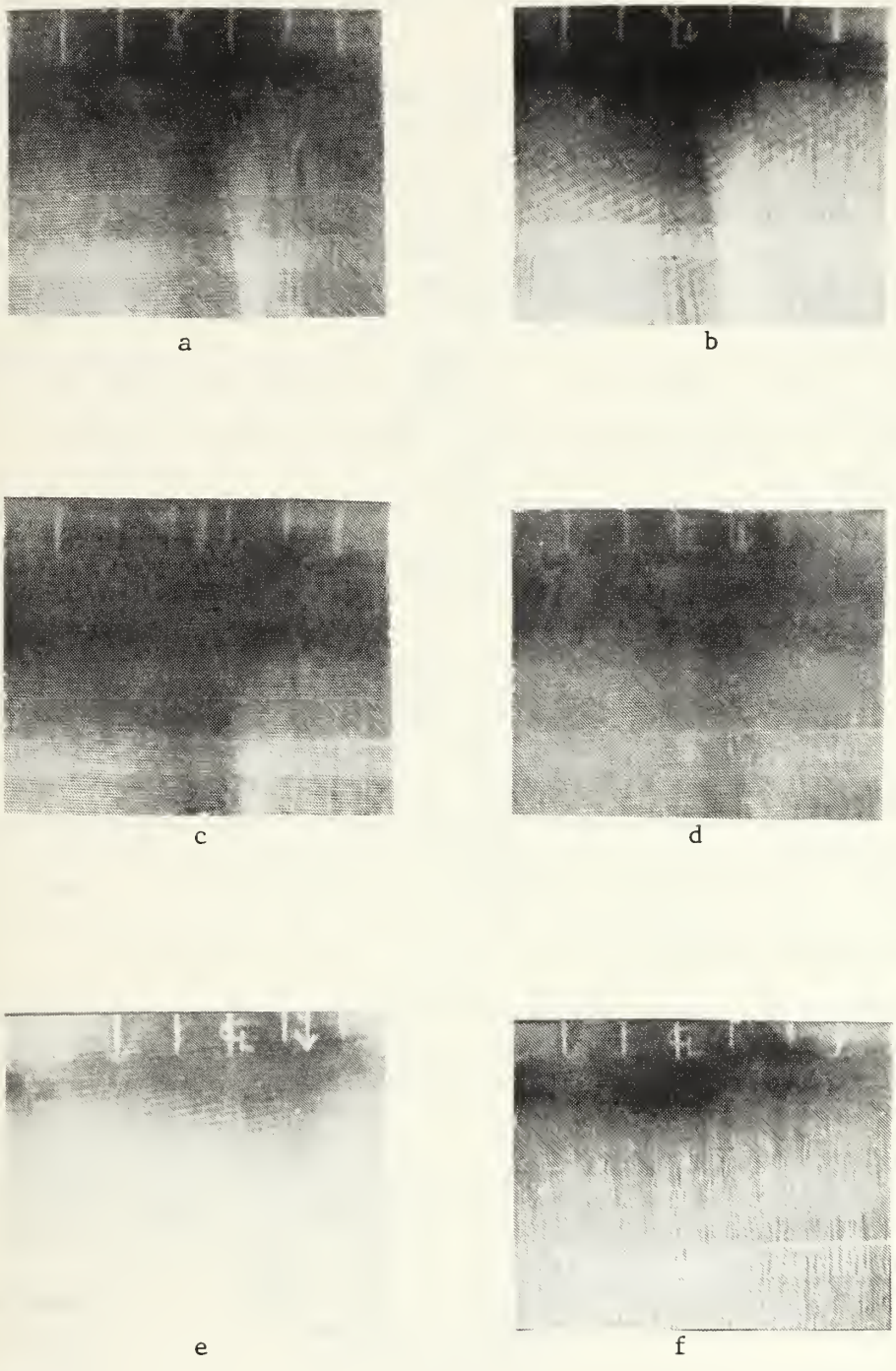

Figure 186. Surface Flow Patterns: Single Injection Hole

APPENDIX B

UNCERTAINTY ANALYSIS

An uncertainty analysis of the key variables and input parameters used in the experimental procedures of this study was performed by Schwartz [Ref. 18]. Schwartz' uncertainty estimates are based on a 95% confidence interval and are determined by considering three orders of replication:

1. Zeroth Order Uncertainty due to the level of accuracy achievable in the measurement (1/2 the least measurement graduation).

2. First Order Uncertainty due to unsteadiness in the taking of the measurement.

3. Second Order Uncertainty due to the uncertainties in the measuring device calibration and bias. [Ref. 18:pp. 267-269]

Uncertainty estimates for key parameters are summarized in Tables XIV and XV (from reference 18).

TABLE XIV. MEAN VELOCITY UNCERTAINTY [Ref. 18:p. 268]

Quantity (units)	Typical Nominal Values	Experimental Uncertainty
Ky, Kp (units/)	0.09	0.0086
Cpy, Cpp	0.7, 0.27	0.02
α , β (degrees)	10.0	1.2
Ux (m/s)	10.0	0.25
Uy, Uz (m/s)	1.0	0.09

TABLE XV. STANTON NUMBER UNCERTAINTY [Ref. 18:p. 269]

Quantity (units)	Typical Nominal Values	Experimental Uncertainty
T_∞ (°C)	18.0	0.13
T_∞ (°C)	40.0	0.21
Pambient (mm Hg)	760.0	0.71
P (mm Hg)	760.0	0.71
P (kg/m)	1.23	0.009
Po-P (mm water)	6.13	0.047
U ,Uc, Ux (m/s)	10.0	0.06
Cp (J/(kg K)	1006.0	1.0
$\dot{q}$ (W)	270.0	10.5
St	0.00196	0.00009
St/Sto	1.05	0.058

APPENDIX C

DATA ACQUISITION, DATA PROCESSING AND PLOTTING PROGRAMS

1. Mean Velocity Survey Software:

ORIENT: This program calculates calibration coefficients for each of the five pressure transducers associated with the five sensing ports of the five hole pressure probe. Additionally ORIENT is used to orientate the five hole probe so that at 0 yaw angle the pressures from the right and left ports are equal.

FIVEHOLE: This program acquires pressure data from each of the five transducers associated with the five hole probe. The FIVEHOLE program controls the Mitas motor controller which, in turn, controls the automatic traversing device on which the five hole probe is mounted. An 800 point pressure survey is conducted of the Y-Z plane normal to the freestream flow. Two data files, FIV and FIVP, are created. The FIV data file consists of mean velocity, center port pressure, average pressure of the four peripheral ports, and the yaw and pitch coefficients for each of the 800 locations sampled. The FIVP data file consists of the pressures P1 through P5 sensed by each of the five pressure probe

sensing ports, the average pressure of the four peripheral ports and the mean velocity, for each of the 800 survey locations.

PADJUST: This program accesses the FIVP data file created by FIVEHOLE and adjusts the pressures to account for spatial resolution problems. Pressure correction is performed using a curve fit to move the measurement location to the center sensing port location.

VELOCITY: This program accesses the data file created by PADJUST and computes the Ux, Uy and Uz velocity components.

UX2: This program accesses the data file created by VELOCITY and plots streamwise velocity (Ux) contours of the Y-Z plane surveyed by the five hole pressure probe.

PTOT2: PTOT2 accesses the VELOCIY program data file and plots total pressure contours of the surveyed Y-Z plane.

VECTOR2: This program accesses the VELOCITY program output file and plots the secondary flow vectors in the surveyed Y-Z plane.

VORCIRC2: This program acquires the velocity component data file created by the VELOCITY program and plots streamwise vorticity contours of the surveyed Y-Z plane. Vortex parameters calculated by this program include: core center location, core radii, vorticity, vortex circulation, non-dimensional core radii and non-dimensional vortex circulation.

2. Mean Temperature Survey Software:

ROVER: This program acquires flow temperature data from the "roving" thermocouple mounted on the automatic traversing device. The traversing device is controlled by the Mitas motor controller which is, in turn, controlled by this program. The ouput data file consists of differential temperatures (Trover - T_∞) for each of the 800 survey locations in the Y-Z plane.

PLTMP2: This program acquires the differential temperature data file created by ROVER, and plots differential temperature contours of the surveyed Y-Z plane.

3. Heat Transfer Measurement Software (No Film Cooling):

STANTON3: This program acquires multiple channel thermocouple data for heat transfer measurements with no film cooling, and creates two output files, TDATA and IDATA. The TDATA file consists of the 126 test plate thermocouple temperatures. The IDATA file records run number, test plate voltage and current, ambient pressure, pressure differential, ambient temperature, freestream velocity, air density and freestream temperature.

STANTON4: STANTON4 accesses TDATA and IDATA files created by STANTON3 and calculates heat transfer coefficients and Stanton numbers for each thermocouple location. This program additionally calculates the average Reynolds number for each thermocouple row. STANTON4 creates three output files: HDATA, SDATA, and STAV. The HDATA file consists of the local heat transfer coefficient, the Stanton number and the X,Z coordinates for each of the 126 test plate thermocouples (H(I), ST(I), X(I), Z(I)). The SDATA file contains only the Stanton number values calculated for each thermocouple location (ST(I)). The STAV file contains the X location, the average Reynolds number and average Stanton number for each of the six thermocouple rows (X(I), Rey(I), ST1(I))

STAVRAT: This program accesses the HDATA files created by STANTON4 and creates an output file which consists of Stanton number ratios and X,Z coordinates for each of the thermocouple locations (STR(I), X(I), Z(I)). STAVRAT is specifically designed to calculate St/Sto ratios for data collected when no film-cooling is used. Sto values are the baseline Stanton numbers (no vortex and no film-cooling); St values are Stanton numbers with embedded vortices and no film-cooling.

PLOTSTR2: This program accesses the Stanton number ratio files created by STAVRAT and plots spanwise variations of St/Sto ratios for all six thermocouple rows.

NFCCOMBO: This program acquires the Stanton number ratios calculated by STAVRAT for various strength vortices and for no vortex. NFCCOMBO plots spanwise variations of ST/Sto ratios for a user specified thermocouple row. The Stanton number ratio spanwise variations for each vortex are superimposed on top of one another in order to show the effects of varying vortex circulation.

4. Heat Transfer Measurement Software (with film-cooling)

SETCOND: This program is used to set conditions for heat transfer data acquisition when film-cooling is employed. SETCOND determines injection velocity, Reynolds number,

blowing ratio and non-dimensional temperature ( ). It requires user input from the terminal of freestream conditions, rotometer percent flow and injection plenum differential pressure. In order to calculate , this program obtains injection plenum temperature from thermocouple channel 148 and surveys all 126 test plate thermocouples to derive average test plate temperature. [Ref. 16:p. 196]

STANFC1: This program is used when film-cooling is employed to acquire multiple channel thermocouple data for heat transfer measurements. STANFC1 creates three data files; a temperature data file, a terminal input data file and a film-cooling data file. The temperature data file consists of the 126 test plate thermocouple temperatures. The terminal input data file records the identical information contained in the IDATA file of STANTON3, discussed above. The film-cooling data file contains the injection rotometer percent flow and the injection plenum differential pressure.

STANFC2: This program accesses the temperature, film-cooling and terminal input files created by STANFC1. The program then calculates Stanton number values for the 126 thermocouple locations and creates a single output file containing these 126 Stanton numbers.

STANR1: This program reads three Stanton number data files and creates a single output file containing two Stanton number ratios for each of the 126 thermocouple locations. The required input data files are: SDATA file created by STANTON4 containing baseline Stanton numbers (Sto) for no vortex and no film-cooling, ST data file created by STANFC2 for film-cooling and no vortex (Stf), and the ST data file created by STANFC2 for film-cooling and embedded vortex (St). The output data file contains the St/Sto ratios, the Stf/Sto ratios and the X,Z coordinates for the 126 thermocouple locations [Str(I), Sfr(I), X(I), Z(I)].

PLSTRVV3H: This program accesses the Stanton number ratio file created by STANR1 and plots spanwise variations of the Stanton number ratios Stf/Sto for film-cooling only, and St/Sto for film-cooling and vortex. Ratios are plotted for the user specified thermocouple row. PLSTRVV3H is used only for single injection hole film cooling data.

PLSTRVVAH: This program is used with 13 injection hole film cooling data. PLSTRVVAH is identical to PLSTRVV3H with the exception of different upper and lower bounds on the plot axes.

3DSTR3H: This program, which is the three dimensional version of PLSTRVV3H, accesses the Stanton number ratio file created by STANR1. 3DSTR3H plots the spanwise variations of the St/Sto and Stf/Sto ratios for all six thermocouple rows. 3DSTR3H is used only for single injection hole film-cooling data.

3DSTRAH: This program is used with 13 injection hole film cooling data. It is identical to 3DSTR3H with the exception of different upper and lower bounds on the plot axes.

3HCOMBO: This program accesses the Stanton number ratio file created by STANR1 for vortices r, w, x, y and z, and for no embedded vortex. 3HCOMO plots the Stf/Sto spanwise variations for a user specified thermocouple row, and then superimposes the St/Sto spanwise variations data for each of the above vortices.

AHCOMBO: This program is the 13 injection hole version of 3HCOMBO, and is identical to 3HCOMBO with the exception of different upper and lower bounds on the plot axes.

5. Combination Plots Software

VECTCOMBO: VECTCOMBO and TEMPCOMBO are specifically adapted
TEMPCOMBO:
versions of VECTOR2 and PLTMP2, which plot the differential mean temperature contours superimposed on top of the secondary flow vectors. VECTCOMBO is run first followed by TEMPCOMBO.

APPENDIX D

DATA FILE DIRECTORY

1. Mean Velocity Data:

Data Run #	Data File	Generating Program	Experimental Conditions
101588.1145	FIV018	FIVEHOLE	Vortex r, x/d=41.9,
	FIVP018	FIVEHOLE	no film-cooling.
	PRS018	PADJUST	
	VEL018	VELOCITY	
101588.1659	FIV015	FIVEHOLE	Vortex s, x/d=41.9,
	FIVP015	FIVEHOLE	no film-cooling.
	PRS015	PADJUST	
	VEL015	VELOCITY	
101688.1054	FIV012	FIVEHOLE	Vortex t, x/d=41.9,
	FIVP012	FIVEHOLE	no film-cooling.
	PRS012	PADJUST	
	VEL012	VELOCITY	
101688.1524	FIV08	FIVEHOLE	Vortex u, x/d=41.9,
	FIVP08	FIVEHOLE	no film-cooling.
	PRS08	PADJUST	
	VEL08	VELOCITY	
101688.2023	FIV04	FIVEHOLE	Vortex v, x/d=41.9,
	FIVP04	FIVEHOLE	no film-cooling.
	PRS04	PADJUST	
	VEL04	VELOCITY	
101788.0113	FIV00	FIVEHOLE	no vortex, x/d=41.9,
	FIVP00	FIVEHOLE	no film-cooling.
	PRS00	PADJUST	
	VEL00	VELOCITY	
101988.1701	F3H18	FIVEHOLE	Vortex r, x/d=41.9,
	FP3H18	FIVEHOLE	3 injection holes.
	PRS3H18	PADJUST	
	VEL3H18	VELOCITY	

Data Run #	Data File	Generating Program	Experimental Conditions
101988.2347	F3H15	FIVEHOLE	Vortex w, x/d=41.9,
	FP3H15	FIVEHOLE	3 injection holes.
	PRS3H15	PADJUST	
	VEL3H15	VELOCITY	
102088.1025	F3H12	FIVEHOLE	Vortex x, x/d=41.9,
	FP3H12	FIVEHOLE	3 injection holes.
	PRS3H12	PADJUST	
	VEL3H12	VELOCITY	
102088.1718	F3H08	FIVEHOLE	Vortex y, x/d=41.9,
	FP3H08	FIVEHOLE	3 injection holes.
	PRS3H08	PADJUST	
	VEL3H08	VELOCITY	
102088.2031	F3H04	FIVEHOLE	Vortex z, x/d=41.9,
	FP3H04	FIVEHOLE	3 injection holes.
	PRS3H04	PADJUST	
	VEL3H04	VELOCITY	
102188.0301	F3H00	FIVEHOLE	no vortex, x/d=41.9,
	FP3H00	FIVEHOLE	3 injection holes.
	PRS3H00	PADJUST	
	VEL3H00	VELOCITY	
102288.2315	FAH18	FIVEHOLE	Vortex r, x/d=41.9,
	FPAH18	FIVEHOLE	13 injection holes.
	PRSAH18	PADJUST	
	VELAH18	VELOCITY	
102288.1839	FAH15	FIVEHOLE	Vortex w, x/d=41.9,
	FPAH15	FIVEHOLE	13 injection holes.
	PRSAH15	PADJUST	
	VELAH15	VELOCITY	
102288.1323	FAH12	FIVEHOLE	Vortex x, x/d=41.9,
	FPAH12	FIVEHOLE	13 injection holes.
	PRSAH12	PADJUST	
	VELAH12	VELOCITY	
102288.0834	FAH08	FIVEHOLE	Vortex y, x/d=41.9,
	FPAH08	FIVEHOLE	13 injection holes.
	PRSAH08	PADJUST	
	VELAH08	VELOCITY	

Data Run #	Data File	Generating Program	Experimental Conditions
102188.2359	FAH04	FIVEHOLE	Vortex z, x/d=41.9,
	FPAH04	FIVEHOLE	13 injection holes.
	PRSAH04	PADJUST	
	VELAH04	VELOCITY	
102188.1933	FAH00	FIVEHOLE	no vortex, x/d=41.9,
	FPAH00	FIVEHOLE	13 injection holes.
	PRSAH00	PADJUST	
	VELAH00	VELOCITY	

2. Mean Temperature Survey Data:

Generating Program: ROVER

Data Run #	Data File	Experimental Conditions
122388.1632	TEM0B	no vortex, 3 F.C. holes, x/d=41.9
122388.1414	TEM4B	vortex z, 3 F.C. holes, x/d=41.9
122288.1653	TEM8B	vortex y, 3 F.C. holes, x/d=41.9
123088.1914	TEM12B2	vortex x, 3 F.C. holes, x/d=41.9
122288.1359	TEM15B	vortex w, 3 F.C. holes, x/d=41.9
122188.1748	TEM18B	vortex r, 3 F.C. holes, x/d=41.9
122888.1154	TEMPER0B	no vortex, 13 F.C. holes, x/d=41.9
122888.1652	TEMPER4B	vortex z, 13 F.C. holes, x/d=41.9
122888.1345	TEMPER8B	vortex y, 13 F.C. holes, x/d=41.9
123088.1444	TEMPER12B	vortex x, 13 F.C. holes, x/d=41.9
122988.1142	TEMPER15B	vortex w, 13 F.C. holes, x/d=41.9
122888.1629	TEMPER18B	vortex r, 13 F.C. holes, x/d=41.9

Data Run #	Data File	Experimental Conditions
010389.1818	TEM15A	vortex w, 3 F.C. holes, x/d=5.2
010489.1712	TEM15C	vortex w, 3 F.C. holes, x/d=82.9
010589.1237	TEM15D	vortex w, 3 F.C. holes, x/d=109.2
010389.2158	TEMPER15A	vortex w, 13 F.C. holes, x/d=5.2
010489.1251	TEMPER15C	vortex w, 13 F.C. holes, x/d=82.9
010689.1136	TEMPER15D	vortex w, 13 F.C. holes, x/d=109.32

3. Heat Transfer Data:

A. STANTON3 / STANTON4 data files -- (no film-cooling):

TDATAxx ---- temperature data file

IDATAxx ---- user terminal input data file

HDATAxx ---- heat transfer coefficient data file

STAVxx ---- row average Stanton number data file

SDATAxx ---- local Stanton number data file

Data Run #	Data File	Experimental Conditions
110288.1805	TDATA0 IDATA0 HDATA0 STAV0 SDATA0	no vortex, no film cooling

Data Run #	Data File	Experimental Conditions
110288.2112	TDATA18	vortex r, no film cooling
	IDATA18	
	HDATA18	
	STAV18	
	SDATA18	
110288.2245	TDATA15	vortex w, no film cooling
	IDATA15	
	HDATA15	
	STAV15	
	SDATA15	
110388.0012	TDATA12	vortex x, no film cooling
	IDATA12	
	HDATA12	
	STAV12	
	SDATA12	
110388.0101	TDATA8	vortex y, no film cooling
	IDATA8	
	HDATA8	
	STAV8	
	SDATA8	
110388.0153	TDATA4	vortex z, no film cooling
	IDATA4	
	HDATA4	
	STAV4	
	SDATA4	
110288.1816	BTDATA0	no vortex, no film cooling
	BIDATA0	
	BHDATA0	
	BSTAV0	
	BSDATA0	
121988.1621	TDATA04	no vortex, no film cooling
	IDATA04	
	HDATA04	
	STAV04	
	SDATA04	
121988.1643	TDATA05	no vortex, no film cooling
	IDATA05	
	HDATA05	
	STAV05	
	SDATA05	

B. Stanton Number Ratio Files -- (no film cooling):

Generating Program: STAVRAT

Data file	Ratio
STR18	SDATA18/SDATA0
STR15	SDATA15/SDATA0
STR12	SDATA12/SDATA0
STR8	SDATA8/SDATA0
STR4	SDATA4/SDATA0
STR0	SDATA0/SDATA0

C. STANFC1 / STANFC2 data files -- (3 hole film-cooling):

TFC3Hxx ---- temperature data file

IFC3Hxx ---- user terminal input data file

FC3Hxx ---- film-cooling parameters data file

SFC3Hxx ---- local Stanton number data file

Data Run #	Data File	Experimental Conditions
110488.2311	TFC3H0 IFC3H0 FC3H0 SFC3H0	no vortex, 3 injection holes
110488.2359	TFC3H4 IFC3H4 FC3H4 SFC3H4	vortex z, 3 injection holes

Data Run #	Data File	Experimental Conditions
110588.0147	TFC3H8	vortex y, 3 injection holes
	IFC3H8	
	FC3H8	
	SFC3H8	
110588.0253	TFC3H12	vortex x, 3 injection holes
	IFC3H12	
	FC3H12	
	SFC3H12	
110588.0351	TFC3H15	vortex w, 3 injection holes
	IFC3H15	
	FC3H15	
	SFC3H15	
110588.0532	TFC3H18	vortex r, 3 injection holes
	IFC3H18	
	FC3H18	
	SFC3H18	

D. STANFC1 / STANFC2 data files -- (13 hole film-cooling):

TAHxx ---- temperature data file

IAHxx ---- user terminal input data file

FAHxx ---- film-cooling parameters data file

SAHxx ---- local Stanton number data file

Data Run #	Data File	Experimental Conditions
110588.0835	TAH0	no vortex, 13 injection holes
	IAH0	
	FAH0	
	SAH0	
110588.1214	TAH4	vortex z, 13 injection holes
	IAH4	
	FAH4	
	SAH4	

Data Run #	Data File	Experimental Conditions
110588.1124	TAH8 IAH8 FAH8 SAH8	vortex y, 13 injection holes
110588.1009	TAH12 IAH12 FAH12 SAH12	vortex x, 13 injection holes
110588.0918	TAH15 IAH15 FAH15 SAH15	vortex w, 13 injection holes
110588.0718	TAH18 IAH18 FAH18 SAH18	vortex r, 13 injection holes

E. Stanton Number Ratio Files (3 & 13 hole film-cooling)

Generating Program: STANR1

RAT3Hxx -- 3 hole film-cooling

RATAHxx -- 13 hole film-cooling

Data file	St/Sto; Stf/Sto
RAT3H18	SFC3H18/SDATA04; SFC3H0/SDATA04
RAT3H15	SFC3H15/SDATA04; SFC3H0/SDATA04
RAT3H12	SFC3H12/SDATA04; SFC3H0/SDATA04
RAT3H8	SFC3H8/SDATA04; SFC3H0/SDATA04
RAT3H4	SFC3H4/SDATA04; SFC3H0/SDATA04
RAT3H0	SFC3H0/SDATA04; SFC3H0/SDATA04

Data file	St/Sto; Stf/Sto	
RATAH18	SAH18/SDATA04;	SAH0/SDATA04
RATAH15	SAH15/SDATA04;	SAH0/SDATA04
RATAH12	SAH12/SDATA04;	SAH0/SDATA04
RATAH8	SAH8/SDATA04;	SAH0/SDATA04
RATAH4	SAH4/SDATA04;	SAH0/SDATA04
RATAH0	SAH0/SDATA04;	SAH0/SDATA04

LIST OF REFERENCES

1. Ligrani, P.M. and Williams, W., "Effects of an Embedded Vortex on Injectant from a Single Film-Cooling Hole in a Turbulent Boundary Layer", ASME Paper No. 89-GT-189, pp. 1-11, ASME Gas Turbine and Aeroengine Congress and Exposition, Toronto, Ontario, Canada, June, 1989, also to appear in ASME Transactions--Journal of Turbomachinery January. 1990.

2. Ligrani, P.M., Joseph, S.L., Ortiz, A. and Evans, D.L., "Heat Transfer in Film-Cooled Turbulent Boundary Layers at Different Blowing Ratios as Affected by Longitudinal Vortices", Experimental Thermal and Fluid Science, Vol. 1, No. 4, pp.347-362, 1988.

3. Ligrani, P.M., Ortiz, A., Joseph, S.L. and Evans, D.L., "Effects of Embedded Vortices on Film-Cooled Turbulent Boundary Layers", ASME-88-GT-170, ASME Gas Turbine and Aeroengine Congress and Exposition, Amsterdam, The Netherlands, June, 1988, also ASME Transactions---. Journal of Turbomachinery, Vol. 111, pp. 71-77, 1989.

4. Blair, M.E., "An Experimental Study of Heat Transfer and Film Cooling on Large-Scale Turbine Endwalls", ASME Transactions--Journal of Heat Transfer, Vol. 96, pp. 524 529, 1974.

5. Goldstein, R.J. and Chen, H.P., "Film-Cooling on a Gas Turbine Blade Near the End Wall", ASME Transactions-Journal of Engineering for Gas Turbines and Power, Vol. 107, pp.117-122, January 1985.

6. Goldstein, R.J. and Chen, H.P., "Film-Cooling of a Turbine Blade with Injection through Two Rows of Holes in the Near-Endwall Region", The American Society of Mechanical Engineers, Paper No. 87-GT-196, pp. 1-7, June 1987.

7. Sato, T., Aoki, S., Takeishi, K. and Matsuura, M., "Effect of Three-Dimensional Flow Field on Heat Transfer Problems of a Low Aspect Ratio Turbine Nozzle", Takasago Research and Development Center, Mitsubishi Heavy Industries, Ltd., 1987.

8. Kobayashi, R., "Note on the Stability of a Boundary Layer on a Concave Wall with Suction", Journal of Fluid Mechanics, Vol. 52, pp. 269-272, 1972.

9. Kobayashi, R., "Taylor Gortler Instability of a Boundary Layer with Suction or Blowing", Report: Institute of High Speed Mechanics, Vol. 32, Series B, pp. 129-148, 1975.

10. El-Hady, N.M. and Verma, A.K., "Instability of Compressible Boundary Layers Along Curved Walls with Suction or Cooling", AIAA Journal, Vol. 22, pp. 206-213, 1984.

11. Honami, S. and Fukagawa, M., "A Study on Film Cooling Behavior of a Cooling Jet Over a Concave Surface", Paper 87-Tokyo-IGTC-72, Tokyo International Gas Turbine Congress, Tokyo, Japan, 1987.

12. Schwarz, S.G. and Goldstein, R.J., "The Two-Dimensional Behavior of Film Cooling Jets on Concave Surfaces", Paper 88-GT-161, ASME Gas Turbine and Aeroengine Congress and Exposition, Amsterdam, The Netherlands, 1988.

13. Joseph, S.L., "The Effects of an Embedded Vortex on a Film-Cooled Turbulent Boundary Layer", M.E. Thesis, Naval Postgraduate School, Monterey, Califronia, December, 1986.

14. Evans, D.L., "Study of Vortices Embedded in Boundary Layers Wtih Film Cooling, M.S. Thesis, Naval Postgraduate School, Monterey, California, March, 1987.

15. Ortiz, A., "The Thermal Behavoir of Film Cooled Turbulent Boundary Layers as Affected by Longitudinal Vortices", M.E. Thesis, Naval Postgraduate School, Monterey, California, September 1987.

16. Williams, W., "Effects of an Embedded Vortex on a Single Film-Cooling Jet in a Turbulent Boundary Layer", M.S. Thesis, Naval Postgraduate School, Monterey, California, June, 1988.

17. Golstein, R.J., Eckert, E.R.G. and Ramsey, J.W., "Film Cooling with Injection Through Holes: Adiabatic Wall Temperatures Downstream of a Circular Hole", ASME Transactions - Journal of Engineering for Power, Vol. 90, No. 4, pp. 384-395, 1968.

18. Schwartz, G.E., "Control of Embedded Vortices Using Wall Jets", M.S. Thesis, Naval Postgraduate School, September, 1988.

19. Kays, W.M. and Crawford, M.E., Convective Heat and Mass Transfer, Second Edition, p. 216, McGraw-Hill Book Company, 1980.

20. Bradshaw, P., Editor, "Aerodynamics Equipment Instruction Manual", IC Aero TN 76-101, (1984 Revision), pp. 2-4-1 - 2-4-3, Department of Aeronautics, Imperial College of Science and Technology, London, England, 1984.

21. Merzkirch, W., Flow Visualization, pp. 53-56, Acedemic Press, 1974.

22. Westphal, R.V., Pauley, W.R. and Eaton, J.K., "Interaction Between a Vortex and a Turbulent Boundary Layer, Part I: Mean Flow Evolution and Turbulence Properties", NASA Technical Memorandum 88361, January, 1987.

INITIAL DISTRIBUTION LIST

		No. Copies
1.	Defense Technical Information Center Cameron Station Alexandria, Virginia 22304-6145	2
2.	Library, Code 0142 Naval Postgraduate School Monterey, California 93943-5002	2
3.	Professor P. M. Ligrani, Code 69Li Department of Mechanical Engineering Naval Postgraduate School Monterey, California 93943-5000	10
4.	Department Chairman, Code 69 Department of Mechanical Engineering Naval Postgraduate School Monterey, California 93943-5000	1
5	Dr. Dick Rivir Components Branch Turbine Engine Division Aero Propulsion Laboratory Department of the Air Force Air Force Wright Aeronautical Laboratories Wright-Patterson Air Force Base, Ohio, 45433	10
6.	Naval Engineering Curricular Officer, Code 34 Department of Mechanical Engineering Naval Postgraduate School Monterey, California 93943-5000	1
7.	Professor C. S. Subramanian, Code 69Su Department of Mechanical Engineering Naval Postgraduate School Monterey, California 93943-5000	1

8. LCDR Douglas W. Craig 2
366 Hermitage Road
Gahanna, Ohio 43230

9. Commanding Officer 1
David Taylor R&D Center
Carderrock Laboratory
Bethesda, Maryland 20084

Thesis
C78233 Craig
c.1 Effect of vortex circulation on injectant from a single film-cooling hole and a row of film-cooling holes in a turbulent boundary layer, part 1: injection beneath the vortex downwash.

Thesis
C78233 Craig
c.1 Effect of vortex circulation on injectant from a single film-cooling hole and a row of film-cooling holes in a turbulent boundary layer, part 1: injection beneath the vortex downwash.

thesC78233
Effect of vortex circulation on injectan
3 2768 000 83935 1
DUDLEY KNOX LIBRARY